



DOCTOR OF ENGINEERING (ENGD)

The Application of Multi-Attribute Optimisation as a Systems Engineering Tool in an Automotive CAE Environment

Sutton, Paul

Award date:
2012

Awarding institution:
University of Bath

[Link to publication](#)

Alternative formats

If you require this document in an alternative format, please contact:
openaccess@bath.ac.uk

Copyright of this thesis rests with the author. Access is subject to the above licence, if given. If no licence is specified above, original content in this thesis is licensed under the terms of the Creative Commons Attribution-NonCommercial 4.0 International (CC BY-NC-ND 4.0) Licence (<https://creativecommons.org/licenses/by-nc-nd/4.0/>). Any third-party copyright material present remains the property of its respective owner(s) and is licensed under its existing terms.

Take down policy

If you consider content within Bath's Research Portal to be in breach of UK law, please contact: openaccess@bath.ac.uk with the details. Your claim will be investigated and, where appropriate, the item will be removed from public view as soon as possible.

The Application of Multi-Attribute Optimisation as a Systems Engineering Tool in an Automotive CAE Environment

submitted by

Paul Sutton

for the degree of Doctor of Engineering

of the

University of Bath

Department of Computer Science

January 2012

Supervisors:

University of Bath: Prof. J.G. Hawley & Prof. P. Johnson

Jaguar Land Rover: R.A. Mitchell & Dr. S.R. Pierson

COPYRIGHT

Attention is drawn to the fact that copyright of this thesis rests with its author. This copy of the thesis has been supplied on the condition that anyone who consults it is understood to recognise that its copyright rests with its author and that no quotation from the thesis and no information derived from it may be published without the prior written consent of the author.

This thesis may be made available for consultation within the University Library and may be photocopied or lent to other libraries for the purposes of consultation.

Signature of Author.....

Paul Sutton

Summary

Multi-Attribute Optimisation (MAO) is proposed as a tool for delivering high value products within the systems engineering approach taken in the automotive industry. This work focuses on MAO methods that use Computer Aided Engineering (CAE) analyses to build a metamodel of system behaviour.

A review of the literature and current Jaguar Land Rover optimisation methods showed that the number of samples required to build a metamodel could be estimated using the number of input variables. The application of these estimation methods to a concept airbox design showed that this guidance may not be sufficient to fully capture the complexity of system behaviour in the metamodeling method. The use of the number of input variables and their ranges are proposed as a new approach to the scaling of sample sizes. As a corollary to the issue of the sample size required for accurate metamodeling, the sample required to estimate the error was also examined. This found that the estimation of the global error by additional samples may be impractical in the industrial context.

CAE is an important input to the MAO process and must balance the efficiency and accuracy of the model to be suitable for application in the optimisation process. Accurate prediction of automotive attributes may require the use of new CAE techniques such as multi-physics methods. For this, the fluid structure interaction assessment of the durability of internal components in the fuel tank due to slosh was examined. However, application of the StarCD-Abaqus Direct couple and Abaqus Combined Eulerian Lagrangian was unsuitable for this fuel slosh application. Further work would be required to assess the suitability of other multi-physics methods in an MAO architecture.

Application of the MAO method to an automotive airbox shows the potential for improving both product design and lead time.

Dedication

For Liz & my family

Acknowledgements

This research was funded by Jaguar Land Rover and the EPSRC through the SEDC.

Firstly I would like to thank my project supervisors Steven Pierson and Rob Mitchell of Jaguar Land Rover and Gary Hawley and Peter Johnson at the University of Bath, for their constant advice and support.

At Jaguar Land Rover, I would like to acknowledge the input of Ian Shilling, Ray Cheung, David Clayton, Matt Butler and all members of the Powertrain CAE team and I.T. support. Mike Powell and the air intake system team for many discussions on airboxes. Paul Foster and Simon Wright for insights into fuel system and tank design. Andy Bowen, Martin Dale and Lawrence Terry for help with the fuel tank rig tests.

I would also like to thank the support staff at the various software vendors; Rachel Fitzsimmonds at CD-Adapco, Anne-Marie Lambert & Leon Cordingly at Simulia and David Mosely at Esteco.

Thanks to Ashley Mills for help with Matlab coding and support throughout the doctorate.

For organising the Doctorate, Guy McCusker at University of Bath, Sharon Henson and Karen Holmes at the SEDC.

A special thanks to Liz Simpson for her patience during this project and for proofreading this work. My final thanks go to my family, I could not have got this far without their love and support.

Contents

1	Introduction	17
1.1	Thesis Summary	17
1.2	Research Aims & Objectives	19
1.3	Contribution to Knowledge	19
1.4	Structure of this Thesis	21
I	Systems and Optimisation	23
2	Literature Review	24
2.1	Introduction	24
2.2	Systems Engineering	24
2.2.1	What is Systems Engineering?	25
2.2.2	Systems Engineering Processes	26
2.2.3	Case studies of the Application of Systems Engineering to Automotive Design Problems	29
2.3	Optimisation	31
2.3.1	Definition of Optimisation	31
2.3.2	Classical Optimisation	31
2.3.3	Solution Methods	32
2.4	Optimisation of Systems	33
2.4.1	Multiple and Conflicting Objectives	33
2.4.2	Optimisation of Multiple Domains & Disciplines	34
2.4.3	Robustness	34
2.5	Approaches to Systems Optimisation	35
2.5.1	Systems Modelling & Problem Solving	35
2.5.2	Design of Experiment (DoE) Methods	35
2.5.3	Single Attribute Optimisation	36
2.5.4	Multi-Disciplinary Design Optimisation	36
2.5.5	Multi-Attribute Optimisation	37
2.5.6	System Modelling	39
2.5.7	Summary	41
2.6	CAE Based Optimisation Problems	42

2.6.1	Reducing Problem Complexity	42
2.6.2	Reducing Computational Time	43
2.6.3	Reducing Engineering Hours	44
2.6.4	Application of Metamodelling	45
2.6.5	Multi-physics CAE Methods	56
2.7	Examples of Optimisation in Literature	57
2.8	Conclusion	58
3	Rationale and Criteria for MAO	60
3.1	Introduction	60
3.2	System of Systems Engineering	61
3.3	Feasibility of Using MAO as a Systems Engineering Tool	61
3.3.1	Current Optimisation Methods in Jaguar Land Rover	62
3.3.2	A System of Systems Viewpoint of The Design Environment	63
3.3.3	A Systems Engineering Approach to a MAO Tool	66
3.3.4	A System of Systems Engineering Approach to a MAO Tool	67
3.4	Requirements for projects	69
3.5	Research Methodology	70
3.5.1	The Jaguar XK Airbox Multi Attribute Problem	70
3.5.2	The Fuel Tank multi-physics Analysis Project	71
3.6	Conclusion	72
II	Project Research	73
4	The Airbox MAO Problem	74
4.1	Introduction	74
4.2	The Automotive Airbox	75
4.2.1	Key Role and Operation	75
4.2.2	CAE analysis and Optimisation of Airboxes	75
4.2.3	Airbox Design Within Jaguar Land Rover	76
4.2.4	Approach to the Multi-Attribute Airbox Optimisation Problem	77
4.2.5	Gathering the Airbox Requirements	77
4.3	Standard CAE Approaches for Attributes	83
4.3.1	CFD Methods for Pressure Loss Prediction	83
4.3.2	Capacity	85
4.3.3	Results	86
4.3.4	Transmission Loss of an Airbox	89
4.4	Variables and Parametrised CAD Geometry	94
4.4.1	Selection of Variables	94
4.4.2	Selection of Variable Ranges	95
4.4.3	Development of a Parametrised CAD Model	96

4.5	Using the Standard CAE for Airbox analysis	96
4.5.1	CFD Mesh dependence Study	98
4.5.2	Ricardo WAVE Modelling	101
4.6	XK Supercharged Airbox Base Line	102
4.7	Conclusion	105
5	Building the Airbox Metamodels	107
5.1	Introduction	107
5.2	NVH Meta-Modelling	107
5.2.1	NVH Metric	107
5.2.2	Initial Metamodel and Further Sampling Experiments	109
5.2.3	Local Error Estimation & Lipschitz Sampling	111
5.2.4	Increasing the Sample Size	113
5.2.5	Comment on the NVH Metamodel	116
5.3	Attributes Assessed by CFD Methods	117
5.4	Validation	119
5.4.1	Pressure Loss Prediction	119
5.4.2	Capacity Prediction	120
5.4.3	NVH Attribute Prediction	121
5.4.4	Discussion	122
5.5	Conclusion	124
6	Optimisation of the Airbox Problem	126
6.1	Introduction	126
6.2	Inputs to the Optimisation Process	126
6.3	Comments on Optimisation Algorithms	127
6.4	Understanding the Attributes	128
6.5	Single-Attribute Methods	129
6.6	Multi-Attribute Trading Methods	131
6.6.1	Dimensionality Reduction	133
6.6.2	Clustering Methods	133
6.6.3	Self Organising Maps	136
6.6.4	Utility Function Methods	137
6.7	Verification of Optimal and Trade-off Designs	141
6.8	Conclusion	144
7	The Multi-Physics Fuel Tank Problem	146
7.1	Introduction	146
7.2	Project Drivers	146
7.3	Fuel Tank Multi-Physics CAE Methods	147
7.4	Exploring the Project Opportunity	149
7.4.1	Fuel Tank Design Stages	149

7.4.2	Multi-Physics CAE Project Application Opportunities	150
7.4.3	Scope and Requirements	150
7.4.4	Summary	153
7.5	Approach to Multi-Physics CAE Evaluation	153
7.6	Unmapped & Uncoupled Analysis Case Study	155
7.6.1	Finite Element Model and Pressure Loading	155
7.6.2	Results	156
7.6.3	Summary	159
7.7	Multi-Physics Analysis Methods	160
7.7.1	Star-CD & Abaqus Direct Couple	160
7.7.2	Abaqus Combined Eulerian Lagrangian	163
7.8	Discussion	167
7.9	Conclusions	169
III	Project Closure	171
8	Discussion	172
8.1	Introduction	172
8.2	MAO Methods as a Systems Engineering Tool	172
8.2.1	The MAO Method	172
8.2.2	MAO Method Contributors	175
8.2.3	Using MAO as a Systems Engineering Tool for the Selection of Component Design	182
8.3	Casestudy: The Jaguar Land Rover Product Design System	183
8.3.1	MAO Project Timings	183
8.3.2	The Airbox Optimisation Example	185
8.4	Airbox Capacity Calculation	186
8.5	Further Work: Metamodelling-based MAO Methods	186
9	Conclusions	188
A	Sample Size, Distribution and Error Estimation Experiments	204
A.1	Introduction	204
A.2	Experiment Outlines and Methods	204
A.2.1	The Branin Function	205
A.2.2	Upfront and Sequential Sampling Methods	206
A.2.3	Error Estimation Methods	208
A.3	Experiments	209
A.3.1	Experiment 1: Examination of the Literature Guidance on Sample Size	209
A.3.2	Experiment 2: Sample Size and Distribution for Error Estimation	210

A.3.3	Experiment 3: Comparing Seeded and Uniform Latin Hypercubes	212
A.3.4	Experiment 4: Comparing Sequential Sampling Methods	215
A.3.5	Experiment 5: Examining the ‘Leave One Out’ Error Estimation Method	220
A.4	Conclusions	222
B	Supporting Documentation for Airbox Project	225
B.1	Airbox Geometry	225
B.2	NVH Metric Method	230
B.3	WaveBuild 3D Automation	232
B.4	CCM+ Attribute Processing	233
B.5	ModeFrontier Implementation	235
B.6	Utility Script	236
C	Fuel Tank Design Study	238
C.1	Fuel Tank Design Stages	238
C.1.1	Concept Design	238
C.1.2	Concept Finalisation	238
C.1.3	1 st Design Iteration	239
C.1.4	2 nd Design Iteration	239
C.1.5	3 rd Design Iteration	240
C.2	Summary	240
C.3	Application of Method throughout fuel system design team	241
D	Slosh Rig Experiments	244
D.1	Introduction	244
D.2	Experimental Setup	244
D.2.1	The NVH Slosh Rig	245
D.2.2	High Speed Camera	245
D.2.3	Pressure Transducers	246
D.2.4	Accelerometer	247
D.2.5	Communications & Channel Locations	247
D.2.6	Procedure	249
D.3	4 & 6 Litre Pressure Results	249
D.4	Revised Pressure Transducers	255
D.5	Testing With Revised Transducers	256
D.5.1	Hydrostatic Tests	256
D.5.2	Motored Slosh Tests	258
D.5.3	Revised Water Supply	260
D.6	Correlation Study	262
D.6.1	Rig Test Results	262
D.6.2	CFD Modelling	262

D.6.3	Correlation Results	263
D.7	Camera Acceleration Input	266
D.7.1	Establishment of Scale	267
D.7.2	Measurement of Distances	267
D.7.3	Processing the Data	268
D.7.4	Reconstructing the Pulse	269
D.7.5	Application of the Video Derived Acceleration Pulse	270
D.7.6	Summary	274
D.8	Conclusion	275
E	Exploring the Slosh Boundary Condition	276
E.1	Introduction	276
E.2	Details of the Tank Geometry	277
E.3	The StarCD Procedure used for Fluid Modelling	278
E.4	Crash Impulse Loads	280
E.5	Prototype Road Testing Event	281
E.6	Rig Tip Testing	285
E.7	Case Loading Forces	285
E.8	Fuel Fill Sensitivity Analysis	288
E.9	Conclusions	289
F	Slosh and MPCAe Scripts	290
F.1	The User Coding for Source Momentum	290
F.2	The Method Taken to Model the JLR Rig Test	292
F.3	Morphing Mesh Method	293
F.4	Abaqus Direct Cosimulation Cards	294
F.5	Example Abaqus CEL Deck	295

List of Figures

2-1	The Systems Engineering 'V' model	27
2-2	Pareto-Sets and Optimisation Objectives	33
2-3	Global Optimum Performance Variation and Robust Optimum Point.	34
2-4	CAE methods within powertrain CAE	41
2-5	Key Controlling Parameters in Meta-Modelling	46
2-6	Examples of sample sizes in literature and regions	53
2-7	The 'leave one out' error estimation process	55

3-1	Current optimisation methods	62
3-2	Relationships between major design systems	63
3-3	A possible MAO application	66
4-1	Attenuation spectra for XK SC pressure loss single attribute optimisation and NVH trade-off designs	77
4-2	Air intake system P-Diagram	79
4-3	Extracted airbox P-Diagram	80
4-4	Air intake system transmission loss target	82
4-5	Directionality of the filter	84
4-6	Correlation studies for pressure loss	85
4-7	The empirical filter capacity model	89
4-8	Meshing of the XK NA airbox	91
4-9	Example setup of transmission loss experiment in Ricardo WAVE	93
4-10	Correlation studies for transmission loss	94
4-11	Simplified airbox with various potential variables	95
4-12	Finalised WAVE model geometry for design 17	98
4-13	Finalised CFD model geometry for design 17	98
4-14	Mesh refinement around the clean side diffuser and MAF	100
4-15	Mesh refinement around the dirty side diffuser	100
4-16	XK SC baseline geometry (CFD model)	103
4-17	XK SC pressure distribution	104
4-18	XK SC z-directional velocity through the filter	104
4-19	XK SC attenuation spectra	105
5-1	Attenuation spectrum for airbox design 4	108
5-2	Error estimation with increasing Lipschitz samples	113
6-1	Main effects plot for pressure loss based on 43 samples	129
6-2	Function plot during the first single attribute optimisation stage	130
6-3	Pareto designs for three way trade	132
6-4	Pareto surface for three way trade-off of airbox attributes	133
6-5	An example of a 4-D bubble plot	134
6-6	Parallel line chart for pareto airbox designs	134
6-7	2 Cluster grouping for airbox attributes	135
6-8	Increasing the number of clusters in a visualisation	135
6-9	Reduction of complexity in parallel line charts via clustering	136
6-10	SOM applied to the airbox Project	137
6-11	Pressure loss utility function	138
6-12	Capacity utility function	139
6-13	NVH attenuation utility function	140
6-14	Pressure loss & NVH attenuation trade surface	141

6-15	Utility optimised attenuation spectra	144
7-1	Deflection sample locations	156
7-2	Kerb island strike deflection and loading for x (top) and y (bottom) directions	157
7-3	16 Kph crash deflection and loading for x (top) and y (bottom) directions	158
7-4	The geometry and fluid fill conditions used in the direct couple assessment	161
7-5	Comparing the coupled model to the fluid only model	162
7-6	Comparing the coupled model with a reduced timestep to the fluid only model	162
7-7	Comparing the coupled model with a steel baffle to the fluid only model	163
7-8	CEL test case geometry	164
7-9	Eularian mesh pressure distribution	165
7-10	Free surface at time 0.0 (top left), 0.1 (top right), 0.4 (bottom left) and 0.45 seconds (bottom right)	166
8-1	The MAO method	173
8-2	Examples of sample sizes in literature	178
A-1	The Branin function	206
A-2	Variation of the R^2 error estimator of seeded latin hypercube sampling method with increasing numbers of samples	209
A-3	Variation of the RMSE error estimator of seeded latin hypercube sampling method with increasing numbers of samples	210
A-4	Metamodel surface based on 20 modeFRONTIER non-uniform latin hypercube sample points	211
A-5	R^2 error estimator comparing sampling method and size	212
A-6	RMSE error estimator comparing sampling method and size	212
A-7	Variation of RBF approximation with 9 point latin hypercube (top left seed=1, top right seed=2, bottom left seed=3 & bottom right seed=4)	213
A-8	Variation of the R^2 error estimator of various sampling methods with increasing numbers of samples	214
A-9	Variation of the RMSE error estimator of various sampling methods with increasing numbers of samples	214
A-10	RMSE with increasing numbers of sample points	215
A-11	RMSE with increasing numbers of sample points	216
A-12	Increasing the number of points via the MACK sampler with 20 (left) and 21 (right) samples	217
A-13	Predicted global maxima locations	218
A-14	Predicted global minima locations	219
A-15	Comparing error estimates based upon 'leave one out' error and actual error for modeFRONTIER latin hypercubes	221
A-16	Comparing error estimates based upon 'leave one out' error and actual error for Ford minimum latin hypercubes	221

A-17	Comparing error estimates based upon 'leave one out' error and actual for EbL sampling	222
A-18	Comparing error estimates based upon 'leave one out' error and actual error for MACK Sampling	223
A-19	Increasing the number of points via the MACK Sampler with 24 (left) and 25 (right) samples.	223
B-1	Simplified Airbox Geometry	225
B-2	Airbox Height Definitions	227
B-3	Airbox Height (l) & Breadth (r) Definitions	228
B-4	Airbox Height Definitions	228
B-5	Airbox Height Definitions	229
B-6	Airbox Height Definitions	229
B-7	ModeFrontier implementation for internal assessment of meta models	235
B-8	ModeFrontier implementation with Matlab Utility function	236
D-1	The slosh rig physical test	245
D-2	PMP 317 3038 pressure transducers	246
D-3	Communication routes in the experiment	248
D-4	Pressure transducer channel numbers	248
D-5	4 litre run 1 pressure traces	252
D-6	4 litre run 2 pressure traces	252
D-7	4 litre run 3 pressure traces	253
D-8	6 litre run 1 pressure traces	253
D-9	6 litre run 2 pressure traces	254
D-10	6 litre run 3 pressure traces	254
D-11	The machined pressure transducers	255
D-12	Revised pressure transducer channel numbers	256
D-13	Hydrostatic test on channels 1, 2 & 4	257
D-14	Hydrostatic test on channel 3	257
D-15	Full test run 1, channels 1, 2, 3 & 4	258
D-16	Full test run 2, channels 1, 2, 3 & 4	259
D-17	Full test run 3, channels 1, 2, 3 & 4	259
D-18	Frothing issue found during hydrostatic tests	260
D-19	Clean water full test run 1, channels 1, 2, 3 & 4	260
D-20	Clean water full test run 2, channels 1, 2, 3 & 4	261
D-21	Clean water full test run 3, channels 1, 2, 3 & 4	261
D-22	Run 33 channel 1 pressure trace	262
D-23	Run 33 acceleration pulse	264
D-24	Channel 1 pressure trace for run 33 acceleration profiles	264
D-25	Free surface comparisons at 3.23 (top images) and 3.40 seconds (bottom images)	265

D-26	Accelerometer frequency response	266
D-27	Measuring points for scale and distance on the fuel tank	268
D-28	Measured distances travelled in video images	268
D-29	Comparing acceleration profiles from the accelerometer and video	269
D-30	Assumed acceleration profile compared to accelerometer data	270
D-31	Channel 1 pressure trace for high speed video derived acceleration profile	271
D-32	Free surface comparisons at 3.23 (top images) and 3.40 seconds (bottom images)	272
D-33	Run 33 accelerometer and assumed acceleration pulse	273
D-34	Channel 1 pressure trace for run 33 acceleration profiles	273
D-35	Free surface comparisons at 3.23 (top) and 3.40 seconds (bottom)	274
E-1	Simplified fuel tank geometry	278
E-2	16 kph crash impulse	280
E-3	Kerb island strike x (top), y (middle) & z (bottom) acceleration	282
E-4	Postel road brake x (top), y (middle) & z (bottom) acceleration	283
E-5	Accel on 5 bumps x (top), y (middle) & z (bottom) acceleration	283
E-6	Chatterbumps x (top), y (middle) & z (bottom) acceleration	284
E-7	Slalom cobblestones x (top), y (middle) & z (bottom) acceleration	284
E-8	Rig test modelling setup.	285
E-9	Forces on the Baffle	286
E-10	Pressures on the Baffle	286
E-11	Free surface within the tank	287

List of Tables

2.1	Tools commonly used in DCOV methods	28
2.2	Examples of Metamodelling in Literature (a)	47
2.3	Examples of Metamodelling in Literature (b)	48
2.4	Examples of Metamodelling in Literature (c)	49
2.5	Abbreviations used in examples table.	50
2.6	Guidance for regions of sample sizes (where N is the number of variables)	53
2.7	Maniverter Design Improvements enabled by use of MDO	58
4.1	Parameters and pressure loss for XK SC pressure loss single attribute optimisation and NVH trade-off designs	76
4.2	Filter resistance parameters	84

4.3	20 mBar (ΔP) pressure loss test samples	88
4.4	25 (ΔP) mBar pressure loss test samples	88
4.5	WAVE transmission loss CAE setup	92
4.6	Current Jaguar Land Rover airbox volumes, breadths and lengths	96
4.7	Variables for 33 latin hypercube sample	97
4.8	Pressure loss mesh dependency study	99
4.9	Gamma mesh dependency study	99
4.10	Parameter & attribute values for XK SC airbox	102
5.1	Rough airbox ranking orders	108
5.2	Airbox NVH metric and ranking	109
5.3	Additional airbox designs for NVH evaluation	111
5.4	Parameters for additional sample points	112
5.5	Airbox ranking changes for full geometry to simplified WaveBuild3D	115
5.6	Error estimators of metamodeling methods based on 129 sample points with 33 error estimation points	116
5.7	Variation of pressure loss measurements over last 200 iterations of CFD model	117
5.8	Variation of gamma measurements over last 200 iterations of CFD model	118
5.9	Additional error estimation airbox designs	119
5.10	Pressure loss on 10 additional airbox designs	120
5.11	Capacity on 10 additional airbox designs	121
5.12	NVH metric on 10 additional airbox designs	121
5.13	NVH metric on 10 additional airbox designs with increasing sample size	122
5.14	Airbox MAO process times	123
6.1	Design variable input parameters in modeFRONTIER	127
6.2	SAO airbox designs	131
6.3	Attribute trade-off airbox design	142
6.4	Comparing metamodel predictions with CAE results	142
6.5	Comparing CAE results for utility optimised and baseline designs	143
7.1	Fuel tank CAE Lists	151
7.2	Revised fuel tank CAE Lists	151
7.3	Pugh selection matrix for multi-physics project	152
8.1	Guidance for sample sizes (where N is the number of variables)& suggested sample sizes for an 8 variable problem	177
8.2	XK SC airbox input variable ranges and sensitivity factors for the NVH attribute values	179
A.1	Global maxima predictions for the various sampling methods	218
A.2	Global minima predictions for the various sampling methods	219
B.1	Primary Parameters	226

B.2	Secondary Airbox Parameters	226
B.3	MAF Parameters	229
C.1	Fuel system design team CAE Lists	242
C.2	Revised fuel system design team CAE Lists	243
D.1	Pressure transducer calibration	247
D.2	Accelerometer calibration	247
D.3	Predicted hydrostatic pressures from ρgh approximation	249
D.4	4 litre tests	250
D.5	6 Litre Tests	250
D.6	Machined pressure transducer calibration	255
D.7	Hydrostatic pressure tests	256
D.8	Scaling measurements	267
E.1	Simplified fuel tank volume calculation	278
E.2	Accelerations in the PASCAR events	281
E.3	Maximum and Minimum Forces of the Baffle	288
E.4	Maximum and minimum directional forces for each of the load cases	289

Nomenclature & Acronyms

ALE	Arbitrary Lagrangian Eularian
CAE	Computer Aided Engineering
CEL	Combined Eularian Lagrangian
CFD	Computational Fluid Dynamics
DCOV	Define, Characterise, Optimise & Verify
DMAIC	Define, Measure, Analyse, Improve & Control
DoE	Design of Experiments
EoS	Equation of State
FE	Finite Element
FEM	Finite Element Method
FSI	Fluid Structure Interaction
HPC	High Performance Computing
INCOSE	International Council on Systems Engineering
kph	Kilometres Per Hour
LH	Latin Hypercube
MAO	Multi Attribute Optimisation
MDA	Multi Discipline Analysis
MDO	Multi-disciplined Design Optimisation
MObjO	Multi Objective Optimisation
MOO	Multi Objective Optimisation
MOOP	Multi Objective Optimisation Problem
MPC	Multi Physics Code
MPCAE	Multi Physics Computer Aided Engineering
MpCCI	Mesh-based Parallel Code Coupling Interface
NVH	Noise, Virbration & Harshness
SPH	Smooth Particle Hydrodynamics
VOF	Volume of Fraction

Chapter 1

Introduction

1.1 Thesis Summary

There are many pressures on companies operating within the automotive industry. Overcapacity in manufacturing[1] and a decline in sales during the recent ‘credit crunch’[2] prompted vehicle manufacturers to reduce costs in all areas of business. Increasing demand for new products and a recovery in sales[3][4] now require the automotive industry to design better products in a shorter space of time[5]. Systems Engineering is a method that can deliver customer-focused products whilst reducing the time and cost taken to design new vehicles[6][7].

Systems Engineering is an interdisciplinary approach to delivering customer requirements[8]. This approach relies heavily on systematic processes and tools to enable system designers to understand the requirements and constraints of systems. Optimisation is a core component of the Systems Engineering process, which ensures that designs best meet the product requirements[9].

Within automotive design, a product will have many different and potentially conflicting attributes. Computer Aided Engineering (CAE) methods have been utilised to predict a product’s attributes early in the design process[10]. Each of these attributes need to be optimised in order to deliver a high value product. However, conflicts between attributes must be resolved by methods which trade-off one attribute against another. Historically, iterative processes have been used to achieve this, whereby each attribute is optimised in isolation and trade-off occurs in a sequential process (see Section 3.3.1). The issue with this approach is that it may not produce the optimal design, as the inter-relationship between the attributes is not considered. Multi-Attribute Optimisation (MAO) methods consider the multi-attribute nature of systems and may therefore provide an improvement in product design, in a reduced development time. In order for the MAO approach to be effectively utilised in an industrial setting, the processes and enablers need to be better understood.

When optimising the design of a system, exploration of the potential design space allows the relationships between the attributes of the product to be established. Metamodelling is a tool that can be used to explore the design space as part of an MAO approach[11]. With this tool, a mathematical function is fitted to predictions or measurements of the attributes within the design space. The function can then be used to predict attribute behaviour in other regions of the

design space. However, there are some problems with using the metamodeling technique; namely, the sample size required versus the cost of collecting those samples[12][13][14] and the cost of calculating the error in the metamodel[11][15]. When using MAO as a tool, ways of exploring the design space, trading attributes and selecting the final design that delivers the best value product must also be considered[16].

The building of metamodels can be based on CAE methods. The method used must be appropriate to the attribute under investigation. While most attributes can be analysed by a single domain CAE code, the multi-disciplinary nature of a system's attributes may cross the traditional CAE domains[17]. In these instances, multi-physics CAE methods are sometimes required in order to capture attribute behaviour accurately[18]. However, there is an issue of the additional cost of such methods versus the improved accuracy of the attribute prediction.

While research in these methods is ongoing to develop new metamodeling, sampling, error estimation, trade-off and CAE techniques, this thesis focuses on the application of such techniques as a systems engineering tool. For this, the constraints of a systems engineering design environment must be considered. In this thesis, the Jaguar Land Rover product design and optimisation processes are used as a case study, providing the context and constraints in which an MAO tool must operate. Within this context, issues connected with metamodeling and multi-physics CAE methods are addressed by two projects. The first is an MAO airbox project that examines sample size, error estimation, trade-off methods and the benefit of a multi-attribute approach to optimisation. The second project is a multi-physics analysis of a fuel tank that investigates the cost versus the benefit of using multi-physics methods. Both projects were constrained to use Jaguar Land Rover software and procedures.

A constructive research approach is taken, using practical application of CAE and optimisation methods. The airbox MAO problem examines the use of the metamodeling approach to the trade-off between three conflicting attributes. The impact of using the current Jaguar Land Rover single attribute optimisation approach to sample size and error estimation is assessed. After a number of improvements to the sampling and error estimation methods are made, an optimised airbox design is presented. The multi-physics analysis of the fuel tank investigates Fluid-Structure-Interaction (FSI) methods for the durability of fuel tank components. The multi-physics problem is outlined and the application of a number of FSI approaches is examined. The results from these projects are then used to build a set of recommendations for using MAO as a systems engineering tool and the implications of these discussed within the context of the Jaguar Land Rover design environment.

The design of automotive components and systems should utilise optimisation to deliver the best value product. The optimisation process must be able to encapsulate the multi-attribute nature of systems. This thesis examines the use of MAO methods within a systems engineering environment, to enable designers to improve product performance by exploration of the design space and reduce development times. The contribution of this thesis is in guiding the use of MAO methods as a systems engineering tool and in particular provides a new approach to scaling MAO projects, allowing the tool to be applied throughout the systems engineering process.

1.2 Research Aims & Objectives

The aim of this research is to investigate the challenges and key benefits of adopting a MAO method as a systems engineering tool to improve product development times and component design. The objectives to achieve this aim are:

1. To review the current knowledge and issues in automotive systems optimisation methods within a systems engineering approach. From this key research areas will be identified as the use of metamodeling to model attribute behaviour within the design space and the use of multi-physics CAE methods as an enabler within MAO. To investigate these areas, further objectives can be specified as:
2. To examine the role of optimisation within an automotive design environment allowing sub-projects to be scoped and bounded.
3. Investigate key enablers and methods required to implement MAO within an automotive design environment, including:
 - (a) Examine issues of sample size and distribution in the generation of metamodels and the estimation of the error in the model fit.
 - (b) Examine techniques and methods for attribute trade-off.
 - (c) Examine the benefits and costs of a multi-physics approach to CAE for use in an MAO architecture.
 - (d) Use an automotive case-study to understand the potential application of MAO methods.

1.3 Contribution to Knowledge

This thesis contributes to systems engineering by guiding the use of MAO for the optimisation of systems. This is intended to be for the use of system designers and CAE engineers working in a systems engineering environment. While this thesis focuses on the application of MAO within an automotive environment, the recommendations suggested for MAO implementation could be used in any design and optimisation process. Other contributions include the development of a method for predicting the capacity of an automotive airbox as well as improving the design by application of the MAO method. Finally, the assessment of a number of multi-physics methods highlights implementation issues within the software codes used.

This thesis takes a systems engineering approach to the implementation of MAO within the context of Jaguar Land Rover Powertrain CAE. This includes a system of systems viewpoint analysis to gather requirements for projects. This analysis is shown in Chapter 3 and was presented to the 2010 IEEE International Conference on System of Systems Engineering.

The key recommendations are focused on the sampling size and error estimation methods used within a metamodeling approach to MAO. These can be summarised as:

1. Based on application of an MAO method to the design of an airbox, scarce sampling is unsuitable for large generic metamodels.
2. To increase predictive accuracy, the number of samples taken to capture attribute behaviour must be increased.
3. However, the guidance from literature for the required sample sizes may be insufficient and lead to unsatisfactory metamodels.
4. This work proposes that the sample size guidance in the literature cannot capture the complexity of large design spaces and suggests the design variable range method as an alternative.

As a corollary to the findings on sample size required to build metamodels, the sample sizes required to evaluate their error was also investigated. The literature showed little consensus for the sample size and distribution that should be applied for metamodel error estimation and concerns were raised over the application of 'leave one out' errors. Key knowledge contributions in error estimation are:

1. That the estimation of true error requires a very large uniform sample which would prove impractical in an industrial setting.
2. The use of alternative 'leave one out' error estimation methods may be misleading.
3. This work suggests the use of both methods.

The metamodeling MAO method was applied to the design of an automotive airbox, this process included developing an empirical model to predict the capacity of the air filter. The model used capacity measurements obtained from physical tests of Jaguar Land Rover airboxes and correlated these values to the dimensions of the airbox and a prediction of the flow uniformity from a CFD model. The correlation equation provides a simpler method for prediction of the capacity when compared to other methods found within the literature. The application of the MAO method to the concept design of the Jaguar Land Rover XK airbox also yielded improved attribute performance as follows.

1. The pressure loss was reduced by 360 Pa, giving approximately 7 b.h.p. improvement in power output at full load.
2. A 25 gram improvement in the dust capacity of the airbox.
3. This improved breathing was also matched by a 23% improvement in the NVH characteristics over the concept baseline.

Recommendations and contributions to knowledge were also gained from the application of multi-physics CAE methods to a fuel tank as follows.

1. The multi-physics fluid structure interaction methods available in standard Jaguar Land Rover CAE codes was not applicable to fuel tank applications.

2. The StarCD CCM+ and Abaqus CAE direct couple approach was shown to be unstable due to the implicit time-step.
3. For the direct couple these results led to the vendor changing the recommended application of the method to air and solid coupling problems only and also to further development of explicit models of multi-fluid couples[19].
4. The element size and penalty methods in the Abaqus CEL (Combined Eulerian Lagrangian) method led to poor hydrostatic pressure and free surface predictions.
5. The CEL limitations were passed on to the vendor and software updates and new implementation advice and revised software were issued[20].

1.4 Structure of this Thesis

This thesis is divided into three parts. The first part contains a review of literature, research and the industrial context relevant to this thesis. Within this, Chapter 2 reviews the literature and research to give an overview of Systems Engineering and Systems optimisation methods. The review then focuses on the issues of using CAE based optimisation methods. Chapter 3 reviews the operation of optimisation methods within an automotive design process. This allows a series of research questions, caveats and constraints to be discussed. Using this as a starting point, the project areas for research in this thesis are defined.

The next part of the thesis contains the research completed on the airbox MAO problem and the multi-physics analysis of a fuel tank.

Chapter 4 defines the airbox problem and the approach taken to the sample size and error estimation dilemmas. The impact of this approach is examined in Chapter 5 where the airbox attribute metamodels are built and their accuracy assessed. The findings of this chapter are supported by additional experiments presented in appendix A. The metamodels generated are then used to examine methods of optimisation and attribute trade-off in Chapter 6. Supporting documentation for the airbox project is given in Appendix B.

Chapter 7 examines the multi-physics approach to the fuel tank analysis. This chapter includes a review of multi-physics approaches to fluid structure interaction in fuel tank simulations. In addition, the findings of applying a number of multi-physics approaches is detailed. Here, the cost and accuracy of the simulation are evaluated. This chapter is supported by a number of appendices:

- C A description of the fuel tank design stages.
- D Correlation of the StarCD free surface analysis method using a half scale rig test.
- E Exploration of the fuel slosh boundary condition.
- F Example scripts for StarCD and multi-physics models.

The final part of this thesis closes the work. Chapter 8 uses the findings from the airbox and fuel tank projects to build a set of recommendations for using MAO as a systems engineering tool. Chapter 9 draws the final conclusions and specifies areas for further research.

Part I

Systems and Optimisation in the Computer Aided Engineering Environment

Chapter 2

Literature Review

2.1 Introduction

The aim of this chapter is to review the current knowledge and issues in automotive systems optimisation within a systems engineering approach.

This chapter starts by defining systems engineering and examining the processes and tools that are utilised in such an approach. Within this, the optimisation of systems was shown to be a key part of the process. However, the optimisation of systems is complicated by multiple and conflicting requirements, the crossing of distinct engineering domains and issues of robustness. Here, the use of MAO can be used to overcome these complexities.

From this, the review then investigates how systems can be modelled and optimised with a focus on system component design optimisation within the automotive industry. CAE methods were seen to enable early problem solving and attribute modelling for physical components. The final part of the review focuses on investigating the methods used in CAE based optimisation. Here, the use of metamodeling is shown to be an efficient way to explore the design space. The issues connected with the metamodeling approach are then examined.

2.2 Systems Engineering

The automotive industry is an extremely competitive industry. Many vehicle manufacturers compete for sales in various global and vehicle role markets. Problems of overcapacity [1] and the recent reduction in sales due to the 'credit crunch', increased the financial pressures on vehicle manufacturers. In the US, year on year light vehicle sales dropped by 27% in September (2007 to 2008) [2]. These pressures have prompted the industry to reduce costs in all areas of business. The subsequent recovery in sales caused by expansion into emerging markets [3] and the drive for new and improved products [4] shows the change in pressures on automotive manufacturers. Products must be developed cheaper and more quickly, while also improving on previous models.

The automotive industry's interest in the Systems Engineering method is part of the natural

progression of design, development and manufacturing methods. While the standard production line process had been utilised for some time, limited resources in Japan have led to more efficient manufacturing methods being developed[21]. The success of the Toyota Production and Kanban System method led to the application of related methods across more of the company's activities[10]. The emphasis on early problem solving has been encapsulated into many automotive product development strategies such as concurrent engineering. The increasing complexity of vehicles means that there is a need to advance product development methods in order to meet future customer demands. Systems Engineering is seen as the next step[6][7].

2.2.1 What is Systems Engineering?

The Systems Engineering approach is summarised by the International Council on Systems Engineering (INCOSE) as:

'An interdisciplinary approach and means to enable the realization of successful systems. It focuses on defining customer needs and required functionality early in the development cycle, documenting requirements, then proceeding with design synthesis and system validation while considering the complete problem:

- Operations
- Performance
- Test
- Manufacturing
- Disposal
- Training & Support
- Cost & Schedule

Systems Engineering integrates all the disciplines and speciality groups into a team effort forming a structured development process that proceeds from concept to production to operation. Systems Engineering considers both the business and the technical needs of all customers with the goal of providing a quality product that meets the user needs.'

INCOSE[8] website: <http://www.incose.org/practice/whatissystemseng.aspx>

This definition shows that a 'systems' approach is required to ensure that the work completed by individual teams working on various aspects and features of a product conform to the overall system and customer requirements. However, this presents the systems engineer with a complex problem, as there may be many different and often conflicting requirements which may require the expertise of many engineers. In order to design systems, this complexity needs to be encapsulated. A Systems Engineering method can be considered a method which enables the practitioner to consider a system as a set of entities with discrete properties, capabilities and behaviours derived from the customer requirements. This method encapsulates the complexity as a function of discrete parts, allowing the problem to be solved[9]. A generalised Systems Engineering process centres

on solving customer problems to deliver a product or service which meets their requirements. Hitchins[9] (pg 199-200) gives the following sequence of activities which constitute this problem solving process:

1. Explore/bound the dynamic problem space.
2. Synthesise a dynamic solution.
3. Develop viable solution concepts.
4. Choose the optimum solution concept
5. Design the dynamic system solution.
6. Select, connect and configure parts to meet the design.
7. Test and tune the dynamic system solution in a representative dynamic problem space
8. Adjust/modify parts and interactions to realise/optmise properties, capabilities and behaviours of the whole.
9. Fit dynamic solution into dynamic problem space.
10. Resolve the dynamic problem.

When this list is considered with the INCOSE definition of Systems Engineering, a number of key points about what constitutes Systems Engineering can be generated. Firstly the structured nature of the list indicates that a Systems Engineering project requires a systematic approach that takes a holistic view of the problem and focuses on developing requirements and solutions[22]. This focus carries through all subsequent steps. Austin [6] describes this as a 'formal process' which manages the support, processes and deliverables of a project. Also, there is a focus on the optimisation of the system in order to best meet the customer requirements. Hitchins argues that balancing the properties, capabilities and behaviours of the whole system is core to the Systems Engineering process [9].

The next step in this chapter is to examine formal Systems Engineering processes that are used in the design of automotive systems. This will include the operation of the processes and the use of optimisation.

2.2.2 Systems Engineering Processes

Within the automotive Systems Engineering, two examples of formal Systems Engineering processes are the 'V-Model' [6][23][24] and the 'DCOV' approach[25][26]. The former is used as an approach to program design while the latter is used for smaller design based projects.

'V' Model Systems Engineering

One Systems Engineering approach is characterised by the 'V' model[6], shown in Figure 2-1 (derived from Austin[6]). The initial stages on the left hand side concern the analysis, development and allocation of the customer requirements. This can be seen as a cascade of requirements in a top-down process. Top level requirements are gathered, then translated and cascaded down as system requirements, then further down to sub-system requirements and verification plans are created at each level. Design and optimisation occurs at the bottom of the Systems Engineering 'V', where the customer requirements are transformed into product features. In the final stages, the design is integrated and verified. This is completed by a bottom-up process. The verification plans created in the requirements stages are used to ensure the product conforms to customer requirements. This process is one of the most widely used Systems Engineering models used[6], as there is a strong focus on customer requirements. The 'V' process is at the core of a number of automotive program design strategies, such as the Ford product development systems for whole program management [23] and the BMW Systems Engineering process [24]. However, as this process is intended to be used as a whole program approach, the optimisation stage is not detailed. For this, the 'DCOV' method for individual design projects can be used.

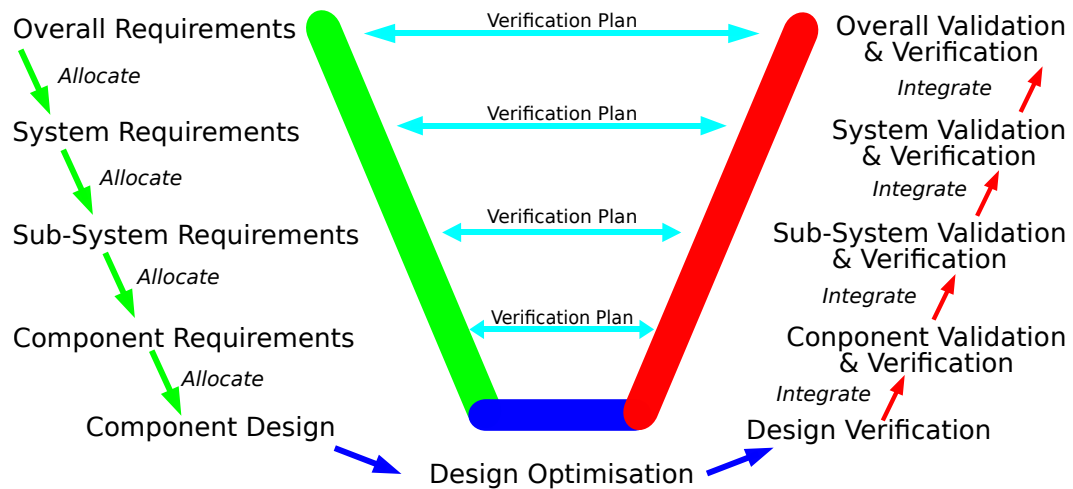


Figure 2-1: The Systems Engineering 'V' model

6-Sigma Methodologies & The 'DCOV' Process for Projects

6-Sigma is a culmination of a number of design and engineering philosophies (Statistical Process Control, Total Quality Management, Lean Engineering, etc.) and utilises the strengths of each[25]. Stamatis[25] and Perreira & Andreassa [27] working at Ford describes two applications of the 6-Sigma approach, both aimed at improving system design reliability. The first is to solve problems of process variability in product manufacturing and the second is as a preventative measure to avoid variability in the design. The second of these is called Design for Six Sigma (DFSS) and in Ford

applications, employs a ‘DCOV’ (Define, Characterise, Optimise and Verify) method to product design[26]. The application of this method allows for greater upfront engineering whereas the traditional DMAIC (Design, Measure, Analyse, Implement and Control) model is used predominantly in manufacturing.

The ‘DCOV’ Process can be summarised as follows;

- *Define*: gather and understand the customer requirements, translate these into “Critical To Satisfaction” (CTS) and functional targets.
- *Characterise*: Here the CTSs are cascaded down and translated to “Critical To Quality” (CTQ) design parameters, these should be used to understand the system and select the concept designs.
- *Optimise*: The design should be optimised to best meet the CTQs and CTSs with an emphasis on product sensitivity.
- *Verify*: Assess the system performance against functional targets.

This method features both a strong connection to the customer requirements and an optimisation phase. It is used by Ford and associated partners within its product development cycle for design projects[27]. To complete the ‘DCOV’ stages, various tools are used, some of which have been demonstrated in the Systems Engineering application examples. Typical tools used in DCOV are shown in Table 2.1 [26]. Specific tools are used at certain times to ensure that each stage is completed effectively and remains focused on the customer requirements. Tools are used to help model requirements and system behaviours to enable the designer to make decisions.

Table 2.1: Tools commonly used in DCOV methods [25][26].

Define	Characterise	Optimise	Verify
Consumer Insight	Concept Generation, Modelling and Selection	Numeric/Heuristic Optimisation	Model Validation
Kano Model	Designed Experiments	Designed Experiments	Test Results
QFD	P Diagrams	CAE Methods	Robustness and Reliability
Market Research	System Functional Diagrams	Taguchi Methods, Parameter & Tolerance Design	Control Plans
Historical Data Benchmarking	Parameter & Tolerance Axiomatic Design		Control Planning

2.2.3 Case studies of the Application of Systems Engineering to Automotive Design Problems

There are many cases in literature where the application of Systems Engineering has enabled more customer-focused design in automotive applications. In these examples the use of the Systems Engineering analysis and tools are highlighted, together with the benefits for the design

When optimising the light-up emissions of a catalytic converter system, the designers were faced with a number of different customer groups, each of which needed to be satisfied. The major groups were the overall vehicle customers and the legislation on emission standards[28]. The requirements for a catalytic converter design were obtained from the customer and the legislation. The requirements for the design were then analysed using a Systems Engineering P-Diagram. When using this tool, the key inputs, control factors and noise factors are all identified along with the ideal function and error states of the system. By analysing the system operation and interfaces with surrounding systems, the P-Diagram allowed the interactions and behaviours of the system to be understood. The knowledge of the system was then used to focus the physical testing and Design of Experiments (DoE) optimisation tool (see section 2.5.2) to specific problem areas. The benefit of this approach was that the new design met the stringent emissions standard with fewer physical tests conducted.

In the design of Occupant Protection Systems (OPS) at Delphi[29], the need for Systems Engineering was driven by the increasing complexity within the system. A Systems Engineering approach was used to capture the requirements for an OPS in various different crash modes. This allowed the critical and conflicting requirements to be identified and appropriate concept designs to be proposed. From the key requirements, the most important system input variables were identified along with the correct boundary conditions. Again, focusing on the key requirements allowed the number of CAE analyses to be reduced to a few specific cases. This example also demonstrated the use of DoE methods as an optimisation tool to understand how the inputs to the system affect the performance. In this example, the application of Systems Engineering enabled a customer-focused product to be developed due to the preliminary work completed gathering the requirements and understanding the system.

Ford applied a 'top-down' approach to vehicle chassis design[30]. The problem featured many part-to-part interactions of the suspension components as well as non-linear interactions between the tyre and the road. This Systems Engineering method allowed the decomposition of this problem into a number of sub-system analyses, but due to the use of Systems Engineering tools, the requirements and interactions were captured at a high level and cascaded down. The top-down approach allowed the engineer to investigate the requirements and the interactions. This allowed assessment of the system as a whole rather than as individual components. A number of systems modelling tools based on CAE approaches were then used to examine the effects of design changes on component parts and the part-to-part interaction. The use of this approach was said to reduce the development time whilst improving the simulation accuracy.

A systems approach was taken to the design and development of an air intake system at Mahindra & Mahindra[31]. This approach took a holistic view of the air intake system in order

to derive customer requirements and develop a system design specification. The targets from this specification were then cascaded down to individual components and the design requirements developed. The approach featured the use of a number of tools to understand and optimise the system. To provide the optimum design, the air intake system was modelled with the CFD (Computational Flow Dynamics) software Fluent to allow the flow through the system to be visualised. This visualisation allowed the engineer to identify regions of poor airflow and then eliminate them. The quality of the design was developed using a 'Failure Modes and Effects Analysis' (FMEA) tool to focus on high risk areas of the design and reduce the amount of failures. The use of these tools allowed the requirements for the system to be met and improved upon. For example, the CFD optimisation reduced the pressure drop by 18% and improved fuel economy by 1% over the baseline.

These four examples have shown that a Systems Engineering focus on customer requirements has enabled improved design. The Systems Engineering process was required to cope with the increasing complexity of the systems being designed, be it multiple customers with varying requirements or high levels of interaction between parts and surrounding systems. The Systems Engineering approach enabled the complexity that these issues presented to be captured then simplified, allowing the design work to be focused on specific issues. Within the Systems Engineering process, tools were used to help the engineer understand the requirements or the behaviours and interactions within the systems. Optimisation tools such as DoE and systems modelling were shown to be important in delivering best value systems to the customer. Improving optimisation tools for a Systems Engineering approach would be of benefit in enabling further improvements in the design of systems.

The Systems engineering methods utilised in the casestudies presented in this section were a response to increasing complexity of the product being designed. As systems become larger and involve a greater degree of communication and interaction with other surrounding systems, the design problem becomes increasingly difficult. To analyse such problems, 'System of Systems' engineering methods have been proposed[32]. These methods allow for greater uncertainty in operational behaviour that requires a highly complex and dynamic design space. In such problems the objective of design may no longer be to optimise, rather to satisfy and sustain required system behaviour[33]. The optimisation of a system in an uncertain, highly complex and dynamic design space can be characterised as a 'WICKED' problem as defined by Rittel and Webber[34]. 'WICKED' problems are those which lack a definitive problem formulation and are unique. They also have multiple solutions which are difficult to measure, compare and validate, requiring a 'one shot' solution that does not allow an opportunity to use trial and error[35]. As the scope of an optimisation problem is increased, such characteristics may need to be considered.

2.3 Optimisation

Hitchins describes optimisation as a core element of the Systems Engineering process[9]. This section introduces optimisation and will discuss how this can be used to obtain best value systems. The complexities of optimisation of systems are discussed in section 2.4, followed by a discussion of the approaches to system design optimisation in section 2.5.

2.3.1 Definition of Optimisation

There are two definitions of optimisation:

1. The mathematical process of finding the maxima or minima of a specified function[36].
2. The action or process of making the best of something; (also) the action or process of rendering optimal; the state or condition of being optimal[37]. With optimum being the best or most favourable point, degree, amount, etc. The greatest degree or best result obtained or obtainable under specific conditions[37].

While the mathematical definition implies a hard and fast point, the second definition suggests a more generalised concept. From the systems approach above Hitchins argues that an optimal system is one where the performance, capabilities and behaviours of one system configuration are of greater value than others[9]. This concept of value is a central idea in decision theory [16], and provides some form of measure that will allow designs to be compared. Capturing what is of value to the customer is a vital part of gathering requirements.

2.3.2 Classical Optimisation

In a classical optimisation problem, algebraic equations are used to model the system so that the output is a function of the inputs, common terms used are listed below [38].

- *Design Variables:* Design variables are the inputs into the design optimisation problem that are used to characterise the range of the design space. These can be continuous or discrete with ranges defined by the side constraints.
- *Design Parameters:* Design parameters, or dependent design variables, are non-variable inputs to the optimisation problem.
- *Design Space:* The design space of a system is defined by the upper and lower limits of all the design variables. For n design variables the space is n -dimensional and represents the area that will be searched for the optimal value.
- *Design & Objective Functions:* The design/objective function is the model of the behaviour of the system given a set of inputs. It is this model that is to be optimised.

- *Constraints*: A system is subject to constraints that also need be taken into account in the solution of the optimisation problem. A design space limited by constraints is called a feasible domain or set. Three types of constraints exist; side, equality and inequality.
 - *Side*: Defines the range of the design space.
 - *Equality*: Behaviour or performance that must be met and defines a value of feasibility.
 - *Inequality*: Behaviour or performance that defines a region of feasibility.

2.3.3 Solution Methods

The solution to the optimisation problem is to find the point of maximum value (be it maximisation or minimisation). Andersson[16] notes that there are two methods of solving optimisation problems; derivative methods and non-derivative methods (or meta-heuristic methods). Derivative methods follow point paths using gradients to find the next point that would give an improved objective function. The iteration continues until the objective function can no longer be improved. For a given objective function, there may be numerous local optimum points but only one global optimum (the point best value in the feasible domain). This can lead to the optimisation process being trapped at a local optimal point but not the global point. Meta-heuristic or non-derivative methods were developed to overcome this issue and are more efficient than the application of derivative methods[39]. Examples of Meta Heuristic methods are simulated annealing and genetic algorithms.

Simulated annealing mathematically replicates the heating then cooling of materials to organise the internal structure. After starting with an initial design, a small population of local designs is generated and the changes in the objective function measured. Where new samples exceed the initial sample, they are accepted and the process repeats. If the sample is worse, acceptance is judged using a Boltzman probability function. Initially the probability of accepting degradation is high. As the sequence iterates, this probability is reduced in a pseudo cooling effect. The process is continued until the probability drops to a minimum level [39].

In genetic algorithms, the design variables are imagined to be genes and the system performance the output of this combination. From an initial population, the outputs are measured and the best performing genes are selected for mating. In a mating sequence, the genes are swapped over to produce the next generation. The children are then measured and compared as the process iterates. The progression of the algorithm continues until either the genes converge to a single set of parameters or a given number of generations occurs [39].

These two examples are just some of the meta-heuristic methods suggested, for further information texts such as Collette and Siarry [39] detail other methods and formulations. Extensions of these solution methods to other optimisation problems such as multiple objectives are also discussed. Many of the commercially available optimisation software codes feature a variety of standard optimisation strategies and formulations [40][41]. Application of these enables non experts in optimisation algorithms to apply advanced optimisation techniques.

2.4 Optimisation of Systems

The discussion of optimisation has included the basics of optimisation theory. However, the application of optimisation to a system poses different challenges, which will be considered in this section.

2.4.1 Multiple and Conflicting Objectives

In the design of systems, it is common to have to optimise for more than one objective, for example minimising the deflection of a structure as well as minimising the weight. Not only does this problem have two objectives but they are opposed to each other. This has the potential to lead to multiple solutions being found, of which only a small subset will be of interest to the designer. The solutions will show how the different objectives are related and in particular the dominance of a solution[39]. The dominance of a particular solution can be defined by the solution being as good as other solutions in most attributes but largely better for a single attribute. Solutions which are dominated by other solutions are of little interest to the designer. Pareto optimal (or non-dominated) solutions can be defined as solutions which are dominant over others but are not themselves dominated. A set of non-dominated solutions is called the Pareto frontier. The possible Pareto frontiers for a double objective optimisation are shown in Figure 2-2. A utopian point can be defined as the solution which satisfies each objective simultaneously. This is also indicated in Figure 2-2.

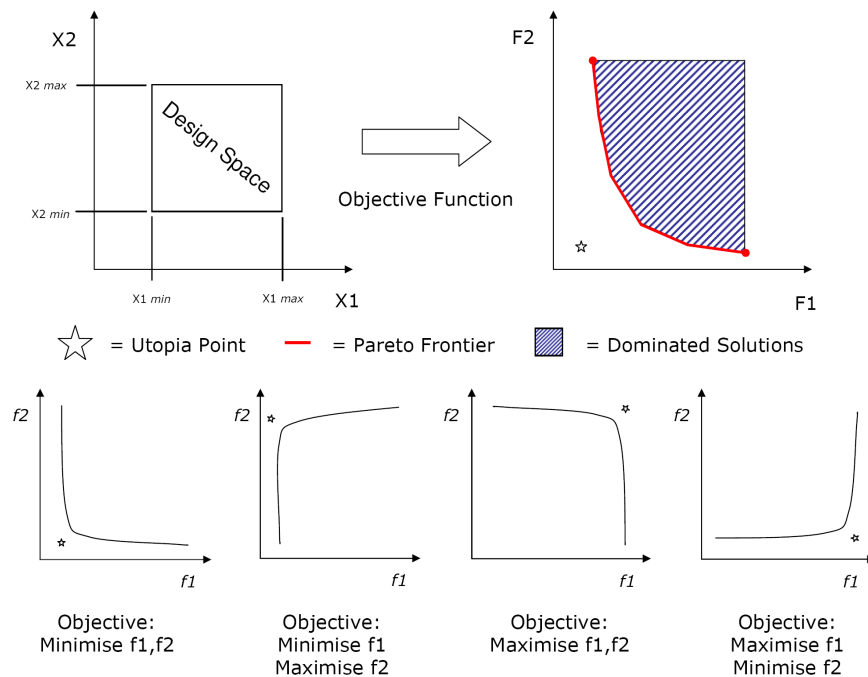


Figure 2-2: Pareto-Sets and Optimisation Objectives

2.4.2 Optimisation of Multiple Domains & Disciplines

The INCOSE definition of Systems Engineering stated that it is “an interdisciplinary approach and means to enable the realization of successful systems” [8]. This means that the optimisation of a system must be able to cover multiple engineering disciplines. In the optimisation of a maniverter for a Fiat gasoline engine [5], the cost of the design was estimated along with a number of engineering attributes. This required a number of different domain analyses to be built using the advice from a number of domain experts. This made the building of the optimisation project a team process. Multidisciplinary projects are inherently a team activity [42] and the optimisation of a design is no longer dependent solely on the optimisation processes but also the on the teamwork within the process. This human factor adds to the complexity of optimisation projects that cover multiple disciplines [43] as not only must the technical aspects of the process be addressed, but so too must enabling effective team working [44] and communication [45].

2.4.3 Robustness

The optimisation of a system will yield a set of design parameters to which the system will be built. However, these input parameters will be subject to variation, either in the manufacturing of the system or noise within the operational environment. If a design is centred on the optimal performance point, then design parameter variability will move the system away from this position. Steep response behaviour could lead to large changes in system performance (Point A Figure-2-3). However, more stable system response behaviours will only lead to small system performance variability (Point B Figure-2-3). The assessment of the robustness requires the examination of the attribute behaviour in the local design space so the stability can be assessed, this requirement increases the complexity of systems optimisation [46].

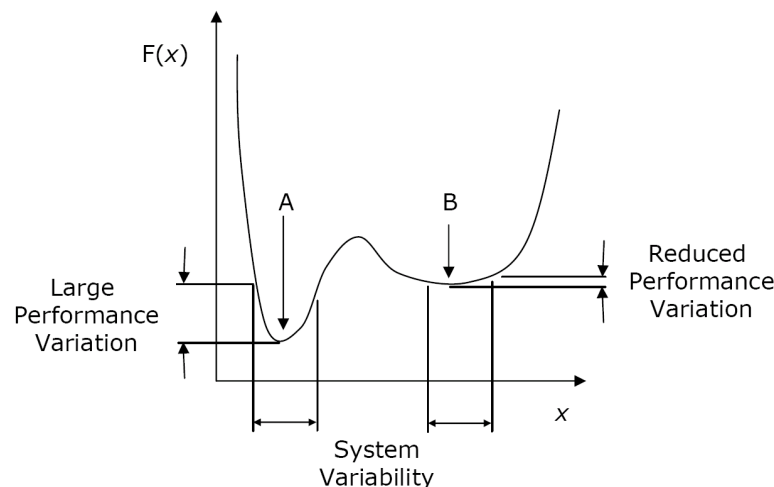


Figure 2-3: Global Optimum Performance Variation and Robust Optimum Point.

2.5 Approaches to Systems Optimisation

The previous section highlighted the complexities of systems optimisation. In this section some of the tools and methods used for optimisation will be reviewed and the case for using MAO established. The literature has shown a number of approaches for the optimisation of systems, these are:

1. Systems Modelling & Problem Solving
2. DoE Methods
3. Single Attribute Optimisation
4. Multi-Disciplinary Design Optimisation
5. Multi-Attribute Optimisation

Each of these will now be examined for their applicability to systems optimisation.

2.5.1 Systems Modelling & Problem Solving

Under the list of optimisation tools in the Ford 'DCOV' process, CAE systems modelling is cited as one of the potential methods for optimisation [25][26]. An example of this was shown in the Systems Engineering case-study of the airbox presented in section 2.2.3. This used a CFD systems model to visualise the airflow and allow problems to be identified[31], which could then be solved by the engineer. While these methods allow the engineer to investigate the behaviour of a design, the CFD system model used is for one set of design parameters. This means that the potential design space is not fully explored and it is unknown whether it is the best value design. Systems optimisation requires exploration of the design space[9].

2.5.2 Design of Experiment (DoE) Methods

The DoE method is also an approach used in the Ford 'DCOV' processes[25][26]. This method proposed by R.A. Fisher [47] uses a number of experiments to explore the potential design space. The number of experiments required for the method is determined by the number of inputs and levels. Statistical analyses such as Analysis of Variants (ANOVA) can then be used to find the effect and interactions of the input parameters on the system behaviour [48]. Knowing which input parameters and interactions yield an improved system performance, the designer can exploit the relationships to maximise the beneficial effects. However, the use of ANOVA, methods may be limited requiring a different approach to the analysis of DoE data. Examples of the DoE method include the optimisation of the light-up emissions of a catalytic converter system and the design of an occupant protection system used in section 2.2.3. In these examples, a mathematical model was fitted to the data collected from the experiment to create a response surface [28][29]. This response surface (or metamodel) can then be used to predict the system behaviour in untested regions of

the design space. The DoE approach has also been extended by both advanced metamodeling and sampling techniques such as Monte Carlo Methods to consider robust optimisation. This allows parameter and tolerance design to be examined to meet quality targets[49]. This advanced sampling and response surface (or metamodeling) method forms the basis for some approaches in advanced optimisation (Single Attribute, Multi-Disciplinary Design and Multi-Attribute Optimisation) and is fully described in section 2.6.

2.5.3 Single Attribute Optimisation

Single Attribute Optimisation (SAO) is used to find the best value design for a system that is characterised by a single output behaviour. In many systems, this optimisation approach may not reflect the true nature of the design as there will not be just a single output behaviour. However, if there is one dominant attribute of the system, or all of the attributes can be amalgamated into a single value metric then this approach can be used. SAO has been applied to the crash structures of automotive vehicles at Ford[50] and Hyundai[51]. In both cases, the objective was to minimise the weight of a number of key components of the crash structures. However, the optimisation was constrained to ensure that the new crash structures still provided an expected level of safety. While both projects achieved some reduction in weight, there was a reduction in the safety performance of the new designs. For the Ford case the weight of the crash component was reduced by 15.6kg, but the roof crush resistance was reduced from 34.7kN to 31.3kN [50]. In the Hyundai case a 7.4kg saving came at the expense of increased head injury criterion and chest acceleration in a high speed crash[51]. While these vehicles still met the expected level of safety, these results raised an important issue of trade-off; how much safety is the engineer willing to trade-off against weight gain? In the SAO taken here, this trade-off is not considered.

While a single attribute optimisation approach may be used in simple cases, its application to the optimisation of systems may not provide the best value design for the system as a whole. Hitchins argues that an optimal system is '*comprised of sub-optimal parts*' [9] (page 197), meaning there may need to be some trade-off to provide the best design. A Systems Engineering tool must be capable of allowing the engineer to explore and exploit the trade-offs within a system.

2.5.4 Multi-Disciplinary Design Optimisation

Multi-disciplinary Design Optimisation (MDO) is an approach to problems that cross the traditional domains in engineering. These have been extensively studied by NASA and other Aerospace engineering companies[42]. Here, the separate domains of aerodynamics and structural mechanics have been combined in a single optimisation project. The MDO approach must consider both the technical and human aspects of completing such projects[43].

In a review of MDO, a number of technical frameworks have been created [52][53] that control the optimisation process and the flow of data. To make the project more manageable, it must be decomposed into domain specific analyses. This is driven by the need to distribute tasks between resources, allowing the design time to be compressed[43]. However, this decomposition

and distribution can lead to disciplines becoming isolated. This is where the optimisation framework is used, coordinating the flow of data to the various domains. Details of these frameworks can be found in works by Sobieski[52][53].

The communication of data in an MDO approach may be complicated when the analysis requires the interaction between domains to be evaluated. For example, where the fluid and structure interact[54]. The fluid flow around the wing is resolved to find the pressure distribution as well as the lift and drag coefficients. From this, the deflection and stresses in the wing structure can be calculated. This requires that the output from one domain is applied as a boundary condition in a 'coupled' approach. The coupling of analysis disciplines in the automotive sector has enabled MDO methods to be applied at the system level[18]. The application of such methods has been seen in the minimisation of weight of key components of a crash structure whilst considering crashworthiness, durability or NVH attributes as constraints on the design [50][51].

To enable such projects, the coordination and communication between teams working in the different domains must be facilitated. As cultural and organisational issues may prevent full integration of the domains[18], traditional aspects of team working and communication should enable the process. For enabling effective team work Waszak *et al*[44] found that clarity of mission, quality of communication among team members, involvement of key experts, experience, willingness to be a team player, team processes, balancing of technologies and high leverage interventions were important to MDO projects[44]. In many projects, the different domain teams will not be co-located, so communication must be mediated by means other than face-to-face conversation. Here, the technological aspects, particularly with regards to communication, are a major area of computer science research such as Computer Supportive Co-operative Work (CSCW) [45].

This section has shown that the MDO approach can address the multi-disciplinary nature of Systems Engineering projects. However, these projects have mainly focused on single attribute problems. The next step for MDO methods is to consider cases that have multiple objectives or attributes[18][43].

2.5.5 Multi-Attribute Optimisation

Multi Attribute Optimisation is a method that addresses the varying number of conflicting requirements that are present in the design of systems. This approach finds the best value system by trading-off attributes against each other, meaning that the design may have sub-optimal performance for one or more attributes to gain performance in other areas[9]. The solution of MAO problems requires that the design space be explored to find the Pareto set of solutions[16][39]. For this, algorithms such as the Multi Objective Genetic Algorithm (MOGA-II) and the Non-Dominated Sorting Genetic Algorithm (NSGA-II) can be used [41]. These algorithms automatically explore the design space and find the Pareto Frontier. The selection of the final design can be completed using methods which enable the designer to use their preferences or by utilising a visual means to display and sort the Pareto solutions.

Decision Analysis Methods

The selection of design is based on the designer specifying a preference for certain solutions over others. These choices will be based upon the overall requirements of the system and many of the techniques employed are based on decision analysis and decision theory[16]. Techniques such as Design Utility[55] and Figure of Merit [56] are methods of multi-objective decision making that use mathematical modelling and functional relationships to weight the objective functions. These methods base the decisions on the system requirements given by users.

With Utility methods, a function is generated that ranks the performance within the possible range. A common approach is to use linear or exponential functions so that the worst utility attains a value of zero and the highest utility a value of one [16]. However, other arbitrary functions within the range may be utilised in order to tune the function to the particular needs of the system. To reduce complexity, the utilities for multiple objectives are normally aggregated by weighted additive or multiplicative functions to produce a single objective function. The utility functions and weightings should all be derived from the customer requirements [56].

The application of designer preferences can occur before, during or after the optimisation process; *priori*, *progressive* and *posteriori* methods respectively [16][39]. In these methods the objectives are weighted against each other, enabling the optimiser to distinguish which objectives it is most important to satisfy. Details of the methodologies used in each of these instances can be found in a review by Andersson[16].

- In a *priori* optimisation cycle, weighted objective functions are used within the optimisation process to balance which attributes are most prevalent within the design. These types of methods can be called aggregated as the weighted objectives transform the multi-objective problem into a single-objective optimisation[39].
- *Progressive* methods stop during the analysis and request decisions from the designer. This method is used when the *priori* preferences are not available and the designer uses the information given about the current solution set to make the design selection. These methods can be slow due to the interaction needed between designer and process [16][39].
- *Posteriori* methods do not require the designer to limit the possible solution set before or during the optimisation process[39]. All Pareto optimal solutions within the design space are found and presented independently of the designer's initial preferences [16]. Due to this, these methods are associated with high computational costs, however they are the most flexible and allow for greater exploration of the design space.

While the application of these methods may provide a single optimised result, it may not represent the best trade-off between attributes. The methods of setting the weights and preferences must be carefully considered. Such methods may be required to enable final design selection when presented with a large Pareto set and should be considered when using MAO methods.

Visualisation Methodologies

With increasing numbers of system objectives, there is an increasing amount of data which needs to be viewed. How to present the data in such a way as to best enable the designer is a complex problem. This issue has roots in the computer science domain of data mining[57]. The visualisation of data is a key enabler for successful data mining. However, as the number of dimensions increases it becomes increasingly complex to display the required data. There are numerous methods to plot one, two and even three dimensional data, but more dimensions require increased sophistication[57].

When using the iSight software for the multi-objective optimisation of an automotive maniverter, it was found that the use of glyphs and other built in methods were not intuitive enough to be used[5]. To increase the visual impact and intuitiveness of the data mining, a new '*Rainbow Plot*' was created. This used coloured contours to rank the objectives from minimum to maximum. The 'Rainbows' for each objective were laid next to each other, enabling easier selection of design.

Another method of visualising highly dimensional data is the parallel coordinates plot [58]. In these plots, each input and output parameter is assigned a vertical axis and each potential design is represented by a line crossing each of the axes at its respective value. Slider bars on the axes allow the design space to be reduced to guide the designer to the optimum design. Even with slider bars and more advanced selection techniques such as brushing [59], increasing the number of samples increases the difficulty for the user to see trends within the data and make the final design selection.

Self Organising Maps (SOM) have the potential to overcome the complexity of large potential design sets in highly dimensional optimisation. These maps are a neural network trained with learning algorithms that allow the data to be visualised on a hexagonal grid [60]. These algorithms cluster designs of similar performance, allowing the whole data set to be seen in groups. The application of this method was found to be most effective when applied to the Pareto data in the optimisation of supersonic wing and fuselage design [61].

The multi-dimensional plots discussed here enable the visualisation and exploration of the design and trade-off space. This provides an opportunity for the designer to learn and understand the effects and interactions that the input parameters have on the system. Such methods are essential for using MAO as a Systems Engineering tool. Many of these methods are included in commercially available optimisation software such as modeFRONTIER [41].

2.5.6 System Modelling

All of the approaches to systems optimisation have been based upon the use of systems modelling to provide data to the optimiser. In the simplest sense, a model takes the system inputs and boundary conditions, simulates the functionality and predicts the behaviour of the proposed configuration. This could be as simple as a flow diagram, as long as it allows for system to system comparison. In the automotive industry, two methods for predicting system behaviour are physical prototypes, as shown in the catalytic converter[28] case study and CAE models as shown in the occupant protection system[29] and the airbox optimisation[31].

Physical prototyping involves the creation of components that represent the system and demonstrate some of its functionality. There are many techniques for the rapid manufacture of components that can show some of the behaviours of the system. However, in the concept design stage, this represents a substantial investment in both time and engineering effort. The application of CAE methods allowed BMW to run a total of 91 crash simulations in the design development process, the results of which gave a 30% increase in side impact crashworthiness [10]. For physical experiments, the number of prototypes needed to gain this level of detail would have proved costly in terms of both time and resources. The increasing proliferation of computers within the industry has led a movement to replace physical prototyping with CAE in early design stages[10].

The use of CAE has not only helped to reduce costs and development times, it has also changed the design process itself. In a 2007 interview for AEI[62], John L. Givens, Director for Engineering Math Processes at GM Powertrain, addressed the changes brought about by math-based analysis. In previous experiment-based methods, the CAE analyst was mainly used for forensic purposes. Only once a part had failed would the analysis methods be used. However, CAE allows the behaviour of systems and components to be partially predicted, allowing simulation to be used before failure occurs[62]. But the changes were not limited to when simulation was used; the inclusion of CAE required both organisational and process changes. CAE was moved from a supporting role to a mainstream position within the product development process, allowing for greater use of virtual prototyping. In some cases, this method of proof is now robust enough to be sufficient as a sign off method, allowing physical testing resources to be utilised more effectively[62]. This is confirmed by the use of CAE in powertrain analysis at Jaguar Land Rover [63]. Here, the CAE teams provide a number of different types of analyses in order to meet the requirements of the system design teams. These can be summarised as[63]:

- *Problem Solving:* This type of analysis is used when there is an issue with design or an unexplained failure. The CAE can be used to gain further insight into the root cause of the issue so the failure mode can be removed.
- *Change Analysis:* A change analysis occurs when the CAD designer has to change the design and the new component needs to be verified, this is usually due to a manufacturing or process issue.
- *Measurement Support:* A measurement support methodology is used to gain insight into the operation of a component when physical tests cannot give the required detail.
- *Design Optimisation:* Optimisation involves exploration of the design space to enable the optimal design to be found.
- *Design Verification:* Design verification analyses allow the designs to be signed off via a virtual analysis.

Figure 2-4 shows the change in analysis methods used since CAE methods were introduced to Jaguar Land Rover[63]. Increasing confidence in CAE technologies has resulted in a shift from issue-based analyses to an increasing amount of design optimisation and verification.

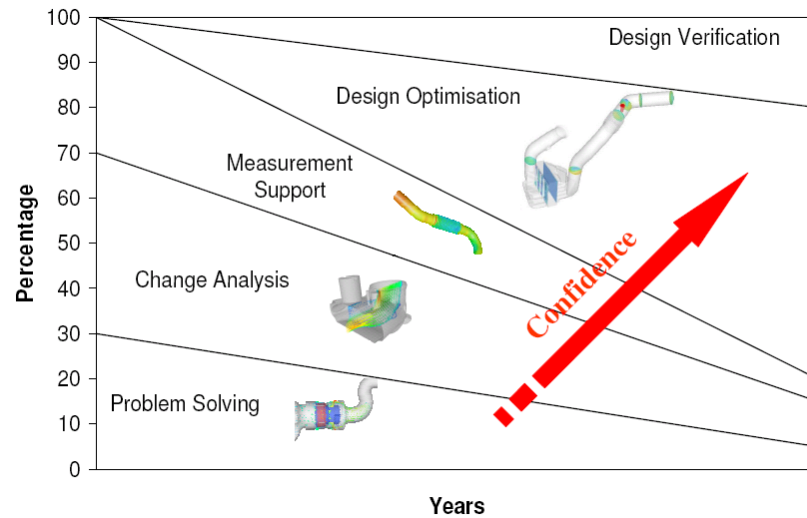


Figure 2-4: CAE methods within Jaguar Land Rover powertrain CAE. Diagram from Pierson[63]

2.5.7 Summary

The review of Systems Engineering processes showed that the optimisation of systems was a core part of delivering high value products. The previous section described optimisation as a mathematical method that can be applied to select input parameters that yield the best value output. However, this approach was complicated when applied to systems due to multiple and often conflicting objectives, multiple domain considerations and robustness.

For the optimisation of systems, a single system model is insufficient to explore the design space and SAO methods do not consider the multi-attribute nature of systems. DoE methods based on ANOVA may explore the design space and interaction. However, the limitations of such approaches have resulted in advanced DoE methods which can be utilised to explore the design space, model the system behaviour and analyse the system robustness. These approaches can be used in SAO, MDO and MAO. While the MDO approach considers the multi-disciplinary nature of systems, these methods have been used mainly for single attribute optimisation. However, moving to a multi-attribute approach was seen as the next step. MAO methods that model different disciplines and explore the design space (globally for optimisation, locally for robustness) can be used as a systems optimisation tool.

The MAO approach was shown to be a method that can encapsulate the system optimisation complexities. However there are issues over how the data from such methods can be used in attribute trade-offs. Finally, it was noted that the systems optimisation techniques were all built on systems modelling methods for attribute prediction. CAE methods were highlighted for their ability to provide accurate attribute predictions early in the design process. From this, MAO enabled by CAE methods is suggested as an automotive systems optimisation tool. However, the use of CAE based optimisation problems requires further investigation.

2.6 CAE Based Optimisation Problems

This review has previously discussed the modelling of automotive systems using CAE techniques as an enabler in an optimisation process (DoE, SAO, MDO or MAO). These models use the design geometry and boundary conditions to predict attribute behaviour. When these CAE methods are used in the optimisation of design problems there are a number of key issues[64]:

- The design problem features many input parameters and output objectives (H - High dimensionality).
- The designs are evaluated by computationally expensive and potentially multiple simulation programs (E - Expensive).
- The system behaviour within the design space is unknown (B - Black-box)

The issues surrounding such HEB problems will be explored in this section. Firstly the methods used to reduce complexity, computational time and engineering hours will be discussed, then the application of metamodelling is examined.

2.6.1 Reducing Problem Complexity

In a review of strategies to tackle high dimensionality and complexity in HEB problems, Shan and Wang summarised the five different methods that have been applied. These are decomposition, screening, mapping, space reduction and visualisation [64].

1. *Decomposition*: In order to reduce the complexity of a large scale problem, analysis can be reformulated into a number of smaller, more manageable problems. These problems could be independent or coupled but these are simpler and more efficient to complete. This is a common approach in MDO [53] which can provide methods to maintain the required coupling between analyses.
2. *Screening*: Screening of the optimisation problem removes parameters which are less important or sources of noise within the design space. ANOVA methods on small samples are useful in understanding the main effects and interactions of the design variables. This can reduce the dimensionality of the problem. However, the accuracy may suffer as a consequence. The application of this may be limited in multi-attribute problems due to differential powers of parameters and interaction in each behaviour of individual attributes.
3. *Mapping*: There are two methods of mapping; firstly to reduce dimensionality by removing correlated variables and attributes and secondly the space mapping method. With this, coarse and fine attribute maps are generated for the same design space. The coarse map is based on a simpler and less expensive CAE model and the fine map is a local map generated with more expensive, accurate methods. The two maps can then be used in conjunction with the predictions from the coarse map being adjusted by the fine map in the local regions. These methods have limited applications to highly dimensional models.

4. *Space Reduction*: The design space is the region encapsulated by the ranges of the input parameters. Reducing these ranges decreases the amount of potential samples and the effort required to gather data points. However, this reduction may come at the cost of removing potential regions of interest and may be difficult in multi-objective cases where the optimums are in separate regions of the design space.
5. *Visualisation*: The need for visualisation methods for highly dimensional problems has already been discussed. It is seen as a key enabler in understanding the design space and enabling informed choices about the complexity reduction methods mentioned here or design selection.

2.6.2 Reducing Computational Time

High numbers of variables increase the complexity and require more samples to be taken, resulting in high computational expense. High fidelity models such as finite elements and CFD are used by CAE for accurate simulations during the design process. However, such models come with high computational cost[65]. The literature shows a number of methods employed in an attempt to address this issue.

In order to reduce computational effort, approximate models could be used, replacing more costly system models[65]. In the optimisation problem of the High Speed Civil Transport wing, a full factorial design resulted in 59049 experiments[66]. Using a low fidelity model, each of these experiments was completed in 2-3, seconds giving a total runtime of approximately fifty hours. For the same wing problem, a medium fidelity model runs in 1.5-2 minutes. This could not be completed for the full factorial design, as the computational expense would be substantial. Instead, the low fidelity model was used to screen the possible data sets to reduce the design space.

However, the use of fast analysis models can affect the accuracy of the optimisation result. The maniverter optimisation tool used a laptop with an Intel Pentium 4 processor[5]. This severely limited the CAE models that could be used in the optimisation. In order to have a faster analysis time, key analyses for the maniverter had to be neglected or the accuracy compromised. The fluid flow analysis over the catalyst was deemed too computationally expensive and the elements used in the frequency analysis were unsuitable.

The previous applications have been methodologies where total runtime has been reduced through reducing the number of experiments or by using lower fidelity models. The use of High Performance Computing (HPC) offers another approach[50]. The minimisation of the weight of a vehicle was conducted using a 512 CPU SGI Origin super computer. This allowed not only for the individual CAE runs to be executed on multiple cpus (4 processors per simulation), but for many simulations to be completed simultaneously. If this were to be completed on a single CPU then the total runtime would be estimated to be 22,500 hours, whereas the actual time taken using HPC was 70 hours.

2.6.3 Reducing Engineering Hours

The requirement for solution points requires the simulation to be run with many different sets of input variables, this requires many models to be set up. This requirement has led to models becoming parameterised, where key features of the system model have constraints which can be modified. In the optimisation of a maniverter there were 46 geometrical variables that could be changed within the optimisation[5]. To complete the geometry by hand for each optimisation iteration would consume a large amount of time and render the process unusable. To avoid this, a CAD package that featured model parameterisation was used.

This reduction of manual input to the CAD can be applied across the rest of the CAE and optimisation process. The optimisation of a maniverter also featured auto-meshing methods and automatic results capture in an integrated optimisation architecture [5]. Such architectures not only reduce the human input to the system but also aid inter-operability and multi-disciplinary problems [67]. While these two examples show customised optimisation architectures, there are commercial software packages that fulfil these roles [40][41]. These codes feature the integration of many CAD and CAE packages, as well as providing in-built DoE, metamodeling and optimisation methods. This allows the user, an expert in CAD/CAE, to focus on the product design and requires only a systems level understanding of the optimisation process. This does mean that there must be close collaboration between the CAE user and the optimisation software vendor to ensure that the most efficient method is applied and the state of the art is maintained in the optimisation code.

2.6.4 Application of Metamodelling

As CAE methods only allow the simulation to be completed for one set of input variables giving a single solution point, the derivatives of the attribute behaviour cannot be calculated. This prevents the application of classical gradient-based optimisation techniques [11]. In order to gain the data needed to predict the system behaviour, the model must be run multiple times. To optimise these systems, meta-heuristic methods are applied by one of two different ways. Firstly, by directly coupling the optimisation software to the CAE. With this method, samples will be gathered for each iteration of the meta-heuristic algorithm applied. Examples of this application approach are shown in the optimisation of a maniverter [5], truck body weight [68], internal combustion airbox [69] and engine components [70]. The aforementioned examples show a high reliance on the optimisation architectures which exploit automation methods. However, the serial natures of such projects makes them increasingly impractical as the cost of the CAE functions increase[11].

As an alternative, the metamodelling or response surface method can be used. The metamodelling approach was developed from the DoE methods and can be used in SAO, MDO or MAO. Here an upfront sample is used to build a low cost model of the system behaviour that can be used to predict the behaviour of the system throughout the feasible domain [71]. This method has a number of distinct advantages. Metamodel methods are seen as more efficient as they are non-sequential and greater degrees of parallelisation can be obtained. The cost of applying the optimisation algorithm is comparatively lower than when using optimisation based on direct sample approaches. Finally, the whole design space will be explored, this gives greater opportunity for the designer to investigate the system behaviour and may reveal different regions of interest than expected [11]. However, questions have been raised about the use of such methods with increasing dimensionality [18][64].

The relationships within the metamodelling method are shown in Figure 2-5. It can be seen that the key enablers in HEB problems are still applicable, but other issues about metamodelling such as the sample method and size, model selection and fitting are now important. The optimisation method must balance each of these competing factors within the constraints of the design system to deliver an improved product. For example, a constraint on analysis time will limit the dimensionality and maximum sample size that can be obtained. This could cause the optimisation method to fail. Thus, the maximum level of information must be obtained for the smallest amount of work possible. The controlling methods in metamodelling must now be explored to see how this can be achieved.

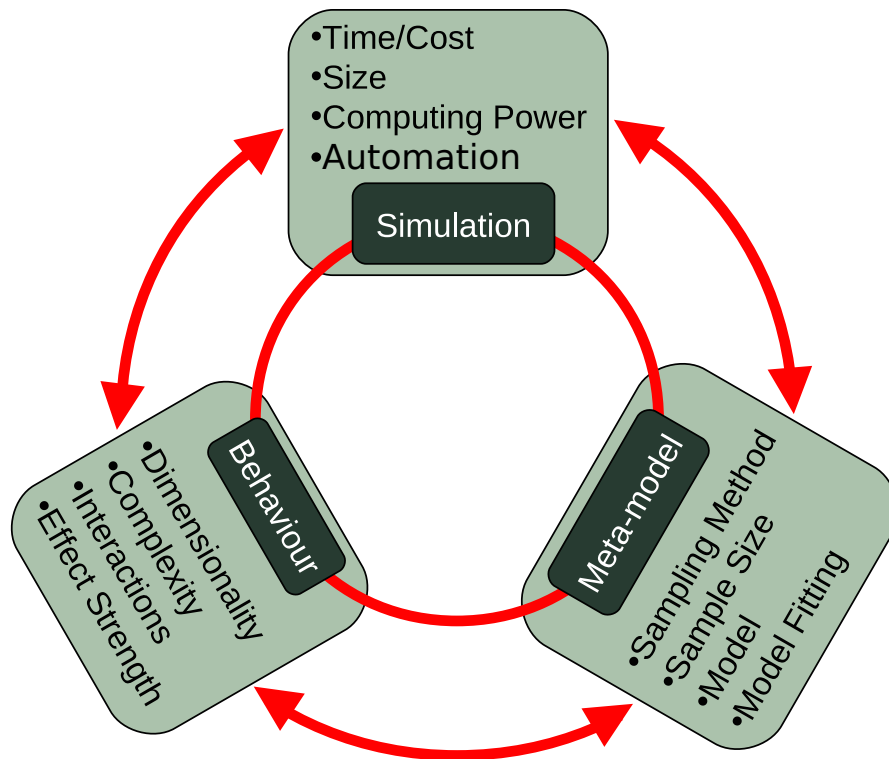


Figure 2-5: Key Controlling Parameters in Meta-Modelling

Examples of Metamodelling

The metamodelling method will be examined using examples from the literature. Tables 2.2 to 2.4 give the details of numerous examples of metamodelling techniques applied to engineering issues. Studies based on mathematical functions alone have not been included. While these tables are not an exhaustive list of all applications, it does represent a cross-section of applications within the field. The table lists the author(s), the type and size of sampling method used plus any additional samples gained, the metamodelling method used, any given errors and comments on the CAE used. A table of the abbreviations used is given in table 2.5.

Table 2.2: Examples of Metamodelling in Literature (a)

Author(s)	Sample Type	Sample Level	Sample Size	Meta Model	Error	Comment
Butkewitsch et al [72]	2 Fractional DoE	16	LR	$R^2 > 95\%$	5 variables on a buggy type vehicle structural FEM	
Clark, Grebsch & Simpson [73]	CCD	27	QR			
	CCD/LH	13	KR	Based on 1000 additional points	3 different test cases with 2, 3 & 4 variables respectively.	
		15	RBF		Shows SVR to out perform both RBF and KR. Simple mathematical models	
		25	SVR			
Fang et al [74]	OA	27	RBF	Error based on 8 Points	RBF error 2-6%, Compared Radial Basis Functions with RSM, RBF better, used on crash structure optimisation, 10 variables	
Fang et al [75]	NG	94	RBF	Examines Local leave one out errors for outliers	Engine simulation code with 15 inputs, data not sufficient for RBF usage.	
Gerhorst, Wirth and Kuhlbach [76]	Fractional DoE	25	QR, MARS	NG	8 variable examination of engine control parameters.	
Gilkeson et al [77]	OLH	40	MLS	10 additional points, value not given.	CFD model of aerodynamic flow around a vehicle and trailer, 3 input parameters.	

Table 2.3: Examples of Metamodelling in Literature (b)

Author(s)	Sample Type	Sample Level	Sample Size	Initial	Meta Model	Error	Comment
Gu <i>et al</i> [78]	OLH		33 36 Final		QR	<1% of attribute on optimised	For weight optimisation in crash structure using FEM with 11 input variables. Sequential area sampling.
Jasper, Rudell & Sakurai [79]	2/3 Fractional DoE	10		LR	NG		Two experiments on race car wings 7 variables each, using CFD. Mainly used DoE approaches to results.
Khandare, Pan and Schoon [68]	ULH	9	8	LR	NG		3 Variable input, CFD of flow around a HGV.
Lee & Kang [80]	LH	100		KR		Leave one out RMSE < 0.2%	Door frame impact model with 7 input variables FEM
Martinelli & Duvigneau [81]	LH	8, 23		RBF, KR		441 Points, Relative error < 0.06%	CFD flow around an aerofoil with 2 variables, system behaviour is simple. RBF out performs KR.
Pan, Zhu & Zhang [82]	LH	15		SVR		R^2 & RMSE based on 8 additional Samples, $R^2 > 0.84$ and RMSE 6%	3 Design variables in automotive crash structure design FEM.

Table 2.4: Examples of Metamodelling in Literature (c)

Author(s)	Sample Type	Sample Size	Meta Model	Error	Comment
Simpson <i>et al</i> [83]	ROA	25	QR	2nd order (4.54%, 0.015%, 0.90%) KR (4.37%, 0.018%, 0.89%) RMSE on Additional 25 points	Examined 3 attributes of an aero spike nozzle, this had 3 input parameters Minimal difference between the two metamodelling methods. CAE is simple mathematical models
Wang, Li & Li [84]	LH	55 initial 118 Final 78 Initial 146 Final	SVR KR SVR	Case 1 $R^2=0.923$ $R^2=0.821$ Case 2 $R^2=0.893$ Errors based on Leave one out methods.	Frontal crash structure FEM, Case 1 simplified 8 input variables, case 2 full model FEM 15 variables. Additional samples gained by intelligent sampling strategy
Yang <i>et al</i> [50]	LH	57	SWR	NG	Earlier work by Yang (2001), Uses 19 inputs and cites 3 N for sample size.
Yang <i>et al</i> [85]	LH	12, 24, 36, 72, 144	LR, RBF, Kr, NN	RMSE additional Points	4 Variables. Experiments with varying sample size to test for accuracy. Crash FEM model. Use sample size >9*Number of variables, little difference in metamodelling methods.
Xiao <i>et al</i> [86]	FF/LH	146	KR	NG	6 Inputs. Examining the port flow on internal combustion engine using CFD.

Table 2.5: Abbreviations used in examples table.

Initials	Name
Sampling Methods	
CCD	Central Composite Design
FF	Full Factorial
LH	Latin Hypercube
NG	Not Given
OLH	Optimal or Orthogonal Latin Hypercube
ROA	Random Orthogonal Array
Metamodelling Methods	
KR	Kriging
LR	Linear Regression
MARS	Multi Adaptive Regression Splines
MLS	Moving Least Squares
QR	Quadratic Regression
RBF	Radial Basis Function
SVR	Support Vector Regression
SWR	Step Wise Regression

Selection of Meta-Model Type

The principle of metamodelling methods is to build an empirical model of the system. The choice of metamodel can heavily influence its accuracy [87]. There are two distinct types of metamodel; parametric (based upon a fixed underlying formula) and non-parametric (sample point fitting techniques) [64]. In the table of examples there are a number of different methods that have been utilised, the most common of which are parametric regressional models and non-parametric Kriging, Radial Basis Functions and Support Vector Regression.

- *Regression Methods:* With these models, predefined functions such as linear or polynomial lines and surfaces are fitted to the data. It has been found that such methods are only suitable when the underlying system behaviour matches the selected function, thus they have limited applicability to complex system behaviour[64]. As the dimensionality increases, they also require increasing amounts of samples to resolve all of the constants. Regressional methods are best used on local metamodels (small parameter ranges) and simple system responses[14].
- *Radial Basis Functions:* In a Radial Basis Function (RBF) each sample point has an associated n-dimensional centred symmetric function and a multiplying weight. The system behaviour is then the total sum of all of the functions in the design domain. These functions can be used in conjunction with a non-uniform set and have been shown to model complexity in surfaces well [12]. There are a number of formulations which can be used, the details of which can be found in work by Buhmann[88] and the modeFRONTIER technical documentation[89].
- *Kriging:* Here the system response behaviour is modelled by an underlying response function and a localised departure. The underlying function captures the bulk behaviour of the data

while the complex surface comes from the departure equations which are based on a probabilistic approach [71]. Both parts of the Kriging method have a number of formulations that can be used, the details of which can be found in the modeFRONTIER technical documentation[90]. The Kriging models have also been found to be applicable to complex and noisy response behaviours.

- *Support Vector Regression*: This method is a relatively new metamodel and is based on the machine learning technique “support vector machines” [84]. This method fits numerous n-dimensional hyperplanes to the data which are then mapped in the design space. The function is then approximated as the sum of the various vectors and weighted map functions. There are a number of examples in the literature to suggest this method may out-perform the more common Kriging and Radial Basis Functions for predictive power on complex surfaces[11]. Details of this improvement, including examples of formulation and application, can be found in work by Clarke *et al*[73] and Wang, Li and Li[84].

These are just some of the metamodel methods that have been applied to engineering optimisation problems. There are also examples of Gaussian Processes [91], Multi Adaptive Regression Splines (MARS) [92] and neural networks [11][85]. There have also been efforts to create ensemble models with multiple types of metamodel on a weighted sum function [93]. Many of the commercial optimisation software codes feature metamodeling modules with various formulations of common models [40].

The large number of methods presents the user with a difficult choice when selecting the metamodel, while non-parametric methods are considered an improvement over parametric regression models, there is no consensus over the best application. There are examples of each being preferable (Kriging [83], RBF [81][74][12] & SVR [11][73][84]). This would seem to suggest that the selection of the metamodel must be made on a case by case basis, balancing the cost undertaken to produce the model with its accuracy. When selecting a metamodeling method, the user should try all approaches with the same sample and error estimation methods to find the model which is most appropriate.

Sampling Methods

Traditional methods of experimental sampling are based on Design of Experiment (DoE) methods. These can be combined with statistical techniques, such as ANOVA, to understand the system behaviour response to the design variables and any interactions. Traditional DoEs use a full factorial approach where every combination of variable and level is examined. As dimensionality and complexity increase, requiring more intervals, the size of the required sample set increases dramatically. The optimisation of wing design of a High-Speed Civil Transport aircraft involved the examination of 10 design variables, each with three intervals, leading to a total of 3^{10} (59049) experiments[66]. The runtime and resource requirements of some CAE would prohibit this many experiments. Thus, there is a need for an alternative approach which efficiently searches the design space.

Fractional DoEs are a structured method that allow for efficient use of simulation points[48]. This is achieved by reducing the number of sampling points. In the design of a rear wing on a Formula Student car there were 7 variables at 3 levels equating to 2187 samples. With a runtime of 12 to 15 hours per simulation, a full factorial approach could not be achieved. Here, the fractional DoE Taguchi orthogonal array method allowed the optimisation to be based on just 18 samples. When using such methods for CAE based optimisation problems there are two issues; firstly repeated sampling and secondly capturing of complexity.

CAE, unlike physical experiments, is not subject to repeat experiment variability. The same input conditions will always give the same results, meaning repeated experiments are a waste of resources. As well as repeat points, traditional DoEs tend to place samples on the boundary of regions [11]. This can be an issue as the complexity of behaviour within the design regions is not resolved. Sacks *et al* [94] stated that 'space filling' sampling approaches were more appropriate to computer experiments. This is supported by Simpson *et al* [95] and Jin, Chen and Simpson[12]. This approach is termed Design and Analysis of Computer Experiments (DACE)[94]. There are many methods suggested for 'space filling' techniques. In a review of sampling techniques, Abdallah *et al* found that latin hypercube methods were an efficient and accurate method of sampling [96]. This method of sampling does not repeat any previous input states, allowing CAE resources to be maximised [65]. The precedence for use of the latin hypercube method is demonstrated in tables 2.2 to 2.4. There are many different formulations of latin hypercube that have been demonstrated, where orthogonal and uniform designs are commonly cited. Ford provide an optimal set of latin hypercubes for sampling the design space[97]. This set of latin hypercube designs was based on methods proposed by Ye [98]. Here the design space is optimally filled by maximising the minimum distance between samples.

Sample Size

The number of sample points is also a key consideration in the metamodeling method. Too few samples will not capture the complexity of the system behaviour sufficiently, but too many make the method less efficient to operate. As the complexity of the black box function is unknown there is no direct formula to calculate how many samples are required. There have been a number of suggestions for approximate sample sizes based upon the number of input variables (N). The guidance from a number of literature sources is summarised in table 2.6. Jin, Chen and Simpson [12] break the sample sizes into three distinct regions defined by the 3 equations given in table 2.6. Kaufmann suggests a size $1.5*N$ to $4.5*N$ samples [13], while Yang at Ford used $3-9*N$ [50][85]. The work of Wang and Beeson[14] at GE Aviation suggested a sample size of $10*N$. A larger set based on the number of unknown variables in quadratic regression models is suggested by Jin, Chen and Simpson[12]. Conversely, in the optimal latin hypercube set, provided by Ford, a minimum sampling approach is taken[97], the governing equation is given in table 2.6.

The sample sizes from the examples presented in tables 2.2 to 2.4 is plotted against the number of input parameters in Figure 2-6, along with the different regimes indicated by Jin, Chen and Simpson[12]. While Figure 2-6 shows there is some variance between the number of variables and

the size of sample used, most examples fall within the scarce to small regimes used by Jin, Chen and Simpson[12]. However, there are examples where the sampling size exceeds this guidance, this will be to increase the accuracy of the metamodel. As the behaviour within the design space is unknown, these guides should be used as a starting point when defining MAO projects.

The problem of sample size presents a dilemma when using MAO as a Systems Engineering tool within a design process. The requirement for accuracy pushes the user towards increased sampling sizes. However, the time and resource constraints mean that smaller samples are preferable in an industrial setting. It can then be seen that the eventual number of samples used will be a trade-off within this conflict.

Table 2.6: Guidance for regions of sample sizes (where N is the number of variables)

Region	Sample Size	Author(s)
Scarce	$1.5 \cdot N$	Kaufmann [13]
	$3 \cdot N$	Jin, Chen & Simpson[12], Yang[50][85]
	$4.5 \cdot N$	Kaufmann [13]
Small	$9 \cdot N$	Yang[50][85]
	$10 \cdot N$	Jin, Chen & Simpson[12], Wang & Beeson[14]
Large	$\frac{3 \cdot (N+1) \cdot (N+2)}{2}$	Jin, Chen & Simpson[12]
Minimum	$2^{\frac{N+2}{2}} + 1$	Gromping[97]

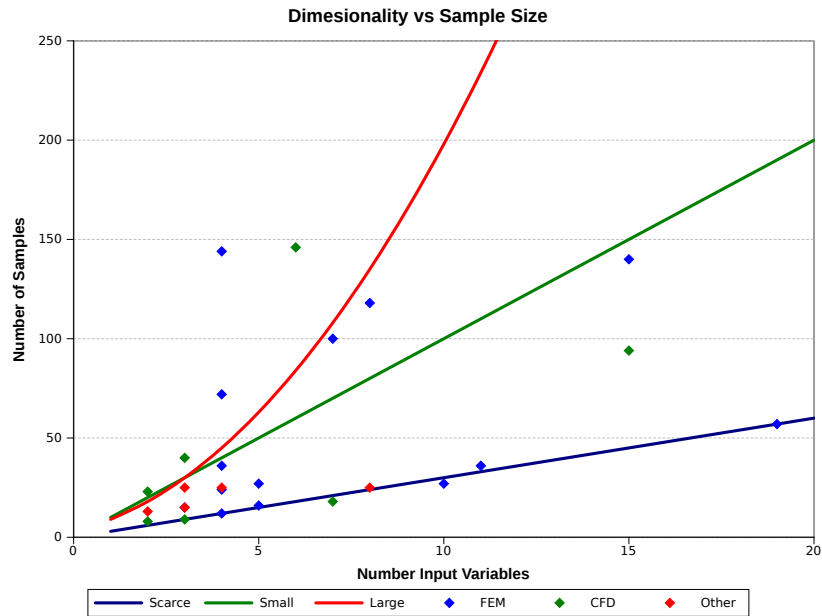


Figure 2-6: Examples of sample sizes in literature and regions, as defined by Jin, Chen and Simpson [12]

Error Estimation

Parametric models use regression methods to fit the metamodel within the region sample data. However, the fitted model does not necessarily pass through the sampled points. This allows the error to be estimated at every sample point. Non-parametric metamodels are interpolative, i.e. the model goes through all the data samples. This means the estimation of error cannot be judged as easily. There are two approaches that are used to assess error of non-parametric metamodels; additional sample points and leave one out methods [11][15].

Additional samples require that the CAE simulations are completed on a second independent sample set. This allows the actual results to be compared to the values predicted by the metamodel. Samples in isolation can only indicate the error in that vicinity; for an estimation of the global error numerous samples must be taken. However, the examples presented in tables 2.2 to 2.4 give no clear guidance on the size or distribution of such samples. However, where multiple points are used there are common methods of measuring the global error such as the R^2 and Root Mean Squared Error (RMSE) found using equations 2.1 and 2.2 respectively. Here a good fit is indicated by an R^2 value approaching 1 and a reducing RMSE (this has the same value as the output but can also be normalised to give a percentage).

$$R^2 = 1 - \frac{\sum_{i=1}^m (y_i - \hat{y}_i)^2}{\sum_{i=1}^m (y_i - \bar{y})^2} \quad (2.1)$$

$$RMSE = \sqrt{\frac{\sum_{i=1}^m (y_i - \hat{y}_i)^2}{m}} \quad (2.2)$$

Where y_i is the observed value, \hat{y}_i is the predicted value from the metamodel and \bar{y} is the mean of all the observed values.

The gathering of additional points increases the cost of the optimisation process, thus there is an incentive to use methods which do not require additional samples. For this, 'leave one out' methods have been suggested [15]. If there are a total of x samples taken in the sampling stage, then a total of x metamodels can be generated based on $x-1$ points. The error in predicting the remaining point can then be calculated. This process is shown in Figure 2-7. Graph *a* in Figure 2-7 shows three points on an arbitrary (x, y) coordinate system. x is the input value and y the output. A quadratic curve (blue) has been fitted to these three to create a relational behaviour for x and y . The process of calculating the leave one out error is then shown in graphs *b-d* in Figure 2-7. One of the points is removed from the set and a line fitted to the remaining points (red). The error can then be estimated by extrapolating or interpolating the behaviour of the red line to the known input value and the difference calculated (green line). Once this has been completed for every point in the sample, the global error can be estimated using the R^2 and RMSE methods. The formulations of the Kriging and Radial Basis Functions metamodels allow this to be calculated at only a small additional amount of computational expense [89]. However, the use of such methods has been questioned as the error is not based upon the final surface created on the whole sample set. Some

consider it to be a measure of sensitivity to the sample points and could potentially be misleading [11].

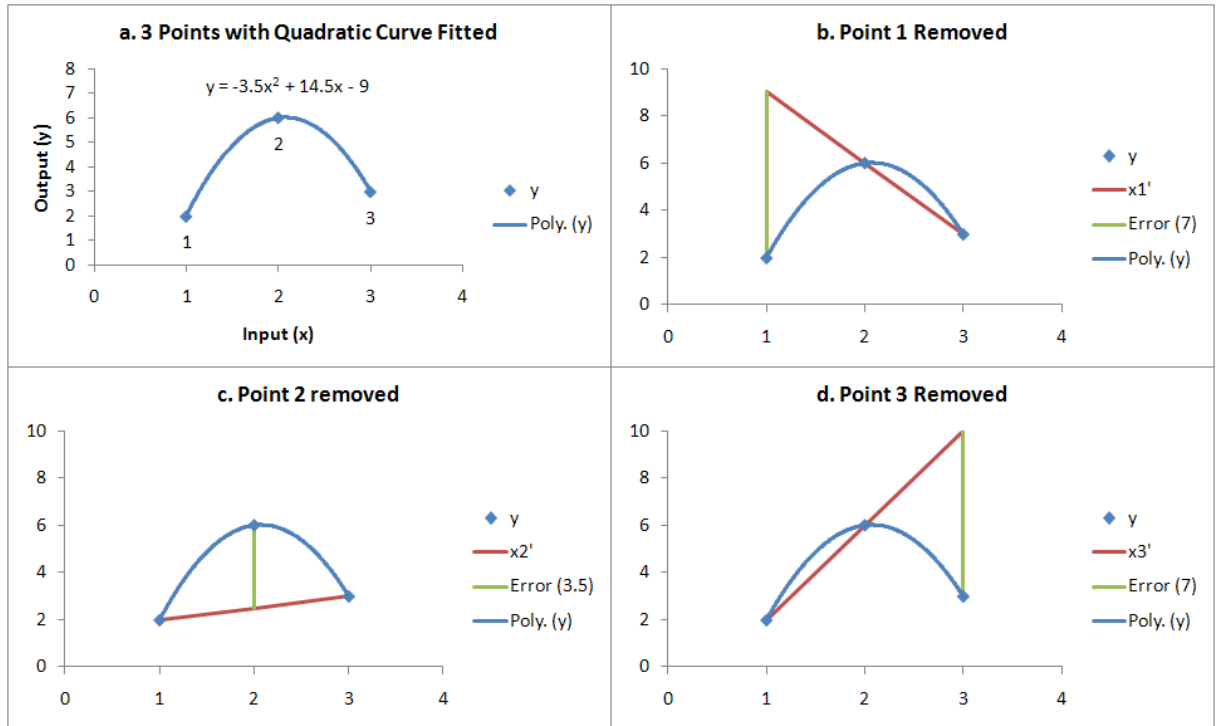


Figure 2-7: The 'leave one out' error estimation process

Understanding the error in a metamodel is key in selecting which metamodeling method is used and for gaining confidence that the metamodel is correct. The assessment of metamodel error presents another dilemma when using MAO as a Systems Engineering tool within a design process. The use of additional samples to estimate error will increase the cost of using the process, however there are a number of unknowns. Firstly, the literature lacks guidance for the number and distribution for the samples used to estimate error. Secondly, it is unclear if the low cost 'leave one out' error method is an accurate prediction of the metamodel error.

Resampling Methods

Where the fitting of the metamodel does prove poor, additional samples are required. Additional points should help to resolve the localised complexities within the metamodel behaviour, allowing for increased predictive performance. Two strategies for the inclusion of additional samples are an optimal guided process and a global sequential method [64].

In an optimal guided approach an initial sample and metamodel generation is conducted, the optimal point is found, then validated. If the metamodel prediction is poor then the design space is reduced and further local samples are taken to improve local performance. This approach is not without risk, as if the initial metamodel is poor then the optimal point may just be an error in the

surface and drive the process away from the true optimal point[64].

To overcome this risk, the additional sample set should be made to improve the predictive power over the whole design space. These samples would have to be guided to ensure that the additional sample points are placed in regions of error or complexity. The literature shows a number of suggestions as to how this can be achieved and it is the focus of much research in the field[84][99][100]. There are also examples of implementation of intelligent sampling methods in commercial optimisation software such as the Lipschitz [101] and Multivariate Adaptive Crossvalidating Kriging (MACK)[102] methods in modeFRONTIER. With the Lipschitz method the complexity is measured by gradients between samples while the MACK sampler examines error on a Kriging metamodel fitted to a subset of the whole sample. The ability of intelligent sample methods has the potential to reduce the error in the metamodel more quickly than simply adding additional points based on a secondary latin hypercube or other applicable method. This is due to the resolution of complexity [99]. When used in conjunction with a sensible initial sample, there is a large potential for computational efficiency savings[100].

2.6.5 Multi-physics CAE Methods

This section has examined the use of CAE methods to model the system and provide predictions of attributes. In order to model multi-disciplinary systems and attributes a new approach is needed within CAE[17]. Traditionally, CAE methods have been split into specific domains, each with a distinctive strategy for solving the physics of that domain[103]. For example, fluids modelled by CFD typically use a finite volume solver, whereas solid mechanic simulations tend to be based on finite elements. However, the multi-domain analyses that are part of MDO present a new challenge[18]. MDO methods specialise in optimisation projects that cross the traditional analysis domains and within this the need to simulate domain interaction was identified. Here, domains would need to be 'coupled' to allow the exchange of data at the boundary interface. Such analyses are termed multi-physics analyses and are of interest to CAE users as both a stand alone CAE tool and an enabler in optimisation projects. Examples of multi-physics problems are[103]:

1. Fluid Structure Interaction
2. Thermo-Mechanical
3. Thermo-Fluid
4. Piezo-Electric

These analyses require the exchange of data at the domain interface to set the boundary conditions for the neighbouring domain. For this, the various domain analyses must be coupled together[17]. The degree of coupling is dependent on the strength of the interactions between the domains[103]. Low level, loose or one-way coupling can be used when one domain significantly affects another but is itself unaffected. A fully coupled solution is required when all domains show significant interaction. The level of coupling has a large impact on the cost and complexity of the multi-physics method.

The desire for such methods has led CAE software vendors to include multi-physics analysis methods within their codes. There are two distinct approaches. The first is to use domain specific codes that communicate with each other via external pathways. The second is to use a single multi-physics code where all domains are solved in a single model and the coupling is handled internally[103]. The use of multiple domain specific codes is seen as more expensive as separate domain models and CAE engineers are required, as well as support for communication during the simulation. However, in a single model approach, accuracy sacrifices may be made as a non-specific software code is used.

The additional costs and benefits of such methods require further investigation if they are to be used as an enabler in MAO/MDO projects. In particular, the attribute prediction accuracy benefits and costs should be established for the various levels of coupling, as well as single versus multi-code approaches.

2.7 Examples of Optimisation in Literature

The previous sections have highlighted many of the complexities that arise when using optimisation within real engineering design problems. However, the cost of applying these methods must be traded off against the benefits that such methods can bring.

The design of vehicle engines has many instances of multiple and conflicting objectives. In the case of port development of SI Engines, both economy and the performance were optimised[104]. Combustion stability is influenced by the tumble number which needed to be optimised for maximum economy. The flow coefficient is used to measure the performance of the engine and this also needed to be maximised. However, there is a trade-off as increased tumble number led to degradation of the flow coefficient. The application of multi-objective genetic algorithms allowed the system to converge on a solution which simultaneously optimised both the tumble number and flow coefficient. This approach yielded information on the effects of the design parameters on the trends in the tumble number and flow coefficient. This was then used to optimise the intake port design which was then applied to a test engine and the improvements verified.

The design and multi-objective optimisation of the Maniverter[5] led to the torque performance index, 1st natural frequency and the catalyst inlet temperature all being improved upon while the cost and weight of the system were minimised when compared to a baseline solution. The Figures are shown in table-2.7. The approach used an integrated approach with parameterised CAD models. The 1st natural frequency was assessed using an MSC.Patran model with 8 mm 4 noded tetra elements and an AVL boost model used to predict the torque performance index and catalyst inlet temperature. This model is a 1D fluid simulation code, flow through the catalyst was not assessed due to the time constraints of the project. The cost and weights were obtained from estimates based on the CAD. While the results may be questioned due to the lack of high fidelity CAE models and some accuracy sacrifices made to enable fast optimisation, the process has shown that it can be used to guide the design. The process also showed significant time and cost advantages. The total development time was reduced from sixty plus days to fourteen (using

Table 2.7: Maniverter Design Improvements enabled by use of MDO[5] page 164.

Performance Attribute	Optimisation Target	Baseline	Selected Solution	Difference
Torque Performance Index	↑↑	129.70	152.96	17.94%
Cost (€)	↓	36.83	18.56	-18.27
1 st Natural Frequency (Hz)	↑↑	340.71	415.26	74.55
Catalyst Inlet Temperature (°C)	↑↑	1178.68	1204.38	25.70
Mass (g)	↓	5945.63	5556.17	-389.46

low-fidelity methods) and development costs were lower. It was also discussed that high fidelity CAE (CFD flow over catalyst) could be included but would require the use of HPC. With increased computing power it was predicted that the design optimisation could take as little as seven days.

High performance computing has been used to optimise crash structures of automotive bodies[50]. An MDO procedure that accounted for full and offset frontal crash simulations, a roof crush model, human occupant modelling and NVH analyses, yielded approximate weight savings of 15kg in the crash structure components. This was achieved while still meeting all safety requirements. The optimisation was completed using HPC at NASA and took a total of three days to complete.

The examples shown in this section demonstrate that a CAE based Multi-Attribute approach to design optimisation could not only provide improved design and trade-off strategies, but also reduce the time it takes to develop system solutions.

2.8 Conclusion

In this review, Systems Engineering was shown to be an interdisciplinary approach to the design of systems. The Systems Engineering approach relies on tools and processes that ensure the product is designed to meet customer requirements. Optimisation is a key part of this process and enables improved products to be designed. However, the optimisation of systems is complicated by multiple and conflicting objectives, multiple domain considerations and robustness. MAO methods were suggested as an approach to system optimisation that could be utilised to overcome these complexities. A key issue identified with these methods is how visualisation and decision analysis methods can be applied to the data obtained from the optimisation process to understand the system and enable attribute trade-offs. Such methods are important for enabling design decisions to be made and should be explored when creating a MAO systems engineering tool.

The systems optimisation methods were shown to be based on systems modelling methods which allow the system attributes to be predicted. For this, CAE methods for modelling physical components are used within the engineering industry as they enable early problem solving and are more cost-effective than physical testing methods. A review of CAE based optimisation revealed two approaches that can be used, firstly direct application of the optimisation algorithm and secondly, using the metamodeling approach.

Metamodeling methods are an advancement of the design of experiment and statistical methods. Direct approaches were shown to be enabled by integration architectures that allowed the automation

of the sampling process. However, the metamodeling approach provides a more efficient use of parallelisation and the sampling of the whole design space within this approach is seen as an improvement over direct application methods. However, as there is still a high cost associated with metamodeling, methods which enable improved models at reduced costs are important. Within this area, there are a number of issues with setting the sample size and estimating the error in the metamodel which affect the cost. These need to be better understood in order to use MAO as a systems engineering tool.

For CAE based experiments, the literature agreed that sample distributions that filled the design space are the most appropriate, an example of which is the optimal latin-hypercube used by Ford[97] based on the work of Ye[98]. However, the guidance over sample size was less clear. Wang and Beeson[14] working at GE Aviation suggested a sample size of ten times the number of inputs. A larger sample size, based upon methods required to solve the unknowns for quadratic regression models, was given by Jin, Chen and Simpson [12]. However, smaller sample sizes are suggested by the minimum latin hypercube approach used in Ford[97] and in the scarce sets suggested by Kaufman[13], Wang & Beeson[14] and from Jin, Chen and Simpson[12]. This presents a major dilemma when using metamodeling within a systems optimisation tool. As the sample size has a large influence on the duration and scale of an optimisation project and the accuracy of the metamodel, there is a conflict between completing the project within the time constraints of the design system and a robust optimisation.

The selection of the type of metamodel used is based on an estimation of the fitting error. The error estimator also gives confidence that the metamodel is sufficiently accurate for use in an optimisation tool. The two approaches for error estimation of non-parametric metamodels are using additional sample points and using 'leave one out' methods. This presents another dilemma in using MAO as a systems optimisation tool in a constrained design environment. The use of additional sample points represents an increase in cost of the process but there are accuracy and interpretation issues associated with the low cost of 'leave one out' method.

The MAO approach is built on CAE methods which have been traditionally split into domain specific applications. However, in instances where an attribute requires a solution covering multiple domains, a new CAE approach is required. Here a multi-physics approach could be used to increase the accuracy of the simulation, but this must be balanced against the additional cost of such an approach. This cost benefit analysis requires further investigation.

Chapter 3

Rationale and Criteria for MAO

3.1 Introduction

The aim of this chapter is to examine the role of optimisation within an automotive design environment and allow technical research projects to be defined. This aim will be achieved by analysing the interaction of the optimisation method with other systems within the design environment, using a 'System of Systems' Engineering viewpoint analysis. While the literature review examined the methods of systems optimisation based on CAE methods, this chapter further explores optimisation within the context of the Jaguar Land Rover product development system.

The chapter begins with a discussion of the 'System of Systems' engineering viewpoint, followed by an examination of the current Jaguar Land Rover optimisation method and the surrounding systems in the design environment. This is then extended to examine the potential effects of introducing a multi-attribute method into the CAE analysis process from a system of systems viewpoint. The previous chapter reviewed the use of metamodeling based MAO and raised specific issues about the implementation of the methods with regards to sampling, error estimation and the CAE used. This analysis provides further insight into the operation of MAO methods in a automotive design environment. The System of Systems viewpoint helps to identify the key roles and enablers within the design process and raises key questions which need to be addressed about the application of MAO as a Systems Engineering tool. The research areas and key questions identified are then focused in to two sub-projects that focus on the application of MAO to an automotive airbox and the multi-physics analysis of a fuel tank. The key questions are then prioritised, then research projects and structures for multi-attribute and multi-physics methods are outlined.

Much of this chapter has been extracted from a paper presented at the 2010 IEEE International Conference on System of Systems Engineering, Loughborough University, 22nd - 24th June [105]. Some sections are extended to include the multi-physics and other aspects of the work that followed on from this paper.

3.2 System of Systems Engineering

Systems Engineering captures the complexity of design problems by viewing the properties, capabilities and behaviours in discrete systems and sub systems. However, a change in viewpoint could allow the observer to see that these systems do not exist in isolation, but as part of many interconnected systems. The term 'System of Systems' can be applied to this situation. This term is used widely within Systems Engineering. Although no hard and fast definition exists[106], it can be used to describe large-scale systems whose components are systems in their own right. A 'System of Systems' approach should be taken in order to gain a holistic view of the system and operational environment. The System of Systems Engineering approach can be considered a development of traditional Systems Engineering. The approach is a useful tool when considering the integration of complex systems in a dynamic environment and allows new challenges to be addressed [32]. Eisner *et al* provides the following definition of 'System of Systems' (cited from [107]):

'A set of independently acquired systems, each under a nominal Systems Engineering process; these systems are interdependent and form in their combined operation a multi-functional solution to an overall coherent mission. The optimisation of each system does not guarantee the optimisation of the overall system of systems.'(pg 486)

A system of systems approach calls for the dynamic nature of system-to-system interaction as well as for each individual system to be characterised. The characteristics of a system of systems are autonomy, belonging, connectivity, diversity and emergence [33]. The autonomy characteristic can be used to differentiate between individual systems and a system of systems. Decisions in an individual system can only be taken at the highest system level, not at the sub-system or component level. Using this definition of decision making, the boundaries of systems in a system of systems can be drawn where each individual system is free to make decisions in order to achieve functionality. This decision making allows systems to belong to a system of systems and add functionality where there is sufficient benefit. This changes how systems are connected. In Systems Engineering, much of this communication is defined at the design stage and hidden in encapsulated systems. However, a system of systems demands a dynamic approach to connectivity. The dynamic nature of autonomy, connectivity and belonging in a system of systems increases its diversity and allows the system to respond to new and unexpected changes in the operational environment. In Systems Engineering, the emergent behaviours of a system are either designed in when beneficial or removed when detrimental. In a system of systems approach, any detrimental emergent behaviour can be eliminated by adaptation (autonomous changes of belonging and connectivity) and any beneficial behaviour can be kept.

3.3 Feasibility of Using MAO as a Systems Engineering Tool

While it could be argued that a vehicle constitutes a System of Systems, this is not the focus of this chapter, instead a System of Systems viewpoint is taken of the automotive design environment;

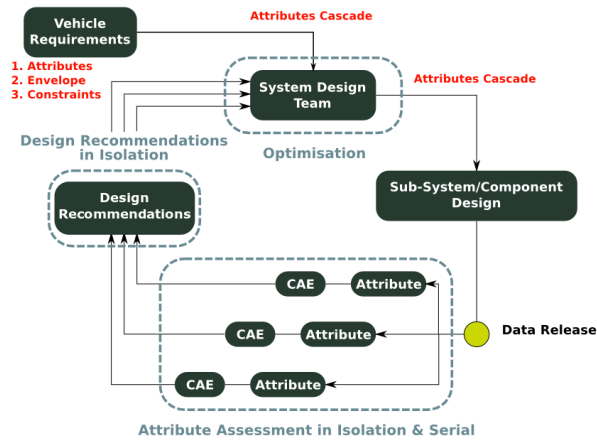


Figure 3-1: Current optimisation methods

treating the application of a MAO tool as the system that is to be implemented by the CAE team within this environment. The first part of this section focuses on current optimisation methods and the environment in which these are completed. To gather the requirements for the assessment of feasibility of using MAO methods, an initial Systems Engineering approach is adopted. This is then expanded to a System of Systems Engineering approach in order to gain a greater understanding of the issues involved. The key questions that could be addressed are raised, considering the System of Systems Engineering characteristics.

3.3.1 Current Optimisation Methods in Jaguar Land Rover

To design a high value vehicle, an automotive manufacturer must first define what is of value to the customer. Targets for attributes such as price, fuel economy and maximum performance are set early in the development of new model programs. Harder to measure attributes, such as aesthetics and refinement, are subjective. In these cases, the targets will be set by strategically placing the vehicle programs according to the company design, brand philosophy and image. The buyer of a vehicle may be the direct customer, but there are also other sources of requirements and targets. Vehicles must conform to various industry and legal standards governing their usage. Once all of these targets, requirements and constraints are finalised, they are decomposed and cascaded to the system, sub-system and component levels. Solutions can then be created to meet the design requirements.

The designs must be analysed to compare competing solutions against each other and against the requirements. Product development attributes such as performance, NVH (Noise, Vibration and Harshness) and durability are analysed using multiple CAE techniques, shown in Figure 3-1. To create a product with the highest value to the customer, the system must then be optimised. Due to the decomposition of disciplines within CAE, the assessment of each attribute is carried out in isolation in a sequential optimisation process. When a system is optimised for one attribute, the performance of other attributes may suffer. Engineering judgement and expertise are used

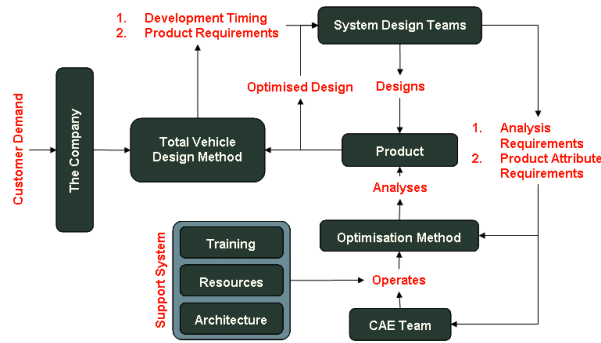


Figure 3-2: Relationships between major design systems

subjectively to trade-off attributes and optimise the whole system. This approach requires several iterations of design and optimisation cycles to allow for attribute trade-offs, conflict resolution and re-assessment of the system.

The serial optimisation method does include methods of single attribute optimisation within the Jaguar Land Rover powertrain CAE process, this is part of the 'DCOV' approach to design problems. In a single attribute process the system behaviour is assessed using the Ford provided optimal latin hypercube method with the minimum number of samples[97]. The data from these CAE points is analysed by the application of metamodels (depending on accuracy) or statistical methods such as ANOVA[26]. These methods provide the CAE user and designer with clear indications on the direction the design should be progressed in.

3.3.2 A System of Systems Viewpoint of The Design Environment

In a System of Systems Engineering approach, the surrounding systems would also be included in the analysis. This will help the engineer to envisage the live design environment in which the process will operate. The overall total vehicle design system, shown in Figure 3-1, has been re-arranged to show the interactions between the major systems for the optimisation of a product in Figure 3-2 . Considering the optimisation method as a system within the live design environment, it can be seen that it must operate on the design of the physical system within the constraints of the other systems. For clarity, in this analysis, the word 'product' is used to describe the artefact which is the subject of the design and optimisation process. This product could be a single component, an assembly, sub-system or even a system of a vehicle.

The Product Strategy Team

The product strategy team is the interface that links products to customer demand. It is here that the top level requirements for a vehicle will be formulated before these are decomposed and cascaded within the total vehicle design method. It is also at this level that assumptions of commonality (across different vehicle lines) and carry over components are created. This represents much of the early advanced design work which precedes the detailed design operations of the system

design teams.

The Vehicle Design Process

Automotive design processes use a Systems Engineering approach to total vehicle design; an example is the Ford Product Development System [23]. This approach takes the requirements of the whole vehicle (customer, legal and corporate) and decomposes them down into systems and sub-systems. The systems approach manages the resources, targets, assumptions, quality, design and timing of new vehicle programs. The system design and CAE teams operate within this framework, with work milestones and targets set by the required product progression targets. The total vehicle design system can be considered the central authority in guiding the efforts of the system design and CAE teams.

The System Design Team

Under the total vehicle design process, there are multiple autonomous system design teams each designing a single on-vehicle system (product). It is the job of the system design teams to translate the system requirements into detailed physical products using methods such as the design for 6- σ and 'DCOV'[25]. These methods require the behaviour of the system to be predicted in order that it can be optimised and verified against its requirements. In order to facilitate early fault detection without expensive prototyping loops, CAE methodologies are applied to the system. The system design teams must use the data from CAE and other verification methods to create the best design possible. This is complicated due to the interaction with other vehicle systems, where there is competition for space and attribute weightings (where one or more vehicle systems contribute to a single customer attribute, relative targets must be set).

The CAE Team

The CAE team supports the total vehicle design system by using various modelling approaches to predict the behaviour of the vehicle systems or components from multiple system design teams. The CAE team uses specialised methodologies that allow particular physical domains to be analysed, e.g. finite element methods for structure and solids and computational fluid dynamics for fluids. These methodologies require various resources such as specialist personnel, computer hardware and software.

The CAE method used must be able to provide data to enable design behaviour prediction. However, CAE methods with increased fidelity may be required to model this system behaviour accurately. This necessitates newer, more advanced CAE techniques, such as multi-physics approaches. To use such methods a number of issues must be addressed, these include evaluation of the maturity, stability and validity of the method. Such methods may also necessitate multi-discipline approaches with one or more CAE analysts included in the process. The use of such methods must balance the need for the multi-physics evaluation against these issues and the available resources.

The Optimisation Method

The optimisation of the product is aimed at delivering the best value product. The selection of an optimisation method depends greatly on the complexity of the product that is being designed and the attributes which are being considered. Although the optimisation of a single component may involve multiple analyses, the optimisation is simpler than one where physical domains and system boundaries are crossed. This is where the MDO formulations have proved successful [52]. Extensions of MDO architectures, by modifications in the degree of control at each hierarchical level, have allowed the optimisation of products that are systems of systems in their own right [108]. This demonstrates a relationship in the requirements for an optimisation method and the product to which it is applied. Any optimisation method must balance the complexity of the method with the capability and constraints of the CAE system and the need for the optimisation method.

The Product

There are many systems on a vehicle which must be integrated. Each will be optimised to meet the specific requirements of each individual system but this may not directly result in an optimised vehicle. For example, the optimisation of a vehicle chassis for weight may cause a deterioration of performance in terms of crashworthiness and NVH [50]. Thus, the boundaries to other vehicle systems may change as the design progresses. This increases the complexity of any optimisation as both the inputs and outputs could be altered.

Support Systems

The completion of the optimisation method will require a number of supporting systems to be in place. The chief among these is the training of the CAE analysts, the resources available and the architectures for information and communication.

The MAO method may require the CAE analyst to use new tools and processes that are not within their current skill set. This is especially evident in cases where the analysis crosses over between specific CAE domains. In this instance the CAE analyst will require training. This will ensure new tools and processes can be used effectively.

The CAE analyses and the optimisation methods require the utilization of hardware, software and engineering time. The requirement of each of these is dependant on the complexity of the CAE analyses and optimisation methods, the size of the product design space and the levels of automation that can be introduced. Thus, there is not a standard requirement for resources and it will vary by application. This will increase the difficulty of planning for optimisation applications.

The CAE analyst can also be considered as a resource within the CAE Team. In order to complete the analysis the person with the correct skill set must be available. Where CAE domain boundaries are crossed, multiple CAE analysts may be required to cover all the necessary analyses within the MAO application.

There are a number of supporting architectures that need to be in place in order to use MAO methods. There is the computing and I.T. infrastructure that is used to deliver the resources to

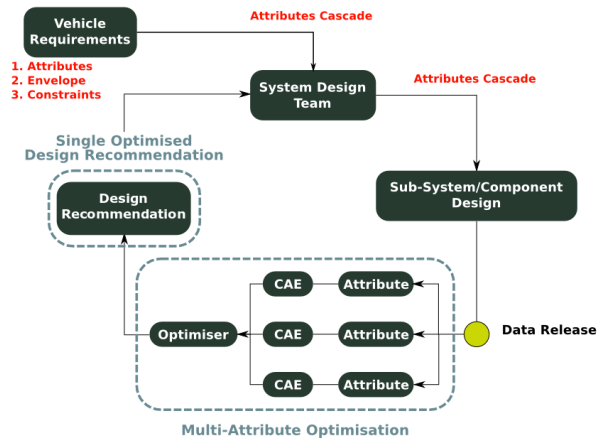


Figure 3-3: A possible MAO application

the CAE analyst and also the structure that supports the wider functionality of the CAE Team. This wider support structure must facilitate the bureaucracy of the MAO method ensuring that the requirements and constraints are understood. There is also a need for the collaborative aspects of the MAO methods to be supported.

Another valuable support structure is the software vendors. These are experts in the operation of the various CAE and optimisation codes that they produce. Their expertise on the set up and coding of the software can help to resolve technical issues. However, there is also the opportunity for close collaboration to develop aspects of the code to suit the specific needs of Jaguar Land Rover, or to inform and train when new technologies become available.

Human-to-human interaction and collaboration is key in the communication of requirements, results and conflicts. While there are many methods to support communication using computers (Computer Supported Collaborative Work (CSCW)) [45], the design process may include many informal forms (telephone, face to face etc). The information contained within such communication may be vital to an optimisation process. When requirements are cascaded from the system design team, it may be in a formal document that lists the hard limits of various attributes. However, communication that is more informal may illicit designer preference for attributes that would guide the optimisation process and help with conflict resolution. Also, the communication of results from the process is of high importance. In many cases, the optimum design point may not represent the best design, especially in areas of trade-off or robustness. In this instance, details of the system behaviour over the whole design range would be of greater interest.

3.3.3 A Systems Engineering Approach to a MAO Tool

The application of a MAO tool would introduce a new stage to the design cycle, shown in Figure 3-3. The optimiser would take input from the CAE performed on a vehicle system, then output a single optimised design. If the optimisation method is isolated from the surrounding system and treated as a 'black box' CAE tool, then the main requirements for a feasible system become the need to

optimise the system with respect to all design attributes and to operate within the time constraints of the design loop.

Meeting these requirements would be controlled by the CAE used, where a trade-off would be required between accuracy of predicted attribute behaviour and computational time. The use of the stable boundaries in this analysis has limited the scope and impact that the application of MAO may have. The assumption of stable boundaries has simplified the interaction between the system design and CAE team so that only rigid requirements and a single optimised solution are communicated. This approach also neglects to assess the effects of reaching an optimal design earlier in the design process. Both of these could affect the fundamental operation of the MAO process and the design system as a whole. The Systems Engineering approach is negating the desired benefits of the MAO approach, thus it is clear that the dynamic boundaries between systems within the design environment need to be considered.

3.3.4 A System of Systems Engineering Approach to a MAO Tool

One of the perceived benefits of MAO is conflict resolution between system attributes. Where a MAO process cannot resolve conflicts then there has to be some negotiation of the system requirements. This could be at the system level or even up to the product strategy level. This could change the assumptions made for common and carry over parts affecting the cost of the product. The MAO process must consider how such negotiations are initiated, directed and justified.

The tool could also affect the total design system as the early optimisation of a product will change the design process downstream. This could affect the timing of various design progression targets and the steps required to integrate all the systems within a vehicle. Possible questions regarding the total design system are:

1. How are the post-optimisation design iterations affected by the introduction of a MAO tool?
2. Does the system require greater or fewer design iterations?
3. Does the method require longer or shorter design iterations?

If the goal of the design process is to deliver a high value product while reducing cost and time of design, then the applicability of a MAO tool to every system must be considered. The resources such a method may use within the System Design and CAE teams may inhibit the analysis application to every product. Such a method may only be cost effective in areas where there are high amounts of conflict between systems or attributes. This raises a number of questions:

1. If the MAO tool is to be considered autonomous, how and when is it decided that the MAO tool should be adopted for a given system?
2. Is this decided by the CAE team alone or by input from both the CAE and system design teams?
3. Does every vehicle system and sub-system require the use of the MAO tool?

4. At what level should the MAO tool be applied?
5. How would process cost trade-off be assessed to find where the MAO tool would be most effective?
6. How would a MAO tool use its perceived effectiveness to belong to the design process?
7. How are the results of a MAO tool integrated with other analyses and optimisations provided by other methods?
8. Where are the various analyses integrated and how are they connected?

The discussion of the optimisation method showed a direct link between the product and the analysis method used to capture its behaviour. Increasing the level of the product from component level to system or system of systems level will require a different approach. Thus, the questions to be asked are, at what design level should the MAO approach be used and what level of detail would this application be able to resolve?

The introduction of a new tool to the work of the CAE team will affect its operation. The analysis of a system with more than one attribute will cross traditional CAE domains. This may require the use of a multi-physics CAE method. Questions addressing team composition and CAE working practices are:

1. Is it beneficial to have experts in domain or system when carrying out an analysis?
2. How would CAE operations change with MAO resource usage?
3. What additional resources are required for MAO?
4. What additional training is required?
5. The new process may also affect the communication and interaction between the system design and CAE teams. How must this be facilitated in the architecture of the support system?
6. What is the best method to input requirements to the MAO tool?
7. What is the most effective use of MAO results?
8. What system architectures need to be in place to facilitate the MAO input and output requirements?

When using multi-physics or other advanced CAE methods within the optimisation, consideration must be given to the following issues:

1. Has the CAE method been validated to ensure that the analysis can predict the system behaviour?
2. Is the new method stable enough to be used for the type and range of boundary conditions within the analysis application?
3. What additional support is required for the analysis method?

Finally, the emergent behaviour poses an unknown risk to the effectiveness of the total vehicle design system. The system of Systems Engineering approach does not attempt to control emergent behaviour as does the Systems Engineering approach. Instead, adaptation from other constituent systems is used to quell any undesirable effects. The risk for the total vehicle design system is that the initial introduction of a MAO tool may actually increase the time and cost required to develop a product, until such time as the other systems adapt. This risk may be unacceptable and prevent the inclusion of the MAO tool.

3.4 Requirements for projects

The System of Systems Engineering method has fundamentally changed how the feasibility of a MAO tool would be assessed. Using the Systems Engineering approach, the feasibility would be established by conformance to the requirements for such a tool. The System of Systems Engineering approach means that feasibility will be assessed on the dynamic emergent behaviour of the design system. The tool would be introduced to the design system and both improvements and deteriorations in the system performance must be measured. Then a cost benefit analysis would need to be established. From here, the requirements for applicability of such methods could then be defined.

However, this approach risks the deterioration in the performance of the product design system. A preliminary pilot tool that runs alongside but is not integrated within the design process should be used to investigate MAO methods that mitigate this risk. For this, strategies to overcoming the issues of design trade-off, sample size, error estimation and CAE modelling raised in the literature review should be further investigated. However, as the pilot project is 'offline' the interaction questions raised cannot be addressed. Instead, the pilot would be used to understand the MAO tool. Here, perceived detrimental effects could be removed or counteracted. This project may not be able to address all the possible effects, as some emergent behaviour may only be evident when the MAO tool is implemented or scaled up for high usage. Thus, any feasibility assessment should address the method over these timescales.

The feasibility study for a MAO tool in the automotive environment may require a number of projects in order to fully understand its effect on enabling an effective design. Firstly, the MAO tool needs to be understood and piloted. From this some implications on the affects of such a tool may be inferred. Secondly, a project examining the long term implications must be performed during the introduction and scaling up use of the tool.

The use of new CAE techniques within a MAO tool, such as the multi-physics fluid structure interaction available in Jaguar Land Rover standard CAE codes, represents a substantial risk. The methods are as yet unvalidated and the application resource requirements, stability and run-time is unknown. Application within a MAO tool may lead to failure due to the CAE being unable to return the system behaviours as required. To mitigate these risks the methods should be first examined as a stand alone tool and the potential impact on MAO inferred.

3.5 Research Methodology

The project requirements call for separate projects to assess the use of multi-attribute and multi-physics methods within the Jaguar Land Rover CAE environment. The methods need to be better understood so risk mitigation factors can be applied to 'online' methods. This requires that the issues of MAO and multi-physics CAE raised in the literature review are addressed. For this, projects based on application of the CAE simulation methods to known powertrain problems will be used.

Firstly, the assessment of multi-attribute methods will be carried out by the application of MAO to a known powertrain trade-off problem, allowing the investigation of trade-off methods, sample size and error estimation dilemmas. Secondly, the maturity of new multi-physics capabilities for fluid structure interaction methods within Jaguar Land Rover-preferred powertrain CAE codes (CD-Adapco StarCD and Abaqus) must be assessed for the cost and benefits of such an approach.

Finally, a discussion of the use of MAO as a systems engineering tool will draw on the findings of both projects. This will be supported by a casestudy to set the findings of the technical projects within the context of the Jaguar Land Rover product development system. The technical research projects are outlined in the following sections.

By applying the MAO and multi-physics methods to known Powertrain problems, the issues raised in the literature review can be explored as well as gaining an understanding of how the methods work in a design environment. The use of a casestudy then allows the opportunities and constraints that the design system could apply when using such methods to be explored.

3.5.1 The Jaguar XK Airbox Multi Attribute Problem

For the MAO project, the attribute trade-off that occurs in the airbox of the air intake system has been selected as the area of application. The design of an automotive airbox is characterised by the trade-off between the pressure loss and NVH attenuation and is a known issue within Jaguar Land Rover powertrain programs. The project will use the Jaguar XK sports car as a baseline for the airbox attributes. For the Jaguar XK Supercharged (SC) model, single attribute optimisation was applied to the design to minimise the pressure loss. However, this process delivered airboxes which were poor for NVH attenuation. This resulted in further work to correct the issue and a compromise on the pressure loss performance. The MAO method will be used to examine the airbox design space and the trade-off between conflicting attributes. To mitigate risk and allow the project to focus on the MAO problem, the CAE methods utilised should be mature and governed by Jaguar Land Rover standards. The project will require the following stages:

1. A review of the air intake system will be conducted to find the role of the airbox and outline the required attributes. The methods to assess the attributes should also be outlined along with the MAO approach, in particular the sampling size and error estimation methods. Here, the current single attribute optimisation procedures for metamodeling will be used as a starting point. A baseline for the performance of the Jaguar XK SC program should also be established.

2. The next stage is to apply the sampling methods to the system attributes, establish the metamodels and examine the accuracy of fit. The output of the CAE for each model should be interrogated to ensure that the model is providing a stable and correct attribute. Once verified the error in the metamodels should be investigated and a preliminary assessment of predictive behaviour established. From this, decisions about further sampling can also be completed.
3. Next, the metamodels should be used to find the best value design possible. Here, the various multi-attribute trading tools and methods available within modeFRONTIER will be used in order to find the best value design according to the criteria from the airbox problem definition. Finally, the optimised design selected from the trade-off methods should be tested with the CAE to find whether the method can deliver improved performance.

3.5.2 The Fuel Tank multi-physics Analysis Project

As there are no standard procedures for the use of coupled Fluid Structure Interaction (FSI) methods within Jaguar Land Rover, potential applications for the multi-physics methods need to be found. For this, the fuel tank was identified as the system of application. This had two distinct advantages, firstly there was a perception that the fuel tank contains opportunities for using FSI methods and secondly, some CAE applications for the fuel tank were in the process of being brought 'in-house' from suppliers. This provided an opportunity to review the analyses that the powertrain CAE department could supply. To assess the maturity of the multi-physics methods available within Jaguar Land Rover powertrain preferred CAE codes, the project will require the following stages:

1. The design progression and CAE requests at the various stages of the fuel tank design process should be explored. These explorations should culminate in the identification of the application for the multi-physics method and the various requirements that constrain the problem.
2. The boundary conditions and customer-use scenarios for the selected application should be explored and characterised. From this, the worst case scenario for the application can be established. This load case can be used to assess the coupling level requirement. Next, the characterisation of the new multi-physics CAE methods, should establish the suitability of the methods for the application. This should be done on simplified models to allow quick assessment of predictive behaviours of the fuel tank attributes.
3. For any applicable methods, the multi-physics CAE model parameters can be examined to see how the model can be set up for the required CAE method attributes stability, accuracy and resource utilisation. This would then require verification to assess the accuracy of the model. The model should be compared to a rig or in vehicle test to ensure that the model can predict the real behaviour of systems.

3.6 Conclusion

This chapter has used the application of optimisation methods in the CAE environment to examine the key enablers within the Jaguar Land Rover product design system. A 'System of Systems' viewpoint analysis was used as a tool to understand the design environment and explore the operation of a MAO method.

The potential impact of multi-attribute and multi-physics methods has been addressed in both a system and System of Systems manner. This identified key research areas, however, as the implementation of MAO methods presented a potential risk to the performance of the design system, risk mitigation strategies were the top priority. For this, the issues of trade-off methods, sample size, error estimation and multi-physics CAE methods raised in the literature review need to be addressed.

From this, a multi-attribute project of the airbox, in the air intake system, was scoped. The sample size and error estimation issues present two dilemmas which must be addressed to mitigate the risks of accuracy of the optimisation and the project time scale. This project will also investigate techniques which can be used to 'trade-off' attributes in the design process. This project will address these issues in three stages; firstly defining the airbox MAO project and the CAE methods to be used, secondly, building the metamodels to assess sample size and error estimation guidance, then finally, optimisation of the airbox design using trade-off techniques, here the benefits of the approach will also be examined. The context of the Jaguar Land Rover design system constrains the project to use standard CAE techniques and current sampling guidance as an initial starting point.

The multi-physics will be applied to the fuel tank, the first stage in this process is to find an application to develop an appropriate multi-physics CAE method. From this, the implementation of multi-physics CAE analyses to the selected application will be explored. This project intends to evaluate the efficiency and accuracy of the multi-physics when compared to single domain approaches. The multi-physics approaches are limited to only methods available within the Jaguar Land Rover tool-set at the time of the project.

Part II

Project Research

Chapter 4

The Airbox MAO Problem

4.1 Introduction

This chapter aims to define the airbox MAO problem, the approach taken to model the system and the sampling of the design space.

This project is based around the current Jaguar XK Super-Charged (SC) airbox. This airbox was designed using the current Jaguar Land Rover optimisation method, where the CAE methods used were completed serially and in isolation. CFD methods first minimised the airbox for least restriction of airflow, this was then compromised when the design failed to meet NVH requirements. This was remedied by the application of diffusers on the dirty side inlet of the airbox. However, these devices restrict airflow and increase the pressure loss across the airbox, representing a major trade-off between attributes.

This chapter describes the role of the airbox, defines the MAO problem and the optimisation approach that is taken. Also, the key performance attributes and relevant control factors are identified. From this, it can be seen that the pressure loss, capacity and NVH attenuation must be modelled with CAE.

The standard CFD modelling approach within Jaguar Land Rover for pressure loss is presented, then extended by using an empirical equation to yield the capacity of the airbox. The Ricardo WAVE method is then presented as the standard NVH attenuation analysis approach.

The parameterised CAD is detailed and the CAE modelling approach to the design space verified. The sample size dilemma is addressed and the minimum sample approach is taken in-line with the context of the project. Finally the base line performance of the Jaguar XK SC airbox is established.

4.2 The Automotive Airbox

4.2.1 Key Role and Operation

The airbox is a part of the air intake system, its key roles are to take ambient air from the environment to the engine, filter out any particulates and reduce engine noise. To achieve this, the airbox is designed with a number of key features such as a shaped volume, porous filter and NVH devices. Components and items before the filter are denoted as 'dirty side' elements and those after the filter as 'clean side'.

The shaped volume is determined by the breathing requirements of the engine and the packaging space available. Typical examples are rectangular cuboid and cylindrical shapes. The airbox volume must house the air filter. This represents a restriction on the airflow which can reduce the available power of the engine. This flow restriction causes a pressure loss across the airbox which must be minimised[69].

The airbox must also prevent any contaminants, such as dust and water, from entering the engine. For this, a porous filter is used to trap particulates but allow the passage of air. Over time, the filters become clogged, increasing the pressure loss of the air intake system and requires replacement at regular service intervals. The filter should be sized so it has sufficient capacity to meet scheduled service interval periods[31].

The airbox also forms part of the NVH package to remove the noise generated by the pistons and other ancillary intake components such as super and turbo chargers that is transmitted through the air intake system. This noise must be attenuated to meet noise standards and sound quality targets. While the volume of the airbox is a key contributor to the NVH attenuation, other devices such as diffusers and resonators can be utilised to reduce noise transmission[31].

The airbox also features Mass Airflow (MAF) sensors which measure the airflow rate through the air intake system to control fuel injection systems. This component should be kept free of contamination and requires uniform airflow in order to provide an accurate reading. These devices are mounted on the clean side of the filter after the airbox[109].

4.2.2 CAE analysis and Optimisation of Airboxes

There are a number of CAE methods that have been applied in the design of airboxes. Full 3D CFD techniques have been applied as a part a Systems approach to air intake development at Mahindra & Mahindra[31] and in the development of a prototype racing car at the University of L'Aquila[110]. Both of these examples used 3D CFD to view the airflow through the airbox volume. From this, design changes could be made to improve the flow characteristics. The research at Mahindra & Mahindra also included the application of 1-D gas dynamic analysis methods to NVH prediction[31]. Again, the CAE was used to understand the NVH characteristics of the design allowing design improvement to be targeted. Such methods have been standardised within the Jaguar Land Rover product development system (CFD methods[111] & NVH methods[112]) and are used in the design of all airboxes.

The next step on from using single CAE models for airbox design is to incorporate an optimisation method into the process. Branney[69] used genetic algorithms to optimise the design of a simple 3D airbox volume. The approach used StarCCM+ as the CFD analysis tool integrated with modeFRONTIER in an automated optimisation process. The research developed an optimisation tool to minimise the pressure loss across the airbox volume. Examples of metamodeling methods for airbox design are provided by Hoyle[113]. Hoyle[113] used a 2D simulation of an airbox for a racing car parameterised by 16 variables. 200 DoE points were used to build a Kriging metamodel of the pressure recovery coefficient, which was then maximised to give best breathing performance for the engine. Both examples show that the optimisation method can be used on airboxes to improve the design.

4.2.3 Airbox Design Within Jaguar Land Rover

Single attribute optimisation has previously been used at an early design stage on the Jaguar XK SC airbox to minimise the pressure loss, however, this design failed to meet the NVH targets. In a sequential approach to trading-off the airbox attributes, a diffuser was introduced on the dirty side inlet to the airbox and the diameter of duct was also reduced. The diffuser is an NVH device used to improve the attenuation performance of an airbox. The introduction of this device improved the NVH attenuation but increased the pressure loss of the airbox. The effect of this change is detailed in Figure 4-1 and Table 4.1. Figure 4-1 shows that the attenuation of the traded off airbox (blue line) is higher than the airbox optimised for pressure loss alone (red line). However this improvement comes at the cost of increasing the pressure loss from 1733 Pa to 2545 Pa. (N.B. These values are based on the simplified geometry and CAE used in this optimisation process, this is to negate the effect of other design changes allowing a direct comparison). This project examines the use of a Multi-Attribute approach to the optimisation and trade off of attributes in the airbox to find if an improved design can be found over the XK SC NVH Trade-Off airbox (hereafter referred to as the baseline).

Table 4.1: Parameters and pressure loss for XK SC pressure loss single attribute optimisation and NVH trade-off designs

Parameter	XK SC Pressure Loss Optimised	XK SC NVH Trade-Off
Breadth (mm)	140.0	140.0
Clean Duct Dia. (mm)	73.0	73.0
Clean Ingress (%)	0.0	0.0
Dirty Duct Dia. (mm)	93.0	68.5
Dirty Ingress (%)	0.0	0.4
Height (mm)	265.0	265.0
Inlet Runner (mm)	11.0	5.0
Length (mm)	233.0	233.0
Pressure Loss (Pa)	1733	2545

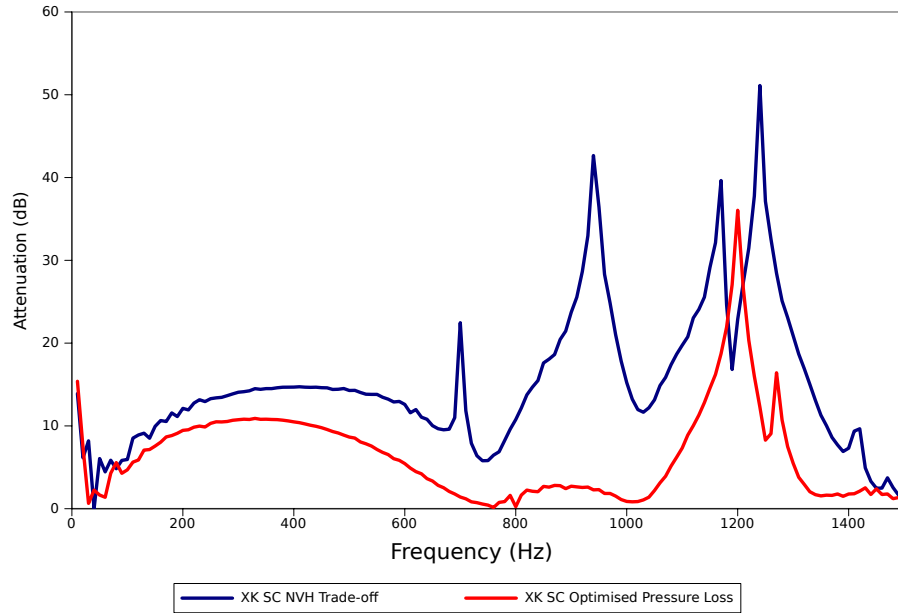


Figure 4-1: Attenuation spectra for XK SC pressure loss single attribute optimisation and NVH trade-off designs

4.2.4 Approach to the Multi-Attribute Airbox Optimisation Problem

The airbox multi-attribute optimisation problem will use a metamodeling approach to build a generic metamodel of the airbox design space. The metamodeling approach has been chosen because the CAE methods require manual input to the setup process. The literature review has shown there are a number of dilemmas when approaching metamodeling based MAO projects. The first is setting the sample size on which to build the metamodel. The second dilemma concerns the cost of estimating the error in the metamodel. The project must also reflect the constraint of working in the Jaguar Land Rover design environment. This means that:

1. The project must use standard Jaguar Land Rover procedures for attribute prediction.
2. The project would use the standard Jaguar Land Rover optimisation code (modeFRONTIER).
3. Due to the cost of the CAE methods, a minimal sample approach would be taken for building the metamodel and error estimation. For this, the standard single attribute optimisation sampling method (Ford optimally distributed latin hypercube[97]) will be used as a starting point. Initially no additional samples will be used as the error will be estimated using modeFRONTIER 'leave one out' methods.

4.2.5 Gathering the Airbox Requirements

This section follows the requirements gathering process that was employed in the optimisation of the airbox. The focus is around the examination and decomposition of the Air Intake System (AIS)

P-Diagram down to the airbox P-Diagram. From this, the attributes are discussed and targets and baselines for the optimisation set.

The operation and environment of the AIS is summarised in the P-Diagram in Figure 4-2 on page 79. The airbox is one of the key components in meeting the various challenges of the air intake system. It houses the filter and a number of expansions and contractions that restrict the air flow and effect noise attenuation behaviour. As structural behaviours are not the prime functions within this system at the concept stage, much of the structural detail remains undefined and will play no part in the optimisation of the airbox. This allows the P-Diagram to be reduced to the form shown in Figure 4-3 on page 80. This reduction also assumes that the airbox is a generic rectangular volume with a filter separating a dirty side inlet duct on the bottom and a clean side outlet duct on the top. Also, the input signal can be reduced to the engine pressure pulsations and the inlet of ambient dirty air as the hydrocarbon trap will not be considered. The key effects of this reduction can be seen in the noise and control factors and ideal function categories of the P-Diagram.

- *Noise Factors:* Some noise factors are out of the control of the designer, such as driver usage and environmental conditions. Other factors, such as part to part variation, require the component performance to be robust against the noise that these factors can introduce.
- *Control Factors:* While the first P-Diagram treated the control factors for the air intake system generically, the reduction to the airbox allows these to be explored in greater detail. Here, the key factors can be considered as the NVH devices, component volume, filter size and duct geometry. These generic terms can be further translated into more specific variables for the airbox such as the length and breadth which contributes to both volume and filter size and height, which contribute to the volume. The NVH devices and duct geometry can be parameterised by the diameter, length and entrance location of any diffusers.
- *Ideal Function:* Focusing on the airbox has allowed more detailed targets for the airbox to be specified; most notably the minimisation of the pressure loss, setting of filter efficiency and capacity targets subject to expected product usage, setting of broadband attenuation (10-600 Hz) and finally the need to provide the MAF sensor with a clean signal.

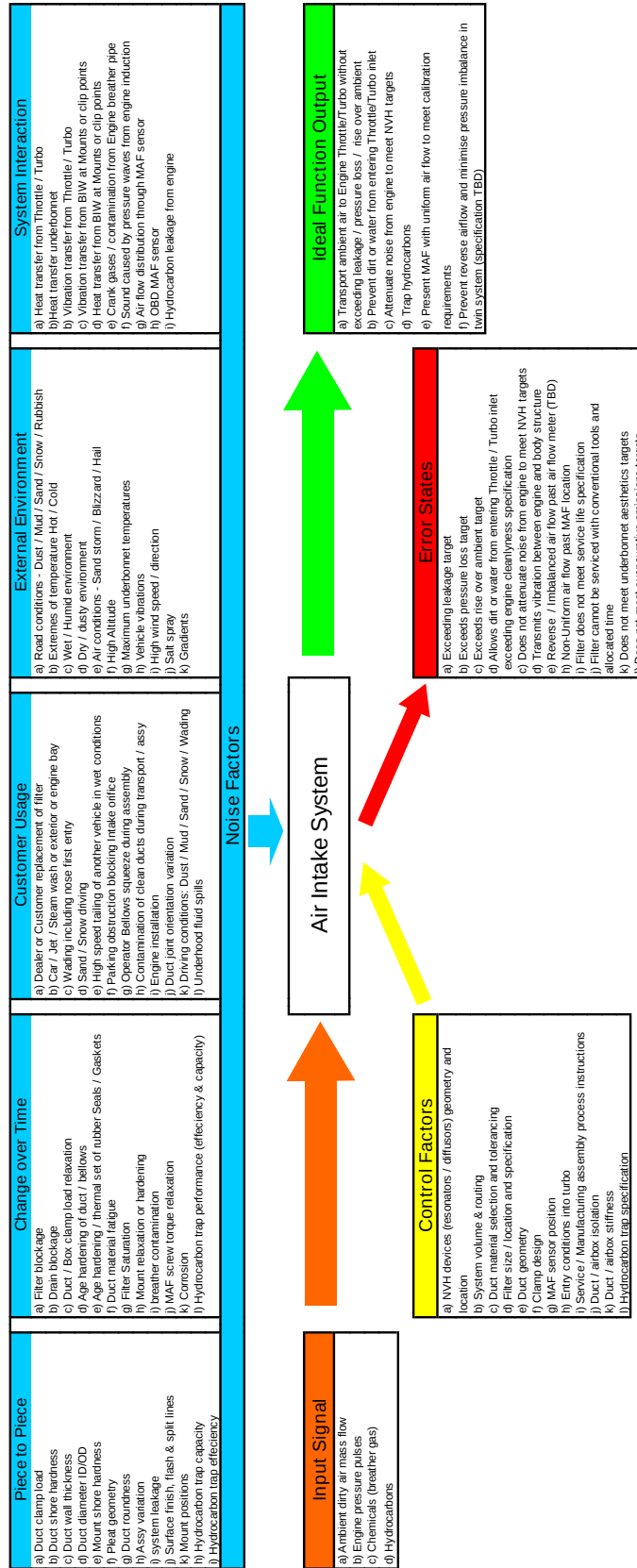


Figure 4-2: Air intake system P-Diagram

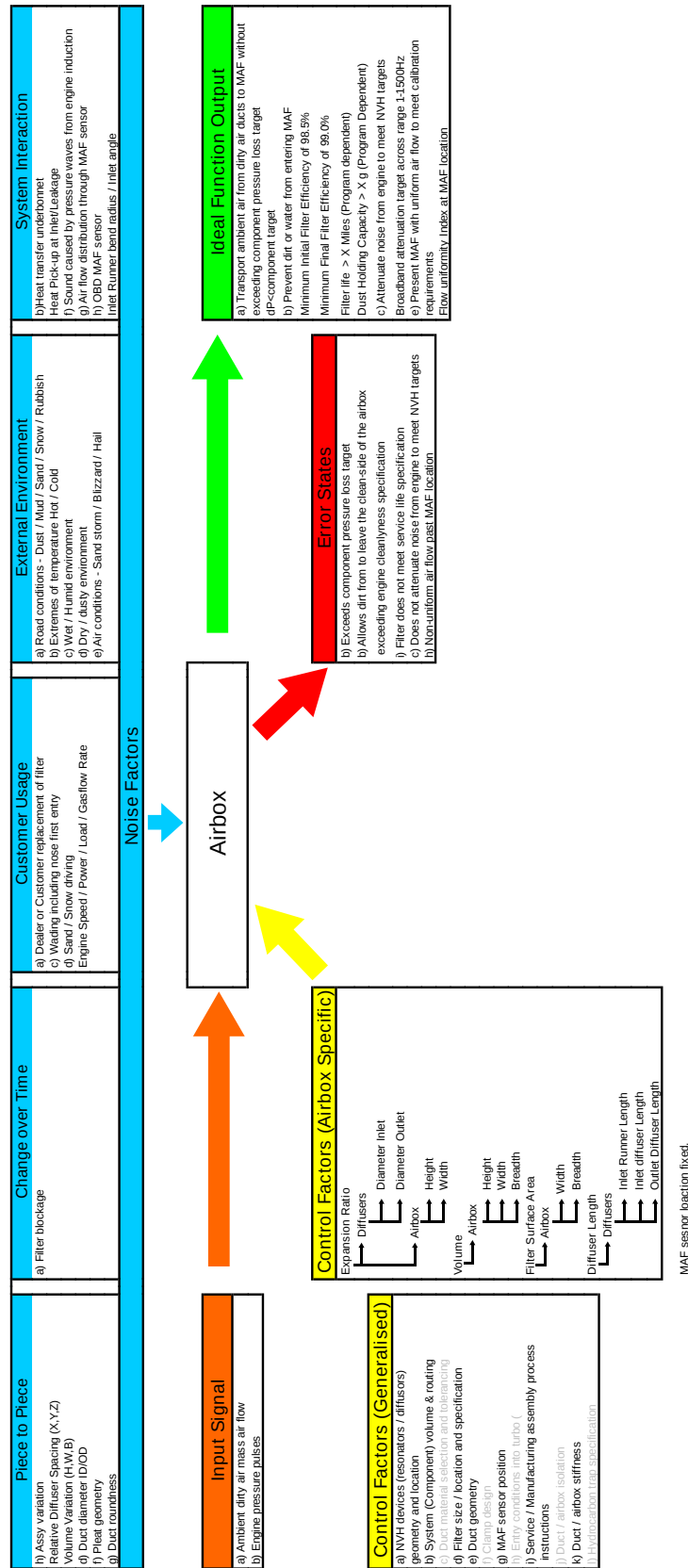


Figure 4-3: Extracted airbox P-Diagram

Using Figure 4-3 the requirements for the multi-attribute optimisation of a supercharged V-8 XK airbox can be summarised as:

- The optimisation method must consider the core control factors as variables, these are:
 - Component volume
 - Filter size
 - NVH devices in the form of diffusers on the clean and dirty side
 - Duct geometry
 - While this method is aimed at the XK SC airbox a more generic approach will be taken to encompass a larger design space.
- Standard CAE Methods will be utilised as the project focus is on multi-attribute methods rather than CAE procedures.
- The geometry will be simplified to represent the concept stage of the concept design phase.
- The standard CFD method applied to air intake systems will be used to measure the pressure loss.
- The pressure loss should be minimised to reduce the restriction effect on the engine.
- To assess filter life, an estimate of the capacity should be predicted from the standard CFD approach for the pressure loss.
- The capacity will be maximised to enable a longer service life.
- Assessment of attenuation must cover both V-8 fourth order noise (433 Hz) and supercharger whine (400-600Hz), using the standard Ricardo WAVE white noise simulation.
- The attenuation over this range must be maximised or approach the air intake system transmission loss target shown in Figure 4-4 and modelled by equation 4.1.

$$f(Hz) = -1.74168E - 17 \cdot Hz^6 + 9.72247E - 14 \cdot Hz^5 - 2.34060E - 10 \cdot Hz^4 \dots + 3.23952E - 7 \cdot Hz^3 - 2.72478E - 04 \cdot Hz^2 + 1.23293E - 01 \cdot Hz \quad (4.1)$$

- The Mass Air Flow (MAF) sensor must be included in the analysis with representative size and attached to the outside of the airbox.
- As no standard CAE method is available that can predict the MAF performance from the CFD model, the conditions that give preferable MAF signals will be implemented in the form of design guidelines and constraints. These requirements will be taken from supplier data and the experience of the AIS Team.
- The XK SC performance will be used as a baseline, this requires that:

- The optimisation method can maintain current attribute performance for one or more metrics if there are significant gains to be made on others.
- At the early concept stage there is a preference for pressure loss gains over NVH attenuation, this is due to the sporting image of the product. If NVH performance is met then the pressure loss becomes the optimisation priority.
- The current Jaguar XK SC airbox must be simplified into the concept form to enable baseline performance to be established.
- The packaging in the Jaguar XK means that a twin system will be used and there will be a volume limit of 9 litres for each single airbox.
- The Jaguar XK requires a total dust capacity of 200g for the whole air intake system or 100g per side.
- The maximum airflow rate is 1700 kg/hr for the total system or 850 kg/hr for a single airbox.

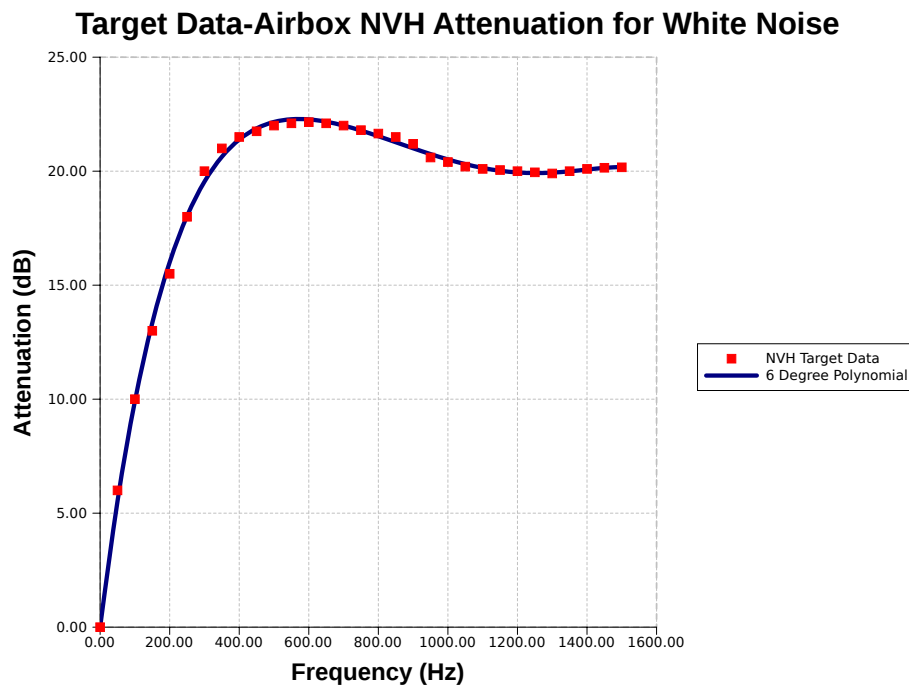


Figure 4-4: Air intake system transmission loss target

4.3 Standard CAE Approaches for Attributes

This section presents the justification for using the standard Jaguar Land Rover CAE methods to predict the pressure loss of an airbox, the capacity of the filter and the NVH attenuation performance.

4.3.1 CFD Methods for Pressure Loss Prediction

CFD is used as a standard method to predict the pressure loss across the air intake system during the design process. This approach has been developed to model the operation of the airbox in the vehicle at full load conditions which is the worst case scenario for pressure loss. The CFD model must represent a number of elements of the airbox such as geometry, filter elements and turbulent flow. To ensure robustness of the analysis, the CFD approach to air intake systems analysis has been standardised within Jaguar Land Rover[111]. The software Star-CCM+ version 3.64 is used at all stages of the airbox project.

Geometry Representation

The geometry representation begins with the CAD model. The detailed internal surfaces are extracted from the CAD and imported into the CFD software. From the geometry, a volume meshing strategy is applied, where the type and density is dependent on the geometry, software and computer platform on which the analysis will be completed. Star-CCM+ features three distinct mesh types; tetrahedral, trimmed and polyhedral. Of these, the tetrahedral meshes may not perform as accurately as polyhedral and trimmed meshes and require a more refined mesh [114]. The selection of mesh type and size should be determined using mesh dependence studies, where local refinements can also be investigated. Another important mesh feature is the prism layers applied to the wall boundaries. These aid in the solution of the boundary layers when using turbulence models[114]. Again, the number and size is determined by the modelling methods used and the geometry.

Filter Modelling in Star-CCM+

The filter representation within Star-CCM+ uses the porous media method. The filter is separated into its own region and then the flow conditions are restricted to represent the effects of a porous filter. The Jaguar Land Rover approach to porous media uses a directional set of viscous and inertial resistances that correspond to the directional features of the filters. Directionality comes from the pleated design of the filter as shown in Figure 4-5. The filter resistance parameters are described in Table 4.2, where ρ is the density of air and μ the dynamic viscosity. These have been provided by the Jaguar Land Rover standard approach to air filter analysis[111]. In Star-CCM+, these values are implemented by user field functions to calculate the resistances which can then be applied in the filter regions.



Figure 4-5: Directionality of the filter

Direction	Pleat Alignment	Viscous	Inertial
XX	Aligned	$4193000 \cdot \mu$	$43.76 \cdot 0.5 \cdot \rho$
YY	Across	$419300000 \cdot \mu$	$4376 \cdot 0.5 \cdot \rho$
ZZ	Normal	$41930000 \cdot \mu$	$437.6 \cdot 0.5 \cdot \rho$

Fluid, Flow & Turbulence Modelling

In the setup of the CFD model there are a number of other parameters that need to be set according to the standard. The flow solvers are set to second order segregated method[114]. The flow is modelled as an ideal gas where the material properties are set to air, using the standard parameters specified in Star-CCM+ material library. The fluid is initialised at a temperature of 298.0 K and zero velocity in all regions [111]. The model is initially solved assuming that the gas is incompressible until a stable solution is reached, then the compressible formulation is used. This approach aids the stability of the analysis.

The analysis standard calls for the realizable K-Epsilon turbulence model with two layer boundary modelling [111]. The initial fluid turbulent conditions are defined by a turbulent dissipation rate of $16.0 \text{ kJ/kg} \cdot \text{s}$ and a turbulent kinetic energy of 4.0 J/kg . The turbulence must also be specified at the inlet and outlet boundaries, this is done by setting the turbulence specification to a length scale. The standard setting calls for a value of 10% of the diameter. Within the filter, the turbulent intensity and viscosity ratios are set to 0 and 1 respectively, this specifies the non-turbulent conditions within

the porous region.

Examples of Application

Figure 4-6 shows the correlation of the pressure losses predicted by CFD methods (blue bars) to that of the measured losses taken during rig (purple bars) or dynamometer (white bars) testing at various flow rates of Jaguar Land Rover airboxes [115]. When the CFD predictions are compared to the actual performance for the 11 air intake system designs, Figure 4-6 demonstrates that the CFD method can be used to predict the absolute values and the trends in pressure loss behaviour and thus is fit for purpose in the airbox project.

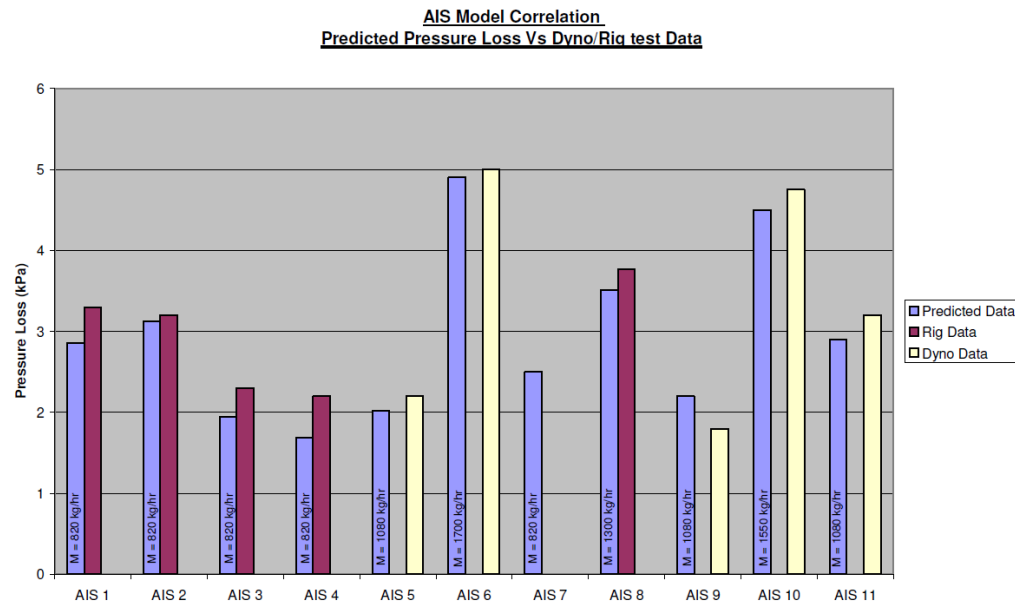


Figure 4-6: Correlation studies for pressure loss [115]

4.3.2 Capacity

The airbox project requires the assessment of the capacity of the air filter which gives an indication of filter lifetime so this can be compared to service intervals. A 100 gram capacity approximates to a 30,000 miles lifetime based on normal driving conditions [116]. Currently, the capacity is determined using a rig test, then this value is used to estimate the service life [116][117]. An attempt to predict capacity with CFD utilised a particle tracking method in a transient simulation[118]. This approach would require a separate analysis within the project. There was a need for a similar analytical predictor for the capacity within the airbox project, using the CFD model that predicts the pressure loss. This section examines the approach taken to fulfil this need. Current understanding of the filter

is that the capacity of the filter is dependent on the uniformity of the flow through it. The capacities obtained from physical rig tests were combined with uniformity predictions from CFD models of the same tests to derive an empirical formula for capacity prediction.

Flow Rig Testing

The capacity of an air filter is assessed using a standard rig test as outlined in BS ISO 5011:2000 [119]. As part of the validation of new vehicle programs, all Jaguar Land Rover airboxes undergo this test. The airbox is attached to a flow rig that allows the injection of dust particles upstream of the filter. Air and dust are put through the airbox at the expected maximum engine flow rate until the buildup of dust on the filter causes a pressure rise of either 20 or 25 mBar. Then the weight of the filter before and after the test is compared to find the capacity [119]. There are a number of test reports available for various models and engines. These have been summarised in Table 4.3 for six tests conducted with a 20 mBar pressure rise and Table 4.4 for the five 25 mBar tests.

Flow Uniformity from CFD Models

The flow uniformity (or gamma value) has been used to rate the performance of catalysts in analyses of exhaust systems. Here, the flow through the catalyst is given a rating based upon the flow velocity normal to the plane compared to the average velocity. The equation for Uniformity is given in equation 4.2 and is taken from the Ford Standard CETP 03.01-C-415 [120]. The CFD method used to obtain the pressure loss across the airbox has been applied to geometries for which capacity data is available. The flow uniformity was obtained from the filter side of the interface between the dirty side of the airbox and the porous region.

$$\gamma = 1 - \frac{\sum_{i=1}^n \sqrt{(U_i - \bar{U})^2} \cdot A_i}{2 \cdot \bar{U} \cdot A_{tot}} \quad (4.2)$$

- γ = The flow uniformity.
- n = The total number of faces on the surface.
- u_i = Velocity of flow normal to the face.
- \bar{U} = Average normal velocity through surface.
- A_i = Area of face.
- A_{tot} = Total area of surface.

4.3.3 Results

The results of the capacity rig tests, uniformity predictions from CFD modelling methods and geometric data for a number of Jaguar Land Rover airboxes is presented in Tables 4.3 and 4.4. The two tables represent the two different pressure rise conditions in the flow rig tests. This data was used to derive an empirical formula that links the capacity of an airbox to its geometric shape

and the uniformity of the flow through the filter. For this, the following logic is used to understand the processes that occur during the rig test:

1. The total weight of dust on the filter is proportional to the mass flow through the filter and the total testing time.

$$W = \dot{m} \cdot dt \quad (4.3)$$

2. The time taken for the test is proportional to the required pressure rise but inversely proportional to the rate of pressure change over time.

$$dt = \frac{\Delta P}{(dP/dt)} \quad (4.4)$$

3. The rate of change of pressure is a function of the change in resistance over the course of the experiment and the velocity of air through the filter.

$$\frac{dP}{dt} = f\left(\frac{dK}{dt}, V\right) \quad (4.5)$$

4. Velocity through the filter is dependent on the area, density and mass flow.

$$V = \frac{\dot{m}}{\rho \cdot A_f} \quad (4.6)$$

5. Resistance will increase as mass flow increases.
6. Resistance will decrease if area is increased.
7. Resistance will decrease if utilisation increases.

$$\frac{dK}{dt} = f\left(\frac{\dot{m}}{A_f \cdot \gamma}\right) \quad (4.7)$$

8. Relating all these equations, the capacity of the filter can be considered a function of the pressure rise, frontal area, utilisation and the mass flow.

$$W = f\left(\frac{\Delta P \cdot A_f^2 \cdot \gamma}{\dot{m}}\right) \quad (4.8)$$

Table 4.3: 20 mBar (ΔP) pressure loss test samples

Model	Engine	Flow Rate (\dot{m}) (kg/hr)	Capacity (W) (g)	Filter Size b_f by l_f (mm) by (mm)	Gamma γ (CFD)
LR322[121]	V8TD	960	420	172 by 370	0.6248
LRT5[122]	V8PSC	992	400	212 by 280	0.6705
LR322/T5[123]	AJ133	850	248	150 by 330	0.6477
LR538[124]	DW12C	670	202	241.5 by 163	0.6765
LR538[124]	SI6	720	195	241.5 by 163	0.6686

Table 4.4: 25 (ΔP) mBar pressure loss test samples

Model	Engine	Flow Rate (\dot{m}) (kg/hr)	Capacity (W) (g)	Filter Size b_f by l_f (mm) by (mm)	Gamma γ (CFD)
X150 (XK) [125]	AJ133	850	99.15	148 by 230	0.7823
LR359[126]	SI6	686	168.3	165 by 250	0.5436
LR359[126]	DW12	662	180.9	165 by 250	0.5443
LR538[124]	DW12C	670	202	241.5 by 163	0.6765
LR538[124]	SI6	720	195	241.5 by 163	0.6686

Figure 4-7 shows the relationship between the capacity and the right hand side of equation 4.8 for both the 20 and 25 mBar test cases. Examining the two rig tests as discrete sets, the R^2 values are 0.9719 and 0.9588 for the 20 and 25 mBar test respectively. The linear functions for both are also given in Figure 4-7, the finalised equation for the 25 mBar test case is given in equation 4.9 where the length (l_f) and breadth (b_f) are in mm, ΔP is in mBar and \dot{m} is in kg/hr.

The rig assessment for capacity is completed at the maximum flow rate for the product in question. As this is also the worst case scenario for the pressure loss, the same CFD model can be used to assess the capacity and pressure loss.

This empirical model for the capacity is a significant contribution to knowledge. Previous attempts to calculate the capacity have required physical testing with prototyped parts or expensive CAE models[118]. As this model can obtain the capacity based upon a standard CAE method then there is a potential cost save for the design process. However, a number of assumptions have been made during the formulation of this empirical relationship. The uniformity is assumed to be constant throughout the rig test. This may not be true due to dust accumulation on different parts of the filter which will affect local flow conditions, changing the uniformity. The range of airboxes was also limited by availability of rig data and does not consider many different sizes and aspect ratios. This could be an area for further work and investigation.

$$W = 10.29 \cdot \frac{\Delta P \cdot (l_f \cdot b_f)^2 \cdot \gamma}{1000000 \cdot \dot{m}} - 174.27 \quad (4.9)$$

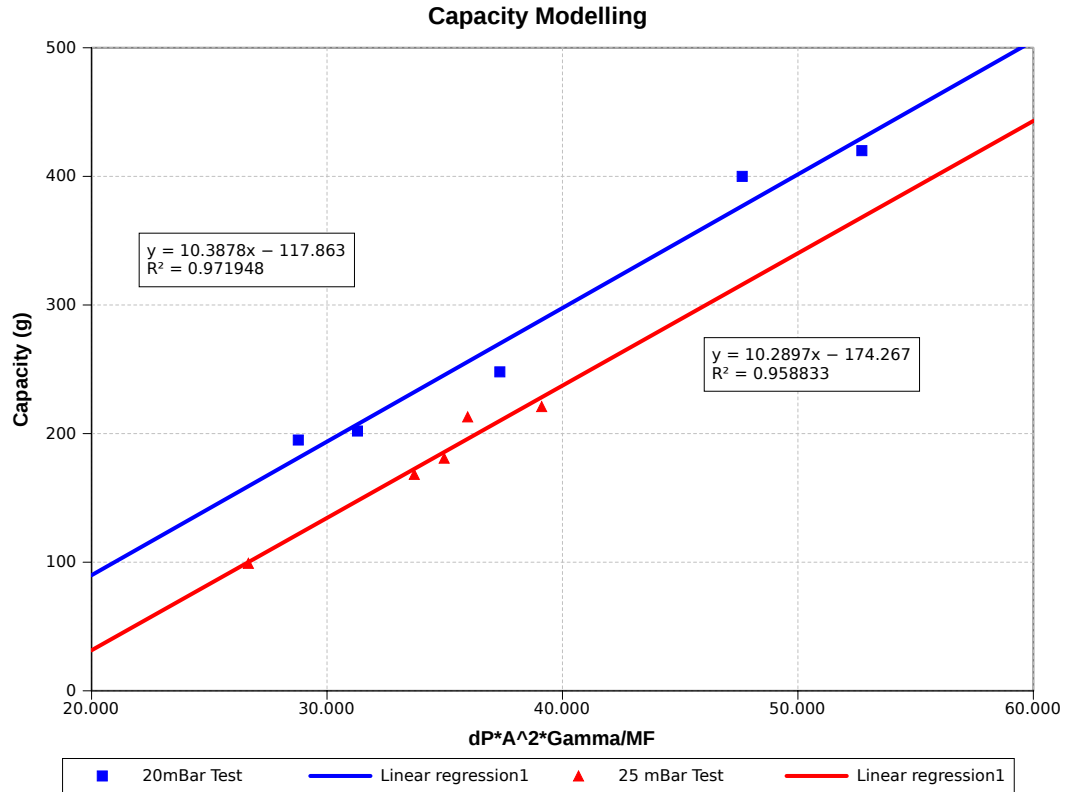


Figure 4-7: The empirical filter capacity model

4.3.4 Transmission Loss of an Airbox

This section examines the use of the 1-D gas dynamic code Ricardo WAVE to assess the NVH characteristics of air intake systems. The standard rig test of NVH attenuation is outlined along with the method used to approximate this test in Ricardo WAVE. The attenuation characteristics of a Jaguar XK Naturally Aspirated (NA) airbox obtained from both a rig test and WAVE analysis will be compared to examine the fitness for purpose of 1D gas dynamic methods.

NVH Rig Testing

The rig procedure for NVH transmission loss evaluation is based around the transfer matrix method[112]. This method is applied as the rig test cannot be conducted in a true anechoic (non-echoing) termination of the airbox as utilised in the WAVE model. To model these conditions, two frequency spectra measurements are taken using a four microphone system. One measurement is taken with the end of the airbox open into the NVH assessment chamber and the other is taken with the end of the airbox closed. A transfer matrix method is then applied to the two known boundary conditions and the anechoic condition calculated. The results from the rig measurements for the Jaguar XK NA airbox is presented as the blue line in Figure 4-10.

Transmission Loss Simulation with Ricardo Wave

As with the CFD model of the airbox, the geometry used in the WAVE model must also be discretised. Meshing breaks down the airbox volume into a network of ducts and complex y-junctions. WAVE provides two methods of doing this. Firstly, simplified shapes and ducts can be created in WaveBuild3D. However, this is limited to simple boxes as some finer detail may not be captured. The second method involves the use of surface geometry files, which are imported, then manually partitioned into the required mesh. The principal advantage of using the WaveBuild3D method is that the geometry definition can be automated, allowing for a shorter pre-processing time where multiple boxes need to be analysed. Also, the simplified geometry allows for a denser mesh for any given box size.

Meshing the Jaguar XK NA airbox

The complexity of the Jaguar XK NA geometry means that WaveBuild3D methods cannot be used and the airbox model must be derived from CAD. The mesh is imported into WaveMesher in *.stl* format which is then repaired and the boundary openings added. From here the geometry must be discretised into smaller volumes, ensuring that relevant expansions and contractions are captured. This is achieved by cutting the volume using various planes. The spacing of these planes will give various refinement levels in the simulation. Closer spacing gives greater mesh refinement and the ability to capture higher frequencies. Figure 4-8 shows three meshing strategies applied to the Jaguar XK NA airbox; coarse refinement (using planes approximately 60 mm apart), median (60 mm through the breadth and height and 40 mm on the length) and refined (40 mm in all directions).

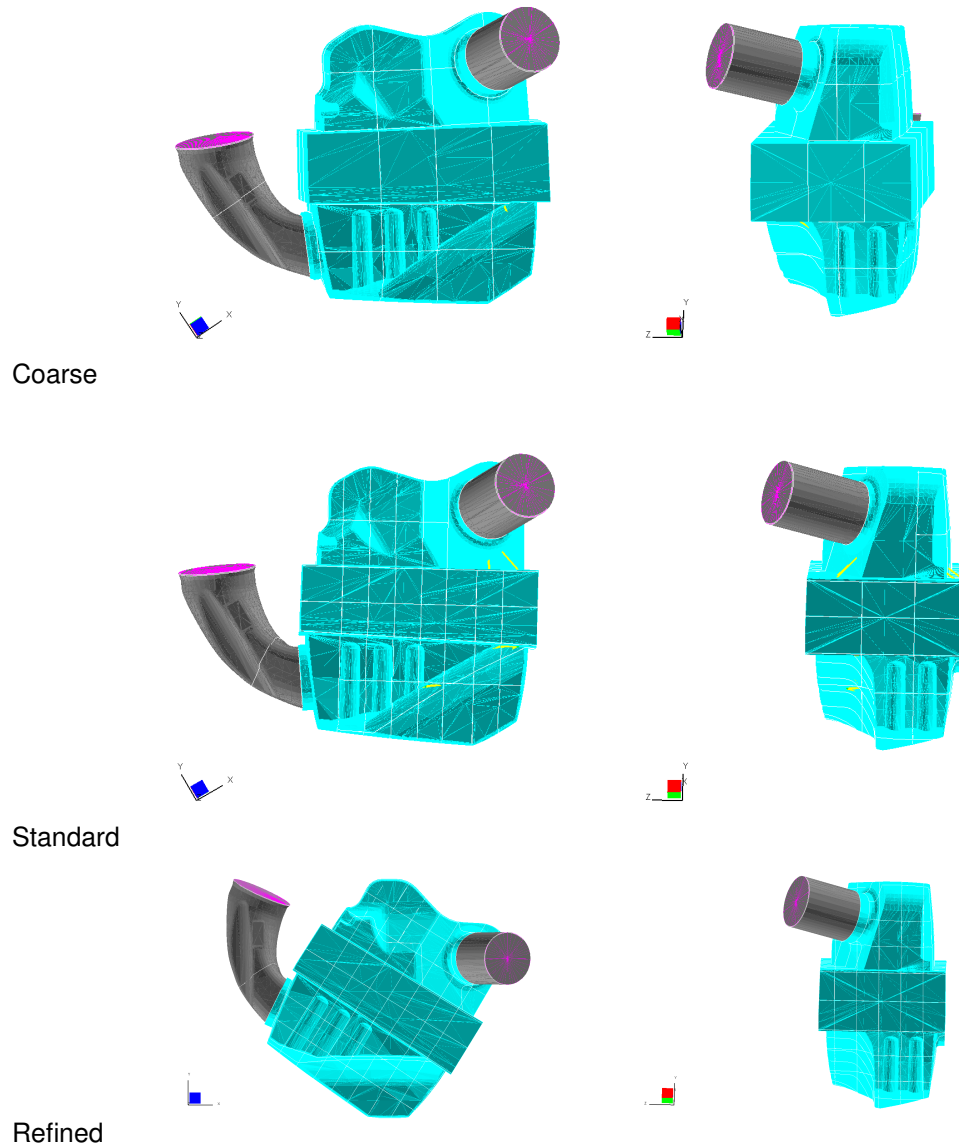


Figure 4-8: Meshing of the XK NA airbox

WAVE White Noise Transmission Loss Study Implementation

The white noise test introduces sound waves of various frequencies at the clean side of the air box where the intensity is measured by two microphones 40 mm apart. The sound waves then travel through the airbox volume where wave construction or destruction occurs depending on the various interaction effects between the geometric lengths and volumes within the airbox and the sound frequencies. The intensity of the sound waves when exiting the box is also captured by two microphones separated by the same distance on the dirty side ducts. When these two

signals are compared, the attenuation of various frequencies can be calculated. The WAVE model set up is outlined in Figure 4-9 with Table 4.5 detailing the setup of the various elements. The sound waves are introduced into the airbox by an acoustic piston. The airbox is represented by numerous complex y junction volumes, with the dirty side duct venting into the open represented by an anechoic termination. The ducts connecting the acoustic piston and the anechoic termination to the airbox are at the same diameter as the clean and dirty side ducts. This is so that no additional expansions or contractions are introduced into the system.

Table 4.5: WAVE transmission loss CAE setup

Tab	Parameter	Value
<i>Acoustic Piston</i>		
Noise - Multi Sine	Steady Velocity Component	0.2 m/s
	Amplitude	0.2 m/s
	Upper Frequency Limit	2000 Hz
	Lower Frequency Limit	10 Hz
Transmission Loss	Upstream Duct	wnp_duct.1
	Downstream Duct	wnp_duct.2
	Up 1 & 2	0.4 & 0.8
	Down 1 & 2	0.2 & 0.6
Ambient Conditions	Pressure	1.0 bar
	Temperature	283 K
Initial Fluid Composition	Fresh Air	1.0
<i>Anechoic Termination</i>		
Initial Fluid Composition	Fresh Air	1.0
<i>wnp_duct.1 & 2</i>		
Duct data	Diameters	Experiment
	Shape	Circular
	Discretization Length	25 mm
	Overall Length	100 mm
Ambient Conditions	Pressure	1.0 bar
	Temperature	283 K
Initial Fluid Composition	Fresh Air	1.0
<i>Simulation Control</i>		
General Parameters	Simulation Duration	10 Cycles
	Time Step Multiplier	0.8
	Max Degree Step	1.0 deg
	End of Cycle Angle	auto deg
Fluid Properties	Ideal Gas	N/A

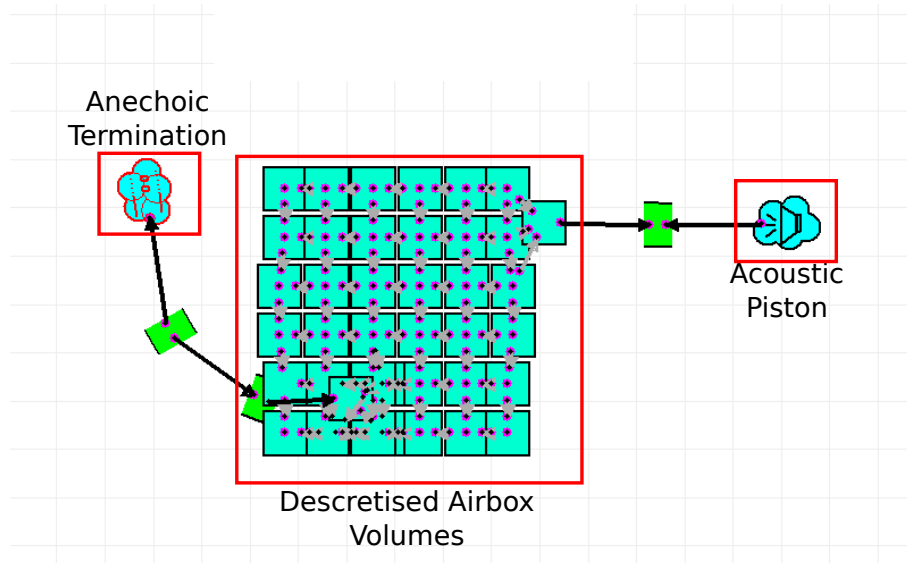


Figure 4-9: Example setup of transmission loss experiment in Ricardo WAVE

Results

Figure 4-10 shows the measured and simulated attenuation spectra for the Jaguar XK NA air box. The blue line shows the results from the physical test on the XK NA airbox. The three yellow lines show the simulated attenuation spectra at the various mesh sizes. The plot shows that the simulation is able to predict the trend of the box to frequencies of up to 600 Hz, after which the correlation becomes poor. This could be due to the oblique angles used in the airbox. These angles cause non-normal wave reflections in the airbox which cannot be fully captured by the meshing method. At frequencies below 200 Hz, the refined mesh correlates most closely to the measured data. As the frequency rises, the coarse mesh predicts values lower than either of the median or refined meshes, giving a better prediction within the 200-400 Hz range. In the 400-600 Hz range the median and refined meshes more closely correlate to the measured attenuation. As V-8 fourth order frequencies are dominant within the 67 Hz (1000 rpm) to 433 Hz (6500 rpm) region and super-charger whine within the 400-600 Hz region, WAVE models using a median to refined mesh can be used to capture the attenuation performance. To improve the NVH prediction above 600 Hz would require further refinement of the mesh. While this may be acceptable for smaller volume airboxes, larger volume airboxes may encounter software stability issues and poor computational performance during the meshing process. A median mesh is considered the best trade-off between speed and software stability for all regions of the design space.

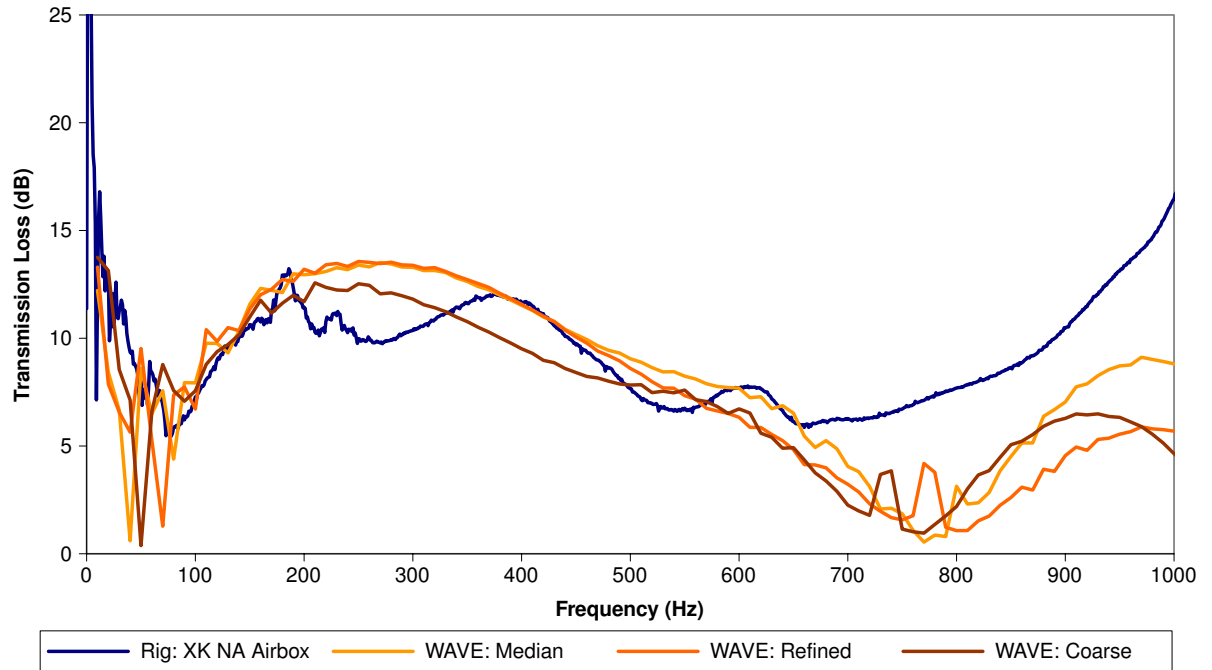


Figure 4-10: Correlation studies for transmission loss

4.4 Variables and Parametrised CAD Geometry

The core control parameters from the airbox P-Diagram and requirements list could be represented by many different design variables in the airbox. This section will show the selection of appropriate input variables, detail the range of the design space and the application of the Ford minimum latin hypercube sampling method[97]. Finally, the translation into a parametrised CAD model is discussed.

4.4.1 Selection of Variables

Some of the potential variables are outlined in Figure 4-11, each of these relates to one of the core control methods discussed in the P-Diagram (Figures 4-3). The first variables to be selected are the length, breadth and height of the airbox volume. These three values are important as they effect the pressure loss, NVH characteristics and the size of the filter.

The optimisation must also consider the NVH characteristics of the airbox design. For this, diffusers will be added to both the inlet and outlet sides. These diffusers are NVH devices that are used to tune the attenuation frequencies within the airbox. They also affect the airflow around the airbox and filter, which will change the pressure loss and capacity attributes. For example, large inlet and outlet diameters would improve the pressure loss attribute as the flow restriction is reduced, but decrease the NVH attenuation as the expansion ratio is reduced. As NVH attenuation is a wavelength problem, the diffuser lengths can be used to tune out undesirable frequencies but

would effect the flow uniformity through the filter. The key parameters for the NVH diffusers are the duct diameters, the length of the diffuser inside the airbox, the entry points and angles.

Increasing the number of variables would require an increase in the number of samples required to examine the design space. However, it is important to ensure that the key variables are selected. It was deemed important that the clean and dirty side diffusers be kept independent, doubling the number of NVH device variables. The key variables selected were the duct diameters (x2), diffuser lengths (x2) and the inlet runner length. This provides a total of 8 variables. All components before the filter are denoted as the dirty side and after the filter, the clean side.

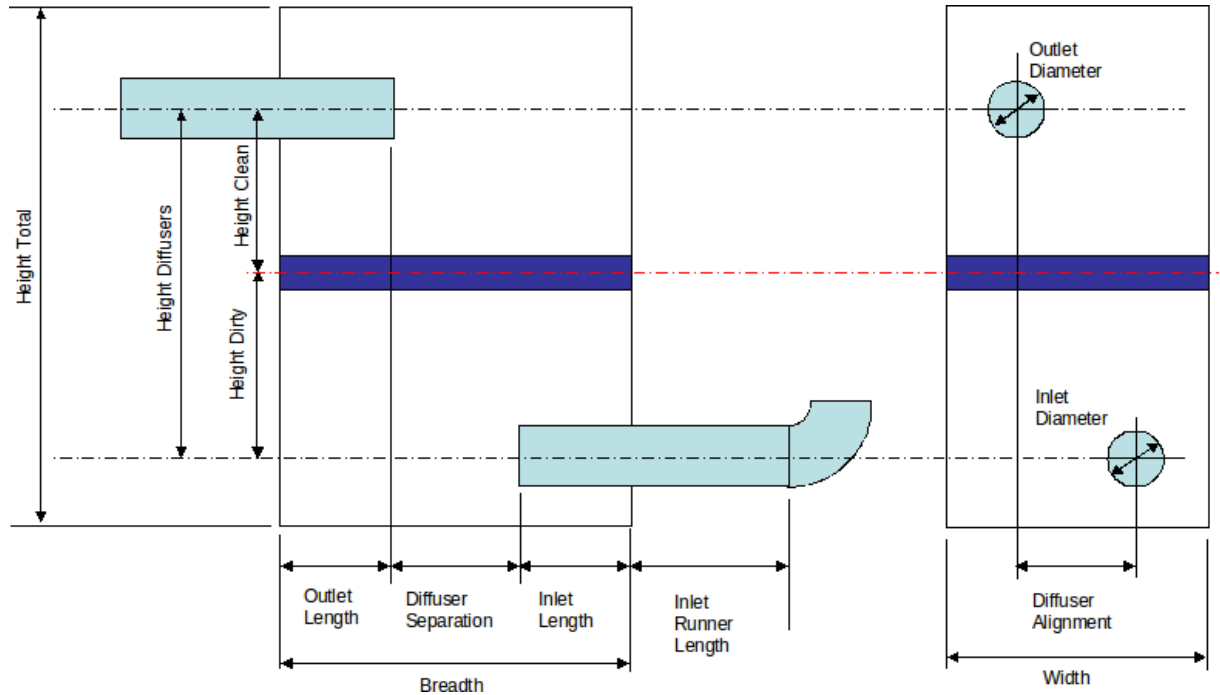


Figure 4-11: Simplified airbox with various potential variables

4.4.2 Selection of Variable Ranges

There is a requirement to approach this optimisation in a generic manner that will allow airboxes not commonly used within Jaguar Land Rover to be examined. The lengths, breadths and volumes of the airboxes used to derive the capacity equation are provided in Table 4.6. From these, the approximate heights can be estimated. These are only estimates as the airbox lids feature sloping faces and other complexities. The table shows that all of the current airboxes have an aspect ratio of greater than one (length is greater than breadth). It is desirable to examine airboxes that have an aspect ratio of less than one. Also desirable would be to include the effect of a larger variation in height. To incorporate this, the lengths and breadths will vary between 140 mm and 370 mm and the height between 260 and 330 mm.

The duct ingresses can be more difficult to set as they must be shorter than the airbox length to

Table 4.6: Current Jaguar Land Rover airbox volumes, breadths and lengths

Model	Variant	Volume m^3	Breadth mm	Length mm	Height mm
L322	V8 Diesel	17.0	172	370	267
T5	V8 Petrol	14.9	212	280	251
T5	V6 Diesel	14.9	212	280	251
T5	V6 Diesel	13.9	150	330	281
L322/T5	AJ133	9.2	148	230	270
L359	DW12C	9.8	165	250	237
L538	DW12C	9.8	163	242	248

ensure a valid geometry, limiting the potential range that could be investigated. To overcome this obstacle, the diffuser lengths would be defined as fractions of the overall length ranging from 0 to 0.75.

The duct diameters and inlet runner lengths were specified after discussions with the air intake systems team leader. The duct diameters will range from 50 to 80 mm and the inlet runner length from 5 to 300 mm. These ranges are broader than the potential use on vehicles allowing more atypical airboxes to be examined.

The minimum latin hypercube method requires a set of 33 samples to be used when the optimisation project involves 8 design variables[97]. This is slightly larger than the 3N scarce set specified by Jin, Chen and Simpson[12]. Using the macro provided from Ford[97], with the variables and ranges discussed, the 33 samples are presented in Table 4.7.

4.4.3 Development of a Parametrised CAD Model

From these eight variables, a parametrised CAD model was produced. This model is representative of an airbox concept within the package space. This includes a 48 mm filter section with the clean and dirty side ducts set evenly on either side. The airbox also features a 10 mm lip around the filter that is visible on the current Jaguar Land Rover airboxes. The MAF is of a representative size from measurements taken from the current sensor in use on the Jaguar XK SC airbox. This is so the duct blockage effect can be included in the CFD model. However, no internal details have been included. The MAF is not included in the WAVE model as it does not effect the NVH attenuation. The specification of variables in the CAD model is further detailed in appendix section B.1. The final airbox WAVE and StarCMM+ CAD models for design 17 are presented in Figures 4-12 and 4-13.

4.5 Using the Standard CAE for Airbox analysis

While the general use of CFD and 1-D gas dynamics for the pressure loss and airbox attenuation has been justified, this section will contain the setup strategy and mesh studies for the airbox.

Table 4.7: Variables for 33 latin hypercube sample

Design	Height mm	Length mm	Breadth mm	Clean Duct Diameter mm	Dirty Duct Diameter mm	Inlet Runner Length mm	Clean Ingress %	Dirty Ingress %
1	305.94	226.25	183.12	63.12	50.94	263.12	0.45	0.70
2	303.75	290.94	175.94	59.38	62.19	5.00	0.02	0.21
3	319.06	183.12	283.75	56.56	58.44	272.34	0.05	0.45
4	316.88	334.06	290.94	57.50	51.88	143.28	0.54	0.02
5	312.50	190.31	240.62	74.38	64.06	281.56	0.68	0.09
6	314.69	312.50	211.88	75.31	52.81	87.97	0.35	0.75
7	308.12	240.62	319.69	68.75	50.00	180.16	0.09	0.07
8	299.38	298.12	312.50	69.69	53.75	14.22	0.75	0.40
9	321.25	140.00	247.81	50.94	66.88	106.41	0.52	0.56
10	330.00	341.25	161.56	62.19	70.62	189.38	0.33	0.16
11	323.44	247.81	370.00	58.44	73.44	51.09	0.19	0.52
12	297.19	348.44	341.25	51.88	72.50	244.69	0.59	0.33
13	325.62	204.69	147.19	65.94	74.38	78.75	0.63	0.26
14	310.31	355.62	233.44	77.19	75.31	235.47	0.14	0.47
15	301.56	147.19	305.31	80.00	68.75	97.19	0.26	0.12
16	327.81	276.56	355.62	76.25	69.69	170.94	0.47	0.61
17	295.00	255.00	255.00	65.00	65.00	152.50	0.38	0.38
18	284.06	283.75	326.88	66.88	79.06	41.88	0.30	0.05
19	286.25	219.06	334.06	70.62	67.81	300.00	0.73	0.54
20	270.94	326.88	226.25	73.44	71.56	32.66	0.70	0.30
21	273.12	175.94	219.06	72.50	78.12	161.72	0.21	0.73
22	277.50	319.69	269.38	55.62	65.94	23.44	0.07	0.66
23	275.31	197.50	298.12	54.69	77.19	217.03	0.40	0.00
24	281.88	269.38	190.31	61.25	80.00	124.84	0.66	0.68
25	290.62	211.88	197.50	60.31	76.25	290.78	0.00	0.35
26	268.75	370.00	262.19	79.06	63.12	198.59	0.23	0.19
27	260.00	168.75	348.44	67.81	59.38	115.62	0.42	0.59
28	266.56	262.19	140.00	71.56	56.56	253.91	0.56	0.23
29	292.81	161.56	168.75	78.12	57.50	60.31	0.16	0.42
30	264.38	305.31	362.81	64.06	55.62	226.25	0.12	0.49
31	279.69	154.38	276.56	52.81	54.69	69.53	0.61	0.28
32	288.44	362.81	204.69	50.00	61.25	207.81	0.49	0.63
33	262.19	233.44	154.38	53.75	60.31	134.06	0.28	0.14

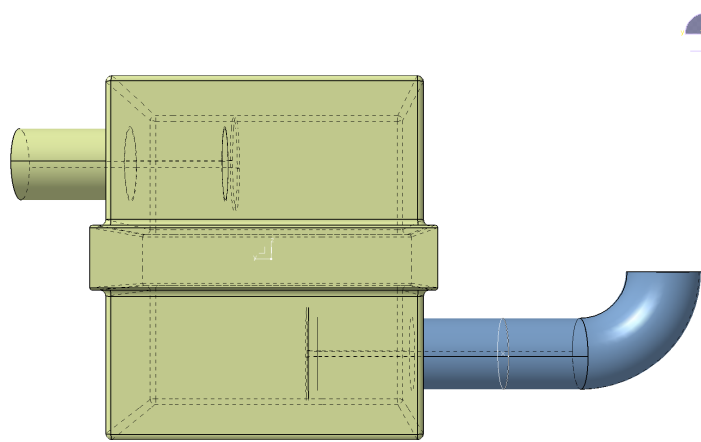


Figure 4-12: Finalised WAVE model geometry for design 17

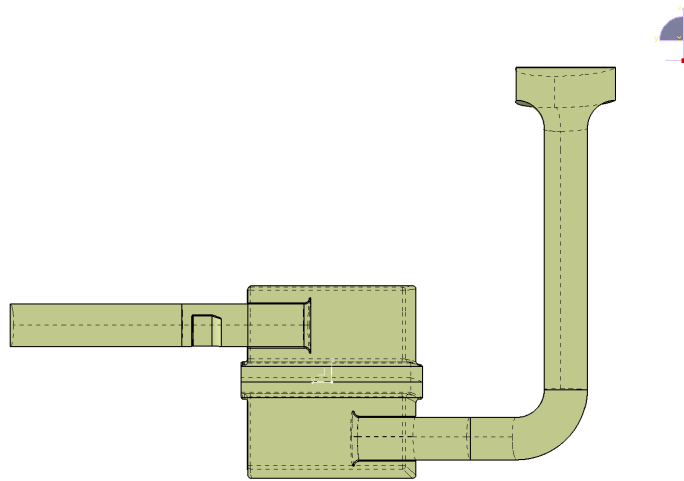


Figure 4-13: Finalised CFD model geometry for design 17

4.5.1 CFD Mesh dependence Study

While the standard procedure for the CFD analysis of airboxes calls for a global mesh size of 4mm [111], the dependency on the mesh should be known. The symmetry within the airbox model is exploited to reduce the model size and runtime. Initial experiments using the standard meshing procedure failed to yield a stable setup, this was shown by poor convergence in the measurable outputs. Using designs 7 and 10, a mesh refinement strategy was developed. This included refinement to 2 mm in the clean duct and dirty duct elbow and 1 mm around the bell mouth and MAF surfaces. This helped the convergence of the outputs and enabled a stable solution to be

found for compressible flow. The global mesh size was then varied to ascertain dependence on global mesh size. Tables 4.8 and 4.9 show that there are only small changes on pressure loss and gamma values except with the 2 mm mesh applied to design 7. When this was further investigated it was found that reducing to this mesh size introduced a pseudo-transient phenomena. The smaller cells were beginning to resolve large eddies around the jetting airflow from the dirty side duct. This meant that a single solution could not be reached causing the the pressure and gamma ratio to change between a number of states. To resolve this would require a fully transient model, which would increase the runtime and complexity of the simulation. Meshing with a 4 mm global size was selected for use in all models. The stability of this set up was then verified on designs 7 and 32, as these were considered worst case scenarios due to the small inlet and outlet ducts. The refinements to the mesh are displayed in Figures 4-14 and 4-15.

Table 4.8: Pressure loss mesh dependency study

Design	Mesh Size	Average (Pa)	Max (Pa)	Min (Pa)	Delta (Pa)	%
7	2 mm	7754	7773	7743	31	0.40
	3 mm	8000	8004	7996	8	0.09
	4 mm	8028	8037	8017	20	0.25
	5 mm	8043	8047	8040	7	0.08
	6 mm	7997	8004	7991	13	0.16
10	2 mm	2868	2868	2868	0	0.00
	3 mm	2878	2878	2878	0	0.00
	4 mm	2877	2877	2876	1	0.02
	5 mm	2881	2881	2880	1	0.02
	6 mm	2936	2936	2936	0	0.00

Table 4.9: Gamma mesh dependency study

Design	Mesh Size	Average	Max	Min	Delta	%
7	2 mm	0.379	0.387	0.376	0.011	2.817
	3 mm	0.419	0.420	0.419	0.000	0.060
	4 mm	0.429	0.429	0.429	0.001	0.130
	5 mm	0.430	0.430	0.430	0.000	0.045
	6 mm	0.466	0.466	0.465	0.001	0.139
10	2 mm	0.839	0.839	0.839	0.000	0.008
	3 mm	0.839	0.839	0.839	0.000	0.000
	4 mm	0.839	0.839	0.839	0.000	0.002
	5 mm	0.839	0.839	0.839	0.000	0.011
	6 mm	0.839	0.839	0.839	0.000	0.005

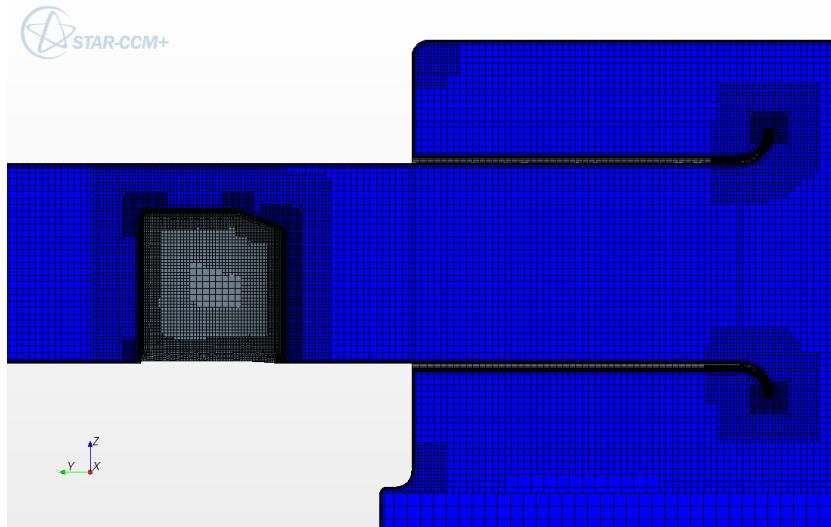


Figure 4-14: Mesh refinement around the clean side diffuser and MAF

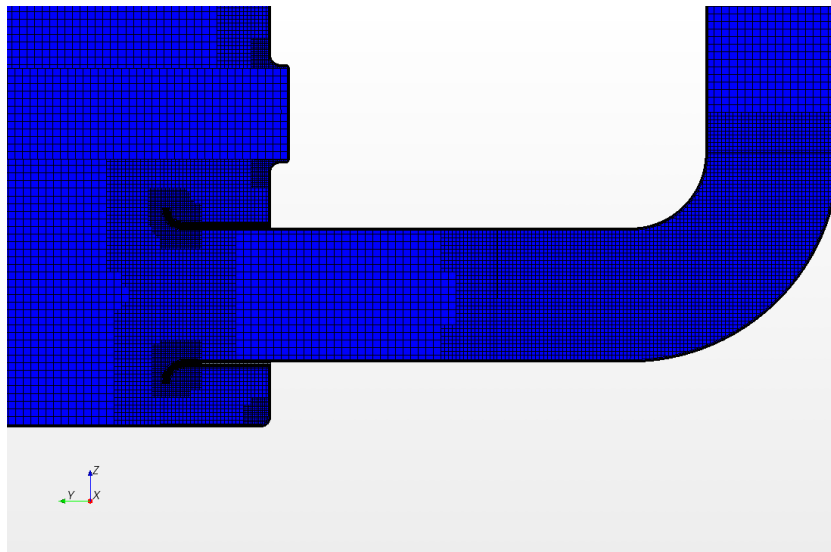


Figure 4-15: Mesh refinement around the dirty side diffuser

Setup Procedure

Star-CCM+ allows for automation of some of the setup procedure by use of java scripts. These must be recorded while one airbox was prepared by hand. This recording can then be played to set up other airbox designs. Not all steps in the CFD model setup could be recorded and these had to be completed manually instead. The geometry and mesh repairs also required some intervention as well as setting the face for gamma. The following is the procedure for the standard set up of the CFD model:

1. Export the airbox geometry from CATIA V5 as a step (.stp) file, import this into Star-CCM+ and repair.
2. Split the airbox into regions using the surface topology. This step introduces an inconsistency in the surface naming, meaning that the gamma functions must be manually set to the correct surface.
3. Run the setup java script, this sets up the physical and mesh conditions to the different regions in the model, sets up the porous media and all user coding. The solver parameters and data outputs are also included.
4. Set the gamma face to the front face of the porous region.
5. Surface mesh the airbox and repair if necessary.
6. Volume mesh the airbox and submit to the parallel solvers.

Once the job has been completed, i.e. the observed monitors and residuals have levelled off, the CFD model can be post-processed. This includes examining the residual plots, pressure loss and gamma convergence, then visualising the pressure and velocity distributions. The pressure loss and gamma measurements are then exported to data files for processing in Matlab. Here the average of the two attributes is taken over the last 200 iterations and the variance between maximum and minimum calculated, this was to gain a measure of the convergence of the model. The setup of a single airbox model takes an average of 60 minutes, the runtime 4-8 hours and the post processing 10 to 20 minutes on 16 cores in the Jaguar Land Rover HPC machines.

4.5.2 Ricardo WAVE Modelling

The approach taken in Ricardo WAVE was based on the standard procedure discussed in section 4.3.4. This showed that a median to refined mesh should be used, meaning that the volume should be partitioned at intervals of between 40 and 60 mm. However, initial applications showed that two key issues needed to be addressed. Firstly, the need to keep partitioning similar for each airbox and secondly, using the smallest discretisation length on the largest volume without causing instabilities within WaveMesher. Here, the large number of partitioned volumes for larger airboxes would cause the software to crash. This meant that a general 60 mm partitioning rule was applied to all the geometries. As the full geometry was used, the partitioning process was completely manual and required that the following features were captured:

1. *Dirty and clean side diffuser expansion:* As the diffuser opens into the airbox volume the expansion needs to be captured. A cut plane is placed 1 mm behind the front face of the diffuser bell mouth.
2. *Dirty and clean side bell mouths:* The expansion within the bell mouth needs to be captured, for this a section is placed at the beginning of the bell mouth.

3. *Filter expansion*: The airbox opens out slightly to allow the filter to be fitted, this expansion needs to be captured with planes just after clean and dirty side sections, i.e. the top and bottom faces of the filter.
4. *Airbox volume*: The volume must be divided up into 40-60 mm spaced sections.
5. *Dirty side duct bend*: Here a section plane is placed on the joint between the inlet runner and the inlet bend.

After the geometry has been partitioned, the resultant model is imported into WaveBuild. Here, the airbox is manually connected to the white noise generator and anechoic termination. The simulation is then completed. To obtain the NVH spectra, the Ricardo WavePost software is used. From this, the frequency and attenuation file have to be manually exported to a data file. The set up time for each wave job varies from 30 to 60 minutes and the runtime varies from 5-10 minutes depending on the volume of the airbox in question. Post processing the model and exporting the attenuation data file takes approximately 10 minutes per airbox.

4.6 XK Supercharged Airbox Base Line

Figure 4-16 shows the simplified geometry that represents a Jaguar XK SC airbox that will be used as a baseline. The airbox input variables are given in Table 4.10. The application of the Star-CCM+ CFD method yielded a pressure loss across the airbox of 2545 Pa and a capacity of 231 g. Images taken from the post-processing of this model give the pressure distribution (Figure 4-17) on the symmetry plane. The gamma metric is a measure of the uniformity of the z velocity through the front face of the filter. A contour plot of the z velocity displayed in Figure 4-18 allowed the uniformity to be visually assessed. The application of WAVE gave the NVH attenuation spectra shown in Figure 4-19 compared to the AIS target. These images along with the residuals were used to ensure that the CAE methods were operating correctly. The values were agreed as an acceptable baseline with the AIS team.

Table 4.10: Parameter & attribute values for XK SC airbox

Height	265.00
Length	233.00
Breadth	140.00
Clean Duct Diameter	73.00
Dirty Duct Diameter	68.50
Inlet Runner Length	5.00
Clean Ingress	0.000
Dirty Ingress	0.391
Pressure Loss (Pa)	2544.77
Capacity (g)	230.90

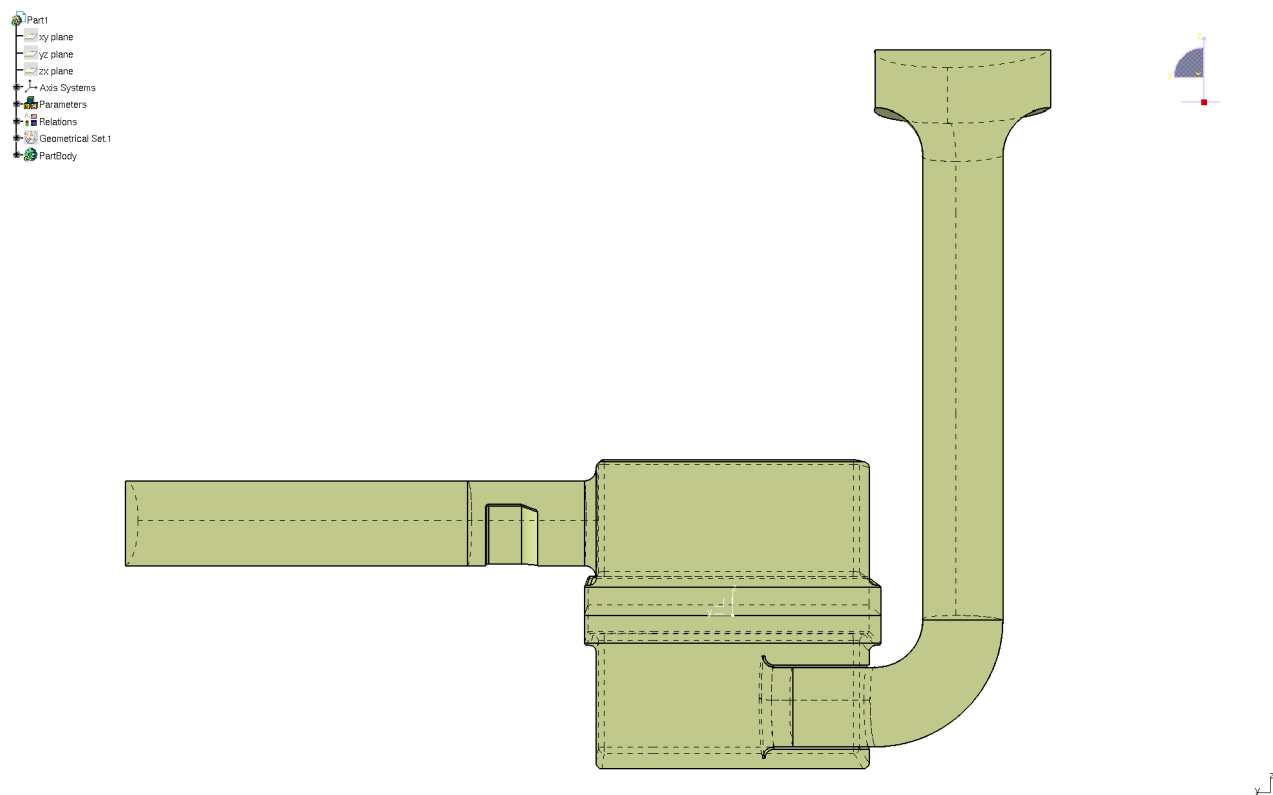


Figure 4-16: XK SC baseline geometry (CFD model)

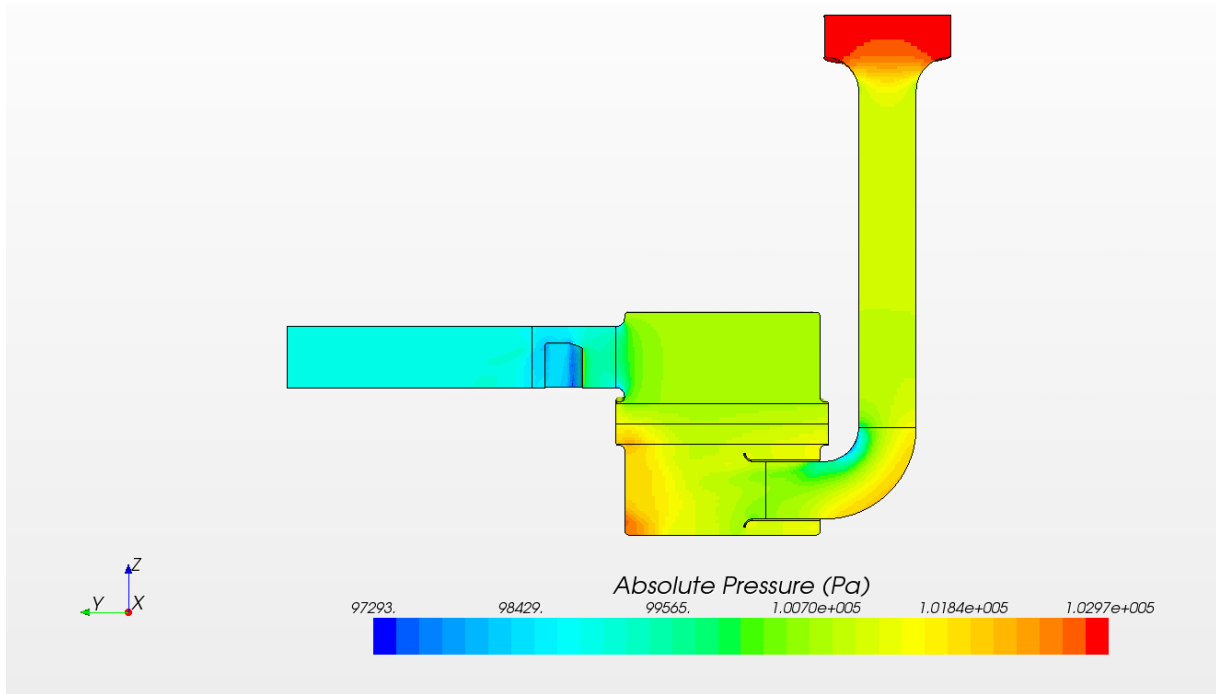


Figure 4-17: XK SC pressure distribution

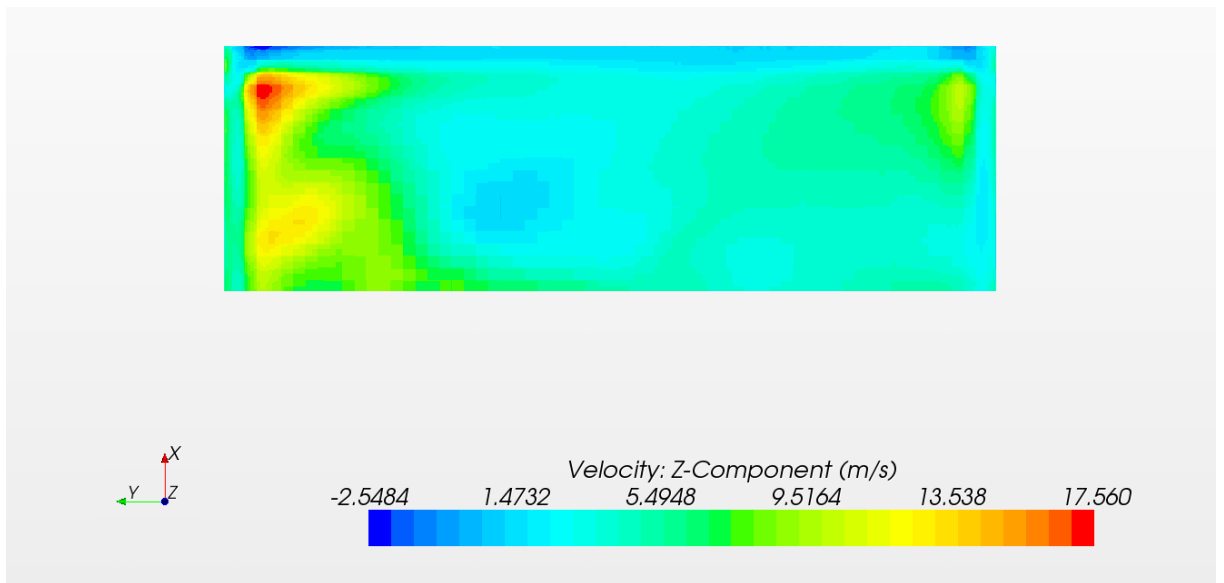


Figure 4-18: XK SC z-directional velocity through the filter

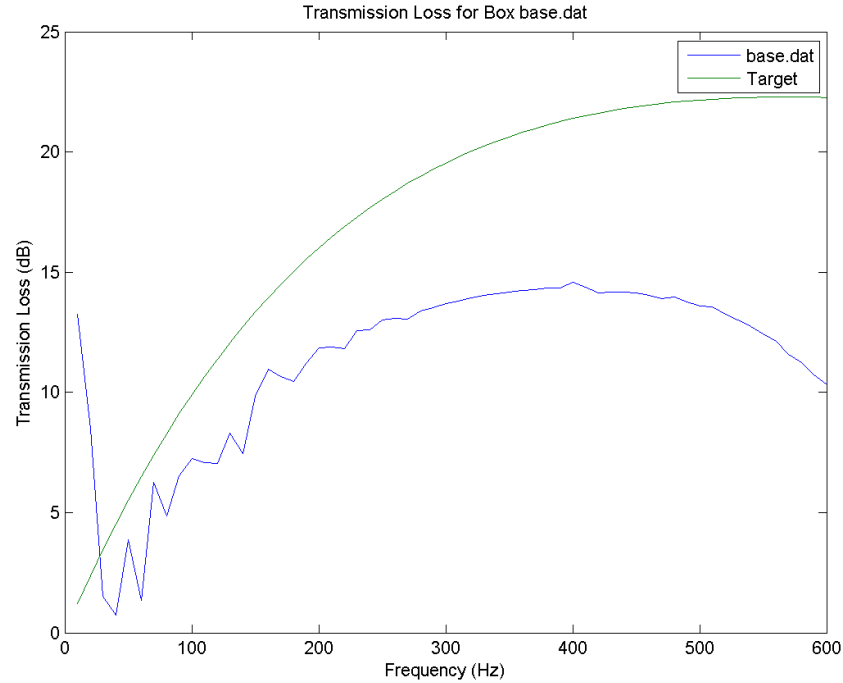


Figure 4-19: XK SC attenuation spectra

4.7 Conclusion

This chapter has defined the MAO problem for a Jaguar XK SC airbox. The trade-off attributes are the pressure loss, capacity and NVH attenuation of the airbox. The key control factors identified have been developed into a parametrised CAD model, with eight variables controlling the airbox volume and NVH devices. The specification for CAE methods were also set, allowing the pressure loss, capacity and NVH attenuation to be predicted with standard CAE methods. The application of standard Jaguar Land Rover approaches has been examined and verified throughout the design space. While there were further requirements to ensure that the airbox provides a clean signal for the MAF sensor, no CAE methods could be used to analyse this. The requirements would be implemented in the form of constraints in the optimisation.

The ranges of the input variables have been set to take a generic approach to allow exploration of the design space. As a starting point, a minimum sample approach has been taken to the metamodel build and error estimation process. This means that a scarce 33 latin hypercube sample has been used and initially, no additional error samples will be taken. Error estimation will be based on the 'leave one out' error methods in-built within modeFRONTIER.

The CAE methods were applied to a simplified version of the Jaguar XK SC airbox to establish a baseline in performance. The pressure loss baseline is 2454 Pa and a capacity of 230 g. The

attenuation spectra for the baseline was also presented in Figure 4-19.

With the requirements for airbox MAO project outlined, along with the definition and justification for the CAE methods used, the design optimisation can proceed. The next chapter details the use of the CAE, sampling and error estimation methods to build the airbox attribute metamodels. The metamodels are then used to find the optimum airbox design in chapter 6.

Chapter 5

Building the Airbox Metamodels

5.1 Introduction

The aim of this chapter is to build the attribute metamodels for the airbox MAO problem. In building the metamodels, the issues of sample size and error estimation will be addressed.

The dilemma between sample size and available time was raised in the previous chapter and for this work, a minimum sample approach was taken. This means that the scarce Ford minimum latin hypercube[97] and 'leave one out' error methods were used. This chapter explores the impact of this approach.

Firstly, the NVH attribute is examined. A single value metric is established and the error assessed. Based upon this result, further experiments on sample size and error estimation are carried out (detailed in appendix A). Further samples are then taken to improve the NVH metamodel.

Finally, the CFD results for pressure loss and capacity are presented. From this the metamodels are built then their accuracy is assessed.

5.2 NVH Meta-Modelling

This section addresses the assessment of NVH attenuation via a single value metric. The application of a radial basis function metamodel is detailed, along with the attempts to improve the predictive performance.

5.2.1 NVH Metric

The results from the Ricardo WAVE model come in the form of an attenuation spectrum (see Figure 5-1), which must be reduced to a single value metric to enable a metamodel to be fitted. The metric must capture the order of preference that distinguishes good NVH performance from poor NVH performance, by measuring conformance to the AIS NVH target model.

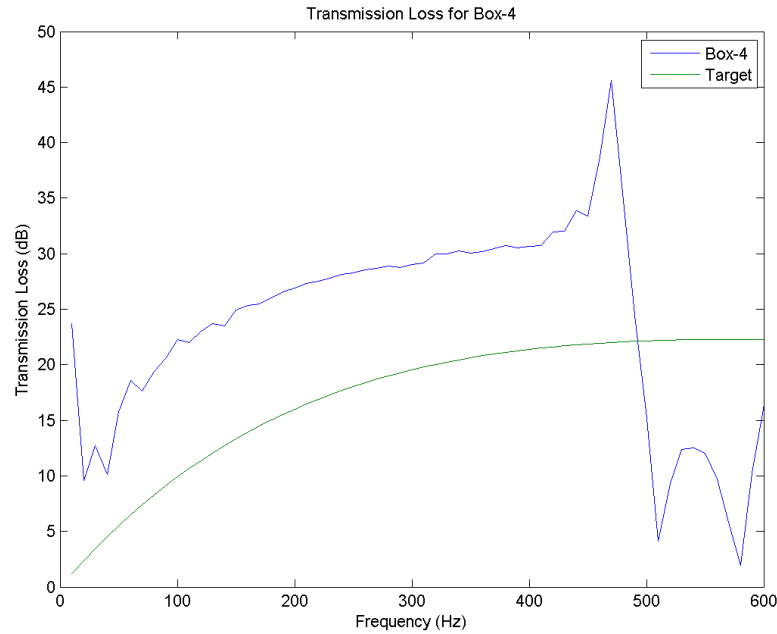


Figure 5-1: Attenuation spectrum for airbox design 4

Table 5.1: Rough airbox ranking orders

Group	Airbox Designs
Good	12, 27, 30, 31 & 32
Median	4, 9, 16 & 18
Poor	13 & 21

The 33 attenuation spectra were presented to a senior CAE NVH technical specialist who put them into an approximate ranking order by grouping the images (given in Table 5.1). While it was difficult to establish an exact best order, the groupings were used to help tune an attribute metric. Figure 5-1 shows that the NVH spectra may exceed the attenuation target in some areas but underachieve in others. While it is useful to exceed the target, there is no real gain compared to missing the target. A metric was derived that examines the area of the spectrum compared to the given target model which considered areas where attenuation is better than target and less than target. The areas above and below the target line were calculated. An individual weighting was then applied to each of these values and the results were added together. The weightings were then adjusted to give the same approximate airbox rankings. The finalised ranking order is given in Table 5.2. The calculation of the NVH metric was completed using the script in Appendix B.2.

Table 5.2: Airbox NVH metric and ranking

Design	NVH Metric	Rank	Design	NVH Metric	Rank	Design	NVH Metric	Rank
1	-1030	19	12	91	1	23	-576	9
2	-2021	28	13	-3888	33	24	-2888	31
3	-1047	20	14	-1193	21	25	-1924	26
4	-662	14	15	-2140	29	26	-903	17
5	-1666	24	16	-989	18	27	-4	5
6	-587	12	17	-622	13	28	-1600	23
7	-576	10	18	-696	15	29	-3361	32
8	44	2	19	-544	8	30	11	4
9	-1839	25	20	-823	16	31	-419	6
10	-2002	27	21	-2787	30	32	14	3
11	-586	11	22	-493	7	33	-1375	22

5.2.2 Initial Metamodel and Further Sampling Experiments

Initially, a radial basis function (Hardy's Multi-Quadratic) was applied to the data. However, the modeFRONTIER error estimator suggested that the metamodel had a poor fit as the calculated 'leave one out' normalised root mean square error was 0.1174 or 11.74%. Further research is required to understand the requirements for sample size and error estimation, however the high costs of the CAE prevent an in-depth study. The use of known mathematical functions to test new metamodeling methods has been demonstrated in the literature[74]. The Branin function has been used in a number of metamodel tests as it has a complex shape and is cheap to compute. Five experiments have been carried out to assess error estimation methods, sample size and distribution. The full details of the experiments are given in appendix A and the summaries are given below.

- *Experiment 1: Examination of the Literature Guidance on Sample Size*

The literature gave three boundaries for sample size guidance (as outlined in Table 2.6 on page 53) and scales the sample size by the number of inputs alone. For a two-dimensional function the smallest sample size would be 6 samples and the largest 20. This experiment incrementally increased the sample size from the smallest to the largest to assess whether this guidance can capture the complexity of the Branin function.

This experiment found that sample sizes guided by the literature are not sufficient to model the complexity in the Branin function. This also suggests that the scaling of sample sizes by the number of inputs alone may not be sufficient.

- *Experiment 2: Sample Size and Distribution for Error Estimation*

As a corollary of increasing the sample size to improve the metamodel fit, the estimation of global error in a metamodel would also be improved by increased sample numbers. The literature gave no clear indication to the size and distribution of any error estimation sample. This experiment examined the requirements for error estimation samples.

The experiment found that the sample size required for error estimation is potentially larger

than that required to build a metamodel. This may make the estimation of global metamodel error impractical. One potential method is to use small additional samples focused on local areas of interest (optimums or expected design regions) to understand local error.

- *Experiment 3: Comparing Seeded and Uniform Latin Hypercubes*

Within this project there are two latin hypercube methods available, the Ford minimum latin hypercube[97] and the seeded modeFRONTIER method. The Ford approach distributes the points uniformly through the design space whereas the seeded method does not. An examination is required to ascertain which approach should be used.

A uniform distribution of sample points is more robust and efficient than a non-uniform sample. This experiment also confirmed the conclusion from experiment 1. A sample size of 20 is insufficient for the Branin function, instead 33 samples are required. This value is 16.5 times the number of inputs.

- *Experiment 4: Comparing Sequential Sampling Methods*

The literature showed there is an interest in sequential sampling methods that place further samples in regions of interest. This experiment assessed the various sequential sampling methods available to the project to see if they can be used to improve metamodel performance.

This experiment showed that a smaller initial sample followed by sequential sampling methods can be more efficient than a larger initial sample. This is because these methods place samples in regions of high error or complexity allowing them to be resolved. Of the three methods available the MACK and EbL methods perform better but are harder to implement than the Lipschitz sampler.

- *Experiment 5: Examining the 'Leave One Out' Error Estimation Method*

The 'leave one out' error assessment method is seen as more efficient than the use of additional samples, however, concerns have been raised over how this metric can be interpreted. This experiment assesses whether this measure is fit for use in the airbox project.

The 'leave one out' error estimation should be interpreted as a dependency metric rather than an error measure. Used in isolation it can be mis-leading and has the potential to under or over estimate the error depending on the model. As this estimator is cheap to obtain it should be used, however, only in conjunction with error estimation based on additional samples.

From these experiments it is clear that further work on the NVH attribute metamodel is required. There is a dilemma as the cheap to compute 'leave one out' error estimation was shown to be a poor measure of the fit, yet the number of additional samples required for a global error estimate is prohibitive in a time constrained design environment. To overcome this the error should be assessed in areas of interest. For this the global maximum and minimum NVH attribute performance should be found, also the error on the baseline performance and additional airbox designs similar to the baseline should be used. The fitting error of these samples should then be used to assess the need for further samples.

The dilemma for further sampling is that the complexity of the NVH attribute behaviour within the design space is unknown, so it is not known if the sample size guidance in literature will be sufficient. However, the project is still operating in a time constrained environment meaning the minimum sample constraint still applies. As experiment 4 showed that sequential sampling methods can be used to resolve complexity in the metamodel this should be the first step.

5.2.3 Local Error Estimation & Lipschitz Sampling

To estimate the local error, the baseline Jaguar XK SC airbox, the maximum and minimum NVH performance airbox designs (obtained by applying a MOGAI optimisation on the NVH metamodel) and three alternative airboxes were selected. The variables for additional samples, the WAVE predicted NVH attribute performance values and the metamodel predicted values are given in Table 5.3.

Table 5.3: Additional airbox designs for NVH evaluation

Parameter	Maximum	Minimum	Base Line	Add 1	Add 2	Add 3
Breadth	370.00	140.00	140.00	140.00	140.00	140.00
CDD	52.00	80.00	73.00	73.00	73.00	73.00
CDI	0.66	0.45	0.00	0.00	0.00	0.00
DDD	50.00	80.00	68.50	68.50	80.00	76.00
DDI	0.65	0.38	0.39	0.00	0.00	0.00
Height	265.50	330.00	265.00	265.00	265.00	265.00
IRL	105.50	5.00	5.00	11.00	11.00	11.00
Length	370.00	140.00	233.00	233.00	233.00	233.00
NVH Metric	346	-5989	-2846	-3522	-4187	-3996
RBF Predicted	1055	-4841	-3086	-2999	-3193	-3125

The error assessment on additional samples showed that further samples would be required to improve the surface fit. The re-sampling examples shown in experiment 4 in appendix A demonstrated that the Lipschitz sequential sampler could be used to improve the metamodel performance. This method was applied to ascertain the effect of doubling the sample size. The additional Lipschitz sample points are included in Table 5.4. The error in the form of the R^2 and RMSE was estimated from the six sample points in Table 5.3 and the modeFRONTIER 'leave one out' error estimator was also used as a guide.

Figure 5-2 shows the changes in the error estimators when the number of samples was increased. All three error estimation methods suggested that the introduction of additional samples did deliver a small improvement in the metamodel performance, after an initial reduction in predictive power. However, the errors were still substantial. Table 5.4 shows that the points were mainly on the borders of the design space, meaning that the interior complexity was not being resolved. It was clear that a much larger sample would be required.

When the 'leave one out' errors are compared to the local R^2 and RMSE error estimation measures, the conclusion of experiment 5 in Appendix A is confirmed. While there is a loose correlation between the trends of the three measures, this is not true throughout the Lipschitz

Table 5.4: Parameters for additional sample points

Lipschitz Sample	Height (mm)	Length (mm)	Breadth (mm)	Clean Duct Diameter (mm)	Dirty Duct Diameter (mm)	Inlet Runner Length (mm)	Clean Ingress (%)	Dirty Ingress (%)
1	260.00	370.00	140.00	50.00	80.00	107.00	0.00	0.00
2	260.00	241.00	247.00	80.00	50.00	63.00	0.00	0.75
3	330.00	370.00	140.00	50.00	71.00	39.00	0.75	0.75
4	330.00	140.00	370.00	80.00	50.00	198.00	0.00	0.75
5	260.00	220.00	140.00	80.00	80.00	5.00	0.00	0.74
6	260.00	140.00	140.00	50.00	50.00	225.00	0.00	0.00
7	330.00	370.00	140.00	80.00	50.00	300.00	0.75	0.00
8	330.00	140.00	140.00	80.00	50.00	300.00	0.75	0.75
9	260.00	294.00	260.00	50.00	50.00	300.00	0.54	0.12
10	330.00	220.00	271.00	58.00	80.00	84.00	0.75	0.75
11	260.00	140.00	370.00	50.00	50.00	265.00	0.49	0.00
12	330.00	191.00	140.00	80.00	80.00	188.00	0.11	0.24
13	330.00	140.00	204.00	50.00	50.00	217.00	0.00	0.30
14	260.00	370.00	245.00	50.00	50.00	104.00	0.00	0.00
15	260.00	140.00	140.00	50.00	80.00	134.00	0.75	0.00
16	330.00	328.00	140.00	50.00	63.00	111.00	0.07	0.00
17	330.00	269.00	262.00	50.00	80.00	240.00	0.75	0.75
18	260.00	140.00	246.00	80.00	50.00	233.00	0.75	0.00
19	260.00	305.00	140.00	80.00	50.00	174.00	0.73	0.38
20	330.00	151.00	370.00	80.00	80.00	300.00	0.75	0.75
21	260.00	338.00	187.00	80.00	80.00	299.00	0.06	0.74
22	330.00	370.00	283.00	50.00	50.00	300.00	0.75	0.72
23	272.00	140.00	370.00	80.00	50.00	5.00	0.02	0.66
24	330.00	297.00	212.00	80.00	50.00	300.00	0.75	0.75
25	260.00	296.00	140.00	50.00	50.00	70.00	0.00	0.00
26	330.00	261.00	184.00	80.00	50.00	188.00	0.03	0.75
27	330.00	140.00	174.00	67.00	50.00	139.00	0.75	0.75
28	260.00	281.00	213.00	51.00	80.00	216.00	0.71	0.37
29	260.00	370.00	370.00	50.00	61.00	95.00	0.75	0.75
30	330.00	140.00	284.00	80.00	80.00	183.00	0.73	0.02
31	329.00	205.00	221.00	50.00	50.00	10.00	0.25	0.00
32	315.00	322.00	222.00	50.00	80.00	153.00	0.54	0.29
33	330.00	370.00	370.00	50.00	80.00	5.00	0.23	0.02

sampling procedure. After sample 48, the metamodel prediction of the 6 additional samples becomes poorer, however, the 'leave one out' error shows the metamodel to be improving. Again this demonstrates the risk of using the 'leave one out' error estimation in isolation.

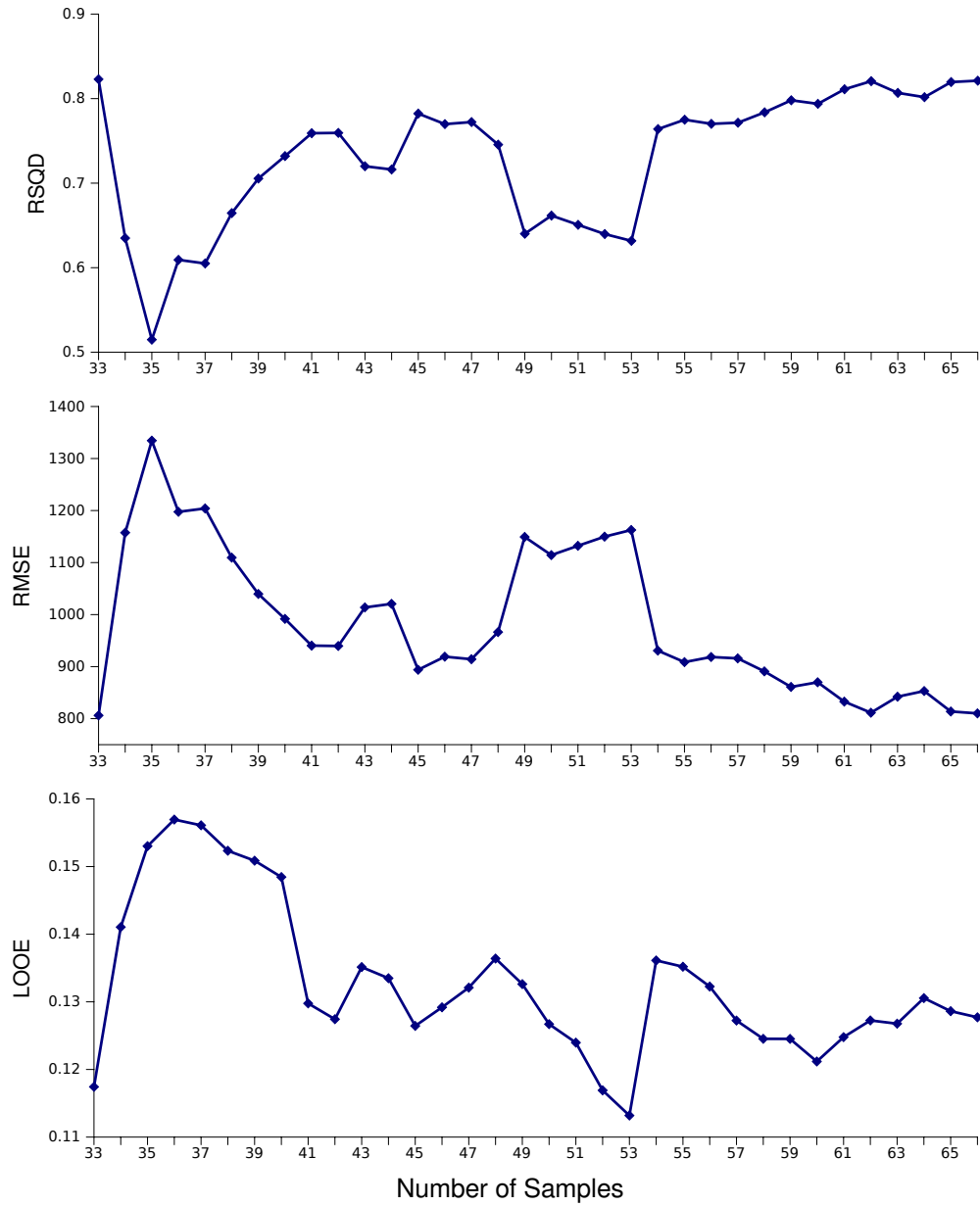


Figure 5-2: Error estimation with increasing Lipschitz samples

5.2.4 Increasing the Sample Size

The use of the Lipschitz sampler has shown that a larger sample is required. As the complexity of the NVH attribute behaviour is still unknown there is a dilemma over how large this sample size should be. The large sample guidance in the literature for an 8 variable problem suggests a sample size of 135 and the estimates from the Branin function 132 points. The closest uniform latin hypercube available is 129 samples, however the 30 to 60 minute set up time per design with the

conventional Ricardo WAVE method was prohibitive. To overcome this time cost the model needed to be simplified and the automation within WaveBuild3D exploited. The approach, automation and set up procedure of the NVH assessment models is described in appendix B.3. This allowed the set up time to be reduced to 10 minutes per design. Due to the simplified geometry a more refined mesh could be applied to the airbox with the discretisation length set to 40 mm. The first step was to assess the effect of the simplified method by comparing the NVH metrics generated by the full geometry with the metrics generated by the simplified method on the original 33 latin hypercube sample. The metrics and airbox ranks are given in Table 5.5.

Table 5.5 shows that the simplification to the WaveBuild3D method changed the airbox ranking orders. For a few geometries, designs 4 and 28 for example, the change is significant. However, generally the approach ranked the designs similarly with most airbox rankings only changing position by one or two places. Some of this could be due to the simplifications made in the geometry used in the WaveBuild 3D method, or the increase in discretisation refinement. The approach was accepted and applied to the 129 sample latin hypercube. The simplified model data, from the original 33 sample, was used to assess the errors in the surface and allowed the various metamodels to be compared.

Table 5.5: Airbox ranking changes for full geometry to simplified WaveBuild3D

Design	WB3D Metric	Full Geometry Metric	WB3D Rank	Full Geom Rank
1	-1633	-1030	23	19
2	-1890	-2021	24	28
3	-1326	-1047	21	20
4	-500	-662	6	14
5	-2249	-1666	27	24
6	-873	-587	16	12
7	-664	-576	11	10
8	-347	44	5	2
9	-2338	-1839	28	25
10	-2125	-2002	26	27
11	-896	-587	18	11
12	-340	91	4	1
13	-4061	-3888	33	33
14	-1510	-1193	22	21
15	-2483	-2140	29	29
16	-1277	-989	19	18
17	-828	-622	15	13
18	-639	-696	9	15
19	-601	-544	8	8
20	-878	-823	17	16
21	-3337	-2787	31	30
22	-777	-493	14	7
23	-563	-576	7	9
24	-2601	-2888	30	31
25	-2121	-1924	25	26
26	-741	-903	12	17
27	86	-4	1	5
28	-758	-1600	13	23
29	-3641	-3361	32	32
30	54	11	2	4
31	-653	-419	10	6
32	-237	14	3	3
33	-1304	-1375	20	22

Metamodel Selection

modeFRONTIER has a number of different metamodels which can be applied to the data. The scarce number of samples meant that the polynomial regression model could not be used. However, the literature shows that polynomial methods perform poorly in real examples and for global metamodels. The main metamodels to be examined were Kriging, Gaussian Processes, Radial Basis Functions and Neural Networks. The metamodel was fitted to 129 samples and the R^2 and RMSE calculated for the 33 latin hypercube sample. Within the main metamodel methods there are a number of different formulations and model optimisation methods that can be applied:

- In Kriging (KR) there are 6 formulations and 3 optimisation methods giving a total of 18 variations.
- With Radial Basis Functions (RBF) there are 3 applicable methods; Hardy's multi-quadratic,

inverse multi-quadratic and gaussian. Two non-applicable methods were the polyharmonic spline which failed during application and Wendland's compactly supported, which supports no more than 5 input variables.

- There are two optimisation methods on Gaussian Processes (GP).
- One formulation for Neural Networks (NN).

The error estimation of the metamodel formulation is compared in Table 5.6.

Table 5.6: Error estimators of metamodeling methods based on 129 sample points with 33 error estimation points

Name	Formulation	Optimisation	RSQD	NRMSE	LOOE
KR.0	Gaussian	Max Likelihood	0.8508	0.0965	0.0801
KR.1	Matern 5/2		0.8557	0.0949	0.0790
KR.2	Matern 3/2		0.8551	0.0951	0.0795
KR.3	Exponential		0.8470	0.0977	0.0872
KR.4	Rational Quadratic 0.5		0.8566	0.0946	0.0785
KR.5	Rational Quadratic 2.0		0.8557	0.0949	0.0787
KR.6	Gaussian	Max Leave One Out Predictive Probability	0.8486	0.0972	0.0798
KR.7	Matern 5/2		0.8543	0.0953	0.0788
KR.8	Matern 3/2		0.8557	0.0949	0.0796
KR.9	Exponential		0.8470	0.0977	0.0872
KR.10	Rational Quadratic 0.5		0.8559	0.0948	0.0783
KR.11	Rational Quadratic 2.0		0.8542	0.0954	0.0784
KR.12	Gaussian	Min Leave One Out Errors	0.7614	0.1220	0.1023
KR.13	Matern 5/2		0.7940	0.1134	0.0980
KR.14	Matern 3/2		0.7985	0.1121	0.0982
KR.15	Exponential		0.7923	0.1138	0.1023
KR.16	Rational Quadratic 0.5		0.7953	0.1130	0.1031
KR.17	Rational Quadratic 2.0		0.7976	0.1124	0.0987
RBF.0	Hardy's Multi-Quadratic		0.8563	0.0947	0.0786
RBF.1	Inverse Multi-Quadratic		0.8570	0.0945	0.0784
RBF.2	Gaussian		0.8597	0.0935	0.0904
GP.0		Max Likelihood	0.7932	0.1136	
GP.1		Min Interpolation Errors	-12.2970	0.9108	
NN.0			0.3095	0.2075	

Table 5.6 shows that there is little difference between the various Kriging and Radial Basis Function formulations with the Radial Basis Functions performing marginally better. It is quite clear that the application of Gaussian Processes and Neural Networks has led to large errors and should not be used for this application. The Radial Basis Functions will be used in this airbox project.

5.2.5 Comment on the NVH Metamodel

The increase in the number of samples for the NVH metric has shown that the global metamodel fit can be improved. However, there are still considerable errors in the surface. The additional 33 samples allowed the error to be estimated in the various metamodeling and input methods but the final metamodel surfaces should be made from all available points. This will be further discussed and validated in section 5.4.

5.3 Attributes Assessed by CFD Methods

There are two results from the Star-CCM+ CFD models that must be examined; the pressure loss across the airbox and the gamma value which is then used to calculate the capacity using equation 4.9. To examine the stability of the predicted results, the average value of the attributes over the last 200 iterations of the model is given, as well as the maximum and minimum allowing the variation to be assessed. The pressure loss results are given in Table 5.7 and the gamma results in Table 5.8. The script for data extraction is given in appendix B.4.

Table 5.7: Variation of pressure loss measurements over last 200 iterations of CFD model

Design	Average (Pa)	Max (Pa)	Min (Pa)	Variation (Pa)	Change (%)
1	7682	7713	7660	53	0.69
2	3846	3847	3845	2	0.05
3	5030	5030	5030	0	0.00
4	7441	7463	7409	54	0.73
5	3532	3544	3514	30	0.86
6	6099	6117	6082	34	0.56
7	8028	8037	8017	20	0.25
8	5867	5868	5867	2	0.03
9	5109	5218	5030	189	3.70
10	2877	2877	2876	1	0.02
11	2699	2699	2698	0	0.00
12	4193	4193	4192	1	0.04
13	2717	2751	2668	82	3.03
14	1842	1845	1837	7	0.40
15	2605	2609	2600	9	0.37
16	2366	2366	2366	0	0.00
17	3365	3375	3358	17	0.51
18	2177	2178	2177	1	0.03
19	2829	2831	2826	5	0.17
20	2406	2406	2405	1	0.03
21	2098	2101	2095	6	0.30
22	3800	3801	3800	1	0.02
23	3304	3312	3292	20	0.60
24	2356	2356	2355	0	0.00
25	2359	2360	2358	2	0.08
26	3383	3383	3381	2	0.04
27	4224	4233	4211	22	0.52
28	5295	5329	5236	93	1.75
29	4504	4505	4504	1	0.01
30	5609	5616	5601	15	0.26
31	6919	6937	6890	47	0.68
32	6364	6370	6357	14	0.22
33	5282	5287	5274	13	0.25

When examining the pressure loss results, it can be seen that most of the models exhibit very little variation (less than 1%) and can be considered to be converged. However, there are a number of airbox designs where there are large changes between the maximum and minimum. Designs 9, 13 and 28 all have variations of over 1%. These variations would seem to indicate some issue in the convergence and that the assumptions made during the mesh dependence study were not true

Table 5.8: Variation of gamma measurements over last 200 iterations of CFD model

Design	Average	Max	Min	Variation	Change (%)
1	0.594	0.595	0.594	0.001	0.123
2	0.743	0.743	0.743	0	0.003
3	0.637	0.637	0.637	0	0
4	0.529	0.53	0.529	0.001	0.188
5	0.732	0.732	0.732	0	0.034
6	0.447	0.448	0.447	0.001	0.28
7	0.429	0.429	0.429	0.001	0.13
8	0.387	0.388	0.387	0.001	0.134
9	0.813	0.818	0.806	0.011	1.41
10	0.839	0.839	0.839	0	0.002
11	0.612	0.612	0.612	0	0.002
12	0.635	0.635	0.635	0	0.046
13	0.853	0.856	0.85	0.007	0.817
14	0.739	0.739	0.739	0	0.008
15	0.722	0.723	0.722	0	0.03
16	0.55	0.55	0.55	0	0
17	0.599	0.6	0.598	0.001	0.215
18	0.664	0.665	0.663	0.002	0.315
19	0.602	0.602	0.602	0	0.006
20	0.703	0.703	0.703	0	0.005
21	0.796	0.796	0.795	0	0.008
22	0.588	0.589	0.587	0.002	0.398
23	0.723	0.723	0.722	0	0.049
24	0.813	0.813	0.813	0	0.001
25	0.825	0.825	0.824	0	0.004
26	0.637	0.637	0.637	0	0.005
27	0.563	0.563	0.563	0	0.085
28	0.778	0.779	0.778	0.001	0.139
29	0.821	0.821	0.821	0	0.003
30	0.396	0.397	0.395	0.001	0.359
31	0.612	0.613	0.611	0.001	0.219
32	0.585	0.585	0.585	0.001	0.088
33	0.765	0.765	0.765	0	0.018

in all cases. In the mesh dependency study, a stable and mesh independent method was derived around design 10 then the stability checked on the assumed worst case scenarios of designs 7 and 32. As these proved to be stable, it was assumed that the method could be applied to all airbox designs. In the airboxes with convergence issues, some region of the flow was not being resolved properly and would require adjustment in the mesh. As these variations represent only a small percentage of the attribute value, they were accepted. However, this may have some effect on the fit of a metamodel. The gamma values showed significantly less variation over the last 200 CFD iterations than the pressure loss and were all accepted as converged. Using the gamma values and the airbox length and breadth, the capacity values can be calculated with equation 4.9. These values were used in the metamodels.

5.4 Validation

This section will examine the validation of the pressure loss and capacity attributes metamodels built from 33 sample optimal latin hypercubes. The NVH metric attribute was based on the combined 161 samples (there was one repeat point at the centre which was only counted once). To assess the R^2 and RMSE error estimators, additional samples were used; The maximum and minimum for each attribute, the baseline XK SC airbox and the three additional samples. The maxima and minima were obtained by applying the modeFRONTIER NSGA II algorithms to the metamodels. The ten additional airbox designs are presented in Table 5.9. Each of the suitable Radial Basis Functions were also assessed. As the error was based on only a few points it is unlikely that it yielded a true estimation of the global error. The results should therefore be treated as a guide.

Table 5.9: Additional error estimation airbox designs

Design	1	2	3	4	5	6	7	8	9	10
Parameter	Pressure Loss Max	Pressure Loss Min	Capacity Max	Capacity Min	NVH Metric Max	NVH Metric Min	Baseline XK SC	A1	Additional A2	A3
Breadth (mm)	319	289	370	140	280.5	140	140	140	140	140
Clean Duct Dia. (mm)	51.5	80	50	65	50	80	73	73	73	73
Clean Ingress (%)	0.73	0.47	0.75	0.75	0.75	0.35	0	0	0	0
Dirty Duct Dia. (mm)	50	80	80	69	50	78.5	68.5	68.5	80	76
Dirty Ingress (%)	0.57	0.4	0.75	0.57	0.28	0.19	0.39	0	0	0
Height (mm)	316	297	330	260	260	326	265	265	265	265
Inlet Runner (mm)	226	152	300	50.5	300	151	5	11	11	11
Length (mm)	311.5	256	370	158	271.5	140	233	233	233	233
Pressure Loss (Pa)	9685	1537	4345	3726	10293	2537	2545	3700	2425	2752
Capacity (g)	976	1523	4238	32	798	-14	231	175	218	212
NVH Metric	-489	-1507	-1117	-4829	505	-6407	-3170	-3565	-4085	-3915

5.4.1 Pressure Loss Prediction

Table 5.10 shows the actual pressure losses for the 10 additional airboxes as well as the predicted values from the Radial Basis Functions. The three formulations for this metamodel method are the Hardy's Multi-Quadratic (HMQ), Inverse Multi-Quadratics (IMQ) and Gaussian (G) methods. Examining the overall trends, it can be seen that the metamodeling method can distinguish between airbox designs of good system performance and bad system performance. However, it cannot fully resolve the correct airbox attribute orders. Comparing designs 1 and 5, 3 and 4, 7, 9 and 10, it can be seen that the order in which they would be placed based on actual system behaviour does not equal the order in which the metamodel sets them. Also, it can be seen that the prediction of maximum pressure loss was affected by the poor metamodel. Design 5 was derived to give the maximum NVH performance but this airbox also exhibited a greater pressure loss than design 1. The predicted values on the metamodels show why this error has occurred; the prediction of the pressure loss of design 1 is greater than the prediction at design 5 (see Table 5.10). This transposition of order has large potential risks when using this metamodel in an optimisation process and would reduce the confidence in any result taken from it.

The table also shows that there is very little difference in the performance of the different Radial

Table 5.10: Pressure loss on 10 additional airbox designs

Design	Actual (Pa)	HMQ (Pa)	IMQ (Pa)	G (Pa)
1	9685	8199	8080	8243
2	1537	492	429	388
3	4346	3859	3949	4122
4	3726	4121	4129	4182
5	10293	8027	7792	7990
6	2537	1507	1635	1562
7	2545	2714	2737	2669
8	3700	2861	2892	2805
9	2425	1641	1858	1789
10	2752	2003	2139	2051
R^2		0.862	0.853	0.864
RMSE		1086	1122	1078
LOOE		0.096	0.098	0.111

Basis Functions. Based on the highest R^2 value and lowest RMSE value, the Gaussian formulation would seem to be the most suitable. However, the modeFRONTIER 'leave one out' error estimator suggests the Hardy's Multi-Quadratic would be the better option. The assessment of the Branin Function showed that the leave one out error could be misleading and as such the Gaussian formulation will be used.

5.4.2 Capacity Prediction

Design 6 of the additional airboxes assessed shows that there is potentially some error in the capacity estimation method. The negative capacity of additional design 6 in Table 5.9 is not physically feasible. The capacity attribute is derived from combining the capacity data from a number of rig tests on Jaguar Land Rover airboxes, the filter size and the uniformity index of flow through the filter from CFD models. As the empirical method only looked at available airboxes, the range of geometries tested was limited. Design 6 represents an airbox that is much smaller than any of the analysed airboxes. This shows that further work is required to examine more airbox designs over the working range to improve the empirical capacity model.

The predictive capabilities of the capacity metamodel show similar trends to that of the pressure loss. The overall trends of high and low capacity are captured but the absolute attribute prediction and airbox order ranking is poor. The lowest errors are seen using the Hardy's Multi Quadratic formulation, therefore this will be utilised.

Table 5.11: Capacity on 10 additional airbox designs

Design	Actual (g)	HMQ (g)	IMQ (g)	G (g)
1	976	1825	1819	1815
2	1523	1445	1448	1451
3	4238	4159	4096	4057
4	32	-246	-220	-200
5	798	1182	1178	1170
6	-14	-29	-4	17
7	231	710	723	736
8	175	762	782	801
9	218	858	876	889
10	212	823	842	858
R^2		0.846	0.841	0.835
RMSE		481	488	495
LOOE		0.076	0.076	0.077

5.4.3 NVH Attribute Prediction

The NVH metric metamodel is based on a much larger sample of 161 points, which should improve the surface predictions. It can be seen from Table 5.12 that the absolute predictions are still poor but the metamodel can predict the trends and airbox attribute ranking orders of the additional points. For example, the ranking order for additional designs using the Hardy's Multi-Quadratic metamodel is correct. The ranking order for the actual designs and the Hardy's Multi-Quadratic metamodel shows the best design is airbox 5, then 1, 3, 2, 7, 8, 10, 9, 4 and the worst design is airbox 6 (from Table 5.12). However, there are large errors in the absolute metric prediction. This shows that some of the surface complexity has been resolved in these regions but there are still errors to be addressed. For the NVH metric the most suitable metamodel based on this sample is the Hardy's Multi Quadratic.

Table 5.12: NVH metric on 10 additional airbox designs

Add. Design	Actual	HMQ	IMQ	G
1	-489	-305	-407	-625
2	-1507	-1248	-1200	-1113
3	-1117	-576	-1071	-2103
4	-4829	-4272	-4148	-4445
5	505	298	99	-349
6	-6407	-5991	-5862	-6124
7	-3170	-1986	-1878	-1703
8	-3565	-2982	-2916	-3058
9	-4085	-3306	-3168	-3232
10	-3915	-3203	-3090	-3164
R^2		0.909	0.888	0.860
RMSE		614	681	762
LOOE		0.077	0.077	0.083

5.4.4 Discussion

Final Metamodels

From the error estimators it can be seen that the scarce sampling has produced metamodels that have significant errors in terms of absolute attribute performance prediction and correct ranking of the airboxes. This suggests that the complexity of the system behaviour can not be resolved with the scarce sample set. The increase in the sampling of the NVH metric did show improvements in the errors of the surface. However, this does not address how many more samples would be required to reach an appropriately refined metamodel. Table 5.13 shows the improvements made on the prediction of the additional ten sample points based on a Hardy's Multi Quadratic Radial Basis Function. While some airboxes see substantial increases in predictive performance, designs 4 and 6 for example, increasing the number of samples deteriorates the performance in other regions (design 7). The sample set size has been increased beyond the large set suggested in the literature (8 input variables would require 135 samples). Despite this it is clear that there are significant errors and that the design space is undersampled. This could be due to the size of the design space which is not accounted for when deciding the sample size. The range of each variable will have a large impact in the complexity that can occur.

Table 5.13: NVH metric on 10 additional airbox designs with increasing sample size

Design	Actual	33	129	161
1	-489	-187	-357	-305
2	-1507	-1991	-1151	-1248
3	-1117	-1475	-830	-576
4	-4829	-2953	-4225	-4272
5	505	593	614	298
6	-6407	-5233	-5987	-5991
7	-3170	-3424	-1782	-1986
8	-3565	-3124	-2745	-2982
9	-4085	-3426	-3245	-3306
10	-3915	-3319	-3093	-3203
R^2		0.845	0.885	0.909
RMSE		801	690	614
LOOE		0.107	0.078	0.077

The NVH metric behaviour within the airbox design space is quite clearly complex and does require more samples. From the small sample error estimation methods it would be difficult to say precisely how many more are required as these may not reflect the true global error. There are larger uniform latin hypercubes that could be applied to ascertain this, however it is beyond the time constraints of this project. The assessment of the additional sample points does suggest that the bulk behaviour of the system attributes has been captured. These surfaces could be used in an optimisation method to examine whether the behaviour captured is sufficient to deliver an improved airbox. This is not without risk, as the poor predictive power of the metamodels would lead to low confidence that any selected trade-off point is the best possible within the design region.

The final metamodels generated, that will be used in the optimisation, will include the data

from the uniform latin hypercube sample and the additional points given in Table 5.9. This gives a final modeFRONTIER 'leave one out' error estimator for the pressure loss metamodel of 0.07715, 0.05256 for the capacity attribute and 0.05833 for the NVH metric.

Cost of Metamodel Generation

Another important aspect of the metamodel build process is understanding the time it would take to build these models. This will allow the MAO project time to be compared to the optimisation intervals available within the Jaguar Land Rover design process. To allow this, a number of assumptions have been made. The first is only methods and samples obtained to build the final metamodel should be taken into account with no time added for the additional experiments completed in Appendix A. The process time does include time to define the requirements and for an experienced CAE engineer to build the necessary CAE methods and any scripts required for process automation and attribute extraction. Another assumption is that only the engineering input is considered. This assumption is made due to the computing facilities available at Jaguar Land Rover and parallelisation of the various jobs involved with the MAO process. Finally, a working week of 35 hours is used. The approximate timings are detailed within Table 5.14, this includes the work completed in the definition stage of the project completed in chapter 4. The total time for the project is given as 277.5 hours or approximately 8 weeks. This breaks down to 2 weeks for defining the airbox MAO problem and 6 weeks for the sampling and metamodel build process.

Table 5.14: Airbox MAO process times

Activity	Time (hours)
Defining the multi-attribute airbox problem and CAD geometry (Chapter 4)	70.0
Defining StarCCM+ meshing and automation strategies	35.0
Latin hypercube StarCCM+ setup (1 hr by 33 designs)	33.0
Latin hypercube StarCCM+ post-process (0.5 hrs by 33 designs)	16.5
Error sample StarCCM+ setup (1 hr by 10 designs)	10.0
Error sample StarCCM+ setup (0.5 hr by 10 designs)	5.0
Defining WAVE meshing and automation strategies	20.0
Large latin hypercube WAVE setup (10 mins by 129 designs)	21.5
Large latin hypercube WAVE post-process (10 mins by 129 designs)	21.5
Small latin hypercube WAVE setup (10 mins by 33 designs)	5.5
Small latin hypercube WAVE post-process (10 mins by 33 designs)	5.5
Error sample WAVE setup (10 mins by 10 designs)	2.0
Error sample WAVE post-process (10 mins by 10 designs)	2.0
Attribute processing, metamodel build & error estimation	30.0
Total	277.5

5.5 Conclusion

This chapter examined the impact to the approach taken of the sample size versus MAO project time dilemma. In this instance the 'leave one out' error suggested that the scarce sample size is not sufficient to model the airbox NVH attribute. To investigate this issue more thoroughly, further experiments were carried out, as detailed in appendix A. The conclusions of this detailed investigation were:

1. The guidance of sample size suggested in the literature may not be sufficient to capture the complexity of the attribute behaviour in the design space.
2. The 'leave one out' error is not an accurate measure of the fit of a metamodel and should be interpreted as a dependency of the sample size, it should be used in conjunction with other error estimation methods.
3. Estimations of the true fitting error with additional samples would require a very large number to be collected, this would be prohibitive in a time constrained environment.
4. Sequential sample methods can be used to resolve local complexity in the metamodel.

Based on these findings it was concluded that the sample size for the NVH model would need to be increased and additional samples should be used to estimate the error. To keep the error sample size to a minimum, the additional samples were obtained in regions of interest (attribute global optimums, baselines and expected trade-off regions). While this would not be able to estimate the global error in the metamodel fit, it would give some inference in the local conditions.

The first stage in increasing the NVH attribute sample size was to use the Lipschitz sampling. However, after doubling the sample size it became clear that this method would require significantly more points to reduce the error to an acceptable level. As the high cost of the set up time per airbox was also prohibitive to large samples, the airbox model was simplified which allowed for some automation of the setup. The reduced setup time allowed a 129 point latin hypercube sample to be taken with an additional 33 latin hypercube for error estimation. This increase was in-line with the guidance within the literature. However, the error estimation of the metamodel still showed significant errors, confirming the conclusions of the experiments in appendix A. The estimation of local error using ten additional boxes on a metamodel built from both latin hypercubes also showed little improvement in the fit. This was represented by an in-ability to place the airboxes in the correct order. The final NVH attribute metamodel was then built using both the 129 and 33 point samples plus the additional ten airboxes used for local error estimation.

For the pressure loss and capacity metamodels the error estimation based upon ten additional samples also showed significant issues with the fit. However, the runtime of such models prohibited further sampling. The final metamodels for these attributes were built from the 33 latin hypercube sample points plus the ten additional samples gained for error estimation.

The literature guidance for sample size is based on the number of inputs. However, this chapter has shown that this approach may lead to undersampled metamodels that cannot capture the

attribute behaviour. To use MAO as a systems engineering tool, other methods to scale the sample size for metamodeling projects may be required.

The pressure loss and capacity attributes also showed a potential issue with the application of the CAE method throughout the design space. Some of the airboxes did display some convergence issues where some portion of the fluid flow could not be resolved. While the variation this caused was small in this case, it raises issues of the suitability of the meshing/CAE method throughout the design space.

Finally, the time taken to complete the initial stage of the project is eight weeks. This includes two weeks for the project definition and six weeks to sample and build the attribute metamodels. The time taken for the optimisation of the airbox will be considered in the next chapter allowing a total time for the project to be defined.

Chapter 6

Optimisation of the Airbox Problem

6.1 Introduction

The aim of this chapter is to investigate techniques that enable attribute trade-off and the benefits of the MAO approach to the airbox. The optimisation will use the metamodels built in the previous chapter and the requirements gathered during the definition of the airbox.

The approach taken to address the dilemma of sample size and project time has resulted in metamodels which contain large errors in the prediction of additional samples. Using these metamodels presents the risk that the optimisation may not yield an improved design of the Jaguar XK SC airbox. However, it does provide an opportunity to examine various approaches to optimise the airbox. Examination of approaches includes reduction of the dimensionality, attribute visualisation and utility value techniques.

The optimisation will be centred on the baseline Jaguar XK SC performance established in section 4.6 on page 102. The benefits of the approach will be established compared to this baseline.

6.2 Inputs to the Optimisation Process

The optimisation of the airbox uses a set of requirements, constraints and baselines derived from the P-Diagram analysis. The requirements outlined in chapter 4 showed the need to optimise an airbox so that both the NVH attenuation and filter capacity are maximised, whilst minimising the pressure loss. The final requirement was to ensure favourable conditions for the MAF signal. For the NVH attenuation, filter capacity and pressure loss, standard CAE techniques were applied and appropriate metamodels built (as outlined in chapter 5). As no standard CAE techniques at Jaguar Land Rover are used to predict the MAF signal, favourable conditions would be implemented using constraints. These conditions were obtained from the supplier design guides [109] and can be summarised as:

1. The minimum duct diameter for the clean side diffuser is 67.5 mm for a mass flow rate of 850 kg/hr.

2. The MAF sensor should be 36.5 ± 15 mm from the clean side duct entrance.
3. The smallest length of box should be 150 mm.
4. Where the clean side diffuser penetrates the airbox volume, the diffuser length should be less than 25% of total airbox length.

Other constraints are a maximum volume of 9 litres and a capacity of 100 g for a single airbox. Whilst there is some drive to increase the capacity above this target, there is little extra gain for additional capacity. This target can be included as a maximisation or as a constraint. The optimisation of the airbox aims to improve the design over the current baseline. Thus, the baseline for the simplified Jaguar XK SC airbox has a pressure loss of 2545 Pa and an NVH attribute of -3170 (from chapter 5 Table 5.9). As the Jaguar XK SC is a high performance product, there is a greater emphasis on pressure loss reduction than NVH improvements. However, it is still desirable to improve the NVH attenuation beyond the Jaguar XK SC baseline.

These requirements and constraints can be implemented in modeFRONTIER by two methods; use of constraint nodes and limiting the variable ranges. The set up of modeFRONTIER is outlined in Appendix B.5 and the limits on input ranges given in Table 6.1. The input variables have also had a step applied, this is to limit the number of decimal places that each variable can change for numerical simplicity.

Table 6.1: Design variable input parameters in modeFRONTIER

Parameter	Min	Max	Step
Breadth (mm)	140.00	370.00	0.050
Clean Duct Dia. (mm)	67.50	80.00	0.050
Clean Ingress (%)	0.00	0.25	0.001
Dirty Duct Dia. (mm)	50.00	80.00	0.001
Dirty Ingress (%)	0.00	0.75	0.001
Height (mm)	260.00	330.00	0.050
Inlet Runner (mm)	5.00	300.00	0.05
Length (mm)	150.00	370.00	0.050

6.3 Comments on Optimisation Algorithms

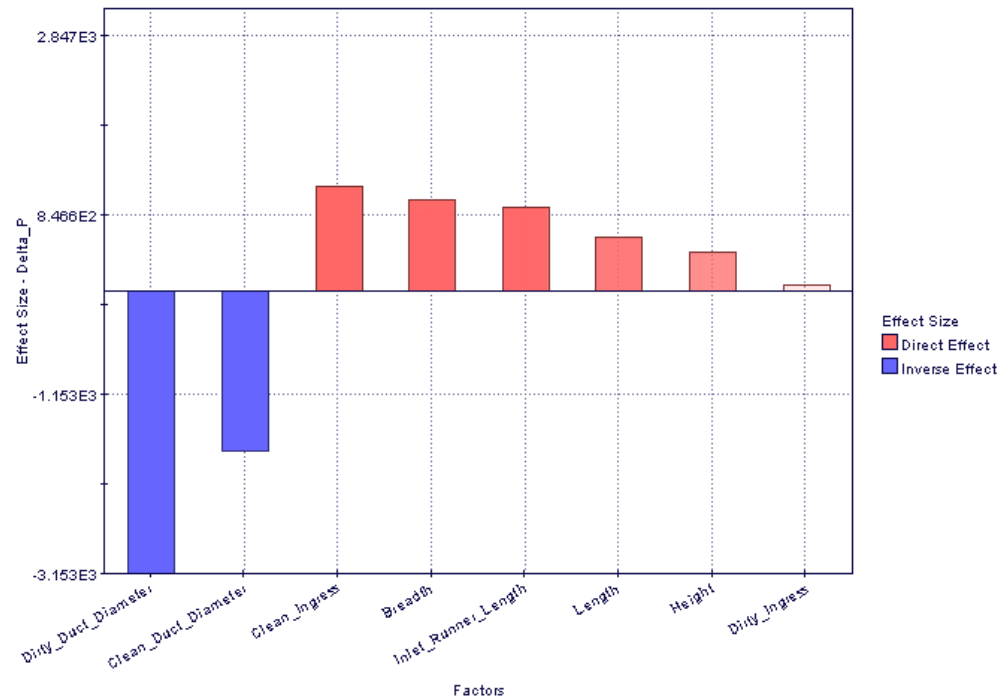
ModeFRONTIER features many different types of DoE sampling methods and optimisation strategies. These can have a great impact on the effectiveness and speed of an optimisation when the samples are gained from an external link. However, when the internal modeFRONTIER metamodeling method is used as the predictor, there is a large increase in the processing speed. In this airbox example, the sampling of 10,000 points took less than two minutes. The rapid assessment allowed many different algorithms to be applied to the same project. This reduces the significance of the applied method and allows approaches considered as computationally expensive, such as full factorial DoE methods, to be applied to the metamodel. In this project the NSGA II algorithm within modeFRONTIER was found to be the most applicable with a large initial DoE, such as a 2 level full factorial DoE.

ModeFRONTIER also features many useful tools for rapidly sorting large sets of data. In particular the selection of feasible and pareto designs is easily completed. Data sorting can be applied to columns to find the maximum and minimum in particular categories. The control of data sets for plotting is also aided by the use of work Tables which can limit the visible points on a graph or chart.

6.4 Understanding the Attributes

When using the metamodeling method it is important to be able to verify the predictive behaviour of the data. For a given metamodel, this can be completed by the use of additional sample points, as shown in chapter 5. But this only considers predictive behaviour at a single point. It is a useful check to visualise what affect each of the main variables will have on the system. This can be achieved using the main effects plots, in this case shown in Figure 6-1 for the pressure loss based upon 43 samples. Here, the main affects are given by changing the duct diameters, which has an inverse affect on the pressure loss. This would be expected as reducing the diameters increases the restriction on the flow. Figure 6-1 also shows the statistical significance of each effect, this can be used to signify effects which are due to the changes in the geometry and which ones occur by chance. The t-student values indicate that it is over 95% certain that the top three main effects are caused by the changes in the geometry. The effect size along with the t-student (or significance) values can be used to look for error and assessing the impact of an input on an attribute.

The main effects plot does not indicate the interactions between the input variables. There are a number of methods to visualise these interactions, such as the box and whiskers plot as well as surface plots. Issues arise with these methods as the dimensionality of the input variables increases. ModeFRONTIER only includes methods of calculating the two-way or second order interactions and the surface plots can only visualise the interaction of two variables while others are maintained constant. This can prevent the user from interpreting the underlying relationships in the system behaviour.



Factors	Effect Size	Significance	t-Student	critical t (sig. = 0.10)	critical t (sig. = 0.05)	critical t (sig. = 0.01)
Dirty_Duct_Diameter	-3.153E3	0.000	6.338E0	1.332E0	1.736E0	2.558E0
Clean_Duct_Diam...	-1.781E3	0.002	2.987E0	1.303E0	1.683E0	2.421E0
Clean_Ingress	1.169E3	0.035	1.863E0	1.303E0	1.683E0	2.421E0
Breadth	1.018E3	0.058	1.606E0	1.303E0	1.683E0	2.421E0
Inlet_Runner_Len...	9.295E2	0.077	1.455E0	1.303E0	1.683E0	2.421E0
Length	5.942E2	0.182	9.184E-1	1.303E0	1.683E0	2.421E0
Height	4.319E2	0.255	6.643E-1	1.303E0	1.683E0	2.421E0
Dirty_Ingress	6.443E1	0.461	9.859E-2	1.303E0	1.683E0	2.421E0

Figure 6-1: Main effects plot for pressure loss based on 43 samples

6.5 Single-Attribute Methods

It is useful to examine the boundaries of performance that the airbox can produce. To do this, each attribute will be optimised in turn within the limits of the Jaguar XK SC baseline for NVH metric, pressure loss and capacity. In Table 5.9 of Chapter 5 (page 119), it can be seen that the maximisation of the NVH metric led to a higher pressure loss than was obtained by optimisation of the pressure loss metamodel itself. This shows that the single shot optimisation method may not deliver the overall global optimums. To overcome this issue, a sequential approach was taken and the design space successively reduced. In the first stage of the pressure loss optimisation, an initial DoE of 25 points was used in conjunction with the NSGA II algorithm with 100 generations. The feasible designs are then extracted and sorted so that the minimum pressure loss was found and selected. The function plot for the metamodel was then examined with the minimum pressure loss design displayed, as shown in Figure 6-2. From this, any further gains were assessed and

the ranges of the design variables reduced. For example, Figure 6-2 shows that the ranges for the clean and dirty ingresses can be reduced to < 0.1 and $0.3 < DI < 0.5$ respectively. Where the optimum of an input variable occurs on the boundary, then the range can be replaced with this value, for example setting the breadth equal to 140mm. The DoE was then reset with the reduced design ranges on all design variables.

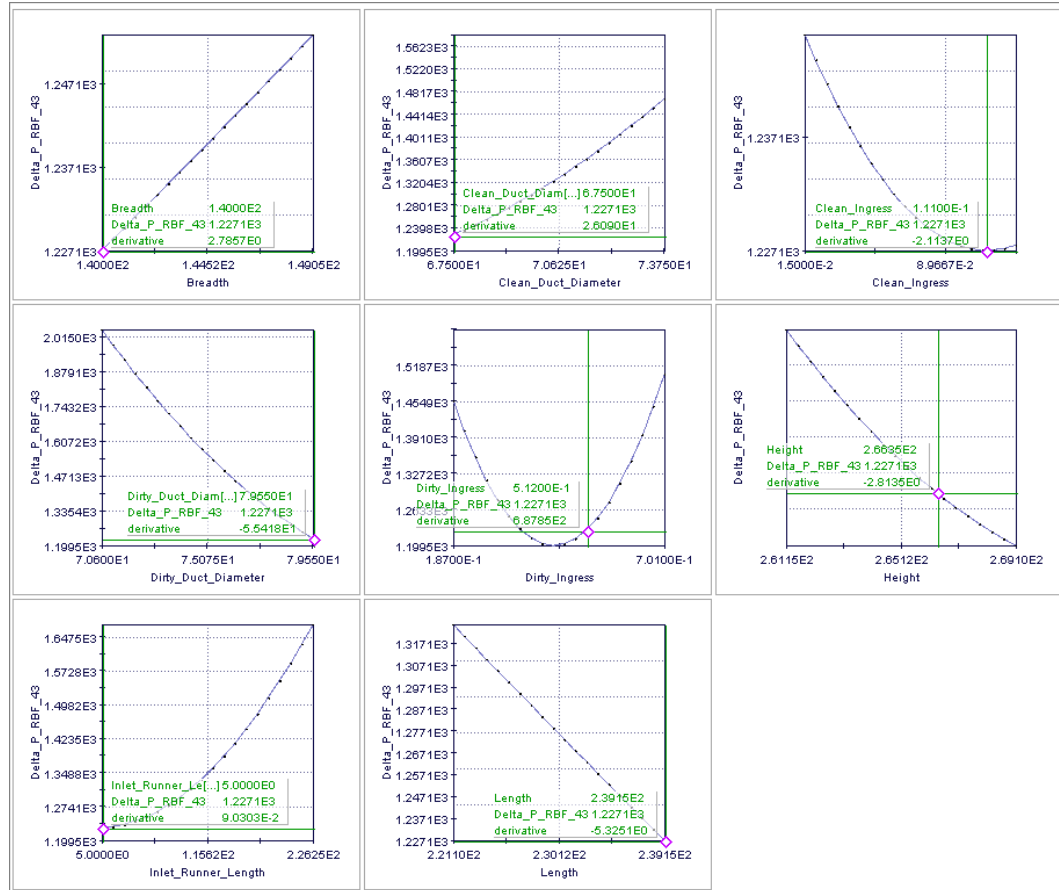


Figure 6-2: Function plot during the first single attribute optimisation stage

This process was repeated until no further improvements were found. Applying this method to each of the attributes in turn provides the airbox designs given in Table 6.2. This shows that there are substantial gains to be made, particularly in the pressure loss attribute. While this approach is more thorough, these points may still not deliver the maximum and minimum achievable in the system. The range reduction was based on the use of function plots which did not consider any interactions amongst individual primary variables.

Table 6.2: SAO airbox designs

	Max NVH Metric	Min Pressure Loss	Max Capacity
Height (mm)	260.20	269.05	261.15
Length (mm)	201.15	238.75	238.35
Breadth (mm)	171.95	140.00	144.55
Clean Duct Diameter (mm)	67.50	67.50	73.85
Dirty Duct Diameter (mm)	69.20	79.75	71.60
Inlet Runner Length (mm)	9.75	5	286.55
Clean Ingress (%)	0.000	0.127	0.000
Dirty Ingress (%)	0.543	0.421	0.639
Delta P (Pa)	2487	1178	2483
Capacity (g)	279	281	478
NVH Metric	-2154	-3055	-3041

The results from the metamodels of the single attribute optimisation approach suggest that there could be significant gains for the airbox design. The optimisation for pressure loss could be approximately halved whilst maintaining the current NVH attribute and capacity. When pressure loss and capacity are maintained the metamodels suggest there is potential for a 32% improvement in the NVH attribute metric. Finally the maximisation of the filter capacity leads to an improvement of around 100%. While individually these represent a significant improvement in one area of airbox design, it may not be the best trade-off. However, this analysis shows that there is a large potential trade-off region which must be explored.

6.6 Multi-Attribute Trading Methods

The airboxes found in Table 6.2 represent improvements of attribute performance but may not represent the best trade-off between all three. This section will examine the various trade-off approaches that can be utilised within modeFRONTIER. In the following images, a large initial DoE of 50 samples was used in conjunction with the NSGA II algorithm and 100 generations. The optimisation used the baseline values as constraints (i.e. airbox designs that failed to improve on current performance were rejected), whilst maximising the NVH metric and capacity and minimising the pressure loss. The pareto data was then extracted as a separate dataset and is presented in the following images.

In Section 6.4, a brief examination of the methods used to understand attribute behaviour found that increased dimensionality increased the complexity. This made the behaviours difficult to visualise and comprehend. This issue is also true for increasing numbers of attributes. Two attributes create a pareto curve and three attributes a pareto surface. These can be seen in Figures 6-3 and 6-4. When just the pressure loss and NVH metrics are considered, Figure 6-3 shows the pareto curve represented by the boundary of blue points. When the capacity is also considered, the three way trade can be seen, this is plotted as a surface in Figure 6-4. This pareto surface is bounded by the three airbox designs in Table 6.2.

The number of attributes that can be visualised in modeFRONTIER can be extended to four

dimensions in a bubble plot as shown in Figure 6-5. Here, the principal visual representations are the NVH metric (X axis), pressure loss (Y axis), the utility (discussed later in section 6.6.4) as distinguished by colour and volume as distinguished by bubble diameter. The parallel line chart, a non-dimensional visualisation technique, is available within the software, as shown in Figure 6-6. Here, the boxes can be selected using the sliding bars on each axis. However, with a large number of samples, airbox design selection and trend spotting can be difficult due to the number of samples involved.

While there are methods of visualising high dimensionality, they become complex when examining a large number of sample points over a large design region. There are approaches that can be used to reduce this complexity and enable the analysts to understand the design space and select a finalised set of design variables. Examples are:

1. Dimensionality Reduction
2. Clustering methods
3. Self-Organising Maps
4. Utility-based methods

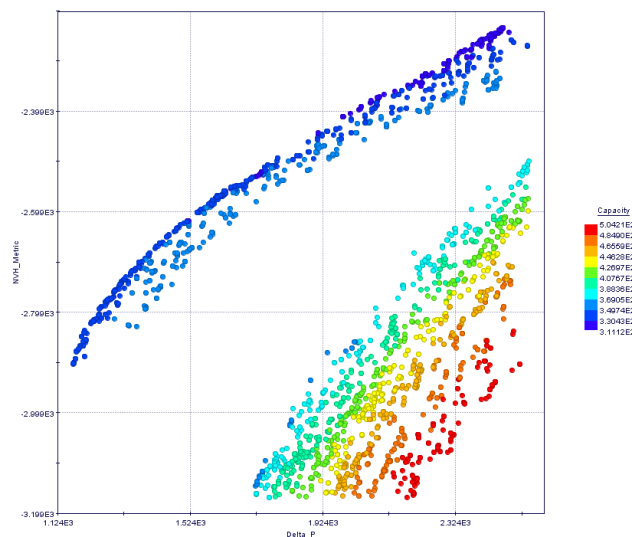


Figure 6-3: Pareto designs for three way trade

6.6.1 Dimensionality Reduction

Figure 6-3 shows that all of the boxes on the pareto front between the NVH metric and the pressure loss satisfy the minimum capacity criteria. One way to reduce the complexity of this optimisation problem is to remove the maximise modeFRONTIER node on the capacity and leave this as a constraint of feasibility. This reduction of the attribute dimensionality allows the trade-off to be conducted between just two attributes, which in turn allows the simpler visualisation methods to be used on smaller data sets, reducing the amount of data that the user must interpret.

6.6.2 Clustering Methods

ModeFRONTIER features algorithms that analyse a set of data to find regions of design that have similar inputs and performance. These are grouped together in clusters. Figure 6-7 shows the application of a clustering algorithm to the data set from Figure 6-3. Here, the data has been split into two distinct groupings; cluster 0 around the high capacity samples and cluster 1 around the NVH/pressure loss pareto front.

This can help to simplify the visualisation of the trade space. The number of clusters displayed can be controlled using the dendrogram shown in Figure 6-8. Here, the number of clusters has been increased to ten. Viewing each attribute trade-off in pairs and in turn on a 2D axis allows for clusters that satisfy all attribute requirements to be identified. In Figure 6-8 it can be seen that clusters 7, 8 and 9 are the areas which best meet the trade-off between the NVH and pressure loss attributes. This process can be repeated for the other attribute pairs until the cluster/s that represent the best trade-off region is identified. Once a cluster has been identified as the best trade-off region, then the work table can be examined. The clustering algorithm also applies the

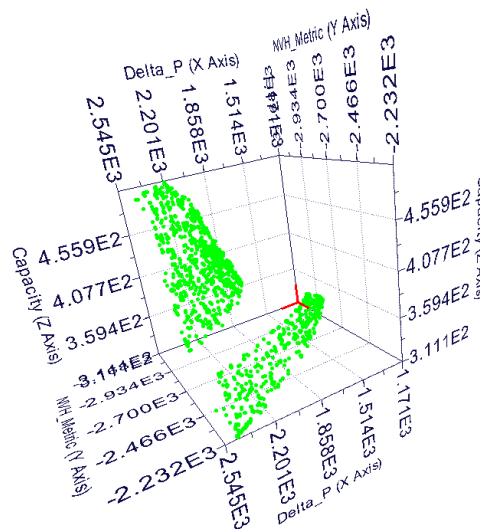


Figure 6-4: Pareto surface for three way trade-off of airbox attributes

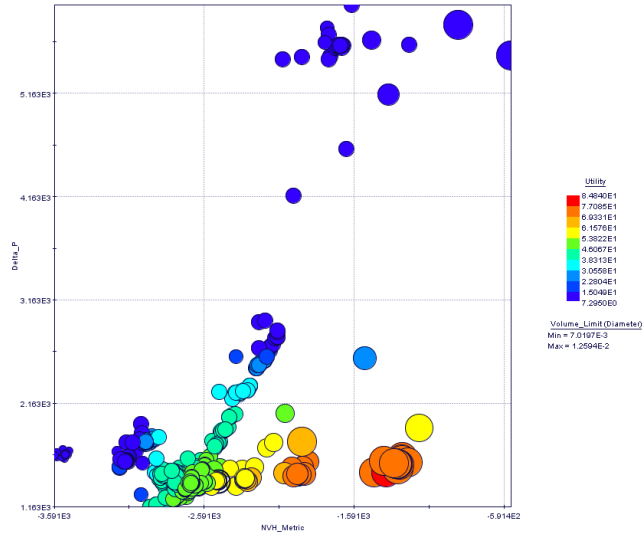


Figure 6-5: An example of a 4-D bubble plot

cluster groups to the work table, where the ranges of design variables and attributes of samples in that cluster are summarised. This helps to reduce the design space. However, as the work table still displays input ranges, there is still a large potential for permutation of design. So, the selection of a final set of design variable values is not fully facilitated. The clustering method can also be applied to the parallel line chart, as shown in Figure 6-9. Here, the application has simplified the

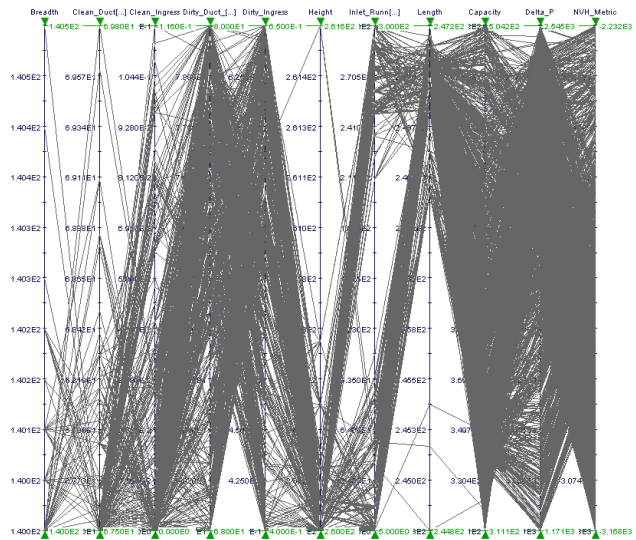


Figure 6-6: Parallel line chart for Pareto airbox designs

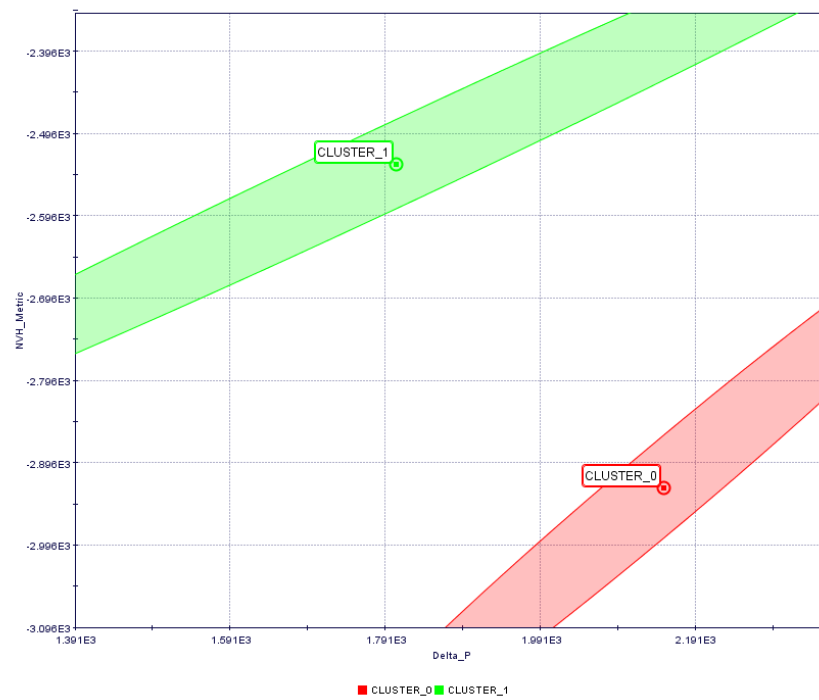


Figure 6-7: 2 Cluster grouping for airbox attributes

number of lines to coloured groupings. This method would help the user to spot design trends and select appropriate clusters in highly dimensional cases.

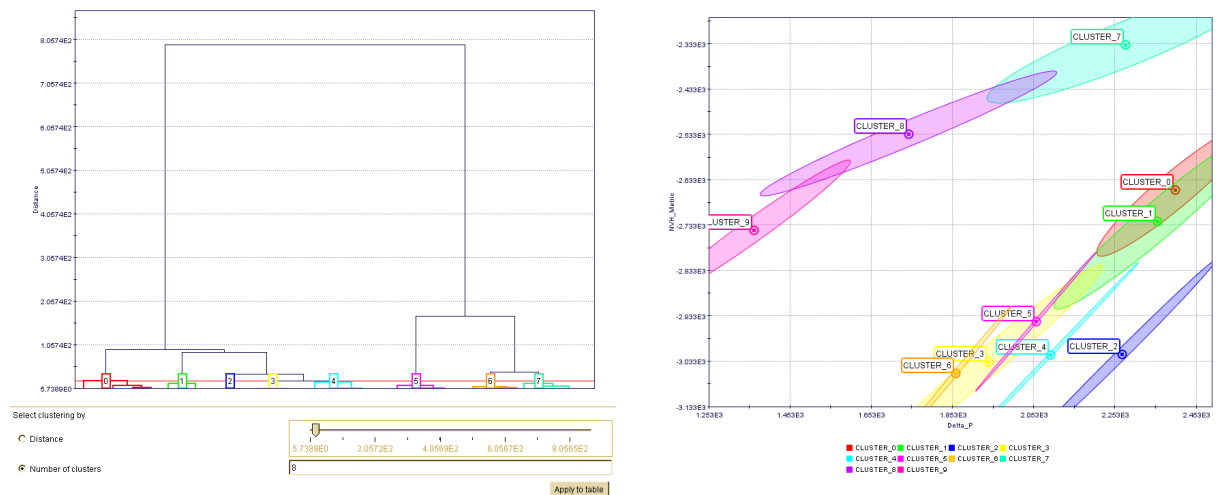


Figure 6-8: Increasing the number of clusters in a visualisation

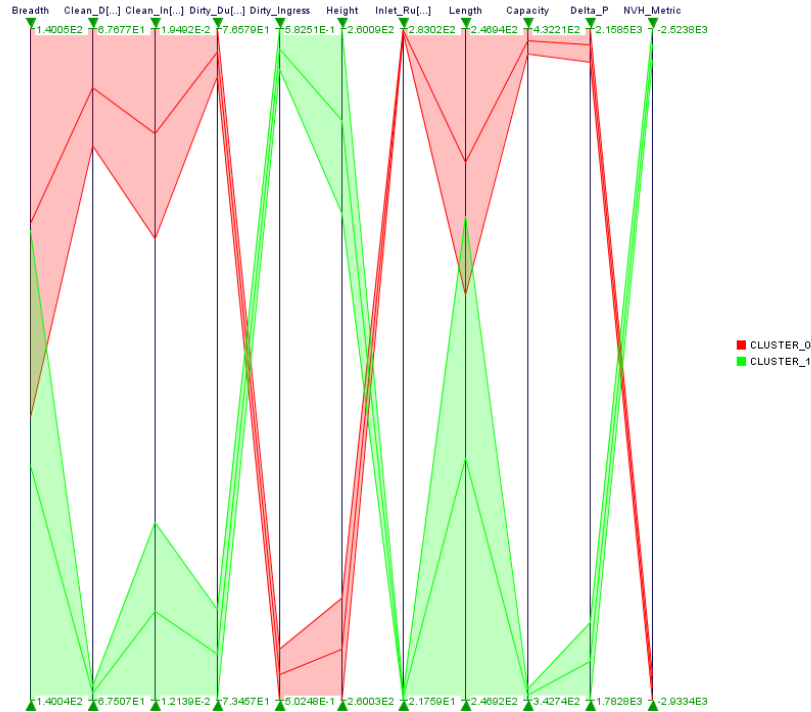


Figure 6-9: Reduction of complexity in parallel line charts via clustering

6.6.3 Self Organising Maps

Another method of visualising highly dimensional data in modeFRONTIER is to apply the self organising map to the data. These are generated by algorithms that are trained on the data set and enable the reduction of highly dimensional data into a simplified map. The maps for each input variable and output attribute is presented in a chart, shown in Figure 6-10. The user can then click on any of these maps and use the slider bar on the side of the chart to see the effect of selecting ranges for specific design variables or attributes. This updates all the other associated maps so that the effect of this selection is transferred across all remaining variables and attributes. The selection removes designs that are not of interest to the designer leaving only designs which are within the selected ranges. Once the user has specified the necessary ranges, the airboxes remaining in any region of the map can be selected and the design variables extracted, either visually from the legends on each map or generating work tables from specific areas of one map. This approach is similar to the clustering method as it can help the user to reduce the design space in order to select a feasible region for the design, but may not necessarily facilitate the selection of a final design.

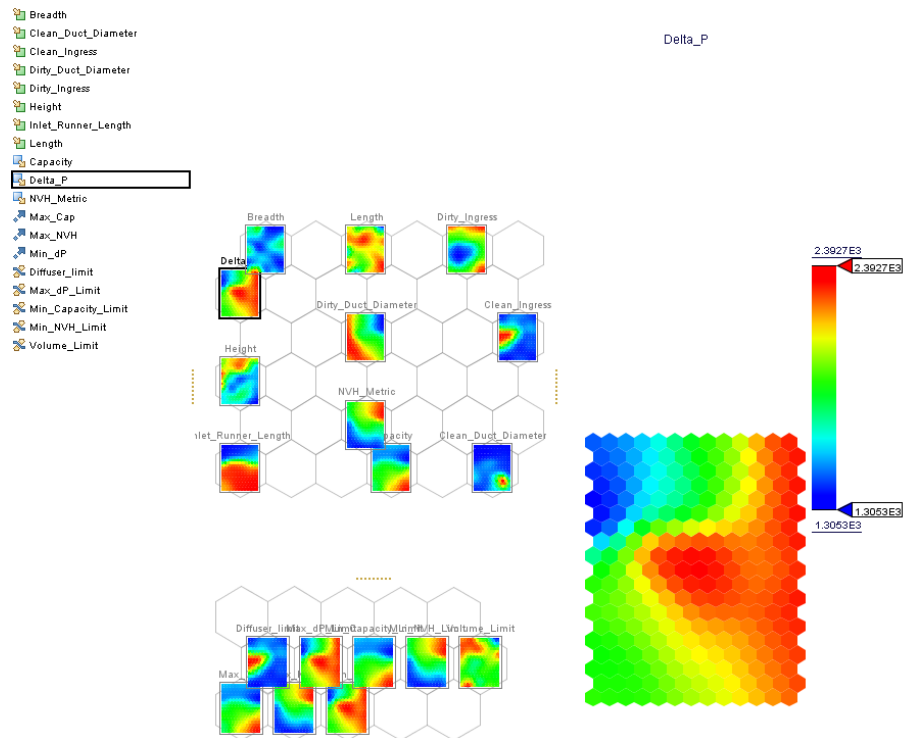


Figure 6-10: SOM applied to the airbox Project

6.6.4 Utility Function Methods

All the methods used up until this point have attempted to reduce the complexity and enable the user to reduce the design space. However, these do not aid in the selection of the final design variables. The utility function method can be used to rank the preference of each of the attributes. A utility function should be derived from the requirements and express the ranking of any attribute within the working range. The functions can then be tuned in order to drive the optimisation in a particular trade direction. In this section, the utility functions for the Jaguar XK SC airbox are derived via the requirements and discussions with the AIS designers.

The initial requirement was to improve the pressure loss of the airbox beyond the initial baseline. However, this was relaxed for utility-based optimisation. The utility at the current baseline was set to an 0.3 acceptance value, with an exponential reduction in utility above this point. An airbox with a pressure loss 30% beyond the baseline was considered to have zero utility. The minimum pressure loss from the single attribute optimisation was used to define the point of maximum utility, given a value of 1. The rise in utility function between the baseline and minimum was then assumed to be linear. The equations for the pressure loss utility function are given in 6.1 and displayed in Figure 6-11.

$$Utility(PL) = \begin{cases} 1 & \text{if } PL < 1160 \text{ Pa} \\ 1.62751 - 5.40958 \times 10^{-4} \cdot PL & \text{if } 1160 \leq PL < 2545 \text{ Pa} \\ -2.19736 \times 10^{-3} \left(1 - e^{6.88646 \cdot \frac{PL-3260}{1000}} \right) & \text{if } 2545 \leq PL < 3260 \text{ Pa} \\ 0 & \text{if } PL \geq 3260 \text{ Pa} \end{cases} \quad (6.1)$$

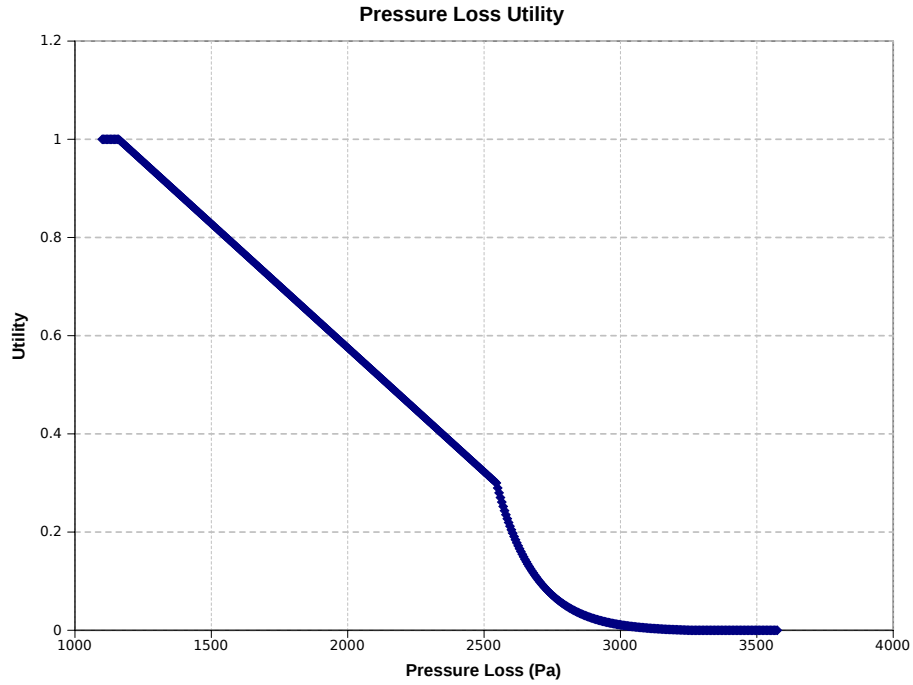


Figure 6-11: Pressure loss utility function

The original requirement for the capacity utility function called for a minimum target of 100 g, once met there were no significant gains for extra capacity. This utility could be modelled as a simple switch function. However, discussions on this requirement yielded further acceptance criteria details. While 100 g is the expected capacity target across all Jaguar Land Rover products, the reality is that airboxes that deliver below target may be accepted. This is due to the Jaguar XK SC being a high performance product where the customer usage may not be as high as other Jaguar Land Rover products. Thus, an exponential penalising function for capacities below targets was applied, the equations for which are detailed in 6.2 and shown in Figure 6-12.

$$Utility(Cap) = \begin{cases} 0 & \text{if } Cap < 80 \text{ g} \\ -6.66667 \times 10^{-2} \left(1 - e^{-13.86294 \cdot \frac{PL-80}{100}} \right) & \text{if } 80 \leq Cap < 100 \text{ g} \\ 1 & \text{if } Cap \geq 100 \text{ g} \end{cases} \quad (6.2)$$

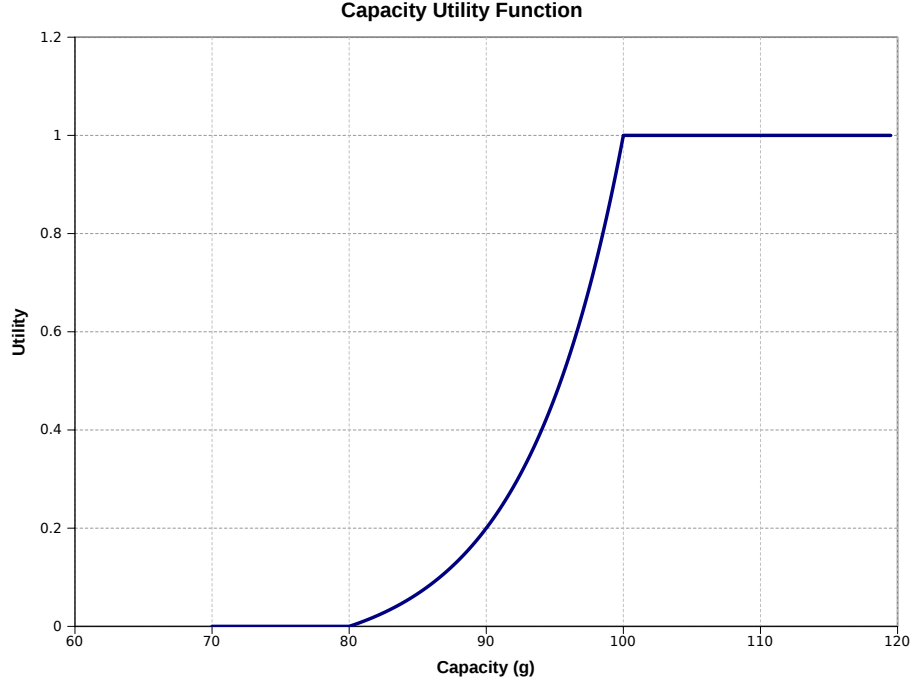


Figure 6-12: Capacity utility function

The utility function for the NVH metric was assumed to be a linear function between the maximum NVH attribute and the baseline. This is shown in Figure 6-13 and the function detailed in equation 6.3.

$$Utility(NVHM) = \begin{cases} 0 & \text{if } NVHM < -3000 \\ 2.60870 + 8.69565 \times 10^{-4} \cdot NVH & \text{if } -3000 \leq NVHM < -1850 \\ 1 & \text{if } NVHM \geq -1850 \end{cases} \quad (6.3)$$

Traditional utility methods have then used the weighted sum methods to optimise the design. Here the utility would be a linear function of the sum of the attributed values. However, these can be limited as the weighting function can only be set at the start of the optimisation. This does not account for the way in which attribute weightings may change based on current performances. Instead, an attribute trade surface can be used as shown in Figure 6-14. Here, the attribute utilities are used as input to a higher utility function. This surface was obtained by stating higher utility at the four corner points characterised by the maximum and minimum attribute performances, as follows:

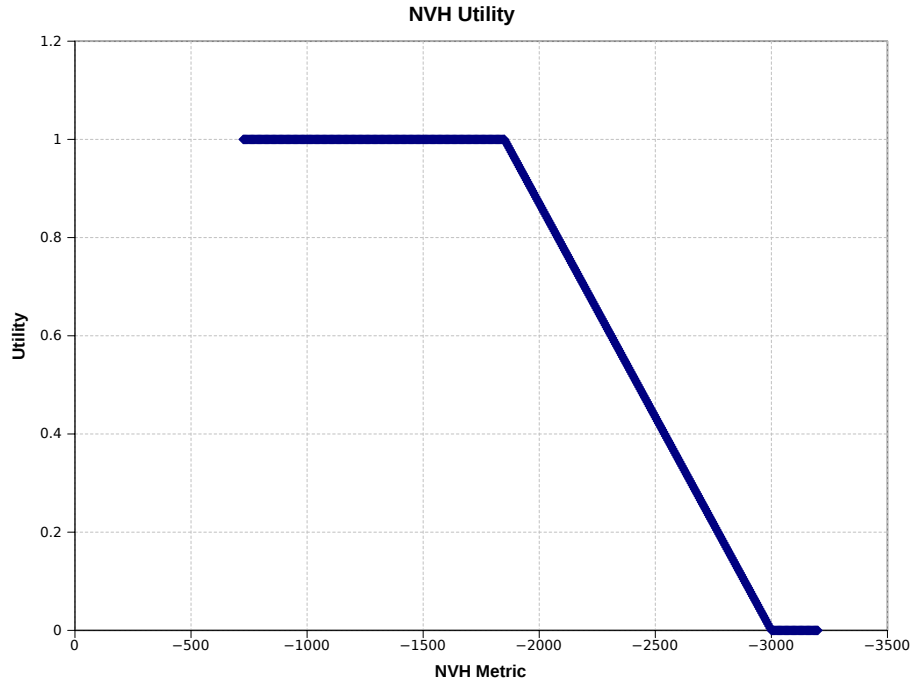


Figure 6-13: NVH attenuation utility function

1. *Minimum NVH Utility, Minimum Pressure Loss Utility:* These attribute performances would not be acceptable and the higher utility is set to 0%.
2. *Maximum NVH Utility, Maximum Pressure Loss Utility:* This would form the utopia point, where both metrics are at best performance giving a higher utility of 100%.
3. *Minimum NVH Utility, Maximum Pressure Loss Utility:* As this surface is for the trade in the Jaguar XK SC airbox there is a slight preference for pressure loss over NVH metric. This can be achieved by setting the higher utility at this point than at the inverse position. Here the utility is set to 20%.
4. *Maximum NVH Utility, Minimum Pressure Loss Utility:* To set the slight preference for pressure loss, the higher utility is set to 10%.

The surface is assumed to be linear between these points and the higher utility can be found using two dimensional interpolation. The surface generated is shown in Figure 6-14. This surface now gives a single value for the utility of the NVH attribute and pressure loss attributes. This must be combined with the capacity metric to give the overall airbox utility. As the capacity utility varies between 0 and 1 and behaves like a switch, it can be used as a multiplier for the higher utility value. Only airboxes below the capacity target will be affected and when above the target, only the trade between the NVH attribute and pressure loss will be examined. The final utility function was maximised in the optimisation and is given in equation 6.4.

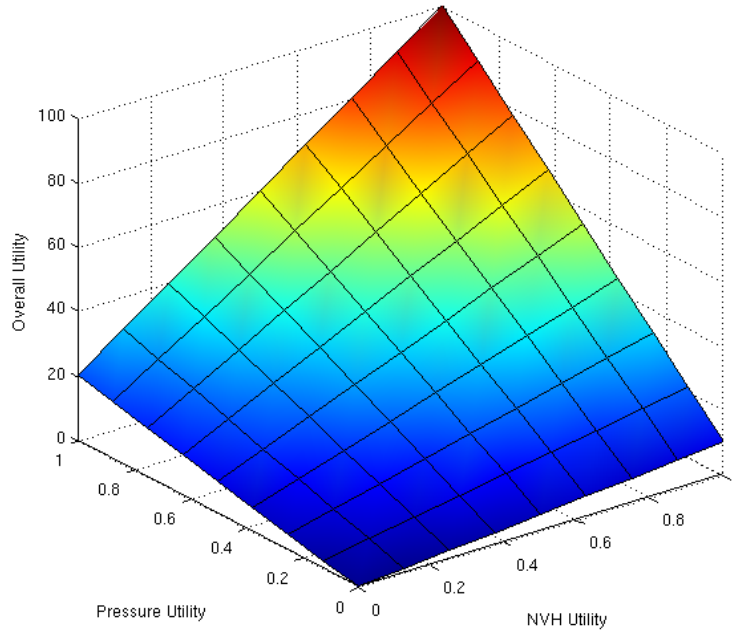


Figure 6-14: Pressure loss & NVH attenuation trade surface

$$Utility_{Airbox} = Utility_{Cap} \cdot TradeSurfaceFunction(Utility_{PL}, Utility_{NVH}) \quad (6.4)$$

The utility functions above were implemented in a Matlab script called by modeFRONTIER. The implementation is given in Appendix B.6. This external interaction slows down the assessment of sample points and means that the large DoEs and optimisation methods take longer to run (approximately three hours for 10000 samples). To reduce this assessment time, a two stage process was used. The first stage was to obtain the pareto front without the utility function evaluation. For this, the baseline constraints on attribute performances were removed and only the trade-off between the NVH metric and pressure loss was optimised. The design parameter values for the pareto boxes were then used as the initial DoE for the second stage of the optimisation. As the pareto front was used, the optimisation focused on the feasible region within the design constraints and contained samples close to the optimum. The utility function was then maximised using fewer NSGAII generations in approximately 20 minutes. The airbox with the maximised utility is given in Table 6.3.

6.7 Verification of Optimal and Trade-off Designs

The airbox designs presented in Tables 6.2 and 6.3 represent large gains in performance of each of the attributes. However, it was known from chapter 5 that the attribute metamodels contained

significant errors. The CAE models were completed on the three optimal airbox designs and the trade-off airbox design to understand whether the gains made were achievable. The results of the CAE are presented in Table 6.4.

Comparing the predicted values from the metamodels with the CAE results shows that there are still large errors in the predictions. There are also issues with the airbox attribute ranking, which can be seen by the way the lowest pressure loss is delivered by the '*utility optimised*' airbox rather than the design optimised for this attribute. This is also the case with the maximum capacities and NVH metrics. These issues led to low confidence that the '*utility optimised*' airbox is the best design possible in the design region.

However, when the CAE results for the utility optimised airbox are compared to the Jaguar XK SC baseline results (Table 6.5) it can be seen that the proposed design does give some improvements. While there is a small improvement in the capacity and pressure loss, the main gain was the NVH attribute. The NVH spectra for the baseline and optimised airbox are shown in Figure 6-15 and show that while the design improves over the whole range of frequencies, the greatest improvement is in the 400-600 Hz range where supercharger whine is prevalent. The pressure loss improvement is important for the XK customer as the 360 Pa reduction in pressure loss would correlate to an increase of approximately 7 b.h.p at max load.

When the optimised airbox is compared to the baseline design it can be seen that the volume of the airbox is slightly larger. The breadth remains the same at 140 mm, the height has been reduced by 5 mm and the length increased by 15 mm. While this will have an improving effect on the airbox attributes, the significant changes will be due to the diffusers and duct diameters. The original

Table 6.3: Attribute trade-off airbox design

	Optimised
Height (mm)	260.00
Length (mm)	247.25
Breadth (mm)	140.00
Clean Duct Diameter (mm)	67.50
Dirty Duct Diameter (mm)	77.20
Inlet Runner Length (mm)	11.60
Clean Ingress (%)	0.017
Dirty Ingress (%)	0.536
Pressure Loss (Pa)	1395
Capacity (g)	343
NVH Metric	-2680

Table 6.4: Comparing metamodel predictions with CAE results

	Pressure Loss (Pa)		Capacity (g)		NVH Metric	
	Predicted	Actual	Predicted	Actual	Predicted	Actual
Max NVH Metric	2487	2547	279	238	-2154	-2596
Min Pressure Loss	1178	2300	281	218	-3055	-3344
Max Capacity	2483	2361	478	248	-3041	-2673
Utility Optimised	1395	2179	343	256	-2680	-2439

design has a clean side duct diameter larger than the dirty side. However, in the trade-off design this has been reversed. The smaller duct diameter on the clean side gives a larger expansion ratio, improving the NVH performance. While this would restrict the airflow out of the airbox, the larger dirty air duct reduces the velocity of the incoming air. This lowers the pressure loss by reducing the shear resistance in the dirty side airflow. The longer dirty side diffuser may also help to improve the flow uniformity over the filter as well as acting as an NVH device.

The reversing of the clean and dirty duct sizes is a key contribution to the design of Jaguar Land Rover airbox design and further investigation should be undertaken to see if such gains are made on airbox designs in other vehicle programs.

This exploration and optimisation process took approximately two weeks. Combining this with the eight weeks to define the project and generate the metamodels, a total of ten weeks would be required for the MAO optimisation of the airbox.

Table 6.5: Comparing CAE results for utility optimised and baseline designs

	XK SC Base	Trade-Off
Height (mm)	265	260
Length (mm)	233	247.25
Breadth (mm)	140	140
Clean Duct Diameter (mm)	73	67.5
Dirty Duct Diameter (mm)	68.5	77.2
Inlet Runner Length (mm)	5	11.6
Clean Ingress (%)	0	0.017
Dirty Ingress (%)	0.391	0.536
Pressure Loss (Pa)	2545	2179
Capacity (g)	231	256
NVH Metric	-3170	-2439

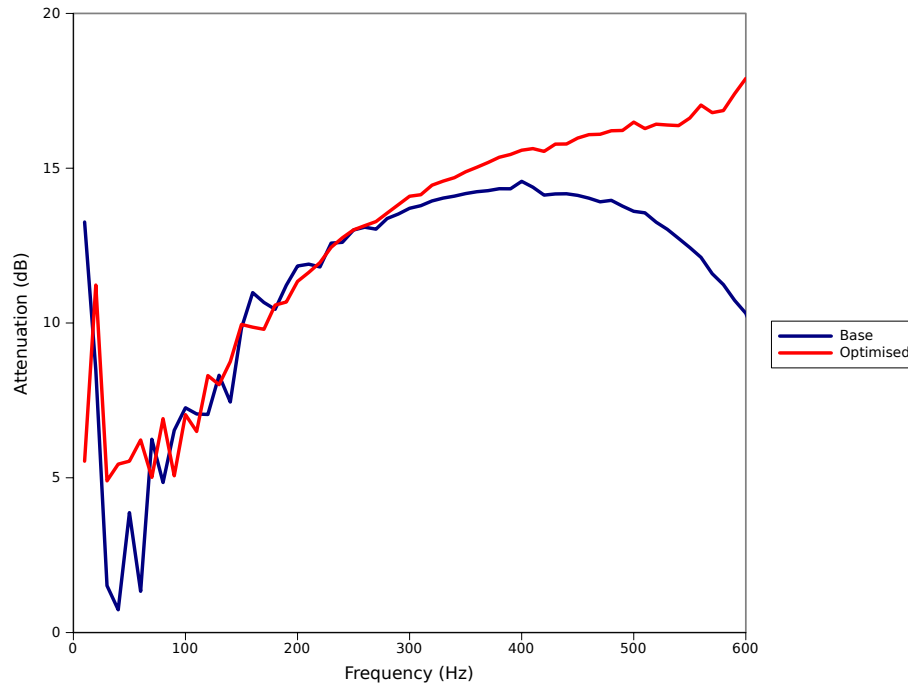


Figure 6-15: Utility optimised attenuation spectra

6.8 Conclusion

This chapter examined techniques to trade-off multiple attributes in an airbox. The first step was to apply reduction techniques allowing the simplification of the design space. The first reduction technique was to use single attribute optimisation for each attribute in turn whilst using the baseline performance of the other attributes as a constraint. While this approach may not present the design with the best attribute trade-off, it does aid the designer to understand what the potential attribute ranges are within the constrained optimisation. A second reduction technique was available within the airbox optimisation as the capacity attribute requirements could be fulfilled by realising the other attributes. However, as these methods do not reflect the best attribute trade-off other methods were examined.

To aid with the attribute trade in the airbox a number of visualisation techniques were then employed. These techniques helped to understand the interactions and relationships. Here, the clustering or mapping techniques proved to be particularly useful in reducing large data sets into patterns and regions. This understanding may help to reduce the design space but due to the large number of potential designs it is difficult to select final design parameters that will be used. This is where utility methods can be employed. The utility functions used in this project were derived from the baseline performance, the single attribute optimised limits and the design requirements. These were then tuned to find the design which had the greatest utility. These methods help select the final design, but further research is required to link the derivation of utility functions to requirements in a systems engineering method. For future projects it is recommended to use both methods first

to explore the design space then select the optimum design.

The optimisation of the airbox also confirmed that the metamodels were under-sampled giving poor attribute predictions. However, when the optimum trade-off design was verified using the CAE methods, the performance was beyond the current XK SC performance. There were modest improvements in the pressure loss and capacity, but the largest gain was in the NVH performance, particularly in the 400-600 Hz range where the supercharger whine is most prevalent. The total time for this analysis was approximately ten weeks. However, this improvement was against the large risk of failure due to undersampling of the design space resulting in the poor metamodels. The improvement in airbox attributes showed that the scarce sampling of the design space had picked up on some of the underlying attribute behaviour. But the insensitivity in discriminating between similar airbox designs means that there is low confidence that the final design is the best within the design space. The sensitivity can only be improved by increasing the number of samples in the design space.

Chapters 4, 5 and 6 have examined the sampling and error estimation methods within a metamodeling method, as an enabler in an MAO method applied to an automotive airbox. Another enabler identified in the Literature Review was the use of multi-physics CAE methods. Such approaches may be required due to the inter-disciplinary nature of systems optimisation to improve attribute prediction. The investigation of such methods, outlined in chapter 3, is presented in the next chapter.

Chapter 7

The Multi-Physics Fuel Tank Problem

7.1 Introduction

This chapter aims to assess the costs and benefits associated with a multi-physics approach to CAE, as both a stand alone CAE tool and for use as an attribute predictor in MAO projects. The assessment is based around the effect of fuel sloshing within a fuel tank and goes through a number of stages. Firstly, the key drivers for this project are re-iterated and the research area identified, this is followed by a brief review of the operation and application of multi-physics methods within fuel tanks. From this, the current CAE analyses for fuel tanks are investigated to find a suitable application for the multi-physics project and the requirements for the CAE method detailed. Finally, the multi-physics methods available to this project are assessed using representative boundary conditions and test cases.

7.2 Project Drivers

From the review of CAE based optimisation, the accuracy of attribute prediction was found to be a key element in the building of attribute metamodels. Applications of MDO identified cases where a system attribute may cross the traditional CAE domains requiring the use of a multi-physics analysis. These analyses come with additional accuracy benefits but at the expense of simulation cost. Within the multi-physics analyses there are two issues which require further investigation; the degree of coupling and the software approach. The degree of coupling determines the strength of interaction between domains and should be appropriate for the application. Two different software approaches can be taken to handle the coupling of domains; using multiple domain specific analysis codes supported by communication methods to exchange data and a single code approach which covers both domains. While the multiple domain specific code may incur an increased modelling cost over a single code approach, there are no accuracy sacrifices in the modelling of domains.

Within the context of Jaguar Land Rover Powertrain CAE, the cost of using a tool includes training and available skill-set. To minimise these costs, the project was constrained to use tools which are available within current Jaguar Land Rover CAE software. The area of application was selected to be the fuel tank, this was due to the high degree of interaction and the potential impact of the tool on future designs.

7.3 Fuel Tank Multi-Physics CAE Methods

The analysis of the motion of fuel within a tank has many applications in guiding design. The phenomenon affects many different design aspects of the vehicle and can provide data before prototyping. The use of CFD has been used to verify the location of valves within the tank to ensure correct operation[127] and for reducing NVH issues[128]. These cases primarily looked at the effect the shape of the tank had on the motion of the fuel.

Initial methods to assess fluid slosh in structural analyses have been to use the Finite Element Method (FEM) and apply pressure boundary conditions to the model[129], or to use software that approximated the mass distribution of a moving fluid[130]. Another method can be to use acoustical elements in a structural solver[131]. However, these elements are better suited to small displacement simulations rather than hydrostatic Fluid Structure Interaction (FSI)[132]. None of these methods properly accounts for the motion of the fluid.

Thus, the FSI multi-physics analysis will need to solve two different physical domains that are linked to each other at a boundary interface. Recalling section 2.6.5 in the literature review the different degrees to which the domains can be coupled are[103]:

- *Uncoupled*: This is where the different domains do not have significant interactions that greatly affect the result. The simulations can be carried out independently using mature methods with a manual exchange of the interface data.
- *Loose/One-way coupled*: In a one way couple one domain will significantly affect another but is itself unaffected. This is similar to the uncoupled approach, however, in a one way couple the one directional exchange of data occurs in an automated fashion, i.e. within a multi or single code multi-physics approach.
- *Fully coupled*: In a fully coupled system the different domains will have a significant affect on each other. This requires the solution of both domains at the same time with exchanges at the interface at regular intervals. This requires a high level of automation within the multi-physics approach.

For FSI methods the uncoupled and one way approaches can be used for small deflections such as thermal problems, but fully coupled methods are required where the displacement of the solid is large and would affect the fluid flow[133]. The coupling of the two FSI domains requires the exchange of surface pressures from the fluid domain and displacements from the solid domain. This exchange can be handled in two different ways; using a single multi-physics code or using a coupled Multi-Code approach.

Multi-physics CAE codes have modules within them to deal with different physics domains. The software is set up to enable the solution of both modules within one global algorithm[132][134]. The Combined Eulerian Lagrangian (CEL) in Abaqus CAE is one such approach to the FSI problem. This features an additional Equation of State (EoS) that simulates the fluid flow and boundary loading, which is then directly applied to the structural model. This EoS is not a full fluid analysis like a CFD code, thus the fluid may not be modelled as accurately as required.

The use of a Multi-Code approach requires that an exchange of data be used as a boundary condition for the other simulation. There are two methods of exchanging this data. Firstly, a third party software such as MpCCI (Mesh-based parallel Code Coupling Interface)[135] can be used. This code automatically takes mapped data from one code to another allowing unmatched meshes to be used in the analysis. Secondly, software vendors are integrating direct couples into their software that allows the data to be exchanged automatically[136]. These approaches require separate models of the different domains and additional computing power to exchange data. However, as domain specific software codes are used, there are no sacrifices in the accuracy of the simulation.

Within these approaches there are a number of methods and algorithms to simulate the interaction between the domains. The type of algorithms affects how the boundaries and interfaces are tracked. Wasfy and Smith[137] outline the different methods of FSI. Fixed fluid meshes with separate deformable meshes for solid elements, Arbitrary Lagrangian Eulerian (ALE) and particle methods were discussed.

- *Fixed Fluid Meshes:* The methodology used in the Abaqus CEL uses a fixed Eulerian mesh that covers the whole domain of possible fluid movement. Within this large Eulerian mesh there is solid Lagrangian mesh. The fluid is then free to move through the Eulerian mesh but the boundary of the Lagrangian mesh is enforced by penalty methods. This prevents the fluid penetrating the solid-[132][134].
- *Arbitrary Lagrangian Eulerian:* An ALE analysis is based around an Eulerian fluid mesh that conforms to a Lagrangian solid mesh. When the solid mesh is deformed, the nodes of the fluid mesh are then moved to conform to this new deformed state. This method was used to find the ballooning of fuel tanks under impact loading[138] and to estimate hydroplaning of tyres[135]. In both of these examples the meshes were critical to the outcome of the simulation. In the ballooning simulation the effect of fluid pressure on the internal structures was also investigated but this increased the runtime of the simulation due to the increased mesh density. The hydroplaning simulation raised another issue with using the ALE method. The deformable fluid mesh led to some local distortion when contact between tyre and road was lost as the fluid mesh did not fill the gap produced. This was rectified using additional modules in the CFD solver but added significantly to the run time. There were also issues with the mesh sizing used; the CFD mesh required a finer grid than did the solid solver. This resulted in non-matching meshes and the requirement for an interpolation algorithm.
- *Particle Methods:* Particle methodologies model the fluid as a set of discrete Lagrangian elements in a mesh-less method. This provides a number of advantages over Eulerian

fluid methods as free surface break up, large deformations and surface tracking are easily modelled[139]. The solid is modelled with Lagrangian mesh and the interface is enforced using a penalty condition imposed on the particle elements[140].

This review has shown a number of issues that need to be addressed when using a multi-physics method to evaluate fuel slosh problems. The first is selecting the correct degree of coupling. Increasing the coupling incurs a higher cost yet may be required for accuracy. The need for a fully coupled solution should be evaluated. The second issue concerns the relative cost and accuracy of the multiple and single code approaches to multi-physics CAE. The method should be able to provide an accurate attribute prediction at a cost feasible within the design or optimisation process.

7.4 Exploring the Project Opportunity

The fuel tank is a system that stores the petrol or diesel liquid for use in the engine and is vital to the safe operation of a vehicle. The tank contains internal components such as Fuel Delivery Modules (FDM) and various valves, all of which contribute to the operation of the fuel tank. These components are mounted to an internal carrier system, which is inserted during the manufacturing process. When the fuel tank is designed, CAE is used to support the design process by analysing the component to ensure manufacturability and performance. The design and manufacture of the system is capital intensive and requires a long lead-time. This is due to the production method of blow moulding which requires the manufacturing of specifically shaped dies which are resource intensive in both cost and time.

Currently, the early designs are sent to the supplier who will conduct CAE on the tank to examine various attributes and manufacturability. Prototype testing is then used to verify and sign off the tank design. While much of the CAE work is completed by suppliers there are efforts to either bring some analyses into the remit of the Jaguar Land Rover Powertrain CAE team or develop new methods to understand the fuel tank in greater depth. The application of a multi-physics analysis was part of this effort. This section details the exploration of fuel tank CAE analyses for the potential application of multi-physics methods. From this relevant applications were identified and the requirements for the project outlined.

7.4.1 Fuel Tank Design Stages

The design stages of a fuel tank are discussed together with the relevant CAE requested in Appendix Section C. The current CAE requests for the fuel tank are given in Table 7.1. The examination of the CAE requests resulted in a revised CAE list for 'in-house' analysis as shown in Table 7.2. The move from supplier completed to 'in-house' CAE required a number of changes such as delaying a number of the structural simulations so that the tank wall thickness data from a supplier analysis can be used. This move also allowed a number of the analyses to be separated, such as the durability and NVH evaluations due to slosh events. While the CAE for these issues is requested, much of the evaluation is completed with physical rig testing. Within this separation a number of

potential applications for multi-physics CAE analyses were found (highlighted in bold in Table 7.2). These examples were identified as the applications where a multi-physics analysis would have the largest impact on the design of a fuel tank.

7.4.2 Multi-Physics CAE Project Application Opportunities

The operation of fuel tanks in vehicles provides an opportunity to use multi-physics CAE. The sloshing of fuel within the tanks is currently the object of NVH and fluid flow CAE. But there is an opportunity to apply FSI methods to gain new insight into the design of fuel tanks. The four possible areas of application are outlined below:

1. The effect of sloshing on tank shell durability.
2. The effect of sloshing on the durability of the tank mounting mechanism.
3. The effect of sloshing on internal component durability.
4. The effect of sloshing on radiated noise from tank surface.

With these applications, the feasibility of each of the new techniques and methods could be assessed on a small scale before being ramped up to larger systems. For a method development project, one of these was selected using a selection matrix, the details are given in Table 7.3.

When selecting the area of application a number of assessments were made. The first is that if a methodology already exists then there would be no extra benefit gained from completing this area within the feasibility study. As methods are already applied to the mounting straps and the tank shell, these areas were marked down.

The second assessment was that the new technologies available would be able to solve both a fluid and solid domain, so only analyses which would require this should be selected. As the radiated noise could be completed without additional domain methods, this area was marked down.

The third assessment was that this project focuses on the application of a FSI method, thus any additional CAE methods beyond the fluid and structure were deemed unnecessary. As the strap and mounting analysis would require the addition of the fatigue code and the radiated noise required then the analysis of the transfer of sound from the tank to the driver, these areas were marked down.

The final assessment was the need to address issues within Jaguar Land Rover fuel tank design. Here, it is desirable to analyse the effect of sloshing on internal components and the NVH issues this causes. These areas are therefore marked up.

From table 7.3, it can be seen that the effect of sloshing on internal component durability has a total of four, meaning that this is the analysis area on which the application of multi-physics methods will have the most effect.

7.4.3 Scope and Requirements

The analysis of the CAE methods applied to the fuel tank revealed a need for an analysis to examine the durability of the internal structures and components. This analysis would need to account for

Table 7.1: Fuel tank CAE Lists

1 st Design Iteration	2 nd Design Iteration	3 rd Design Iteration	Design Verification
Initial pressure/vacuum cycling analysis of fuel tank (supplier /in-house)	Pressure/vacuum cycling analysis of fuel tank repeated		
Initial stress/strain analysis of fuel tank (supplier /in-house)	Stress/strain analysis of fuel tank repeated		
Initial blowmould simulation of fuel tank (supplier)	Blowmould simulation of fuel tank repeated, including initial assessment of carrier over-moulding (if applicable)(supplier)	Blowmould simulation of fuel tank repeated, to finalise carrier over-mould parameters (supplier)	
Initial NVH/slosh evaluation of fuel tank	NVH/slosh evaluation of fuel tank repeated (initial tank internal features added, e.g. basic models of baffles, FDM)	NVH/slosh evaluation of fuel tank repeated, using latest internal child part models	
Initial crash worthiness analysis (fuel tank, fuel filler, filters)	Crash worthiness analyse repeated	Crash worthiness analyses repeated	
Vibration/modal analyses to verify mountings design and fixing point locations	Vibration/modal analyses repeated		

Table 7.2: Revised fuel tank CAE Lists

1 st Design Iteration	2 nd Design Iteration	3 rd Design Iteration	Design Verification
	Initial crash worthiness analysis (fuel tank, fuel filler, filters)	Crash worthiness analyse repeated	Crash worthiness analyses repeated
Initial blowmould simulation of fuel tank (supplier)	Blowmould simulation of fuel tank repeated, including initial assessment of carrier over-moulding (if applicable)(supplier)	Blowmould simulation of fuel tank repeated to finalise carrier over-mould parameters (supplier)	
Initial slosh evaluation of fuel tank based upon early internal geometry to determine need for baffling	Slosh evaluation to determine possible damage to internal components based upon detailed CAD of internal components	Slosh evaluation for NVH based upon detailed tank thicknesses	
	Slosh evaluation for durability of mountings		
Pressure/Vacuum cycling analysis of Tank	Pressure/vacuum cycling analysis of fuel tank repeated*		
	Stress/strain analysis of tank	Stress/strain analysis of fuel tank repeated	

Table 7.3: Pugh selection matrix for multi-physics project

	Existing Methodology	Technology Availability	Additional CAE Required	Current JLR Need	Total
Tank Shell Durability	0	1	1	0	2
Tank Strap Durability	0	1	0	0	1
Internals Durability	1	1	1	1	4
Radiated Noise	1	0	0	1	2

the loading that occurs when the fuel is sloshed. This loading can cause internal components in the tank to fail, causing the vehicle customer to be dissatisfied. Currently there is no standard CAE method in place to analyse this issue.

Fuel sloshing occurs with most vehicle manoeuvres. Intensity of direction, velocity and acceleration changes during these manoeuvres will affect the levels of sloshing within the tank. The loading changes on the internal tank components caused by different events should be assessed, along with tank conditions that could have significant effects on the internal components.

This analysis aims to find the best multi-physics approach for assessing the durability of internal tank components exposed to fuel slosh. The scope of this analysis will include all internal components. The analysis will not include NVH issues, nor the assessment of durability of the fuel tank shell or external components of the fuel tank system. The software to be used will be limited to current availability and expertise within powertrain CAE. However, within these restrictions, any viable method can be explored.

Fuel System Design Team

The Critical-To-Quality (CTQ) requirement for the fuel system design team is that the analysis should provide an accurate and timely result to enable data driven design. As a stand alone tool, this means that the analysis method will need to be completed within the virtual series loop. This gives the requirement that the CAE process must report out within eight weeks of the job request[141]. Within an MAO method, the analysis will need to be repeated a number of times when building the attribute metamodel, the sampling must be completed within the MAO project time.

Vehicle Customer

The CTQ requirement for the vehicle customer is ensuring that the structural integrity and safety of the internal components within the tank are not compromised due to the sloshing of the fluid during road usage. The assessment of structural integrity requires that the analysis examines metrics related to component failure, for example stress, strain and safety factors. The analysis must also be able to incorporate road acceleration load data as an input, to ensure that customer usage is modelled.

Powertrain CAE Team

The CTQ for the powertrain CAE team is to deliver an accurate and timely analysis that uses an acceptable amount of resources. The CAE method should be able to measure the desired attributes and must be robust enough to meet the model requirements. The resource metrics here will be the usage of computer cores, software licences, solver runtime and engineering hours. The accuracy will be dependent on the type of analysis used and the parameters specific to each code. However, these represent a trade-off; increased accuracy will use a greater amount of resources and will greatly effect the timeliness of the reporting out.

7.4.4 Summary

From these requirements it is clear that there are two issues that need to be addressed before any application of a fluid structure interaction method can be applied to a full tank geometry. Firstly the correct boundary condition needs to be explored to ensure that the inputs requirement is met. And Secondly, the stability and accuracy of the various coupling methods available must be investigated. This is to ensure that the methods can predict the required attributes robustly. The first issue is addressed in appendices D and E, the details of which are summarised below. The investigation into available multi-physics methods forms the remainder of this chapter.

The current Jaguar Land Rover approach to free surface analysis is to use the Volume of Fraction (VoF) model within StarCD. To justify this approach, a correlation study was carried out. The work and results of this is presented in Appendix D. While full correlation could not be achieved due to issues with the accelerometer used, the work did show that the VoF method could predict pressure loading of the correct magnitude.

The assessment of multi-physics methods requires the evaluation of fuel slosh load cases that are representative of vehicle use. A boundary condition exploration was conducted on a simplified fuel tank with an internal baffle. The approach and results of this exploration is presented in Appendix E. This study established that the worst case scenarios for fuel slosh was a 16 KpH frontal crash for single event loading and Kerb Island Strike for multiple event loading. The maximum loading in these events occurred with a 60% fill volume.

7.5 Approach to Multi-Physics CAE Evaluation

There are a number of multi-physics methods available for use within the current Jaguar Land Rover tool-set. This section will describe the approaches and define the steps required to assess the degree of coupling required.

Previous work in Jaguar Land Rover had examined the application of acoustical elements for fluid slosh in Abaqus. This method was used in the assessment of fatigue of external components, such as the fuel tank straps and mounting points [131]. This method applied prototype testing event data to a finite element model of a fuel tank, internal and external components and used acoustic elements to model the fuel. Closer inspection of the acoustical element revealed that the

acoustical elements were not suitable for large deformation, non-linear or hydrostatic fluid structure interactions [132]. This means that for the assessment of internal component durability this method would not be able to capture the loading caused by the fluid flow around the tank. A different approach was required.

At the time of this project there were four possible methods that can be used to assess the structural integrity of fuel tank components. These were:

1. An un-mapped un-coupled method, where the surface pressures generated by the CFD model are exported and applied to a structural model of the fuel tank internal components. Each model was run in isolation and sequentially. First the surface pressures were obtained for the whole load case, then applied to the structural model. As this method does not require any specialist simulation software, additional programming or support for communication between the simulations, it was the simplest to use. However, the un-mapped un-coupled nature meant that it would also be the least accurate.
2. The CFD code StarCD includes a finite volume solid domain model. In this simulation method, both the fluid and solid domains are modelled within StarCD and the pressures on the boundaries of the fluid domain are used to calculate the stress and deflection of the solid domain. However, these deflections are not used to move the fluid domain. This method is an example of a single multi-physics code with a one way couple approach. This means the method is most suited to applications with only small solid deflections. As Most specialised solid domain solvers use the finite element approach, the finite volume approach to the solid domain may not be the most efficient or accurate.
3. The StarCD-Abaqus Direct Coupling method is an example of a two code approach where domain specific solvers are used, an Eulerian finite volume approach for the fluid and a Lagrangian finite element for the solid. The direct coupling method can operate as both a one way couple or a fully coupled approach. The one-way coupling approaches, here fluid to solid for stress and deformation and solid to fluid for thermal multi-physics analyses, are applicable for small deflections. This is extended to the fully coupled approach using the mesh-morphing capability in StarCD for large deformation. This method requires two models and additional resources to support the communication between the codes, however, using domain specific solvers means that no accuracy or efficiency sacrifice has been made for either domain.
4. The Abaqus Combined Eulerian (CEL) method is a single code, fully coupled multi-physics approach. Within this method the fluid is modelled by a simpler Equation of State rather than the full Navier-Stokes equations. This means that there is a compromise on the fluid modelling which may effect the accuracy. However, this approach requires only a single model which covers both domains meaning that there are no additional solver requirements.

The first step in evaluating the multi-physics CAE methods was to understand the requirements for using more advanced methods. As both the direct couple and CEL method show significant disadvantages in overall costs (modelling, setup and running), the uncoupled method would be

first used. This is due to the speed and simplicity of the method. By examining the deformations and structural behaviour of a test case, the need for fully coupled methods can be evaluated. To support this evaluation the two high load cases (kerb island strike and 16KpH frontal crash) and the simplified fuel tank and baffle were used in the assessment of the unmapped and uncoupled multi-physics methods.

7.6 Unmapped & Uncoupled Analysis Case Study

The average pressure loading on each of the individual surfaces on the baffle was output from the StarCD models in the engineering data file. These pressures could be applied to a simple finite element model of the baffle in an uncoupled approach. This section details the model setup and results of this investigation. The aim of this section is to explore the need for fully coupled methods given the example loadings from the fuel slosh study.

7.6.1 Finite Element Model and Pressure Loading

The baffle surfaces from the CAD model were imported into Abaqus CAE viewer. The solid volume was then meshed with polynomial tetrahedral elements at an approximate size of 3mm, which allowed three elements to be placed across the baffle thickness. The four baffle feet were given non-displacement boundary conditions in the three principal directions locking the baffle in position. The material selected for the baffle was high density polyethylene which has a density of 876 kg/m^3 , a Young's modulus of 903.114 MPa and a Poisson's ratio of 0.39. The model was assumed to remain linear elastic as this allowed for a simpler model.

The pressures from the StarCD model needed to be applied to the individual surfaces on the finite element model of the baffle. This was done by creating surface sets and applying a pressure load boundary condition on that surface. Each surface then had its own boundary condition that allowed the pressures through the simulation to be varied using the *amplitude card within Abaqus. A Matlab script was required to extract the pressure data from the StarCD engineering data file and put it in the correct format for these *amplitude cards. This Matlab script also computed a running average on the data to reduce the number of increments in the finite element model. For the kerb island strike the 7000 StarCD timesteps were reduced to 200 increments in Abaqus using an averaging factor of 35. For the 16 kph crash case the 20,000 StarCD timesteps were reduced to 400 Abaqus increments using an averaging factor of 50.

To assess the need for a fully coupled analysis of the load cases, the deflection of the baffle needed to be measured throughout the duration of the simulation. To achieve this, the displacement of all nodes was saved into the simulation output database every 5 increments. The model was run in Abaqus standard using the *dynamic card to control the time increments. The use of Abaqus CAE as a preprocessing tool means that the input deck was automatically written.

7.6.2 Results

The deflections of the baffle are taken at the four points shown in Figure 7-1. For point D, the x-directional deflection will be of the greatest interest, while the y-directional displacement is examined at points A, B and C.

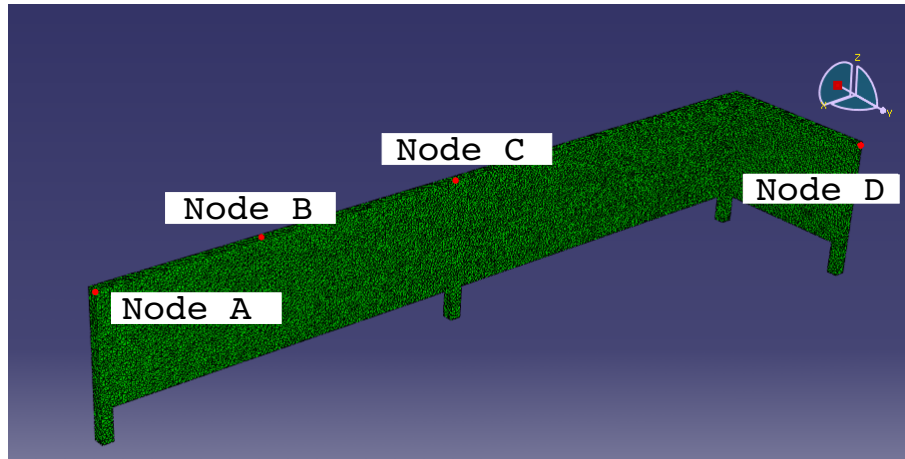


Figure 7-1: Deflection sample locations

Kerb Island Strike

Figure 7-2 shows the deflections of the baffle in the x and y directions along with the load applied during the kerb island strike case. It can be seen that the maximum deflection is less than 1 mm away from the starting point in any direction. The deflections also follow the loading and do not show any vibrational behaviour. This small, steady deflection would not displace the first layer of cells in a fluid mesh. Hence, the application of a fully coupled fluid structure interaction may not be appropriate.

16 KpH Crash Case

The displacements from the 16 kph crash case demonstrate the need for a fully coupled method. Figure 7-3 shows maximum deflections of 12 mm in the x direction and 14 mm in the y direction. This displacement is greater than the base mesh size within the fluid models. The displacement also shows some vibrational behaviour, this is clearly seen in the x direction and as the load is released in the y direction. In reality, the fluid surrounding the baffle would have a dampening effect on this behaviour. This effect cannot be included in an uncoupled or single directional (fluid to solid) coupled method. It can be seen that for this tank and baffle combination undergoing the 16 kph crash loading, a fully coupled method is required.

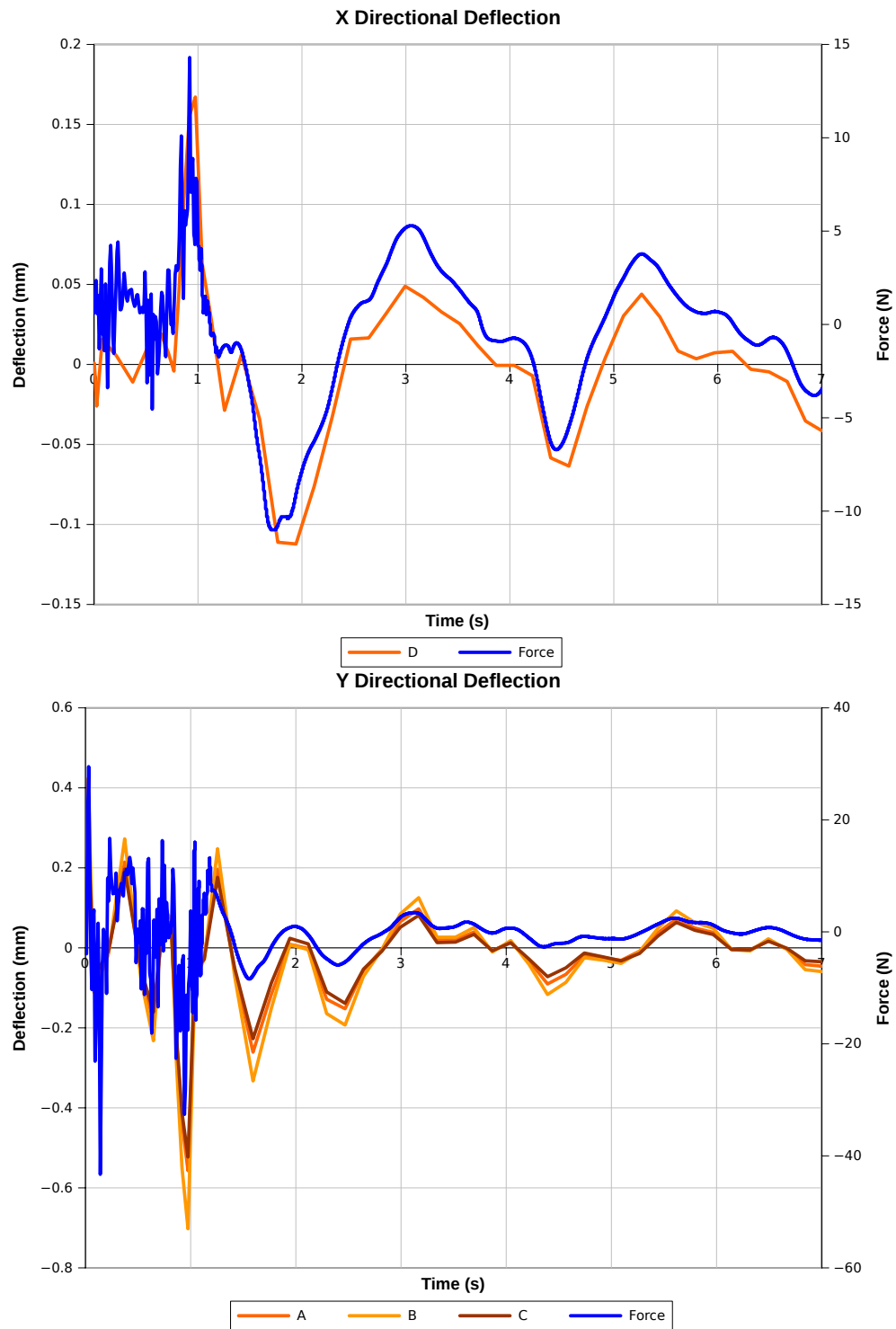


Figure 7-2: Kerb island strike deflection and loading for x (top) and y (bottom) directions

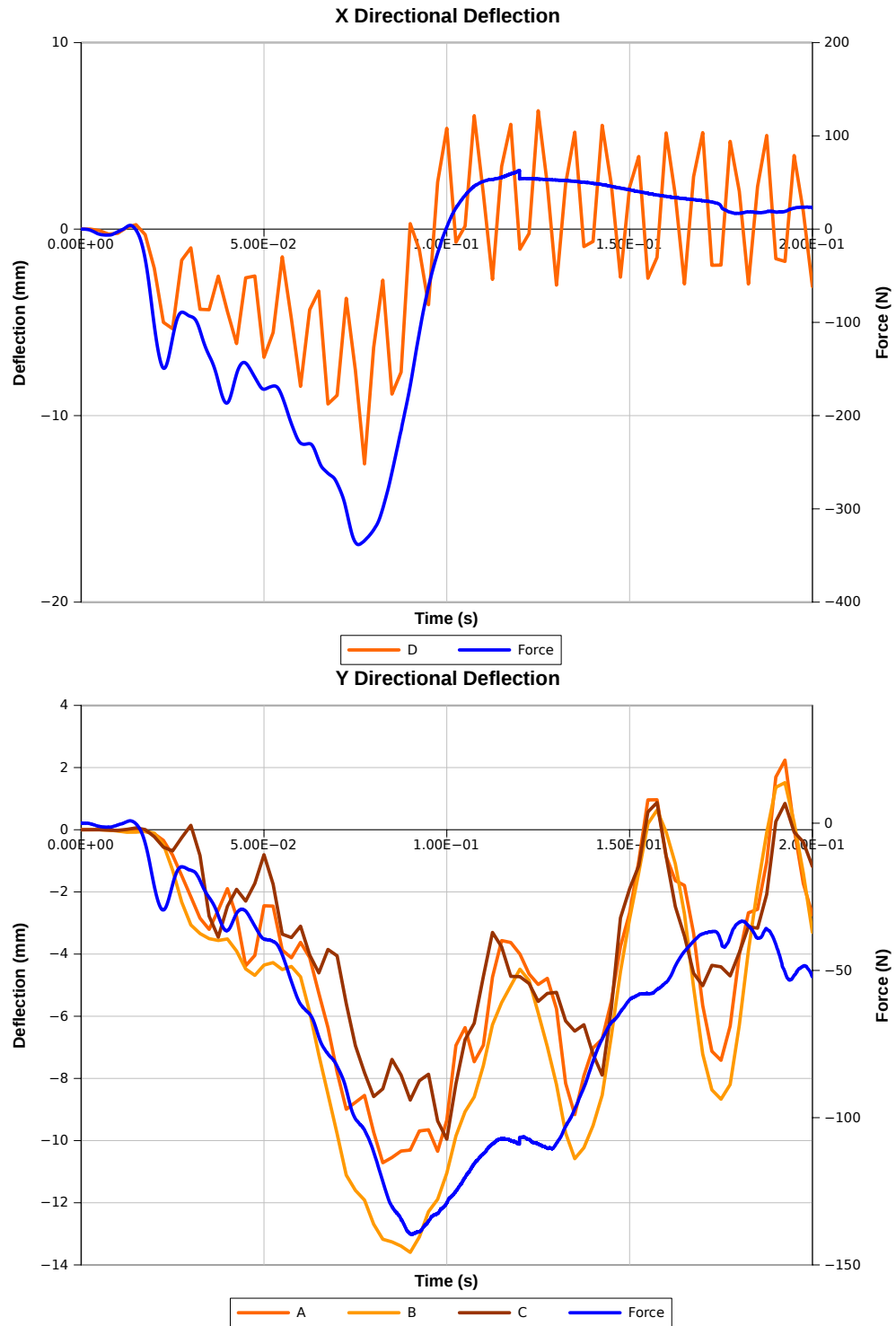


Figure 7-3: 16 Kph crash deflection and loading for x (top) and y (bottom) directions

7.6.3 Summary

The aim of this experiment was to assess the need for fully coupled methods to assess the durability of internal components of the fuel tank when exposed to fluid slosh. For this two cases were tested. The first of these, Kerb Island Strike, had lower loading forces but the event could be repeated many times during the vehicle usage, while the second, the 16 KpH crash case, was an example of single event shock loading.

In the first case the internal baffle in the fuel tank experienced only a small deflection meaning the application of fully coupled methods would not be beneficial for the additional costs involved. Whereas the high deflection and vibrational behaviour exhibited in the 16KpH crash case indicated that a fully coupled solution would be required. While the requirements for different degrees of coupling between these two cases are clearly visible in the results, it is unclear where the switch over point between different coupling approaches occurs. This should be the subject of future investigations.

However in this project, the unmapped and uncoupled method was shown not to be applicable for cases of high deformation and vibrational behaviour, but this result also rules out the use of the StarCD finite volume solid solve approach. This is because this method only uses a one way coupling approach meaning the damping effect of high deformation would not be captured. This case requires a fully coupled domain approach to capture the large deflections and vibrational behaviour interaction between the fluid and solid domains. The fully coupled methods available to this project were then tested to see the fluid structure interaction in the 16 KpH crash case is captured.

7.7 Multi-Physics Analysis Methods

The project was constrained to use multi-physics methods available within standard Powertrain CAE codes. This limitation meant that only two approaches could be taken to model the fully coupled fluid structure interaction analysis. Firstly, a two code direct couple approach between StarCD version 4.08 and Abaqus version 6.8EF, and secondly a single code Combined Eulerian Lagrangian approach in Abaqus 6.8EF. As these approaches were both new, the first step was to assess the methods for the key requirements of any CAE analysis, stability and accuracy. As the direct software couple used well understood single domain solvers, the focus was on the stability of the coupling method. The CEL method featured a new equation of state model for fluid dynamics, this is much simpler than the full Navier-Stokes equations solved in most CFD methods. This was tested to ensure that it could accurately predict the free surface and pressure within the fluid and on the surfaces. The stability of this method also needs to be established. In order to assess these methods, simplified cases were generated that represented the requirements of the case. These models were developed from models provided by the software vendors.

7.7.1 Star-CD & Abaqus Direct Couple

The StarCD/Abaqus direct couple is an explicit code where information between the two distinct domains is shared only at timesteps. The surface pressures are output from the Star-CD fluid domain and mapped onto the appropriate solid surfaces. The solid domain is then solved and the deformation of the surface is written to a file. The mesh in the fluid section then needs to be moved accordingly, this is achieved using mesh morphing techniques within ProStar.

CD-Adapco provided a proof of technology model that featured air flowing through a duct and encountering a flexible baffle [142]. This case was then developed to make the model more representative of the fluid sloshing within the fuel tank. The tank was assumed to be a 3D rectangular box, featuring a solid baffle. The VoF method was implemented as in the load case study (see Appendix section E.3) and was assumed to be 50% full of diesel fuel. The geometry setup is shown in Figure 7-4. To simplify the model, all additional fluid models such as turbulence and surface tension were removed. A small load would be applied to the fluid by implementing the tip case via `sormom.f` (see Appendix F.1). The mesh morphing was implemented using the events method within StarCD. This called a ProStar sub-routine which moved the mesh in the baffle region. This sub-routine was provided by CD-Adapco for the proof of technology model and modified to suit this case, the code is shown in Appendix F.3. The necessary Abaqus deck commands for coupling are given in Appendix F.4. The force on the baffle was captured within the engineering data file and was used to examine the progression of the simulation. The baffle was modelled as linear tetrahedral elements to ensure that the mapping of the surfaces occurred without error. The material for the baffle was assumed to be the same high density polyethylene used in the uncoupled case.

As a comparison, the model without the direct couple was completed for 0.2 seconds with a timestep of 0.001 seconds. The coupling was then engaged for this model and the results shown in Figure 7-5. It can be seen that the initial predictions of the force on the baffle from the coupled

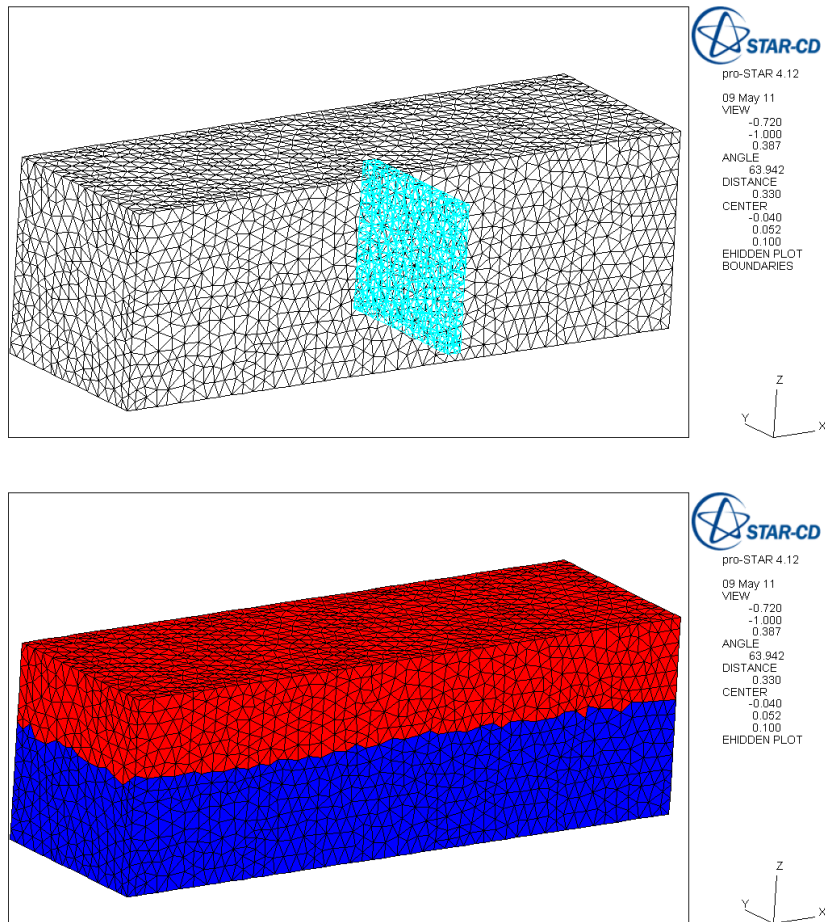


Figure 7-4: The geometry and fluid fill conditions used in the direct couple assessment

case agree with the loading in the fluid only case. However, after approximately 0.15 seconds the loading on the baffle began to oscillate and eventually diverged. In order to understand this instability two further cases were investigated. In case 2 (Figure 7-6) the timestep was reduced to 0.0005 seconds. This showed a greater amount of instability and again the solution diverged. In the final case the material of the baffle was changed to steel with a density of 7860 kg/m^3 and a Young's modulus of 200 GPa. This case was shown to be stable throughout the duration of the simulation as shown in Figure 7-7. These issues were referred back to CD-Adapco support for discussion.

The issue displayed in the results is that increasing the density of the fluid compared to the solid causes the program to diverge. Discussions with CD-Adapco confirmed that this occurs due to the explicit method used to communicate surface pressures and deformations [19]. As the simulation increments from one timestep to the next, the solid boundary face will be displaced by a small amount. This displacement will cause a rebounding force as the fluid opposes this motion. If the density of the fluid domain is small (e.g. air) then this force is small when compared to other

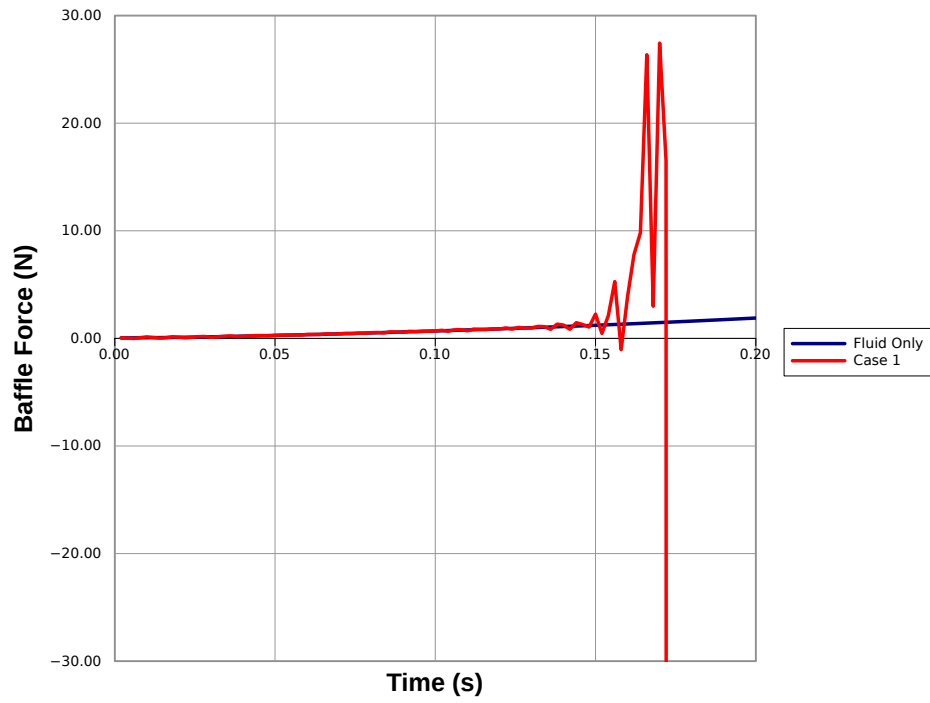


Figure 7-5: Comparing the coupled model to the fluid only model

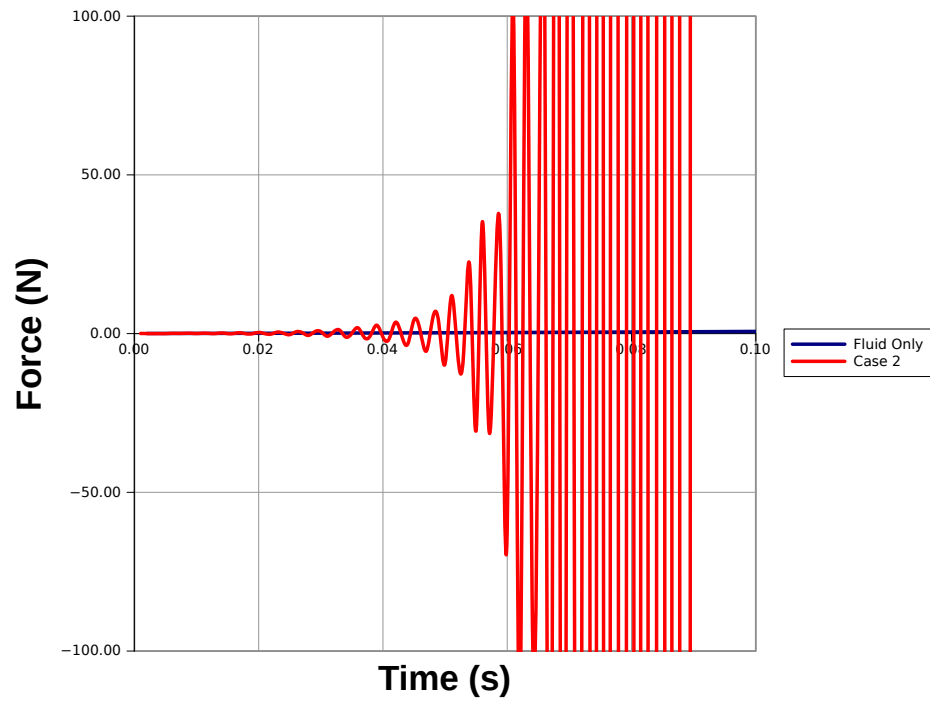


Figure 7-6: Comparing the coupled model with a reduced timestep to the fluid only model

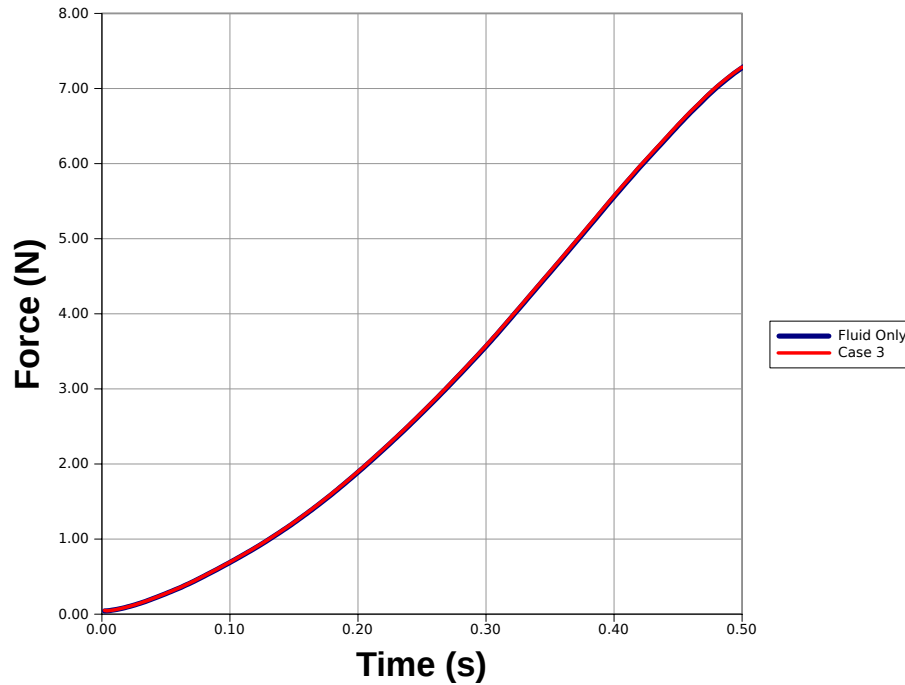


Figure 7-7: Comparing the coupled model with a steel baffle to the fluid only model

loadings within the simulation and does not cause a problem. However, if the density of the working fluid is much larger, then for the same volume of displaced fluid, a much larger rebounding force will be generated. This causes an unrealistic rebounding effect. These oscillations steadily increase until the simulation fails. This explains why stability was found in the case completed with the steel baffle. Further reductions in the timestep could be used to keep the model stable. However, the limit of stability will be dependent on the loading and deformation and may change during the simulation. The conclusion was that this approach is not suitable for applications where the density of the fluid region approaches that of the solid region. The problem has been confirmed with the vendor (CD-Adapco), whom have since changed the usage guidance and are developing a new approach to analyse such cases[19]. However, the direct couple could be used for applications of air-solid coupling. Such applications are beyond the scope of this project but should be part of future research.

7.7.2 Abaqus Combined Eulerian Lagrangian

The CEL method within Abaqus is a very different approach to modelling fluid structure interaction. The fluid is modelled by a simpler equation of state in an Eulerian mesh. However, the interaction with the solid domain is not modelled by morphing the mesh to conform to the Lagrangian solid. Instead the Lagrangian meshes are able to pass through the Eulerian domain. This approach reduces the mesh distortion in high deformation cases. A VoF method is used to track the fluid material interfaces and the interactions defined by the general contact rules within Abaqus.

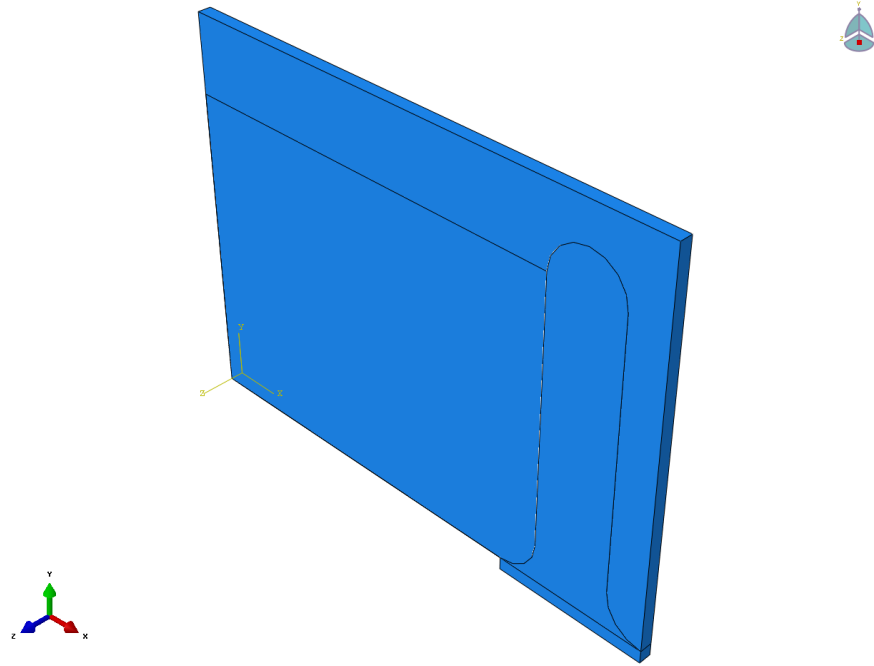


Figure 7-8: CEL test case geometry

As the fluid module within Abaqus is new it was tested on a representative test case to ensure that hydrostatic pressures and free surfaces can be predicted. The case selected was a baffle with dimensions of a similar order of magnitude to those seen on the internal components of fuel tanks. The geometry for the test case is shown in Figure 7-8; the radii at the base and top end of the baffle were 15 mm and the baffle was 150 mm tall. The Eulerian mesh size was set to 3 mm as guidelines suggest that radii feature five mesh elements for a right angle. Also, this was a reasonable representation of a locally refined mesh in a StarCD model. The CEL model was defined using the example given in the tutorial documentation [134]. For model simplification, the solid was set as a rigid body which would not deform but act as a wall. It is meshed using 3mm poly hexagonal elements. The water was defined as an equation of state of type $U_s - U_P$ with a EoS shear property. This required the fluid density, speed of sound and viscosity to be defined. As water is used in this case, the density was 1000 kg/m^3 , the speed of sound was 1483 m/s and the viscosity was 0.001 kg/ms . The contact between the solid and fluid was modelled as rough friction and all exterior contacts were included. The initial water volume was defined using the volume fraction tool within Abaqus. Here, a part with the same shape as the initial volume of fluid was used to define what fraction of fluid each mesh element contained. Zero velocity boundary conditions were applied to Eulerian mesh to prevent fluid leakage, encastre boundary conditions on the base of the baffle and gravity loading on the fluid. To enable the solved free surface and pressures to be examined the VoF and average pressure in the Eulerian domain were output to the results database. The simplified Abaqus Deck for this problem is supplied in Appendix F.5. The pressures and VoF free surface for this model are displayed in Figures 7-9 and 7-10 respectively.

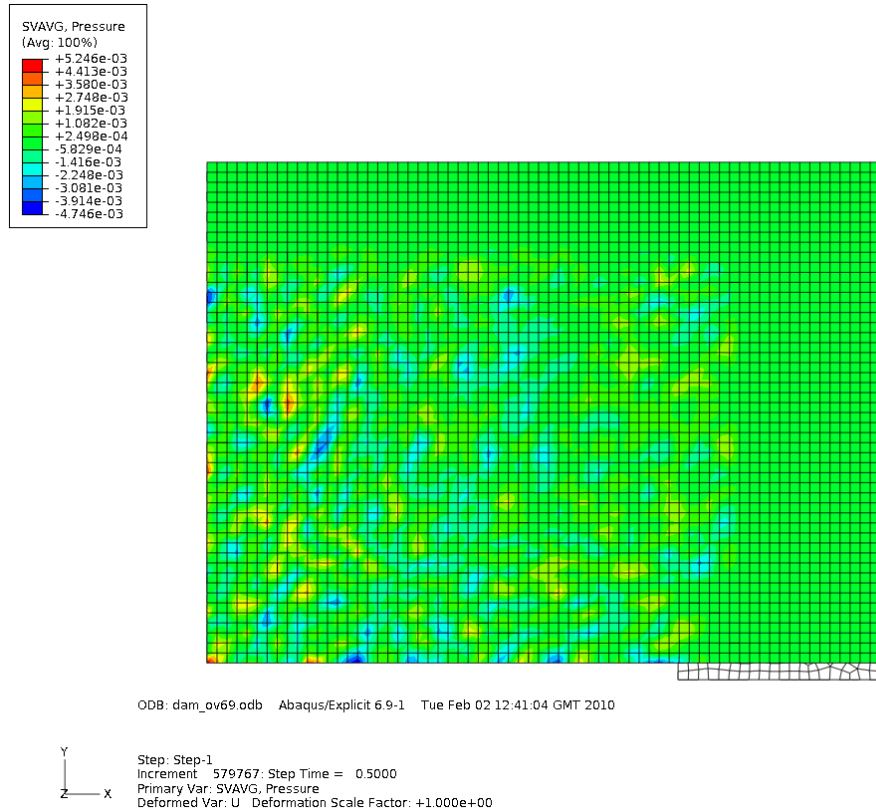


Figure 7-9: Eulerian mesh pressure distribution

As gravity is applied as a boundary condition, the pressure should increase with depth according to ρgh , but the pressure distribution shown in Figure 7-9 shows just noise with no discernible graduation. The prediction for the free surface is also poor, it can be seen that the instability increases throughout the duration of the simulation. These issues were raised with Simulia support in an attempt to find the cause and solution. The following issues were found with this model[20]:

- The simplified model featured a 3 mm mesh which was intended to be representative of the potential refinement required to capture internal tank geometry. This mesh size is small and can represent much higher frequency content. Any pressure noise would be dampened by larger elements in the mesh but small meshes will transmit this information. These small elements not only slow the simulation down but also cause instability.
- The use of rough friction introduces further noise to the system and should not be used with the small meshes.
- The formulation of the CEL method allows some fluid to penetrate the solid domain. A penalty constraint method is then used to enforce the solid boundary. This pushes the fluid back into the Eulerian domain. When the model is initialised with some fluid penetration, the resulting correction of over closure can result in additional fluid velocity noise being added into the

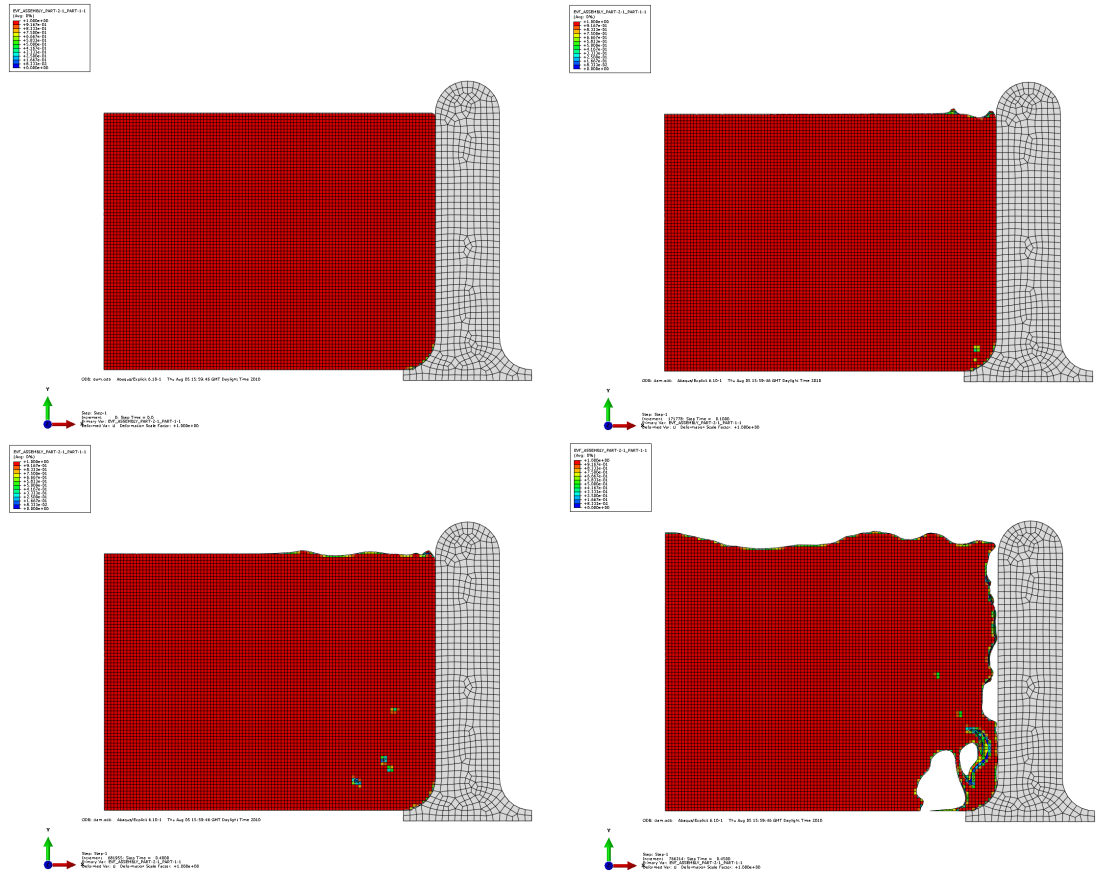


Figure 7-10: Free surface at time 0.0 (top left), 0.1 (top right), 0.4 (bottom left) and 0.45 seconds (bottom right)

Eulerian domain. Again, in this case the small mesh has transmitted this noise, resulting in an unstable free surface. The usual solution for this is to add a fillet to the Lagrangian mesh and locally refine the Eulerian mesh to match the Lagrangian. As this model already has a fillet which is meshed to the refinement guidelines, another approach needs to be taken. Once this was raised with Simulia, a new Abaqus environment file was supplied that modified the initialisation of the VoF surface, which remains untested at this time.

A final suggestion to improve all issues with the CEL model was to ramp the gravity boundary condition on over time and allow the fluid in the tank to settle. However, this would substantially increase the runtime of any simulation.

Unfortunately, due to the time constraints of the project and the timing of these discussions with Simulia, the improvements remain untested in this case. However, from these discussions it became clear that smaller mesh sizes affect the stability and robustness of the solution and that larger meshes should be used[20]. This would mean that detailed geometry may not be captured and the accuracy of the simulation would suffer. Another drawback of this method is the Eulerian meshing method. The element type and implementation mean that it cannot be formed

into a conformal mesh for complex shapes, nor can the local refinement in areas of interest be implemented easily. From this it must be concluded that the CEL method is not a feasible FSI method for the assessment of durability of internal tank components at this time.

7.8 Discussion

The application of the direct StarCD-Abaqus couple and CEL methods have shown that the fully coupled fluid structure interaction methods available in Jaguar Land Rover are not suitable for the assessment of internal component durability in large shock events at this time. Due to this, the relative merits of using a multiple or single code approach to fully multi-physics CAE for this case could not be established. However, the one directional methods did show suitability for cases where the deflection of the baffle was small and did not exhibit any vibrational behaviour that would be dampened by the surrounding fluid. This could be applied to fatigue or NVH slosh evaluations where lower loading forces are expected.

The aim of this project was to establish the additional costs and benefits of using a multi-physics approach as a stand alone CAE tool as well as an attribute predictor in MAO projects. From the work completed on MAO methods it can be seen that establishing the accuracy versus cost balance is critical in metamodel based MAO projects, as the metamodel is sensitive to both error from unstable or inaccurate CAE methods as well as the number of samples used. This project has examined two ways to approach this balance; the first is the degree of coupling and the second the use of multiple or single code approaches.

The experiment conducted using the two load cases and the uncoupled approach showed that both the simpler uncoupled/one way and fully coupled approaches would have use in a multi-physics analysis of a fuel tank. The uncoupled/one way approach can be used for small deflection and a fully coupled when the solid movement is large. However, what was not detailed was the switching point between choosing which approach to take. Determination of this would be vital in the running of a multi-physics analysis as the degree of coupling has a large impact on the cost of modelling. Resources could be wasted if a fully coupled approach was taken when only a one way approach was required. The requirement for multi-physics methods should be assessed in further research.

By using the two fully coupled approaches available to Jaguar Land Rover, the multi-physics project aimed to allow the efficiency-accuracy balance between the domain specific coupled software approach and the single multi-physics code to be examined. The direct couple would require two models to be created; one in StarCD and the other in Abaqus. These would need to be solved together in an approach that supported communication between the two software codes. As these codes are specialised to solve that particular domain there would be less compromise with the accuracy of the model. The single code approach requires only one simulation model for both domains. However, with this there is a compromise on the accuracy of the fluid flow predictions due to the simplified 'equation of state' model. As both these methods were not suitable for this case, the impact of the single versus multiple code could not be assessed. Further work should be

conducted to examine other multi-physics opportunities and methods, examples of which include:

1. *Direct Couple*: The examination of the fully coupled StarCD-Abaqus showed that this method could be applied where there are large differences in the densities of the two domains, e.g. air and plastic or liquids and steel. The need for fully coupled methods involving such materials should be examined. The direct couple can also be used in a one-way coupling method. Here the pressures or temperatures can be mapped to an Abaqus model, but in this case the structural deflections are not used to morph the mesh leaving the shape of the fluid domain constant. This method would only have applicability in cases of small deflection. A guide for what constitutes small deflection suggested by this work would be where the maximum deflection is less than the general cell size used in the fluid mesh and where no oscillating behaviour is present.
2. *CEL Multi-physics*: The cause of the poor pressure prediction was found to be the transmission of noise through the fluid domain due to the small elements used to represent the geometry. This also contributed to the unstable free surface prediction along with the penalty constraint resolution for fluid penetration. Simulia support advised the use of larger elements and released upgraded environment files to fix fluid penetration in the initialisation of the model which remain untested at this time. The use of larger elements may prohibit assessment of slosh loading on internal tank components as the small elements would be required to capture the geometrical detail. However, the application to tank shell assessment, where geometrical features are larger, requires further investigation. This should also include an assessment of the updated software code.
3. *Un-coupled or One-way Coupled Methods*: The manual transfer of pressure data from the StarCD model to the Abaqus model was an example of an uncoupled FSI method. The next step on from this is to use a mapped transfer of pressure data. While this could still be achieved by manual means, (by writing out data files with location and pressure data for each cell and applying it to a structural model,) the use of one-way couples is more attractive as this process would be automated. Examples of one-way couples are the finite volume solid solver within StarCD/CCM+ and the direct couple (when the deflections are not used in mesh morphing). These could be applied in sloshing cases where the deflection is small, meaning there is little deformation into the fluid domain. In the fuel tank analysis, this could include NVH and external tank applications. These two methods also offer an opportunity to investigate the efficiency-accuracy balance of a two-software code approach and a single multi-physics approach. In this application the compromise for accuracy is made in the finite volume solid solver and would need to be compared to more widely used finite element methods.
4. *Other Codes*: One of the restrictions placed on the project was to limit the fluid structure interaction methods to preferred Powertrain software codes, primarily StarCD and Abaqus. These methods have been shown to be unsuitable for the assessment of fuel tank internal component durability, however, there is still a need to analyse the problem. Another line of research that could be followed is to expand the CAE tool-set beyond those currently in use

in Jaguar Land Rover Powertrain CAE. The literature shows examples of LS-Dyna [143] and MSC-Dytran [144] being used for such applications. Also updates and new methods from preferred vendors should be investigated.

7.9 Conclusions

Of the three methods applied to the multi-physics analysis of a fuel tank, only the uncoupled, unmapped method was able to be used. This approach showed that it could be used for loads which cause small deflections. However, the accuracy of the method is severely affected for high load events such as the crash case. This event shows a high degree of deflection and cycling behaviour which would be damped by the fluid, meaning for this load case a one way couple is insufficient. From the experiments on multi-physics methods assessed in this chapter it can be concluded that:

1. It is not feasible to use StarCD-Abaqus Direct couple or Abaqus CEL multi-physics codes to assess the durability of internal components of fuel tanks.
 - The explicit timestep in the direct couple approach means that it is unsuitable where the densities of the solid and fluid domains approach each other. This has since been referred back to the vendor and guidance for usage has been updated.
 - The CEL errors stem from the use of small elements which transmit high frequency noise through the fluid domain. This could be solved by using a larger mesh. However this may compromise the ability of the model to capture the detail of the tank internal structures. These issues were also returned to the vendor, whereupon new guidelines and environment files were issued. These have yet to be tested within Jaguar Land Rover.
2. While the analysis of fuel tank internal component durability cannot be assessed by these methods, other applications and areas of work and research are:
 - One-way coupled methods for fatigue life or NVH slosh evaluation. This could be a further development of the uncoupled method or the application of the finite volume solid solver in StarCD or the one-way coupling available in StarCD-Abaqus direct couple.
 - Using the fully coupled StarCD-Abaqus fluid structure interaction method where the working fluid is air. This would first need an exploration of application as completed in the define stage of this project.
 - Assessment of the new guidelines and environment files in Abaqus CEL to examine improvement in performance.

As the multi-physics methods cannot be used for this application at this time, the assessment of the benefits that such approaches bring to a multi-attribute optimisation architecture could not be addressed. However examining the different methods it is possible to infer further research questions that need to be addressed in more suitable applications.

The various different methods addressed two different approaches to modelling multi-domain problems. The direct coupling between StarCD and Abaqus represents a two model solution with each model accounting for a specific domain. This would require two separate models (one CFD and one FEM) plus additional architecture to support the communication between the two codes. This would increase the cost of the approach. However, it uses tools specialised to the specific domain meaning no compromise has to be made with regards to the accuracy of the model.

On the other hand, the Abaqus CEL approach is an example of single code, multiple domain analysis technique, i.e. both the fluid and the structure are solved in a single model. While this is cheaper in terms of modelling costs, a compromise is made in the modelling of the fluid. This may not be as accurate.

Future projects examining multi-physics methods within multi-attribute architectures must address this balance of the need for simulation accuracy versus the additional cost of such models. This should include an assessment of the degree of coupling required in a multi-physics analysis, as this has a large impact on the cost of a simulation. The degree of coupling used should be appropriate to the case to balance both the accuracy of the simulation and the cost of completion. Further work should be conducted on the switch over point between coupling methods.

Part III

Project Closure

Chapter 8

Discussion

8.1 Introduction

The aim of this chapter is to use the work completed in the airbox MAO problem and multi-physics analysis of a fuel tank, to demonstrate the use of MAO methods as a systems engineering tool. This chapter will then use an automotive case study to understand the potential application of a MAO systems engineering tool. Finally, further research areas to improve MAO as a systems engineering tool are detailed.

8.2 MAO Methods as a Systems Engineering Tool

In this section, the use of MAO as a systems engineering tool to enable improved design is discussed. Firstly, a review of the MAO method is given, detailing the MAO process. From this, key contributors for using a MAO tool are identified. Each of these is then discussed in turn. Where applicable, further work to improve the MAO contributors is given.

8.2.1 The MAO Method

The MAO of an automotive airbox used a metamodeling approach to trade-off three attributes. The process and findings of this approach were discussed in Chapters 4 to 6. Using these chapters as a guide, the metamodel based MAO method can be summarised by the flow diagram presented in Figure 8-1. This diagram shows the key contributors and processes that occur in the creation and use of metamodels in a MAO method.

A MAO project should begin with the definition of the key design attributes, the contributing input variables with appropriate ranges and the requirements and constraints of the design. In the airbox optimisation these were identified by using a systems engineering P-Diagram (see Figures 4-2 and 4-3 on pages 79 and 80). This tool identifies the inputs, control factors, noise factors, error states and the required function of the system to be designed. With this understanding of the system, the

engineer can then focus the optimisation on the most important issues and control factors. From this, the key attributes and their control factors can be established, along with the requirements and constraints for the attributes and design parameters that will be used in the optimisation.

Once the key attributes and inputs of the system to be designed have been established, the parameterised CAD and the CAE analysis methods need to be defined. As multiple attributes may require multiple CAE models, the CAE build process may need to be repeated a number of times. There may also be changes to the parameterised CAD model to reflect the use of multiple models, i.e. the CAD model may have to produce a number of geometries in different formats. The CAE build process is required to investigate the suitability and stability of the analysis setup to ensure robust application of the model to the entire feasible design range. In the airbox project, this was completed by using a number of example airbox designs that were judged to be the worst case scenario. The airbox project also showed how methods of automation can be used to increase the efficiency of the analysis process. For the StarCD CCM+ model, automation was achieved through the use of java scripts which were applied to set up the CFD model. The use of automation for Ricardo WAVE was limited to the geometry definition for the WaveBuild3D models. The ability to use automation methods should be examined and the processes set up alongside the initial CAE build processes.

Once the CAD, CAE and automation methods have been defined, the sample size and distribution must now be set. At this point, the approach to the accuracy versus sample cost must be defined. When metamodeling based MAO methods are used within a design environment, there may be constraints on the time or resource usage, limiting the number of samples that can be taken. However, for confidence in the metamodel, a larger sample size may be required. The setting of the sample size may require a trade-off process. Using information from the initial CAE model builds and an engineer's experience, the cost and time of running the CAE models can be estimated. From this, estimation combined with guidance on the sample size required, the total cost and runtime of the metamodel sample can be estimated. However, if the cost and runtime is greater than is available, the inputs to the project must be adjusted to allow the cost to be reduced. The adjustment may be to remove one or more of the attributes or controlling factors. This cost and runtime analysis must also include the definition of the approach taken to estimate the error in the metamodel as this also represents a conflict between cost and accuracy. Finally, the estimation of the sample cost may also need to consider the potential need for further re-sampling methods should the initial sample prove insufficient.

The next stage is to complete the initial sample and generate the metamodel for each attribute. To have confidence that the metamodel can be used within the MAO method, the error must be assessed. From this, the need for further sampling is determined. In the airbox project, a number of re-sampling methods for the NVH attribute were explored. Firstly, the use of the Lipschitz sampler available in modeFRONTIER and then secondly, a larger latin hypercube was applied enabled by a simplification of the CAE. While the application of these methods did reduce the error in the NVH metamodel, large errors in fit were still present resulting in low confidence in the accuracy of the metamodel. However, in this case the project proceeded to examine multi-attribute trade-off methods. For other MAO projects, the re-sampling methods should be used to reduce the error to

an acceptable level. From this, the metamodels can then be used to optimise the design.

To find the optimum design, the design space needs to be explored. The airbox project used a number of exploration techniques to understand the effects of the main parameters on design and the trade-offs within the design space. Use of single-attribute optimisation techniques enabled the maximum potential performance to be established. However, the designs did not represent the best attribute trade-off. To enable the multi-attribute trade-off in the airbox the NSGA II algorithm was applied to the metamodels, this enabled the pareto set to be calculated. These were then sorted using visualisation and decision method techniques to find the optimum airbox for all three attributes. These techniques to find the optimum trade-off design were guided by the requirements and constraints defined at the start of the project.

The final step in the MAO method is to verify the optimum. This can be accomplished using the same CAE methods or by prototype testing.

8.2.2 MAO Method Contributors

From the description of the MAO method it can be seen that there are a number of key contributors. The role of the CAE methods, the sample size and distribution method (including re-sampling techniques), metamodel selection, error estimation and automation of the process can all have a significant effect on the outcome of a project.

CAE Methods

CAE methods must represent a balance between accuracy and cost. Higher sampling costs will reduce the number of samples that can be obtained, however lower cost models may not be able to capture the system behaviour adequately.

In single attribute optimisation, the main effects plot can be used to drive the optimisation in the correct direction. While there is low confidence that this will result in the global optimum, the design will be moving towards this point. However, when multiple and conflicting attributes need to be considered, the metamodel surfaces need to be as accurate as possible so the trade-off region is correctly defined. The CAE methods have a large influence on the accuracy of a metamodel.

When selecting the CAE models to use, the estimated sample size must be considered in order to find the most accurate system metamodel for the lowest cost. This can be seen with the Ricardo WAVE methods used in the airbox project to predict the NVH metric. The manual WaveMesher method represented a high setup cost and could not be applied when the number of samples needed to be increased. Thus, a lower cost, WaveBuild3D model was utilised. This method simplified the airbox designs down to a simple volume and set of pipes, with more complex features such as bell mouths and fillets removed, allowing automatic generation of the airbox geometries. This may have affected the accuracy of the result, but did allow more designs to be tested in a shorter space of time.

The requirement for increased accuracy for attributes which cross traditional analysis domains was identified as part of MDO methods[18]. Such multi-physics approaches represent an increase

in modelling cost as multiple domains must be included in the simulation[17]. This can be achieved by either coupling domain specific codes, requiring multiple models and support for the data exchange, or a single multi-physics code which solves both domains within a single software[103]. In this thesis, the multi-physics analysis of a fuel tank was used to examine the relative benefits and costs of using such methods. However, due to the unsuitability of the available software codes for the selected application, a direct discussion of using multi-physics CAE methods as an enabler for MAO cannot be completed at this time. Despite this, some relevant issues were raised in this part of the work.

Part of the Multi-Physics examination was to look for the degree of coupling required to assess the durability of internal fuel tank components. This found that for the Kerb Island Strike load case, the deformation of the structure was small, requiring a one-way couple, but the large un-damped deformation exhibited by the baffle structure in 16 Kph Crash case would require a more expensive, fully coupled solution. This raises important questions about the switch over point between various coupling levels in a multi-physics approach. When using multi-physics methods as an enabler to MAO, the requirement for coupling must be assessed. The coupling level must be appropriate to capture the attribute behaviour as well as for cost. Establishing heuristics to guide transition between the different degrees of coupling should be one area of further research.

The work on the multi-physics methods also showed some of the potential dangers of using new CAE methods in MAO projects. Both the CEL and direct coupling methods were not ready for application to fuel tank sloshing problems within powertrain CAE. These methods were unstable in this application or had poor accuracy on attribute prediction. An optimisation process based on such methods would fail. One recommendation for future MAO projects is that only mature and validated analyses are utilised in an optimisation process.

The StarCD CCM+ also demonstrated another important issue with using attributes predicted by CAE methods. Any errors or convergence issues in the CAE will contribute to the error in the metamodel. In the airbox project, this is demonstrated by airbox designs 9 and 13 in the initial 33 latin hypercube sample (see Table 5.7 on page 117). When the pressure loss attribute for these designs was captured over the last 200 iterations of the simulation, the attribute value varied by over 3%. This convergence issue occurred due to poor resolution of the flow within some region of the mesh and may have contributed to the poor fit of the metamodel in the design space around this sample. The root cause of this was the strategy used for meshing the CFD models.

The meshing method was derived by a trial and error approach to ensure stability on the worst case scenario for the airbox design. The finalised meshing strategy represented a balance between the runtime and the stability of the CFD model. The approach was then tested on a number of designs before application to all cases in the latin hypercube. However, this generic 'one strategy fits all' approach led to a number of designs displaying high amounts of variation in the attribute values. Thus when the CAE approach is developed, it must be robust in all regions of the design space. Again this emphasises the fact that stable and known CAE methods should be used for MAO projects.

Sampling Size for a Metamodel

The discussion of the MAO method showed that the setting of the sample size was important for both the accuracy of the metamodel and controlling the runtime and resource cost of the project. If the sampling number is too low, then the attribute behaviour may not be captured, too high and the project may not be able to be completed within the constraints of the design environment. However, setting the sample size is not straightforward as the complexity of the attribute behaviour within the design space is unknown.

The approach taken in the literature to estimate the attribute behaviour complexity is based on the number of inputs with various multiplication factors applied. The largest sample size given by Jin, Chen and Simpson[12], was based upon methods required to solve the unknowns for the quadratic regression model. A sample size of ten times the number of inputs was suggested by Wang and Beeson for practical applications of metamodeling[14]. Smaller sample sizes have been suggested by Jin, Chen & Simpson[12], Kaufmann[13] and the minimum sample approach used in Ford[97]. When testing the performance of various metamodeling approaches Jin, Chen & Simpson[12] used the regimes defined in Table 8.1 along with the minimum sample size defined by Gromping at Ford[97]. The literature review also analysed sixteen examples of the metamodeling method for the number of inputs and samples. This was plotted in graphical form as shown in Figure 8-2.

Table 8.1: Guidance for sample sizes (where N is the number of variables)& suggested sample sizes for an 8 variable problem

Size	Number	8 Variable Problem
Scarce[12]	$3 \cdot N$	24
Minimum[97]	$2^{\frac{N+2}{2}} + 1$	33
Small[12]	$10 \cdot N$	80
Large[12]	$\frac{3 \cdot (N+1) \cdot (N+2)}{2}$	135

The initial sampling of the NVH attribute in the airbox project used the minimum sample latin hypercube[97]. This meant that 33 samples would be taken in a scarce approach. However, this was found to undersample the design space requiring a larger sample. The sample size was then increased to 171, beyond the values suggested in Table 8.1. This suggests that the guidance in the literature may be insufficient when generating large generic metamodels. This finding was corroborated by the third sampling experiment carried out in Appendix A. Here, a 2 input variable metamodel required approximately 33 samples to capture the function behaviour. The work also shows that the scarce sampling methods used in current Jaguar Land Rover optimisation processes are not sufficient for large generic metamodels such as the airbox example. Confirmation of this issue can also be found by examining the sample sizes in the metamodeling examples. Examining Figure 8-2 again, it can be seen that while most of the sample sizes for the metamodeling examples are bounded by the regimes suggested by Jin, Chen & Simpson[12], some projects have sample sizes beyond these. From this, it can be seen that the sampling size for metamodels with large

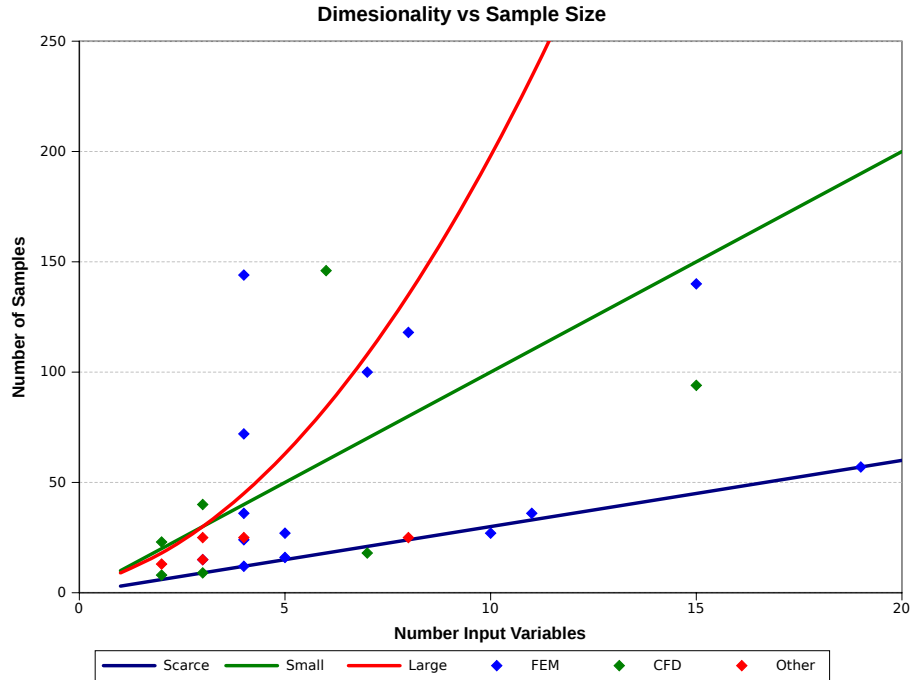


Figure 8-2: Examples of sample sizes in literature

design regions cannot be based on the number of input variables alone. However, as the complexity of the system behaviour is unknown prior to the sampling, the guidance must be based on information available when defining the attributes, control factors and their ranges.

For any optimisation project, the define stage sets out the principal input variables and their ranges. The decisions about which variables should be included is based on prior experience and judgement over what the main factors are that contribute to system performance. Increasing the number of inputs increases the complexity of the problem, so the sample size should be scaled by the input dimensionality. The ranges are then set based on available packaging space, current designs or ideas about potential improvement. However, increasing the range allows for more variation in the attribute behaviour within the design space, increasing the complexity. Thus, the range of variables should also be included when scaling the sample size.

When considering the airbox optimisation detailed in this work, it can be seen that the parameterised design featured eight input variables over a wide range to enable many different airbox designs to be considered. The input variables and their ranges are given in Table 8.2. Within each of the ranges of these variables there are only a finite number of designs that could realistically be used. For example, for the length parameter, a reasonable design step may be every one millimetre or every quarter millimetre on the duct diameters. Applying this step to the variable range will give a total number of potential designs for a given input. However, in optimisation problems with a large design space, the number of potential designs will be high. To reduce this, the sensitivity of the attribute behaviour to the design variable could be used to scale the number of potential designs.

The application of scaling factors would rely on the experience of the engineer, knowledge of

the underlying physics of the attribute or a small main effects study to understand which inputs have the greatest affect on the attribute behaviour. The operation of the sensitivity scaling factor can be seen as a need to test one out of a number of designs. For highly sensitive inputs the scaling value should be low (one or two) and as sensitivity decreases higher scaling factors should be used. The estimated sample size for each variable can be found using equation 8.1. Where $V_n(max)$ and $V_n(min)$ are the limits of the input variable range, V_{step} is the variable design step and SF_n is the variable sensitivity scaling factor. The inclusion of the number of variables (n) allows the sample size (S) to vary with dimensionality as before, however now the range is also considered. Once this has been calculated for each variable, the maximum and minimum values can be used as a guide for the upper and lower bounds of the sample size required. Although no firm value for the sample size required to produce an accurate metamodel of the NVH metric was found, it should be greater than the 171 samples used. The application of this range variable method to the airbox problem is shown in Table 8.2. Each of the design variables was assigned a reasonable step; one or two mm for the main box lengths, a quarter of a mm on each of the duct diameters, five mm on the runner and 0.005 on the percentage ingress. The P-Diagram in the definition of the airbox optimisation problem detailed the importance of the volume and expansion ratios to NVH performance. This led to low sensitivity factor values on the height, length, breadth and duct diameters. This process indicates that the number of samples for the NVH attribute should be between 187 and 320 samples.

$$S_n = n \cdot \left(\frac{\left(\frac{V_n(max) - V_n(min)}{V_{step}} \right)}{SF_n} \right) \quad (8.1)$$

Table 8.2: XK SC airbox input variable ranges and sensitivity factors for the NVH attribute values

Parameter	V(min)	V(max)	Step	SF	Sample Size
Height (mm)	260	330	1	3	187
Length (mm)	140	370	2	3	307
Breadth (mm)	140	370	2	3	307
Clean Duct Diameter (mm)	50	80	0.25	3	320
Dirty Duct Diameter (mm)	50	80	0.25	3	320
Inlet Runner Length (mm)	5	300	2	5	236
Clean Ingress (%)	0	0.75	0.005	5	240
Dirty Ingress (%)	0	0.75	0.005	5	240
Max					320
Min					187

This method will require further work to see if it provides a better guide to the sample size than the number of input variables alone. The first stage in this validation should be to use a number of mathematical functions, such as the Branin surface function, shown by Fang *et al* [74] and others such as those as shown in Jin, Chen and Simpson [12], over different variable ranges. If this proves to be an improved guide then further tests should be conducted on CAE-based optimisation problems.

A recommendation for future metamodeling-based MAO projects is that all available guidance should be used when deciding on the number of samples that are to be taken; the variable based method from literature and the range variable method proposed here. However, the cost of this must be traded off against the time constraint of the project. Therefore, the estimated time for completion of the CAE is required. This will account for setup, run, and post-processing time. If the time taken to obtain the results for the sample exceeds the time available, then the project must be simplified. Previously this may have required that an input variable was removed to simplify the attribute behaviour in the design space[64]. However, the ranged variable method may provide a different approach. As the required sample size for each variable is known, the user can identify the variables that are increasing the sample number or are less significant. This would allow the number of inputs to be reduced or a reduction in the ranges of significant variables.

Sampling Distribution Methods and Re-sampling

As well as the sample size, the distribution of the sample points was shown to be highly influential on the performance of the metamodel. The examples in Tables 2.2 to 2.4 on pages 47 to 49 in the literature review showed that the latin hypercube is commonly used. This is due to its space filling ability[94]. Experiment 3 conducted in Appendix A showed that a uniform distribution of the latin hypercube sample points helped to reduce the variability in metamodel performance. However, the use of the minimum Ford latin hypercubes is limited due to the discrete sample size available[97].

The literature also discussed the potential use of intelligent sampling methods to improve metamodel performance. These methods use some measure of the localised complexity or error within the metamodel to select new sample points[84][99][100][101][102]. The literature showed a number of potential methods of implementation, however the scope of this work limited re-sampling methods to those available within modeFRONTIER. These were the Lipschitz[101] and MACK[102] sampling methods. Experiment 4 in appendix A tested these methods on the Branin function and showed that they have the capacity to improve metamodel performance, however there was the potential for degradation in the performance. New methods should be implemented within modeFRONTIER and research into new re-sampling methods continued.

While research into new re-sampling methods should be continued, their effect on the sample size and metamodel build costs must be investigated. When selecting sampling size and methods to be used in metamodeling projects, the balance between efficiency and complexity resolution should be considered. Large initial samples allow for a greater degree of parallelisation to be applied. However, this efficiency is lost when sequential methods are applied as the placement of a new sample is based on all other points. There is potential use for a heuristic measure that guides the user to the ratio of initial samples versus sequential samples and the potential efficiency savings. This heuristic can then be used to guide the setting of the sample and estimation of the cost and runtime of building the metamodel. Such heuristic measures require further research.

Metamodel Selection

The literature review showed a number of metamodel formulations, out of which the Radial Basis function was selected for use in the airbox optimisation project. This metamodel was selected as it minimised the error in the metamodel predictions of ten additional box samples. The selection of the metamodel was limited to those available within modeFRONTIER. While modeFRONTIER included the most commonly used metamodel formulations, it did not include the Support Vector Regression model cited in the literature. In such instances where new metamodels are not available, collaboration with the software vendor is key in ensuring that the state of art is maintained within the code and the advantages are communicated to the users.

Error Estimation

This discussion has twice mentioned the examination of metamodel errors to guide further work in optimisation projects. This is necessary in deciding whether further samples should be obtained and the selection of the metamodels. The literature review demonstrated two approaches; the use of additional samples and 'leave one out' errors[11][15]. These approaches held a dilemma; additional samples incur higher costs but the 'leave one out' method may not be accurate.

When using additional samples, Tables 2.2 to 2.4 on pages 47 to 49 showed there was no consensus in the literature as to the size and distribution of samples needed to assess error. The requirements for additional sample size and distribution for global metamodel error estimation were investigated in experiment 2 in appendix Chapter A. The experiment found that small samples could lead to variability in the prediction of error. However, large and uniform samples would tend towards a true error value. This has the potential to make the prediction of metamodel global error impractical to find in the time-constrained design environment. Samples in regions of potential interest such as maxima and minima for attributes, as well as any baselines and trade-off points were suggested as an approach to assess local error.

Error estimation methods that do not require additional samples are attractive when it comes to practical applications. However, the literature raised issues about what error the approach measured[11]. It was suggested that 'leave one out' errors were a measure of sample dependency, this idea was confirmed in experiment 5 in Appendix A. The 'leave one out' errors in the modeFRONTIER Kriging and Radial Basis Functions were found to be more a measure of dependence on the sample point rather than the overall global error. This experiment also showed that the method can both under and over estimate the error in the metamodel, reducing confidence in using the method in isolation.

It can also be argued that a metamodel with a close fit to the attribute behaviour may have a large 'leave one out' error. Section 8.2.2 discussed the use of re-sampling methods that placed samples in regions of complexity to resolve the model. In a 'leave one out' error estimation method, each sample is removed in turn, a metamodel built out of the remaining samples and the error estimated to the left out sample. The total 'leave one out' error of the metamodel is then a function of all the individual 'leave one out' errors. In the case where an intelligent re-sampling method has placed a sample in a region of complexity, the 'leave one out' error may be large. When there are a

large number of intelligent samples, the total 'leave one out' error of the metamodel may be large. It follows then that the minimisation of 'leave one out' errors could lead to over sampling of the design space.

A recommendation for future metamodeling and MAO projects is that both error estimation methods should be used. When using additional samples a uniformly distributed sample should be used for global error, or samples in regions of interest for local error. However, this area of metamodeling needs further research to develop error estimation methods that consider both the accuracy of the error prediction and additional costs to the process. Here, sampling methods for building metamodels which include samples for error estimation will be of interest.

MAO Process Automation

A number of the examples in the literature described automation mechanisms as a key method in reducing the engineering expense of CAE based optimisation projects[5][40][41][67]. The work on the airbox also demonstrated these benefits by using java scripting methods within the StarCCM+ set up and in the automation of WaveBuild3D. In the latter, the use of a Matlab script to edit the base files for the NVH analysis allowed the geometry for 129 airboxes to be generated in minutes rather than weeks. Interaction with common CAD and CAE codes is a core feature of modeFRONTIER. The use of MAO as a systems engineering tool should utilise such interfaces within the current CAD/CAE technology setup.

The use of automation takes the user away from the pre and post-processing of the CAE. While this saves time, it removes the opportunity for model review, issue identification and scrutinising the results. In the case of the airbox, some variation was found in a number of designs for the pressure loss attribute. In this project, each airbox was not only post-processed to gain the attribute values, but also to view the flow field. This was to identify issues with the setup and solution of the CFD. If the attributes were obtained automatically, then there is a potential for unstable results to be used in the metamodeling process, increasing the error in the metamodel behaviour.

However, as the number of samples increases, it becomes prohibitive to check each model. The instance of CAE model failure can be reduced by using known and stable methods and, where applicable, with mesh parameters verified for expected worst case scenarios for model instability. While this approach was completed for the StarCCM+ airbox model, some of the designs did show convergence issues. Here, the inclusion of attribute value checks in the automation scripts could be used to flag up models that have not run correctly and require interaction with the CAE user.

8.2.3 Using MAO as a Systems Engineering Tool for the Selection of Component Design

The airbox optimisation project examined the use of modeFRONTIER visualisation methods and showed how they can be used to explore the design space. A combination of the optimisation algorithms and the function plots were used to explore single attribute optimisation but were limited as interactions between the design variables could not be considered.

The clustering and mapping techniques seemed the most useful at aiding the spotting of trends and the reduction of highly dimensional data. While these methods were good at reducing the whole design space to a region of interest, these methods do not lend themselves to the final selection of design. This was achieved by using design utility functions for each attribute. The functions ranked the attributes according to the obtainable scale and the baseline performance. A tuned 'trade plane' was then used to drive the higher utility trade-off between NVH metric and pressure loss. This project outlined the use for such methods and derived utility functions and higher trade surfaces from the customer requirements. However, there is scope for developing these methods further to relate them directly to the customer satisfaction measures. There are systems engineering tools available to gather these requirements in use in the 6-Sigma and 'DCOV' processes employed[25][26]. Further research should investigate the interaction of a MAO systems engineering tool and other common tools used to find enablers for the MAO design selection process.

The metamodelling method may have use as a bargaining tool. Each project will have constraints that are imposed on the design by the packaging of the analysis component within the vehicle space. This will be a trade-off between all systems that compete for space. The metamodel can be used to examine regions beyond the component constraints and detail the potential gains that could be made by adjusting them. For example, the volume constraint on the airbox. Figure 6-5 (page 134) shows that if the volume is allowed to increase then there are gains to be made in all attributes, particularly the NVH performance. A data driven bargaining process would be most useful in the packaging or early concept design stages where there is more freedom to make design changes. However, this could be problematic as this bargaining process may need metamodels of other systems to examine impact on design.

8.3 Casestudy: The Jaguar Land Rover Product Design System

This discussion has so far examined the enabling aspects of MAO, in this section the application of the process within a systems engineering process is examined. The Jaguar Land Rover product design system is used as the example in this study. This section will examine the application of the MAO method within the available design process windows. From this, changes to the airbox project to improve the metamodels and timing of the analysis is discussed.

8.3.1 MAO Project Timings

A review of the process was conducted and found that the critical aspect for the application of such methods is the duration of the project and the resource utilisation[141]. This research has shown that the cost and runtime of a MAO project is determined by the sample size required to model the attribute behaviours in the design space. Also, the number of samples is highly dependant on the dimensionality and size of the model. This could lead to sample sizes that prohibit practical implementation within a design process. The review of the Jaguar Land Rover product development

system also revealed that potential application of multi-attribute methods may occur within three time-scales during the design process[141]:

1. Offline - characterised by no time constraints on an MAO project.
2. Early / concept design phase - characterised by an application window of approximately six months.
3. Design iteration loops - characterised by an application window of approximately eight weeks.

For the two time constrained periods, the MAO project would have to be defined, completed and results reported within the analysis window.

In an 'offline' application of MAO, the time constraint from the design process would be removed, allowing large generic models to be built. To maximise the use of such models, the model should be made highly generic to allow the concept designs for projects across the whole Jaguar Land Rover program range to be derived from a single set of metamodels. Such an approach would require highly detailed models across the whole range of potential designs. This would lead to models that are highly dimensional and require a very large number of samples. These projects should be used for known attribute trade-off problems that occur in every vehicle program.

Consideration should be given to the allocation of resources for 'offline' MAO projects. The generic nature of such metamodels would be highly valuable in packaging an early concept design work. Once the generic metamodel has been built it could be applied to multiple Jaguar Land Rover programs by changing the constraints applied during the optimisation and attribute trade-off. However, the generic model must cover every possible design scenario, requiring a large amount of samples and a high computational cost. As this cost is not directly connected with any vehicle or engine program, resources must be specifically allocated or obtained for such projects. There is also the potential to outsource such projects.

The review of the design process at Jaguar Land Rover indicated that there is a six month window during the concept design stage, where MAO methods could be applied. Within this timescale there would need to be one month allocated to defining the project, implementation methods and parameterised CAD model. Another month would be required at the end to change the design and trade-off with other systems. This would leave approximately four months to gather the initial metamodel build and error estimation samples as well as to carry out any additional sampling. Here, some accuracy may have to be traded against the time allowed. The sample size and approximate CAE runtime would need to be estimated and from this the number and range of variables would then need to be adjusted to suit the time available. This type of approach would be more suited to focused optimisation problems where use is limited to only one Jaguar Land Rover design program.

The application of the MAO method within the design iteration loops is highly constrained by the time available. During these stages, the CAD will be more mature and the simplification of the CAE methods may not be possible. In these cases, the application should focus on only a few design variables over small ranges.

The decision of when to apply MAO as a systems engineering tool to product design raises the dilemma of whether the tool should be used as a design or development tool. When MAO is used later the design process, some of the major trade-offs may have already been made which may limit the impact of the approach when compared to the 'offline' and 'early / concept design phase' applications. The impact of early trade-off on designs was one of the key questions identified in Section 3.3.4 on page 67 and should be subject to further investigation.

The application of MAO to offline and early/concept design phase projects was said to require metamodels which covered the whole potential design space in a generic approach. From this it can be seen that if a metamodel is built to be generic enough that it could be used in multiple vehicle programs, then there is a large potential for reuse. While such metamodels would require a large initial cost in terms of time and resources, the reuse of multiple vehicle programs means that large savings in time and computational expense can be achieved. The application of the metamodeling process to such applications should be subjected to further research.

However, the reuse of metamodels will require a much larger design space and may push the optimisation problem towards the characteristics of a 'WICKED' problem[34][35]. The constraints and the time available to optimise a design during the design iteration loops meant that only a limited analysis could be carried out. This simplifies the design space and means the problem is constrained and does not exhibit the characteristics of a 'WICKED' problem. However, when considering using MAO during the two earlier application windows (offline and the concept design stage), such characteristics become more prevalent. Not only is the design space more complex, due to the need to reuse the metamodels, but the effect of early optimisation of one system will affect the design of others. Thus, the early optimisation of design may result in the need to use optimisation techniques guided by research in the 'System of Systems' and 'WICKED' problem domains.

8.3.2 The Airbox Optimisation Example

The airbox MAO optimisation used two CAE methods to analyse the pressure loss, capacity and NVH attenuation within a generic design space. The process used a minimum sampling technique to build metamodels for the three attributes, these were then used to optimise the airbox performance. When completed by a CAE expert, the process would take approximately ten weeks. While the optimisation of the airbox did deliver an improvement in performance, there were still significant errors in the attribute metamodels which need to be improved. The airbox example could be revised to enable completion of the project within any of the three windows described in the previous section. The changes to the input variables and sampling within the project would depend on which application window is chosen.

To complete the airbox as an 'offline' project a more generic metamodel would be required to examine a wider range of potential designs. This could also include introducing more variables to the parameterised model or increasing the input variable ranges. The sample size would have to be increased in-line with estimations from the ranged variable method. This metamodel would have a large potential for reuse in future programs.

Improved Jaguar XK SC attribute metamodels could be produced for the early/concept design phase by increasing the number of samples. This project would retain the original eight variables, but larger samples would be taken to improve the metamodel performance. The number of samples should be increased to fill a large proportion of the six month window. While this metamodel will not be as generic as the one generated in the 'offline' approach, there is still some potential for reuse for similar vehicle programs, i.e. next generation XK and other high performance products.

The airbox project took approximately ten weeks and produced metamodels with large fitting errors. Both the time and error would need to be reduced in order to complete the optimisation within the eight week window given for a design iteration loop. To achieve these reductions, the project would have to become more focused by reducing the number of variable inputs and their ranges. For example, if the volume of the airbox was fixed, then the metamodel could focus on the trade-offs caused by the design of NVH devices. However, such metamodels may only solve issues for a single vehicle program, limiting the the potential reuse.

Finally, further verification work could include the rapid prototyping and physical testing of a number of the designs. This would allow the accuracy of the CAE throughout the design space to be examined. This prototype testing could also be extended to include finding the capacity of designs, enabling improvement in the empirical capacity model presented in this work.

8.4 Airbox Capacity Calculation

The pressure loss CFD analysis of the airbox was extended to use the uniformity of the flow in the filter to predict the dust holding capacity. This extension was based on an empirical formula derived from physical and CAE tests on current Jaguar Land Rover airboxes. However, one of the additional airboxes, obtained for the error estimation of the airbox attribute metamodels, gave a negative capacity in the CFD analysis. The airbox designed for the minimum NVH attribute gave a capacity of -14 grammes (data from table 5.9 on page 119). This result shows that further work is required to confirm or revise the empirical formula given by equation 4.9. The equation was derived from a limited data set, representing only a small range of the design space assessed in the airbox optimisation problem. The empirical equation also assumed that the flow uniformity in the filter would remain constant during the test however, this will not be the case. Further tests should be carried out on some of the more extreme airbox designs presented in the latin hypercube and additional samples shown in tables 4.7 and 5.9. This would also provide an opportunity to gather more data; the capacities at numerous pressure losses should be taken as well as the time for such tests. Methods that can measure the flow uniformity through the filter should also be investigated and compared to the StarCD CFD model.

8.5 Further Work: Metamodelling-based MAO Methods

The discussion of further work for metamodelling-based MAO methods can be split into two areas; improvements in the MAO method enablers and implementation of the method within an automotive

systems engineering approach to product design.

This discussion has outlined guidance for the number of samples that attempts to scale the project by both the number of inputs and the size of the design space, this must be examined for suitability. The distribution of the sample points was also shown to be of importance and further research into initial distribution and effective re-sampling methods would be advised. As the sampling and re-sampling methods are implemented in modeFRONTIER, along with the metamodelling methods, there should be collaboration with the software vendor (Esteco) to ensure that the newest methods are available in the software and implemented in projects.

The estimation of error also poses significant challenges in MAO projects. Obtaining the value of true error requires a large uniform sample to be taken, error estimates based on small samples and 'leave one out' methods were found to be unreliable. Improving the reliability of error estimation should be further explored and would have significant value to industrial application of MAO methods. This should examine the use of additional samples as well as error estimation methods that only use information based on the single sample set. The latter of these should look to building the error estimation method within the initial sample size and distribution.

The automation methods used in the airbox optimisation project, the java scripting in StarCCM+ and the geometry file modifier written in Matlab, showed that these can reduce the cost of building large samples. Methods of automation and integration with modeFRONTIER should be pursued.

Many questions raised about the implementation of MAO within the Jaguar Land Rover design environment (Section 3.3.4 page 67) required the method to be operating within the environment so the downstream effects could be measured. As this presented a risk of deteriorating the performance of the design process, the initial experiments using MAO methods were required to be conducted 'offline', allowing the benefits and issues of the method to be investigated. The work on the Branin function and airbox showed that the sample size is critical to the effectiveness of the method. Highly complex behaviour and/or expensive CAE methods could render the process unusable within the time constraints of the design process. The solution suggested here was to scale the size of the MAO project accordingly; a highly dimensional large generic model for 'offline' projects, single system models for early concept work and specific design for projects within the design iteration loops. As the timescales shorten, the number of input variables and their ranges should be reduced. The scaling of a MAO project can be achieved using the ranged variable method and estimations of the cost to run the sample size. Using this approach the risks of a MAO project can be mitigated allowing 'online' projects to be completed addressing the questions raised in Section 3.3.4. The most pressing of these are the logistical aspects of MAO application. The integration of MAO projects into the design process will require resources such as CAE personnel, computers, software and licenses. The I.T. structures supporting powertrain CAE may need to be modified to allow the automation of CAE jobs. MAO projects that utilise different domain analyses may require a number of CAE engineers to work together, the structure and hierarchy of which needs to be arranged. Once these issues have been addressed, the downstream effects of MAO on the design process can be observed.

Chapter 9

Conclusions

The aim of this project was to investigate the challenges and key benefits of adopting a MAO method as a systems engineering tool to improve product development times and component design. Within this research the objectives were:

1. To review the current knowledge and issues in automotive systems optimisation methods within a systems engineering approach.

A review of systems engineering methods used within the automotive industry showed that the optimisation of systems is used to deliver products that meet customer requirements.

The optimisation of systems was shown to be complicated by the presence of high dimensionality in both the input variables and output attributes, working across multiple disciplines, the large number of potential solutions and robustness issues. CAE methods were shown to be an enabler in systems optimisation methods.

For CAE based optimisation of systems, metamodeling methods were presented as an approach that enabled the user to explore the entire design space as well as to optimise designs. However, this process required further investigation into issues of sample size, test point distribution method and error estimation.

From this, two significant research areas were identified; the use of metamodeling to model attribute behaviour within the design space and the use of multi-physics CAE methods as an enabler within MAO.

2. To examine the role of optimisation within an automotive design environment allowing sub-projects to be scoped and bounded.

The potential application of MAO was explored in relation to the surrounding design systems to identify potential opportunities and issues with implementing the method. This identified a potential for risk of deterioration in design system performance and required an 'offline' MAO application to explore the method and find risk mitigation factors.

The airbox was selected for application for the MAO method and the project was scoped. Within the MAO method there was also a need to explore the potential of new multi-physics

methods. To explore this need, opportunities in the fuel tank would be found and an application defined. The project would then explore the benefits and costs of multi-physics methods within a multi-attribute architecture.

3. Investigate key enablers and methods required to implement MAO within an automotive design environment, including:

- (a) Examine issues of sample size and distribution in the generation of metamodels and the estimation of the error in the model fit.

The work on the airbox MAO problem and the experiments conducted in Appendix A investigated the issue of sample size. The results showed that a scarce sample was not sufficient to capture the complex behaviour in large generic metamodels. Attempts to increase the sample sizes in both studies, in accordance with guidance from the literature, resulted in limited improvement in metamodel performance. The implication of this result is that the number of samples required cannot be predicted by the number of input variables alone. Based upon this, an alternative method is suggested using both the number of input variables and their ranges to scale the sample size.

As well as sample size, the distribution of the test points was important for metamodel accuracy. This work suggests the use of an initial space-filling uniform sample, where the size is guided by the literature or ranged variable method. Then, based on an assessment of error, intelligent sampling methods can be applied to improve the metamodel fit.

The estimation of error was also examined in Appendix A. A significant result of this was showing that the two commonly used error estimation methods, small additional sample set and 'leave one out' methods, are unreliable. However, the sample size required to find the true value of error would be prohibitive in a practical application. This work suggests the use of a small number of additional samples in regions of interest to assess the local error in the metamodel, as well as using the 'leave one out' error as a guide.

- (b) Examine techniques and methods for attribute trade-off.

The airbox project used visualisation techniques and utility based decision methods to explore the design space and select the final design. Visualisation techniques were useful in examining the potential design space and exploring design options. However, the selections of a single design was difficult due to the high number of potential designs. To overcome this difficulty, utility functions and trade surfaces were used to guide the optimisation according to the product requirements. Both approaches should be taken when using MAO as a systems engineering tool to understand the design space.

- (c) Examine the benefits and costs of a multi-physics approach to CAE for use in an MAO architecture.

The work to examine multi-physics methods first explored CAE usage for fuel tank applications. The durability of internal components of the fuel tank due to fuel slosh was identified as a multi-physics problem and the boundary condition explored. The

need for fully coupled multi-physics methods was established by examination of two load cases in an un-mapped, uncoupled approach. Following this, the project then examined the application of the StarCD-Abaqus direct couple and the Abaqus CEL multi-physics method to the analysis of the fuel slosh problem. However, both of these methods were shown to be unsuitable for this application, meaning the relative benefits and costs of both approaches could not be established.

While the costs and benefits of the multi-physics methods could not be established for this application, the use of such methods in MAO requires consideration of the degree of coupling and the software approach. The degree of coupling is important in determining the cost and accuracy of a multi-physics method and should be assessed for each application. The software approach may incur additional modelling costs (multiple domain specific codes) or sacrifices to accuracy due to non-domain specific solvers being used (single multi-physics code). The balance between accuracy and simulation cost must be established to maximise the use of resources.

- (d) Use an automotive case-study to understand the potential application of MAO methods.
- Using the Jaguar Land Rover design process as a case-study, three potential applications of MAO were identified; offline, early concept work and design development. The examination of these applications showed that early application came with a larger time frame to complete the optimisation. However, these projects would be larger as they would need to address more potential designs. Conversely, covering a larger design space gives the possibility that the metamodels can be used again for other vehicle programs. This poses a dilemma for the use of MAO in the automotive design environment. Use in the early stages of a design project resulting in higher modelling costs for a larger design space, or use in later development projects in which the design could already be compromised.

Other issues in the metamodeling approach to MAO can be summarised as:

- Metamodel accuracy is also dependent on the stability and robustness of the CAE analysis methods used to obtain data points. For future MAO projects applied within an automotive product design system, only mature, stable and validated CAE methods should be used.
- Automation was cited as a key enabler in the MAO method. This can reduce the human input needed in the sample gathering process, reducing the time required to set up each model. However, some consideration must be given to methods that allow unstable or poorly converged simulations to be identified as variation in the attribute behaviour could affect the fit of the metamodel.
- Collaboration with the MAO software vendor is also important in maintaining the state of art in the various sampling methods, metamodel formulations and visualisation techniques.

The benefit of the MAO approach can be shown in the Airbox project. The application of the MAO method to the attribute trade-off of a concept design level Jaguar XK SC airbox showed a reduction in the pressure loss of 366 Pa. This was achieved whilst improving the

NVH performance by 23% (as measured by the single value NVH metric) and increasing the dust capacity by 24 g. This result demonstrated the potential of MAO methods to deliver improved product design. The improvement in the design came from increasing the dirty side duct diameter whilst reducing the clean side diameter, this is contrary to Jaguar Land Rover design philosophy. Further experiments should be conducted to see if airbox attribute gains could be made within other programs by following this example.

The opportunities for further work can be identified in three different areas; improving metamodel sampling techniques, exploring the application of MAO and metamodeling within a larger design system and examining new multi-physics techniques to improve attribute prediction.

1. The work on the airbox showed that the number of inputs alone was not sufficient to determine the sample size required to build an adequate metamodel. In the discussion, the ranged variable method was suggested for the estimation of sample sizes in MAO projects. However, this required further research to support or improve the method. Here, the examination of a number of mathematical functions over varying range sizes could be used to test and improve the method. From this, the ranged variable method could be applied to real optimisation problems. This project should also seek to improve the understanding of and guidance on sampling and re-sampling methods, including:
 - (a) Establishing heuristic measures to guide the balance between initial and re-sample sizes.
 - (b) Investigating new methods for guiding re-sampling.
 - (c) Improving the error prediction when using both additional samples and 'leave one out' methods.
2. To explore the application of MAO and metamodeling within a larger design system, further optimisation projects should be completed on known attribute trade-offs. These projects should explore the timing of the MAO project and its effect on the design process. Of interest would be:
 - (a) The interaction of a MAO tool with other systems engineering tools. In particular, establishing methods to derive utility functions and trade surfaces based on customer requirements and satisfaction data. This will enable large generic metamodels to be applied to different vehicle programs by a simple change of utility function.
 - (b) Examining the operation of MAO within powertrain with a focus on logistical and resource issues. The impact on other projects and programs would also need to be monitored.
 - (c) Establishing the downstream effect of early attribute trade-off on the number of design changes throughout the product development process.
 - (d) Establishing the requirements for enabling metamodel reuse across programs and investigate the benefits of this approach.

3. Finally, due to the unsuitability of the available multi-physics software codes for the fuel tank application, there is still a requirement to examine the use of such methods as an enabler in MAO. Examining other opportunities and applications for multi-physics analyses would allow the relative benefits and costs to be assessed. This should include an assessment of the degree of coupling required to model the system attribute accurately. Here, the development of heuristics to guide what degree of coupling is required would be of interest. These methods should then be validated against a suitable rig test case.

References

- [1] KPMG International. Kpmg concerned over automotive industry's view of over-capacity, January 7, 2005.
- [2] KPMG International. A rough road: The effects of today's financial crisis on the global automotive industry, November 2008.
- [3] KPMG International. Kpmg's global automotive executive survey 2011, 2011.
- [4] KPMG International. Issues monitor: Sharing knowledge on topical issues in the automotive industry, October 2010.
- [5] M. Usan. Automotive component product development enhancement through multi-attribute system design optimisation in an integrated concurrent engineering framework. Master's thesis, Massachusetts Institute of Technology, 2005.
- [6] T.E. Austin. Why have a systems engineering (se) capability for automotive product development? questions and answers. (2007-01-0782), 2007. SAE International, Warrendale, Pennsylvania, USA.
- [7] G. Loureiro, P.G. Leaney, and M. Hodgson. A systems engineering framework for integrated automotive development. *Systems Engineering*, 7(2):153–166, 2004. Copyright 2004 Wiley Periodicals, Inc.
- [8] Incose. <http://www.incose.org/practice/whatissystemseng.aspx> (Accessed 20/03/2012).
- [9] D.K. Hitchins. Systems engineering in search of the elusive optimum. *Engineering Management Journal*.
- [10] S. Thomke and T. Fujimoto. The effect of front-loading problem-solving on product development performance. *Journal of Product Innovation Management*, 17, March 2000.
- [11] G. Wang and S. Shan. Review of metamodeling techniques in support of engineering design optimization. *Journal of Mechanical Design*, 129(4):370–380, 2007.
- [12] R. Jin, W. Chen, and T.W. Simpson. Comparative studies of metamodeling techniques under multiple modelling criteria. *Structural and Multidisciplinary Optimization*, 23:1–13, 2001. 10.1007/s00158-001-0160-4.

- [13] M.D. Kaufmann. Variable-complexity response surface approximations for wing structural weight in hsct design. Master's thesis, virginia polytechnic institute and state university, April 1996.
- [14] L. Wang and D. Beeson. Valuable theoretical lessons learned from the application of metamodels to a variety of industrial problems. *ASME Conference Proceedings*, 2009(49026):789–804, 2009.
- [15] M. Meckesheimer, A.J. Booker, R.R. Barton, and T.W. Simpson. Computationally inexpensive metamodel assessment strategies. *AIAA Journal*, 40:2053–2060, 2002.
- [16] J. Andersson. A survey of multiobjective optimization in engineering design. Technical report, Department of Mechanical Engineering, Linkoping University, 2000.
- [17] D.P. Mahoney. Multiphysics analysis. *Computer Graphics World*, 23(6), June 2000.
- [18] J. Agte, O. de Weck, J. Sobieszczanski-Sobieski, P. Arendsen, A. Morris, and M. Spieck. Mdo: assessment and direction for advancementan opinion of one international group. *Structural and Multidisciplinary Optimization*, 40:17–33, 2010. 10.1007/s00158-009-0381-5.
- [19] R. Fitzsimmonds. Personal correspondence: Cd-adapco support, 2009.
- [20] L. Cordingley and A.M. Lambert. Personal correspondence: Simulia support, 2010.
- [21] Y. Kusunoki, K. Cho, F. Uchikawa, and S. Sugimori. Toyota production system and kanban system materialization of just-in-time and respect-for-human system. *International Journal of Production Research*, 15(0020-7543):553–564, 1977.
- [22] D.K. Hitchins. *Putting Systems to Work*. John Wiley & Sons, Inc., New York, NY, USA, 1993.
- [23] M. Lubraico, J.C. Frias, and T. de Sousa Pereira. Vehicle program management concept. novembro 2003.
- [24] J. Schlosser. Requirements for automotive system engineering tools. In *Computer Design: VLSI in Computers and Processors, 2002. Proceedings. 2002 IEEE International Conference on*, pages 364–369, 2002.
- [25] D. H. Stamatis. Design for six sigma (dfss) and reliability. (2003-01-1374), 2003. SAE International, Warrendale, Pennsylvania, USA.
- [26] Dcov 110: Dcov process fundamentals, 2006. Internal Jaguar Land Rover Intranet.
- [27] M.C. Andreassa and G.A. Parreira. Applying six sigma with the theory of inventive problem solving (triz) to reduce the time to solve problems. (2007-01-2585), 2007. SAE International, Warrendale, Pennsylvania, USA.
- [28] R. Hurley, D. Eade, A. Fraser, S. Brett, R. Shrieves, J. Kisenyi, and B. Rutter. Robustness design of experimental approach to the optimization of fast light-off of catalytic vehicles emission systems. *IMechE Conference Transactions*, 1996.

- [29] H.L. Zhang and D. Ma. A systems engineering approach to occupant protection system design and optimization through modeling and simulation. *Systems Engineering*, 8(1):51–61, 2004.
- [30] B. Shahidi, U.K. Stuhel, B. Shahidi, S. Tavakkoli, Y.Q. Liu, and N. Nelson. System level durability engineering in cae. (2006-01-1981), 2006. SAE International, Warrendale, Pennsylvania, USA.
- [31] A.S. Patil, K.C. Vora, and V.G. Halbe. A system approach to automotive air intake system development. (2005-26-011), 2005. SAE International, Warrendale, Pennsylvania, USA.
- [32] M. Jamshidi. System of systems engineering - new challenges for the 21st century. *Aerospace and Electronic Systems Magazine*, 23(5):4–19, 2008.
- [33] J. Boardman and B. Sauser. System of systems - the meaning of of. *System of Systems Engineering*, 2006.
- [34] H. W. J. Rittel and M. M. Webber. Dilemmas in a general theory of planning. *Policy Sciences*, 4:155–169, 1973. 10.1007/BF01405730.
- [35] R.E. Horn and R.P. Weber. New tools for resolving wicked problems: Mess mapping and resolution mapping. Online, 2007. MacroVU Inc, Strategy Kinetics LLC.
- [36] The concise oxford dictionary of mathematics (online). <http://www.oxfordreference.com> (Accessed 14/01/2010).
- [37] Oxford english dictionary online. www.oed.com (Accessed 14/01/2010).
- [38] P. Venkataraman. *Applied Optimisation with MATLAB Programming*. Wiley-Interscience, 2001.
- [39] Y. Collette and P. Siarry. *Multiobjective Optimization Principals and Case Studies*. Springer, 2003.
- [40] G.J. Park, U.P. Hong, and K.H. Hwang. A comparative study of software systems from the optimization viewpoint. *Structural and Multidisciplinary Optimization*, 27(6):460–468, March 2000.
- [41] Esteco. The concept behind modefronter, 2008. Introductory Course Material.
- [42] J. Haftka and R.T. Sobieszczanski-Sobieski. Multidisciplinary aerospace design optimization: survey of recent developments. *Structural Optimization*, 14(1):1–23, 1997.
- [43] K. Lewis and F. Mistree. The other side of multidisciplinary design optimization: Accomodating a multiobjective, uncertain and non-deterministic world. *Engineering Optimization*, 31(2):161–189, 1998. <http://www.informaworld.com/10.1080/03052159808941369>.

- [44] M.R. Waszak, J.F. Barthelemy, K.M. Jones, R.J. Silcox, W.A. Silva, and R.H. Nowaczyk. Modeling and analysis of multidiscipline research teams at nasa langley research center: A systems thinking approach. Technical report, 1998.
- [45] A. May and C. Carter. A case study of virtual team working in the european automotive industry. *International Journal of Industrial Ergonomics*, 27(3):171–186, 2001.
- [46] S. Mahadevan. Design optimization for reliability and robustness. (2004-01-0237), 2004. SAE International, Warrendale, Pennsylvania, USA.
- [47] J. Fisher-Box. R. a. fisher and the design of experiments, 1922-1926. *American Statistician*, 34(1):1–7, 1980.
- [48] G.R. Mutha, N.H. Walke, N.V. Marathe, S A. Gothekar, and K.C. Vora. Design of experiments: A systems approach to engine optimization for lower emissions. (2007-26-012), 2007. SAE International, Warrendale, Pennsylvania, USA.
- [49] H.M. Junior, J.B. Turrioni, J.F. Mologni, and M.M. Fernandes. Capability prediction through design of experiments (doe) and monte carlo simulation on automotive innovation activities. outubro 2008.
- [50] R. J. Yang, L. Gu, C. H. Tho, and J. Sobieszczanski-Sobieski. Multidisciplinary design optimization of a full vehicle with high performance computing. 2001. AIAA-2001-1273.
- [51] M.S. Kim, S.J. Heo, and B.J. Kim. Aluminum space frame biw optimization considering multidisciplinary design constraints. *International Journal of Automotive Technology*, 6(6):635–641, 2005.
- [52] R. J. Balling and J. Sobieszczanski-Sobieski. Optimization of coupled systems - a critical overview of approaches. *AIAA Journal*, 34(1):6–17, 1996.
- [53] S. Sobieszczanski-Sobieski and J. Kodiyalam. Multidisciplinary design optimization - some formal methods, framework requirements, and application to vehicle design. *International Journal Of Vehicle Design*, 25(1):3–22, 2001.
- [54] J.J. Reuther and J.R.R.A. Martins. Complete configuration aero-structural optimization using a coupled sensitivity analysis method. *9th AIAA/ISSMO Symposium on Multidisiplinary Analysis and Optimization*, (AIAA 2002-5406), Sept 2002.
- [55] J.V. Carnahan, D.L. Thurston, and T. Liu. Optimization of design utility. *Journal of Mechanical Design*, 116(3):801–808, 1994.
- [56] D.L. Thurston. A formal method for subjective design evaluation with multiple attributes. *Research in Engineering Design*, 3(2):105–122, 1991.
- [57] D.J. Hand, H. Manila, and P. Smyth. *Principles of Data Mining*. MIT Press, 2001.

- [58] K. Witowski, M. Liebscher, and T. Goel. Decision making in multi-objective optimization for industrial applications - data mining and visualization of pareto data. *7th European LS-DYNA Conference, Salzburg Austria*, (May 14-15), 2009.
- [59] H. Hauser, F. Ledermann, and H. Doleisch. Angular brushing of extended parallel coordinates. In *Proceedings of the IEEE Symposium on Information Visualization (InfoVis'02)*, INFOVIS '02, pages 127–, Washington, DC, USA, 2002. IEEE Computer Society.
- [60] S. Parashar, N. Fateh, V. Pediroda, and C. Poloni. Self organising maps (som) for design selection in multi-objective optimisation using modefroniter. (2008-01-0874), 2008. SAE International, Warrendale, Pennsylvania, USA.
- [61] S. Obayashi and D. Sasaki. Visualization and data mining of pareto solutions using self-organizing map. In Carlos Fonseca, Peter Fleming, Eckart Zitzler, Lothar Thiele, and Kalyanmoy Deb, editors, *Evolutionary Multi-Criterion Optimization*, volume 2632 of *Lecture Notes in Computer Science*, pages 71–71. Springer Berlin / Heidelberg, 2003. 10.1007/3-540-36970-8.56.
- [62] B. Morey. Improving product development at general motors powertrain. *Automotive Engineering*, 115(3):28, March 2008.
- [63] S.R. Pierson. Jaguar land rover presentation to leeds university, 2005. Internal Jaguar Land Rover Intranet.
- [64] S. Shan and G. Wang. Survey of modeling and optimization strategies to solve high-dimensional design problems with computationally-expensive black-box functions. *Structural and Multidisciplinary Optimization*, 41:219–241, 2010. 10.1007/s00158-009-0420-2.
- [65] V. Toropov, A. Wood, and P. Zadeh. Metamodel-based collaborative optimization framework. *Structural and Multidisciplinary Optimization*, 38(2):103–115, 2009.
- [66] A. A. Giunta, V. Balabanov, D. Haim, B. Grossman, W.H. Mason, L.T. Watson, and R.T. Haftka. Multidisciplinary optimisation of a supersonic transport using design of experiments theory and response surface modelling. *Aeronautical Journal*, 101(1008):347–356, 1997.
- [67] F. Maier, W. Mayer, M. Stumptner, and A. Muehlenfeld. Ontology-based process modelling for design optimisation support. In John S. Gero and Ashok K. Goel, editors, *Design Computing and Cognition '08*, pages 513–532. Springer Netherlands, 2008. 10.1007/978-1-4020-8728-8_27.
- [68] M. Khandare, F.P. Pan, and R. Schoon. A multi-objective design optimization for an integrated tractor trailer vehicle. (2011-01-0066), 2011. SAE International, Warrendale, Pennsylvania, USA.
- [69] C., G. Cunningham, S. Spence, and G. McCullough. Development of optimization techniques for the design of an internal combustion engine airbox. November 2006.

- [70] W. Zottin, A.P. Curty Cuco, M. Vinícius, F. dos Reis, R. Ferraz, and A.F. da Silva. Application of optimization techniques in the design of engine components. April 2008.
- [71] T.W. Simpson, T.M. Mauery, J.J. Korte, and F. Mistree. Comparison of response surface and kriging models for multidisciplinary design optimization. 1998. AIAA-98-4755.
- [72] M. de Freitas, L. Giovanni, I. Kotinda, S. Butkewitsch, and J.A.F. Borges. Meta-modelling, optimization and robust engineering of automotive systems using design of experiments. (2001-01-3848), 2001. SAE International, Warrendale, Pennsylvania, USA.
- [73] S.M. Clarke, J.H. Griebisch, and T.W. Simpson. Analysis of support vector regression for approximation of complex engineering analyses. *Journal of Mechanical Design*, 127(6):1077–1087, 2005.
- [74] H. Fang, M. Rais-Rohani, Z. Liu, and M.F. Horstemeyer. A comparative study of metamodeling methods for multiobjective crashworthiness optimization. *Computers & Structures*, 83(25-26):2121–2136, 2005.
- [75] X. Fang, L. Wang, D. Beeson, and G. Wiggs. A practical robust and efficient rbf metamodel method for typical engineering problems. *ASME Conference Proceedings*, 2008(43253):873–882, 2008.
- [76] F. Gerhorst, M. Wirth, and K. Kuhlbach. Application of monte-carlo-simulation and most probable limit state on gasoline di combustion system optimization. (2010-01-0712), 2010. SAE International, Warrendale, Pennsylvania, USA.
- [77] C.A. Toropov, V.V. Thompson, H.M. Wilson, M.C.T. Foxley, N.A. Gilkeson, and P.H. Gaskell. Aerodynamic shape optimization of a low drag fairing for small livestock trailers. *12th AIAA/ISSMO Multidisciplinary Analysis and Optimization Conference. Proceedings. 12th AIAA/ISSMO Multidisciplinary Analysis and Optimization Conference, 10 - 12 September 2008, Victoria, British Columbia Canada*, 2008. (AIAA 2008-5903).
- [78] L. Gu, R.J. Yang, C.H. Tho, M. Makowskit, O. Faruquet, and Y.Li. Optimization and robustness for crashworthiness of side impact. *Int. J. of Vehicle Design*, 26(4):348–360, 2001.
- [79] H. Sakurai, M. Jasper, and K. Rudell. The application of design of experiments to cfd studies of racecar wing configurations. (2006-01-3645), 2006. SAE International, Warrendale, Pennsylvania, USA.
- [80] K.H. Lee and D.H. Kang. Structural optimization of an automotive door using the kriging interpolation method. *Proceedings of the Institution of Mechanical Engineers, Part D: Journal of Automobile Engineering*, 221(12):1525–1534, 2007. 10.1243/09544070JAUTO403.
- [81] M. Martinelli and R. Duvigneau. On the use of second-order derivatives and metamodel-based monte-carlo for uncertainty estimation in aerodynamics. *Computers & Fluids*, 39(6):953–964, 2010.

- [82] F. Pan, P. Zhu, and Y. Zhang. Metamodel-based lightweight design of b-pillar with two structure via support vector regression. *Computers & Structures*, 88(1-2):36–44, 2010.
- [83] T.W. Simpson, J.J. Korte, T.M. Mauery, and F. Mistree. Kriging models for global approximation in simulation-based multidisciplinary design optimization. *AIAA Journal*, 39:2233–2241, Dec 2001.
- [84] H. Wang, E. Li, and G.Y. Li. Probability-based least square support vector regression metamodeling technique for crashworthiness optimization problems. *Comput. Mech.*, 47:251–263, March 2011.
- [85] R.J. Yang, N. Wang, C.H. Tho, J.P. Bobineau, and B.P. Wang. Metamodeling development for vehicle frontal impact simulation. *Journal of Mechanical Design*, 127(5):1014–1020, 2005.
- [86] M. Xiao, P. Breitkopf, R.F. Coelho, C. Knopf-Lenoir, M. Sidorkiewicz, and P. Villon. Model reduction by cpod and kriging. *Structural and Multidisciplinary Optimization*, 41(4):555–574, 2010. 10.1007/s00158-009-0434-9.
- [87] K. Shimoyama, J.N. Lim, S. Jeong, S. Obayashi, and M. Koishi. Practical implementation of robust design assisted by response surface approximation and visual data-mining. *Journal of Mechanical Design*, 131(6):061007, 2009.
- [88] M.D. Buhmann. Radial basis functions. *Acta Numerica*, 9:1–38, 2000.
- [89] E. Rigoni. Technical report 2007-001: Radial basis functions response surfaces. Technical report, Esteco, April 2007.
- [90] A. Lovison. Technical report 2007-003: Kriging. Technical report, Esteco, Dec 2007.
- [91] D.J.C. MacKay. Introduction to gaussian processes. *NATO ASI SERIES F COMPUTER AND SYSTEMS SCIENCES*, 168:133–166, 1998.
- [92] J.H. Friedman. Multivariate adaptive regression splines. *The Annals of Statistics*, 19(1):1–67, March 1991. Institute of Mathematical Statistics.
- [93] E. Acar. Various approaches for constructing an ensemble of metamodels using local measures. *Structural and Multidisciplinary Optimization*, 42:879–896, 2010. 10.1007/s00158-010-0520-z.
- [94] J. Sacks, W.J. Welch, T.J. Mitchell, and H.P. Wynn. Design and analysis of computer experiments. *Statistical Science*, 4(4):409–423, November 1989. Institute of Mathematical Statistics.
- [95] T.W. Simpson, A.J. Booker, D. Ghosh, A.A. Giunta, P.N. Koch, and R.J. Yang. Approximation methods in multidisciplinary analysis and optimization: a panel discussion. *Structural and Multidisciplinary Optimization*, 27:302–313, 2004. 10.1007/s00158-004-0389-9.

- [96] A.A. Abdallah, B. Avutapalli, G. Steyer, Z. Su, and K. Yang. Effective nvh analysis and optimisation with cae and computer experiments. *International Journal of Vehicle Noise and Vibration*, 3(1):1–26, 2007.
- [97] U. Gromping. Catalogue of orthogonal column latin hypercube designs according to ye (1998). Technical report, Ford, 2001. Available from Jaguar Land Rover Intranet.
- [98] K.Q. Ye. Orthogonal column latin hypercubes and their application in computer experiments. *Journal of the American Statistical Association*, 93(444):1430–1439, Dec 1998. American Statistical Association.
- [99] R. Rai and M.I. Campbell. Qualitative and quantitative sequential sampling. *ASME Conference Proceedings*, 2006(4255X):381–391, 2006.
- [100] D. R. Jones, M. Schonlau, and W. J. Welch. Efficient global optimization of expensive black-box functions. *Journal of Global Optimization*, 13:455–492, 1998. 10.1023/A:1008306431147.
- [101] A. Lovison. Technical report 2008-002: Lipschitz sampling for improving metamodels in modefrontier. Technical report, Esteco, July 2008.
- [102] Esteco. modefrontier documentation: Multivariate adaptive crossvalidating kriging. Technical report, Esteco, 2009. Version 4.2.2 Documentation, Accessed November 2009.
- [103] M. Cross and A. Slone. Fenet - multi-physics analysis (mpa) theme: A review of commercial mpa capability in 2005. *PROCEEDINGS OF FENET MEETING*, 2005.
- [104] A. Schmidt, O. Lang, P. Schmitt, P. Adomeit, and M. Hopp. Cae-based port development and flow design for si engines. (2005-01-0243), 2005. SAE International, Warrendale, Pennsylvania, USA.
- [105] P. Sutton. Requirements for a feasibility assessment for multi-attribute optimisation techniques: A system of systems engineering approach. In *System of Systems Engineering (SoSE), 2010 5th International Conference on*, pages 1–7, june 2010.
- [106] M.W. Maier. Architecting principles for systems-of-systems. *Systems Engineering*, 1(4):267–284, 1998.
- [107] A. Gorod, B. Sauser, and J. Boardman. System of-systems engineering management: A review of modern history and a path forward. *IEEE Systems Journal*, 2(4):484–499, 2008.
- [108] J.E. Jr Dennis, S.F. Arroyo, E.J. Cramer, and P.D Frank. Problem formulations for systems of systems. *IEEE International Conference on Systems, Man and Cybernetics*, 2005. DOI: 10.1109/ICSMC.2005.1571123.
- [109] Installation guidelines of afm: Aflos5, 2010. Denso Corporation.

- [110] A. De Vita, L. Andreassi, and L. Di Angelo. Experimental and computational study for the optimization of race car intake air flow. 12 2001.
- [111] Air intake system analysis. Procedure Reference: PPR-600100-01.
- [112] R. Cheung. Transfer matrix method. Technical report, Land Rover, 2003.
- [113] N. Hoyle, N.W. Bressloff, and A.J. Keane. Design optimization of an engine air intake. 2005.
- [114] User guide: Star-ccm+ version 5.06.007. Technical report, CD-Adapco, 2010.
- [115] S.R. Pierson. Cfd preformance for air intakes. Internal Jaguar Land Rover Work.
- [116] N.J. Bugli. Service life expectations and filtration performance of engine air cleaners. outubro 2000.
- [117] N.J. Bugli. Automotive engine air cleaners - performance trends. March 2001.
- [118] B. Huurdeman and H. Banzhaf. Cfd simulation of flows in air cleaners with transient dust loading of the filter element. April 2006.
- [119] Inlet air cleaning equipment for internal combustion engines and compressors - performance testing. Technical Report BS ISO 5011:2000, British Standards Institutes, 2000.
- [120] Steady state analysis for catalytic converter gas flow, 2005. Ford Procedure: CETP: 03.01-C-415, page 18.
- [121] Land rover l322 v8 diesel air cleaner test results. Technical report, Mann & Hummel, 2006.
- [122] Land rover t5 v8 petrol n/a air cleaner test results. Technical report, Mann & Hummel, 2004.
- [123] Component testair cleaner land rover l322/t5 v8 n/a s/c. Technical report, Mann & Hummel, 2008.
- [124] L. Wolf. Test report: Air filter element, jaguar land rover l538. Technical report, Mann & Hummel, 2009.
- [125] C. Harris. Jaguar x150 na - air induction system: Air filter efficiency & capacity testing. Technical report, Siemens VDO Automotive, 2005.
- [126] M.A. Pinch. Laboratory report: Pv tests on vp6h5u-9601-ac (ag1628). Technical report, SOGEFI Filtration Ltd, 2006.
- [127] F. Fortunato, P. Oliva, N. Fiore, M. Martinetto, and L. Di Matteo. Sloshing analysis of an automotive fuel tank. (2006-01-1006), 2006. SAE International, Warrendale, Pennsylvania, USA.
- [128] S.H. Cho, J.I. Park, and W.J. Roh. Simulation of sloshing in fuel tanks and parametric study on noise reduction by decreasing impact pressure. (2005-01-1913), 2005. SAE International, Warrendale, Pennsylvania, USA.

- [129] H. Kumagai, K. Morohoshi, and H. Himeki. Fatigue behavior analysis and durability evaluation of plastic fuel tank. (2006-01-0782), 2006. SAE International, Warrendale, Pennsylvania, USA.
- [130] P. Qin and S.F. D'Souza. Cae fatigue prediction of fuel tank straps using proving ground loads. (2005-01-1405), 2005. SAE International, Warrendale, Pennsylvania, USA.
- [131] Internal jlr work. Completed by Richard Tyrrell.
- [132] Abaqus manual. Simulia Documentation for Version 6.8EF.
- [133] S.M. Rifai, Z. Johan, J.A. Landers, A.B. Glendinning, and J.C. Buell. Automotive engineering applications of multiphysics simulation. (1999-01-1022), 1999. SAE International, Warrendale, Pennsylvania, USA.
- [134] DSS Simulia. Coupled eularian-lagrangian analysis with abaqus/explicit. Technical report, Dassult Systemes, 2008. CEL Training Course Material.
- [135] C. Dinescu, B. Leonard, O.U. Baran, A.W. Platschorre, R. Alessio, D. Belluzzo, and Charles Hirsch. Fluid-structure interaction model for hydroplaning simulations. (2006-01-1190), 2006. SAE International, Warrendale, Pennsylvania, USA.
- [136] Starcd user guide. Cd Adapco Documentation for Version 4.08.
- [137] S. Smith, T.M. Wasfy, and J. O'Kins. Experimental validation of a time-accurate finite element model for coupled multibody dynamics and liquid sloshing. (2007-01-0139), 2007. SAE International, Warrendale, Pennsylvania, USA.
- [138] B.R. Tang, S. Guha, T. Tyan, J. Doong, L. Shaner, and D. Bhalsod. Simulation of sloshing and ballooning in fuel tanks for high speed impacts. (2006-01-0314), 2006. SAE International, Warrendale, Pennsylvania, USA.
- [139] N.E. Bedewi and T. Omar. Modelling of automotive fuel tanks using smoothed particle hydrodynamics. (2007-01-0682), 2007. SAE International, Warrendale, Pennsylvania, USA.
- [140] C. Riedel, M. Brusoe, and Z. Penzar. Improvement of an ls-dyna fuel delivery module (fdm) crash simulation. (2008-01-0253), 2008. SAE International, Warrendale, Pennsylvania, USA.
- [141] P. Sutton. Internal report: Jaguar land rover design process and virtual series. Technical report, Jaguar Land Rover, 2008.
- [142] Cd-adapco starcd example: Direct-coupling method, 2009. Available from CD-Adapco Support.
- [143] M. Anghileri, L.M.L. Castelletti, and Maurizio Tirelli. Fluid-structure interaction of water filled tanks during the impact with the ground. *International Journal of Impact Engineering*, 31(3):235–254, 2005.

- [144] E. de Vries and K. Kamiya Y. Yamaguchi. Simulation studies of sloshing in a fuel tank. (2002-01-0574), 2002. SAE International, Warrendale, Pennsylvania, USA.
- [145] Djb instruments website: Piezo-electric accelerometers - a/131/v. Website. <http://www.djbinstruments.com/> (Accessed 20/03/2012).
- [146] Fuel tank internal component slosh test, 2004. Ford Procedure: CETP: 10.01-L-300, page 18.

Appendix A

Sample Size, Distribution and Error Estimation Experiments

A.1 Introduction

The aim of this chapter is to investigate the issues of sample size and error estimation to support the work in the airbox project. The review of the literature and the Jaguar Land Rover CAE environment highlighted a number of issues regarding the number and distribution of sample points for building metamodels and estimating error. This chapter examines the use of various sampling methods of a known function that features some complexity that can be computed cheaply. A metamodel based upon the sampling technique will then be created and the performance assessed on the prediction of the function at known points.

A.2 Experiment Outlines and Methods

The large leave one out error obtained from the NVH attribute metamodel, based upon a 33 latin hypercube sample, requires a greater understanding of a number of issues around sample size and error estimation. As the CAE is costly in both computational effort and time, some simple experiments of fitting a metamodel to a two-dimensional mathematical function will be used to assess sampling and error estimation issues. The five experiments are outlined below.

1. Experiment 1: Examination of the Literature Guidance on Sample Size

The literature gave three boundaries for sample size guidance (as outlined in Table 2.6) and scales the sample size by the number of inputs alone. For a two-dimensional function the smallest sample size would be 6 samples and the largest 20. This experiment will incrementally increase the sample size from the smallest to the largest and assess whether this guidance can capture the complexity of the mathematical function.

2. Experiment 2: Sample Size and Distribution for Error Estimation

As a corollary of increasing the sample size to improve the metamodel fit, the estimation of global error in a metamodel would also be improved by increased sample numbers. The literature gave no clear indication to the size and distribution of any error estimation sample. This experiment will cover both issues to assess the requirements for error estimation samples.

3. Experiment 3: Comparing Seeded and Uniform Latin Hypercubes

Within this project there are two latin hypercube methods available, the Ford minimum latin hypercube[97] and the seeded modeFRONTIER method. The Ford approach distributes the points uniformly through the design space whereas the seeded method is not. An examination is required to ascertain which approach should be used.

4. Experiment 4: Comparing Sequential Sampling Methods

The literature showed there is an interest in sequential sampling methods that place further samples in regions of interest. This experiment will assess the various sequential sampling methods available to the project to see if they can be used.

5. Experiment 5: Examining the 'Leave One Out' Error Estimation Method

The 'leave one out' error assessment method is seen as more efficient than the use of additional samples, however, concerns have been raised over how this metric can be interpreted. This experiment seeks to assess whether this measure is fit for use in the airbox project.

The result of these experiments will then be used to guide the next steps in the airbox optimisation project.

The experiments will use the two-dimensional mathematical Branin function which has been used to test metamodels in the literature [74]. This is discussed along with the available sampling methods and error estimation methods in the following sections.

A.2.1 The Branin Function

In order to understand the operation of the various sampling methods, a representative surface is required that features some complexity as well as changing features. The function selected is the Branin function from Fang *et al* [74]. The equation for the surface is given in equation A.1 which is then plotted in Figure A-1:

$$f(x) = \left(x_2 - \frac{5 \cdot x_1^2}{4 \cdot \pi^2} + \frac{5 \cdot x_1}{\pi} - 6 \right)^2 + 10 \cdot \left(1 - \frac{1}{8 \cdot \pi} \right) \cos(x_1) + 10 \quad (\text{A.1})$$

As this experiment is to assess the various sampling methods, only a single metamodeling method will be used. Fang *et al* [74] found the Radial Basis Function (RBF) using Multi-Quadratic approximations was the best at predicting the surface. The Branin function has a global maximum of 305.9563 located at $x_1 = -5$ and $x_2 = 0$ as well as a local maximum located at $x_1 = 6.2$ and $x_2 = 15$ ($F_{Branin} = 215.5444$). Figure A-1 shows that there are a number of local minima, but the global minimum of 0.4018 is located at $x_1 = 9.4$ and $x_2 = 2.2$. These points will be used to assess the sensitivity of the fitted metamodel to the maximum and minimum.

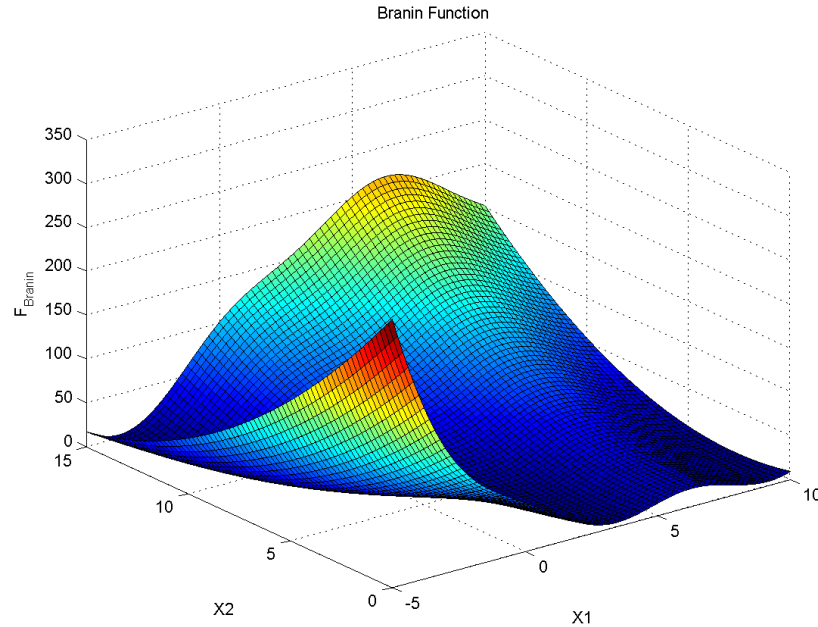


Figure A-1: The Branin function

A.2.2 Upfront and Sequential Sampling Methods

This experiment assesses the various sampling methods available, which are as follows:

1. Latin Hypercubes (LH)
2. Lipschitz (L)
3. Multivariate Adaptive Crossvalidating Kriging (MACK)
4. Error based Lipschitz (EbL)

These can be split into two generic methods; upfront methods (LH) and sequential sampling (L, MACK and EbL). Of the sequential sampling methods, the Lipschitz and MACK methods are in-built within modeFRONTIER, while the EbL method was developed within this project as a new approach to using the Lipschitz sampler.

Latin Hypercubes

There are two Latin Hypercube methods which can be utilised in this project. The first is a seeded latin hypercube available within modeFRONTIER and the second is the Ford minimum latin hypercube designs which are optimally distributed through the design space[97].

The modeFRONTIER latin hypercube methods are based on a seeding point and have 1000 variations. The sample points in this method are not uniformly distributed throughout the design

space. This means that in some areas of the design space the samples are more densely packed than others. The distribution also varies with the seeding number used which can lead to variability in the robustness of the sampling. Unless stated otherwise, in these experiments the default seed of 1 value was used.

The Ford minimum latin hypercube designs[97] are based on the work of Ye [98]. In these designs the sample points are distributed throughout the design space with optimal uniformity. This means that all areas of the design space have the same sample point density. 9, 17, 33, 65, 128, and 257 sample designs are available for use.

Lipschitz Sampling

The Lipschitz sampler is a sequential method that uses an assessment of the surface complexity to judge the next best position for a sample [101]. The process is as follows:

1. An initial sample of the design space is taken.
2. An n-dimensional Delauney tessellation on normalised data is applied to the sample set and the Voronoi vertices calculated
3. The Lipschitz criterion (based upon gradients in the output values) is calculated at each of the Voronoi points
4. At the Maximum of these a point is placed which can then be obtained from the analysis function either automatically (when using CAE tools integrated with modeFRONTER) or manually running the analysis and inputting the result
5. The information from this sample is then added to the total design space
6. The process then repeats

Multi-Variate Adaptive Cross-Validating Kriging Sampling

This method again needs an initial sample of the design space, then using a kriging metamodel on a defined number of points it calculates the interpolation error. New points are then placed where the interpolation error is largest [102]. The new sample point is assessed and the process repeated. This method requires an automatic assessment of new sample points and does not work for cases where manual intervention is required.

Error Based Lipschitz Sampling

The Lipschitz sample uses a simplified gradient function to assess complexity in the metamodel surface, which does not consider error. In the creation of the radial basis function metamodel, 'leave one out' errors can be captured. As 'leave one out' error can be interpreted as a dependence on that point. Lipschitz sampling on this would highlight large changes in dependence/error and place samples to resolve these. The process for this method is completely manual and more time consuming than others mentioned. The process is as follows:

1. Import initial Branin sample and create and an RBF model, exporting the leave one out errors to an .x/s file.
2. Arrange the error data so that it shows the sample point locations and error estimation.
3. Import error sample set into another modeFRONTIER file.
4. Perform a Lipschitz iteration to get the next sample point.
5. Sample this point and add it to the Branin data sample.
6. Create a new RBF model and repeat the process.

A.2.3 Error Estimation Methods

There are a number of error assessment methods that can be applied to compare metamodel predictions with actual computed data. The review of literature suggested the R^2 and RMSE given in equations 2.1 and 2.2. These measures are limited in the fact that only the global fit of the metamodel is assessed. While this may be acceptable in terms of a global optimisation, it gives no information as to the localised errors, i.e. the measures may suggest a poor global fit. This could be the product of poor fit in only one area but generally there is good correlation else where.

It must be noted that the radial basis function is interpolative, i.e. the model will return the sample value at a given sample point. This means that either additional sample points or leave one out methods are required for error assessment.

The advantage of using additional sample points is that the error estimation can be made on the final surface. However, this comes at the cost of reduced efficiency of use as these points must be generated. This may be acceptable for low cost CAE functions but becomes increasingly prohibitive as CAE cost functions rise. When CAE costs are increased, leave one out error estimators become attractive as no additional samples are required to assess the error in a surface.

Leave one out methods function by building a total of n surfaces each based on $n-1$ data points, where n is the total sample size. The prediction error to this remaining point can then be assessed and the final surface error estimated by an averaged value across all the surfaces created. modeFRONTIER quotes this as the root mean square for Kriging metamodel methods and normalised root mean square for radial basis functions. As these errors are not assessed on a surface of all data points, the error measurement is not an absolute figure. Instead it can be interpreted as a dependency on a given sample point. A large leave one out error at one point would be given by a metamodel where the fit to other local points does not capture the true behaviour. The behaviour of these errors must be compared to errors assessed by additional samples to confirm that it is fit for use within projects.

A.3 Experiments

A.3.1 Experiment 1: Examination of the Literature Guidance on Sample Size

The guides for sample size in the literature are given in Table 2.6 on page 53. for a two-dimensional function, such as the Branin function, the smallest sample size suggested is 6 (3 times the number of inputs) and the largest 20 (based on the small set 10 times the number of inputs, for the two dimensional case the large sample set would require 18 samples). In this experiment the sample size of the modeFRONTER default seeded latin hypercube was increased incrementally from 6 to 20. In this case the small set The changes in metamodel fit were measured using the R^2 and RMSE based upon an additional sample of 20 points. This additional sample used a modeFRONTIER latin hypercube with a seed of zero. The measured error results are presented in Figures A-2 and A-3.

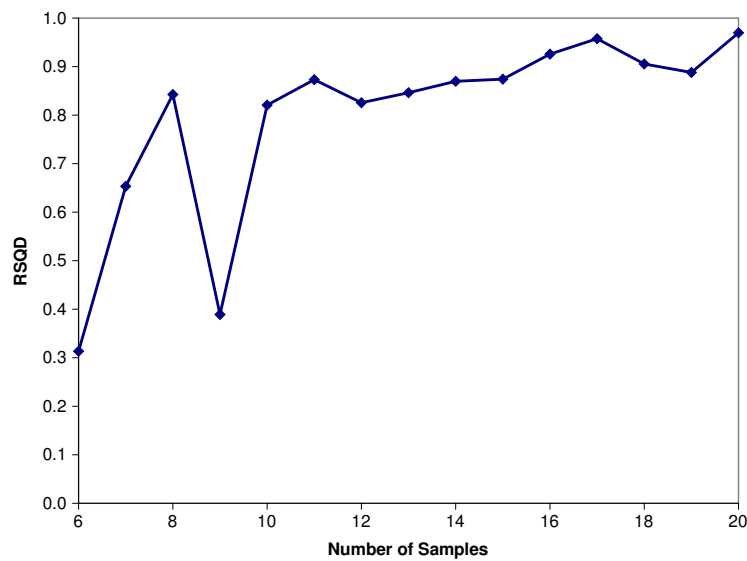


Figure A-2: Variation of the R^2 error estimator of seeded latin hypercube sampling method with increasing numbers of samples

From both the error measures it can be seen that increasing the sample size does improve the fit of the metamodel as the R^2 value increases and the RMSE reduces. However, it can be seen that from samples 8 to 9, 11 to 12 and 17 to 19 that the inclusion of additional points has reduced the fit of the metamodel. This is due to the new sample revealing a region of complexity that was not present in the previous model. The local fit of the metamodel would be improved in the region of the new sample, however the global fit may be severely affected.

For 6 samples the low R^2 value of 0.3 and high RMSE value of over 30 show that the scarce sample size is insufficient to model the complexity of the Branin function. At 20 samples the R^2 value has been improved to approximately 0.97 while the RMSE reduced to approximately 5. This would suggest that 20 samples is sufficient to capture the complexity of the Branin function. However, when the metamodel is visualised, it would suggest that the metamodel has a poor fit.

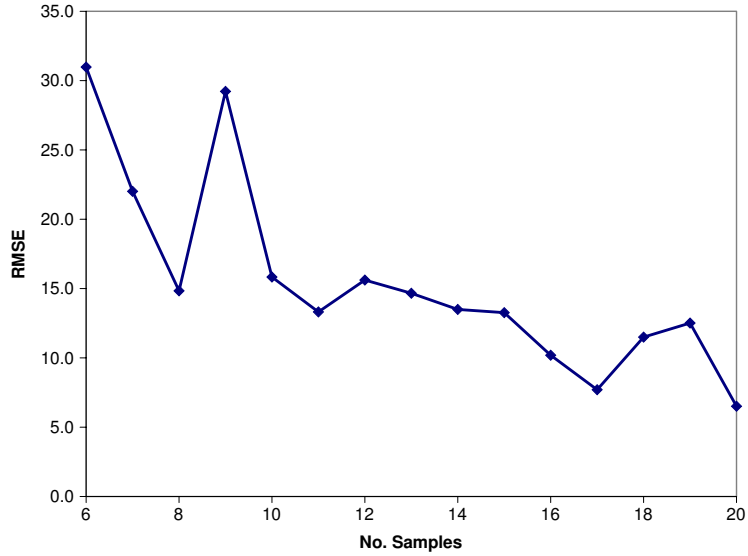


Figure A-3: Variation of the RMSE error estimator of seeded latin hypercube sampling method with increasing numbers of samples

Figure A-4 compares 20 sample metamodel surface (Red Surface) with the actual plotted surface. From this it can be seen that there are still significant errors, particularly in the global maximum region ($x_1 = -5, x_2 = 0$). This would seem to suggest that the error measures are under-estimating the total error in the fit. This should be further investigated.

Figure A-4 also suggests that the guideline of 20 samples may also be insufficient to capture the complexity of the Branin function. This means that the use of number of inputs to scale the size of samples may also need to be examined and another method scaling devised.

A.3.2 Experiment 2: Sample Size and Distribution for Error Estimation

The error in the metamodels created in the previous section were assessed using an additional twenty sample points created by the modeFRONTIER latin hypercube algorithm. However, the use of the error sample was questioned when comparing the measured error results with a visualisation of the metamodel surface. The fit of the metamodel was shown to be sensitive to the number of samples. A corollary of this is that any error estimation using this sampling method would also show the same sensitivity and variability. A consequence of this is a need to understand the best sampling method for error estimation as well as for metamodel creation.

This experiment was conducted using the metamodel created from the twenty point sample modeFRONTIER latin hypercube (shown in Figure A-4). To assess the requirements for error estimation of metamodels three different sampling methods of varying sizes were applied to the Branin function. The error was assessed by the RSQD and RMSE measures.

Figures A-5 and A-6 show the effect of increasing the sample size used in the error estimation

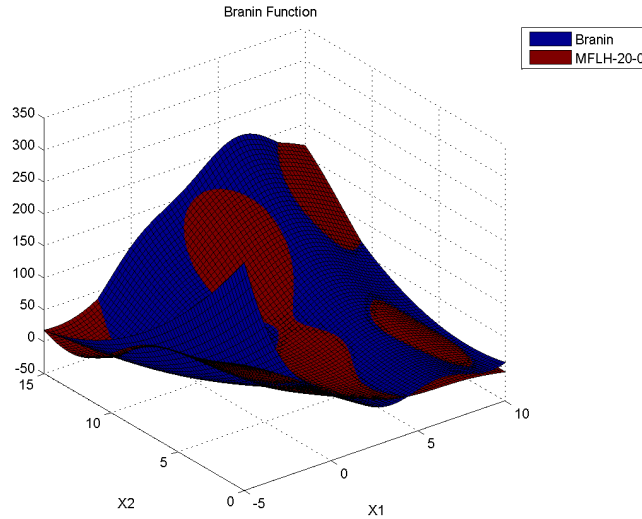


Figure A-4: Metamodel surface based on 20 modeFRONTIER non-uniform latin hypercube sample points

for three different sampling methods. A full factorial with increasing numbers of levels and two types of latin hypercube methods have been employed; the minimum Ford and modeFRONTIER seeded method. From these plots it can be seen that as the sample size increases, the error estimation tends towards a single value. However, it is subject to a diminishing return with increasing the sample size. The uniform latin hypercube method can under-predict the error, however, it tends towards the true error value in fewer samples than the full factorial method. In all error sample distribution methods, the number of samples required for assessment of the error is much larger than expected, this is suggesting that a metamodel built with 20 samples may require more than 257 samples to assess the error.

The initial error estimation of the 20 sample metamodel suggested an R^2 value of 0.97 and a RMSE of 5. The visualisation of the surface in Figure A-4 suggested that these values may have underestimated the metamodel error. This suggestion is confirmed as the true global error is approximately 0.9 and 18 according to the R^2 and RMSE measures respectively. Based on these results it also confirms that a sample size of 20 is insufficient for this example. The sample size required to assess the Branin function needs further investigation.

The large sample sizes required to estimate the global error present a dilemma as it requires a large cost to complete in a constrained environment. While global error estimation by additional samples may be impractical, small focused samples in regions of interest could be used to predict the local error. This may be a more practical method of estimating the error and could include samples of the predicted optimums and baselines.



Figure A-5: R^2 error estimator comparing sampling method and size



Figure A-6: RMSE error estimator comparing sampling method and size

A.3.3 Experiment 3: Comparing Seeded and Uniform Latin Hypercubes

The Latin Hypercube method used in modeFRONTIER is based upon an initial seed value. Therefore, variations in this initial seed can lead to perturbations in performance. This occurs as the positions of the sample points change, meaning different regions will be captured. Figure A-7 show the variation of the radial basis function surfaces for a nine point latin hypercube at four different seed

values.

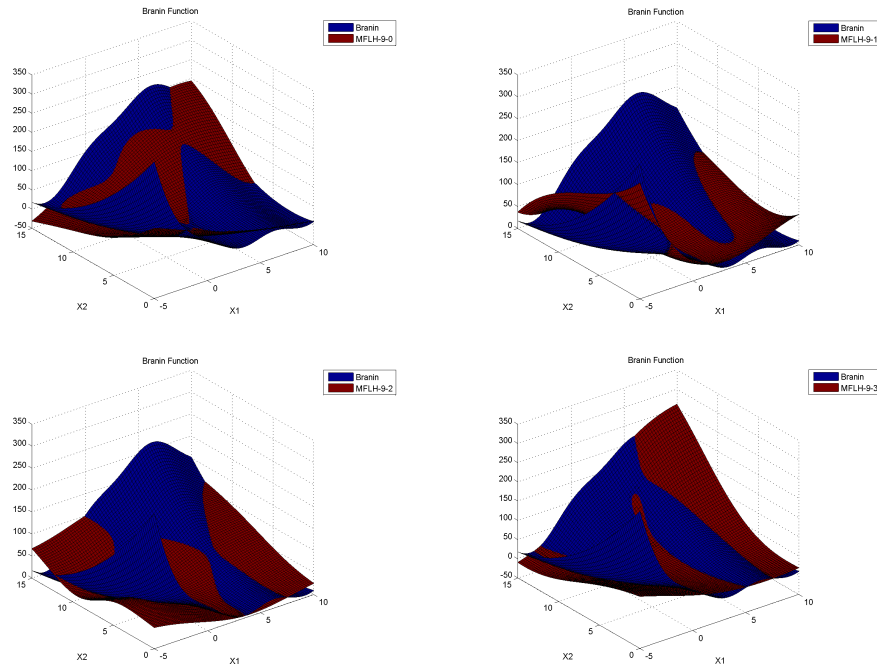


Figure A-7: Variation of RBF approximation with 9 point latin hypercube (top left seed=1, top right seed=2, bottom left seed=3 & bottom right seed=4)

Surfaces show large amounts of variation depending on the seed point and could result in non-robust metamodels. In this experiment, the efficiency of this method is compared with performance of an uniformly distributed latin hypercube, as provided by Ford[97]. The Ford minimum latin hypercube method provides 9, 17, 33, 65, 129 & 257 sample point designs for two-dimensional problems. These are compared to the default seed modeFRONTIER latin hypercube of the same size. The global metamodel errors are estimated based on 5776 additional data points from a full factorial design.

Seeding of the initial sample set can have a substantial effect on its predictive power. This is not advantageous for an unknown function as it could give variable results from application to application. By all measures the optimal latin hypercube outperforms the modeFRONTIER method. This happens up until a critical sample density where they then perform equally, as shown in Figures A-8 and A-9. From this it could be argued that global metamodel performance is a function of the complexity of the surface, number of inputs and the distribution of the sample.

Both methods seem to indicate a diminishing returns behaviour for increasing the number of sample points as the fit tends toward that of the actual surface. This suggests that there is a trade-off point at which increasing the number of samples becomes inefficient when compared to the gains made. This trade-off point would be vital to any industrial application as sampling beyond this point would be a waste of resources. For this example the trade-off sample density seems to be at around 33 optimal samples, there is little change in the R^2 value and the RMSE represents

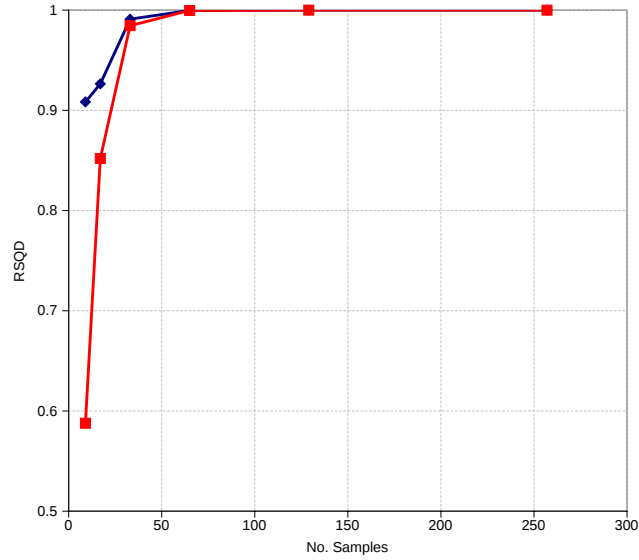


Figure A-8: Variation of the R^2 error estimator of various sampling methods with increasing numbers of samples

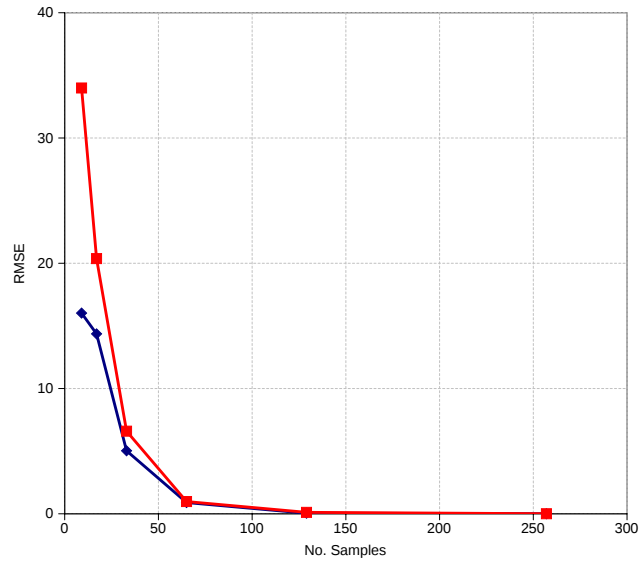


Figure A-9: Variation of the RMSE error estimator of various sampling methods with increasing numbers of samples

approximately 2% of the function range. This is where the prediction performance of the surface is traded off against the effort required to gain further data. At 17 there are insufficient samples to correctly predict global bulk behaviour, i.e. the trends in the metamodel do not match the trends in the function. However, the improvement gained from 65 samples is small. The literature guidelines called for three times the number of inputs for scarce sampling and ten times for small sets.

However, this surface required 16.5 times the number of inputs. This also supports the findings of experiment 1, that the guidance in the literature may not be sufficient to capture complexity. A new approach considering the potential complexity of the surface may be required.

A.3.4 Experiment 4: Comparing Sequential Sampling Methods

The previous section demonstrated that a sample size of approximately 33 points would be sufficient to model the Branin function. In this experiment the sequential sampling methods available within modeFRONTER are used to examine whether this value can be reduced by better placement of samples in regions of interest. The experiment will start with an initial sample, in this case the 17 sample Ford latin hypercube, which represents an under-sampling of the design space. Each of the sequential methods are then used to increase the sample numbers up to 33. To compare the methods the R^2 and RMSE values for each increment is measured using 5776 full factorial sample. The methods are also compared by examining the location of the global maximum and minimum. A more efficient sampling method would reduce the global error and find the global maximum and minimum in fewer samples than other methods.

Error Estimation

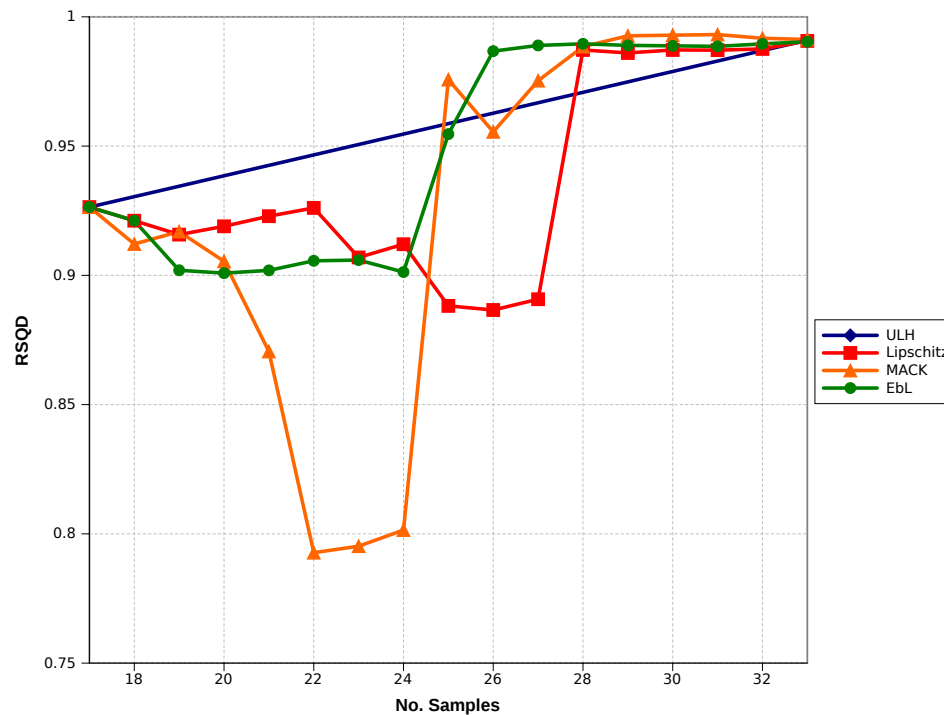


Figure A-10: RMSE with increasing numbers of sample points

Figures A-10 and A-11 demonstrate the fit performance of the various sampling methods with increasing numbers of samples. The plots show that the sequential methods can both improve

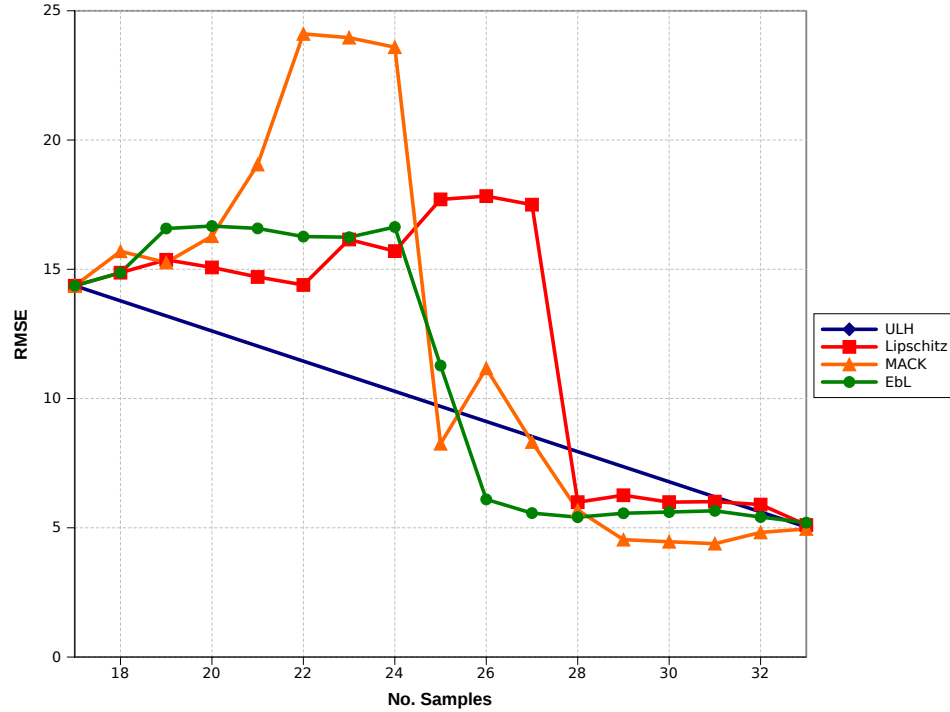


Figure A-11: RMSE with increasing numbers of sample points

and reduce the fit performance of the model on the introduction of a new point. However, all of the sequential methods reach a similar level of performance as the 33 optimal latin hypercube in a fewer number of samples. This suggests that complexity of surfaces can be resolved using sequential methods. In these examples, the methods based on error estimations (MACK and EbL) outperform the Lipschitz method, but these methods are limited by their implementation requirements. The MACK sampler requires automation and the EbL requires a greater degree of human interaction.

However issues can occur with sequential sampling methods. Figure A-12 demonstrates how the metamodel performance can be reduced when new samples are introduced. The addition of a new point may improve the local performance of the model in the region of the sample, but it can affect the overall fit of the function. In the illustrated case, the new sample point dramatically alters the prediction along the borders, increasing the error.

Global Maximum and Minimum Predictions

As well as error sensitivity, the metamodel should also be able to predict the global maximum and minimum locations. In this assessment the maximum and minimum are located using the full factorial sampler used to generate the surface meshes. The maximum locations are given in Table A.1 and the minimum locations in Table A.2. The results from these are displayed in Figures A-13 and A-14.

Viewing the original function (Figure A-1) it can be seen that the maximum is in a region of large gradients on the boundary of the Branin region. This means that the application of the sequential

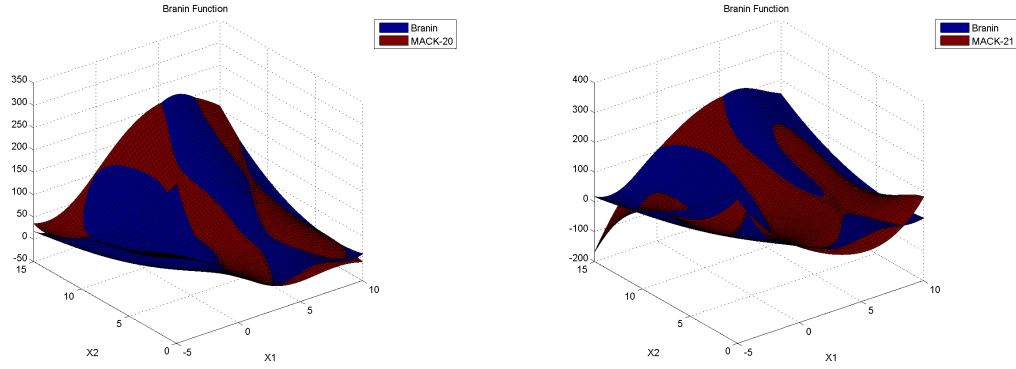


Figure A-12: Increasing the number of points via the MACK sampler with 20 (left) and 21 (right) samples

sampling methods are able to capture this point within a few samples. The large gradients will draw in the lipschitz sampling method and the low sample density will lead to large error in this region, forcing the MACK and EbL methods to add points in this region. However, this is not the case for finding the global minimum as this is located in a shallow trough surrounded by low gradients with multiple local minima. The steep gradient assumption in the formulation of the lipschitz sampling method means that this area is not sampled and therefore is insensitive to this minimum. The relatively low complexity in this region would lead to lower error estimators resulting in the MACK and EbL methods also being insensitive. Any optimisation based on surfaces created using these methods may not deliver the global minimum.

Sample	EbL		Lipschitz		MACK		LH	
	x_1	x_2	x_1	x_2	x_1	x_2	x_1	x_2
17	6.00	15.00	6.00	15.00	6.00	15.00	6.00	15.00
18	6.00	15.00	6.00	15.00	5.60	15.00	-	-
19	6.00	15.00	6.60	15.00	5.80	15.00	-	-
20	7.00	15.00	6.80	15.00	5.80	15.00	-	-
21	6.80	15.00	6.00	15.00	-5.00	0.00	-	-
22	6.80	15.00	6.00	15.00	-5.00	0.00	-	-
23	6.00	15.00	6.00	15.00	-5.00	0.00	-	-
24	5.80	15.00	6.20	15.00	-5.00	0.00	-	-
25	-5.00	0.00	6.00	15.00	-5.00	0.00	-	-
26	-5.00	0.00	6.00	15.00	-5.00	0.00	-	-
27	-5.00	0.00	6.00	15.00	-5.00	0.00	-	-
28	-5.00	0.00	-5.00	0.00	-5.00	0.00	-	-
29	-5.00	0.00	-5.00	0.00	-5.00	0.00	-	-
30	-5.00	0.00	-5.00	0.00	-5.00	0.00	-	-
31	-5.00	0.00	-5.00	0.00	-5.00	0.00	-	-
32	-5.00	0.00	-5.00	0.00	-5.00	0.00	-	-
33	-5.00	0.00	-5.00	0.00	-5.00	0.00	-5.00	0.00

(Actual= $(x_1 = -5.0, x_2 = 0.0)$)

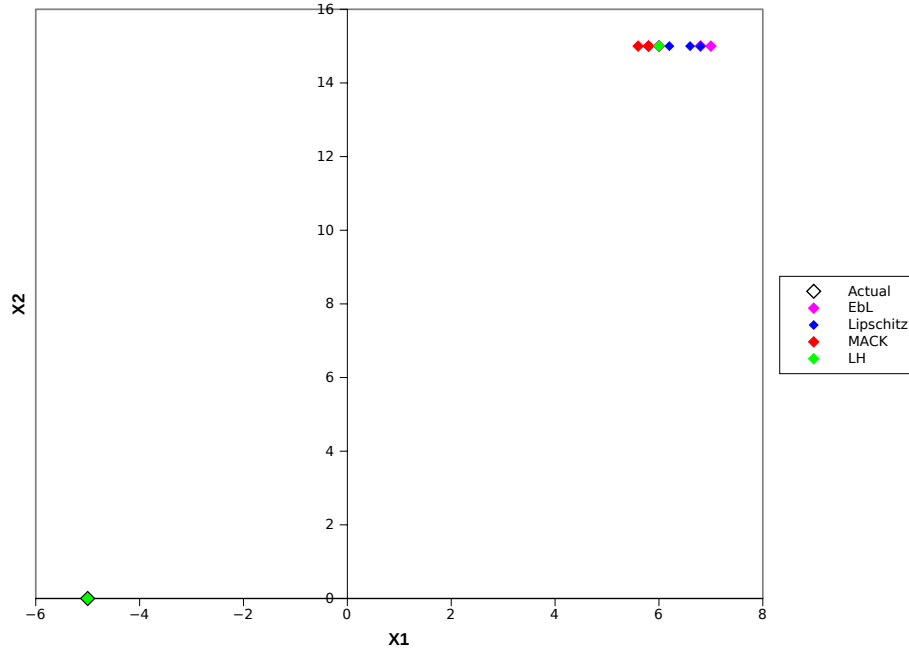


Figure A-13: Predicted global maxima locations

Sample	EbL		Lipschitz		MACK		LH	
	x_1	x_2	x_1	x_2	x_1	x_2	x_1	x_2
17	10.00	0.00	10.00	0.00	10.00	0.00	10.00	0.00
18	10.00	0.00	10.00	0.00	4.60	0.00	-	-
19	3.60	2.00	10.00	0.00	4.60	0.00	-	-
20	10.00	0.00	10.00	0.00	10.00	0.00	-	-
21	10.00	0.20	10.00	0.00	-5.00	15.00	-	-
22	4.60	0.00	10.00	0.00	10.00	0.00	-	-
23	3.80	1.80	10.00	0.00	10.00	0.00	-	-
24	3.60	2.00	4.60	0.20	10.00	0.00	-	-
25	5.80	0.00	3.80	1.20	4.20	2.40	-	-
26	4.20	1.20	3.80	1.20	4.20	2.40	-	-
27	4.40	0.80	3.60	1.40	3.80	2.60	-	-
28	5.00	0.00	4.80	0.00	10.00	1.40	-	-
29	-3.60	15.00	-3.40	12.60	3.60	2.40	-	-
30	4.40	1.40	4.40	0.20	3.60	2.20	-	-
31	4.40	1.20	4.40	0.20	3.60	2.20	-	-
32	4.00	1.80	4.80	0.00	3.60	2.20	-	-
33	10.00	0.00	4.60	0.00	3.60	2.20	10.00	5.40

(Actual= $(x_1 = 9.4, x_2 = 2.2)$)

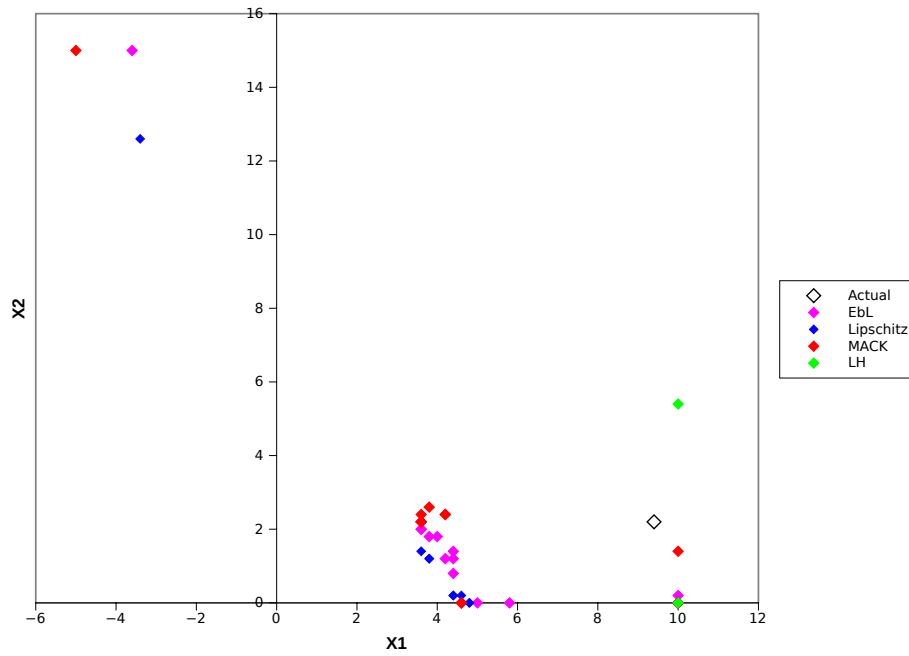


Figure A-14: Predicted global minima locations

A.3.5 Experiment 5: Examining the ‘Leave One Out’ Error Estimation Method

modeFRONTIER uses the normalised RMSE based on a ‘leave one out’ (LOOE in the following figures) method to estimate the surface fit of the radial basis function. This method is meant to guide the user in understanding the fit of the surface without the need for additional data points. While this may be more efficient, as no additional samples are required, it may also not reflect the true state of errors in the model. This experiment compares the use of the modeFRONTIER error estimator against measures taken from additional samples. The experiment also examines how the ‘leave one out’ error can be interpreted and what the changes mean in terms of surface fit. For this experiment the RMSE values obtained in experiments 3 and 4 are normalised against the range and compared to the ‘leave on out’ errors obtained from the same experiments.

Firstly, comparing the additional sample error estimators, hereafter called the measured error, with the modeFRONTIER ‘leave one out’ error over the 9 to 257 sample uniform latin hypercubes shows the general trend of the predictors. However, the Figures A-15 and A-16 show that the error can be over-estimated which increases the risk of gathering more samples than required. These plots demonstrate that the leave one out method can pick up errors in the predictions when there are large variations in the surface fit. But it must be questioned if the ‘leave one out method’ can pick up on differences when there may be only small changes in surface fit?

While Figures A-15 and A-16 show there is a general correlation of the two error estimation methods when there are large variations in the surface fit, Figures A-17 and A-18 show that this may not be true for small variations. Some of the trends shown in Figures A-17 and A-18 show correlation in the ‘leave one out’ and the additional sample error measure. However, the trend is not followed when the sample size is increased from 25 to 26 using the Error based Lipschitz re-sampling method (Figure A-17). This figure shows that while this increase in sample size leads to a reduction in the measured error, there is a corresponding rise in the ‘leave one out’ error. This may drive the user to obtain more samples, however this type of error holds less risk than an underestimation of error.

When the two error estimation methods are compared in the MACK method (Figure A-18) it can be seen that an overall rise in the measured error, from samples 20 to 21, corresponds to a reduction in the ‘leave one out’ error. This introduces a large risk in the use of the surface as the user perceives the model performance to be better than it actually is. The source of these differences needs to be understood.

High leave one out errors show that the final surface requires that point to be there as the other local sample points cannot predict the surface at that point. Conversely, low leave one out errors mean other local samples can be used to predict that point accurately. This means that the ‘leave one out’ error can be seen as a measure of dependence on points in the data set. With this in mind, the two scenarios above can be understood.

In the first case, where a decrease in the measured error corresponded to an increase in the leave one out error, the new sample point resolves a region of complexity which was previously unknown. Thus, when the ‘leave one out’ error is formulated there is a large error at this point as the model surface is highly dependant on that sample. This is demonstrated by Figure A-

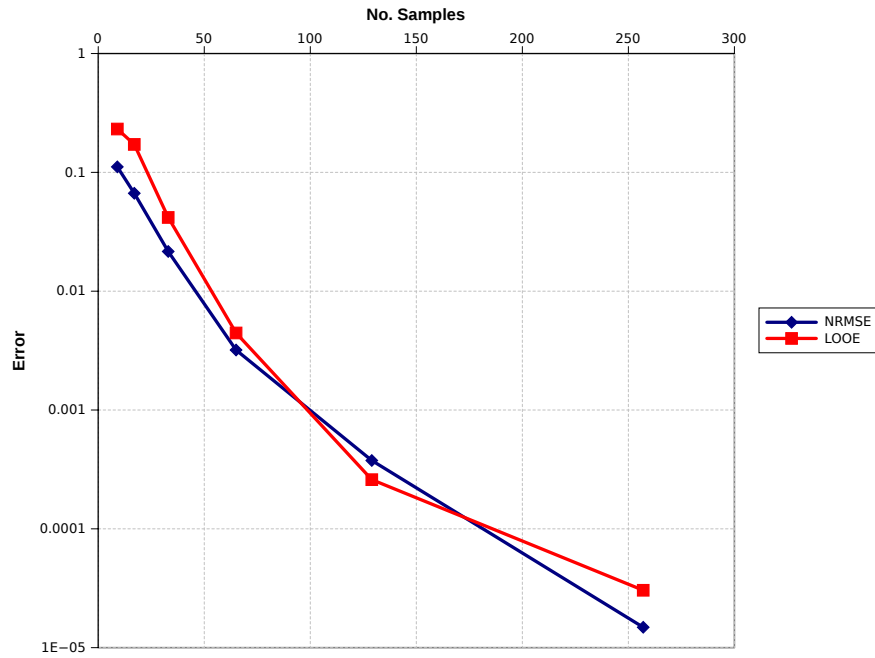


Figure A-15: Comparing error estimates based upon 'leave one out' error and actual error for modeFRONTIER latin hypercubes

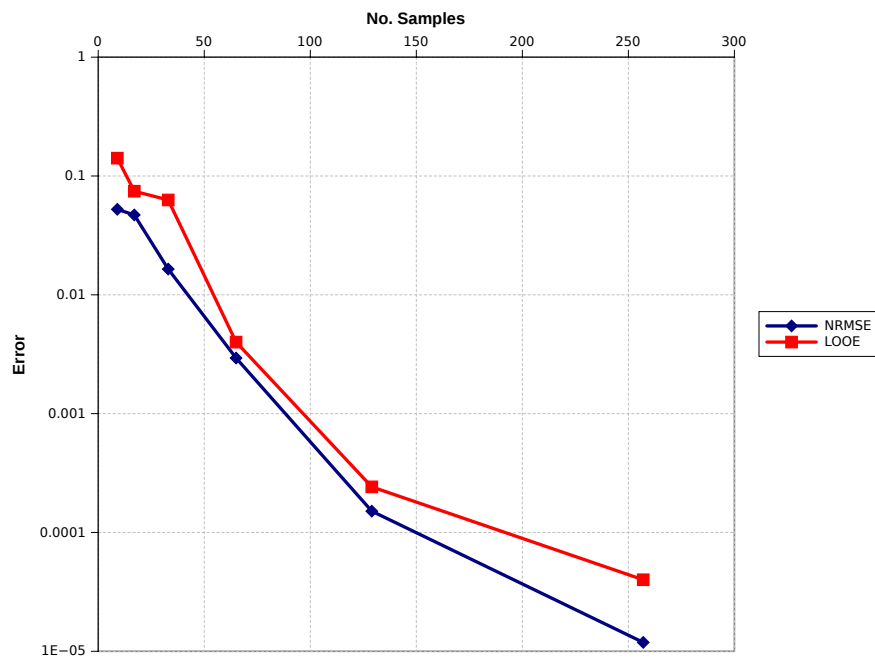


Figure A-16: Comparing error estimates based upon 'leave one out' error and actual error for Ford minimum latin hypercubes

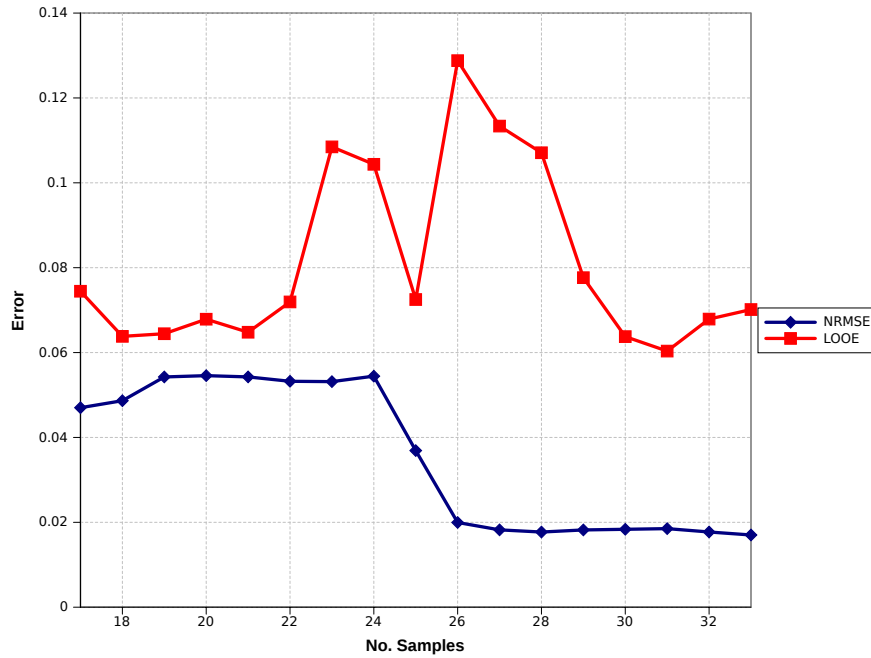


Figure A-17: Comparing error estimates based upon 'leave one out' error and actual for EbL sampling

19. Here, the increase in sample points via the MACK sampler has improved the global fit of the model, particularly on the border regions, but without this point the error estimation would be based on the previous surface. The second scenario is also demonstrated in the MACK sampler, examining Figure A-12 again shows that the global surface prediction has been reduced. However, this corresponds to a steep decrease in the 'leave one out' error as shown in figure A-18. This would occur when the introduction of a new point improves local performance but drastically changes the surface in other regions. When the 'leave one out' surfaces are created, the local improvement reduces the dependence on the metamodel on each sample point, leading to lower 'leave one out' errors. Both of these scenarios mean that using the modeFRONTIER error estimator without additional samples increases the risk of the optimisation method failing.

This section has shown that the 'leave on out' error value can be misleading with both optimistic and pessimistic predictions of the metamodel error. This was particularly significant for small sample sizes. However, as the number of sample sizes increases, so does the confidence in this value. This would mean that fewer additional points would be required to verify the metamodel. This error estimator may be used when no additional points are available, but only as a guide for the surface fit.

A.4 Conclusions

The conclusions from each experiment are as follows:

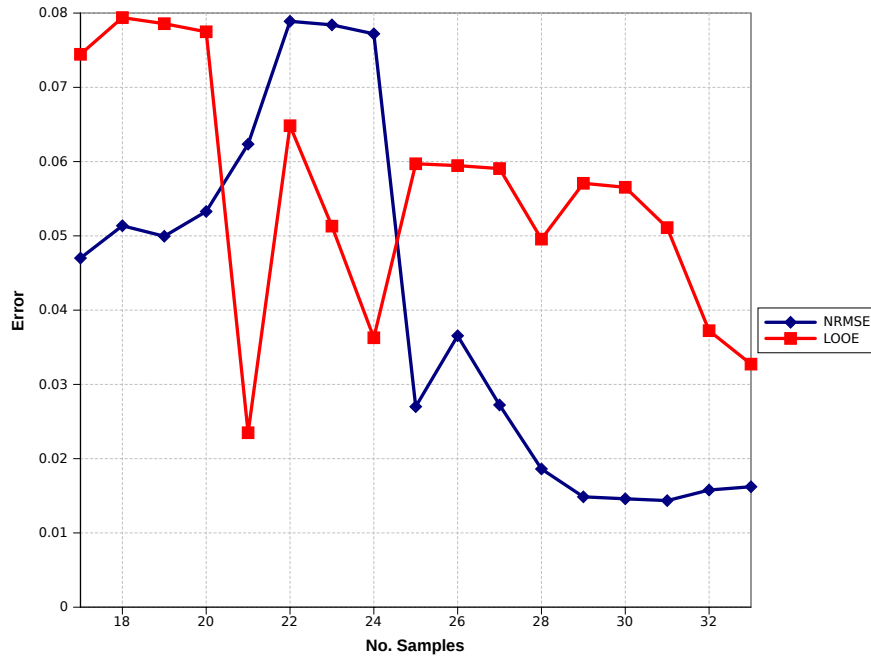


Figure A-18: Comparing error estimates based upon ‘leave one out’ error and actual error for MACK Sampling

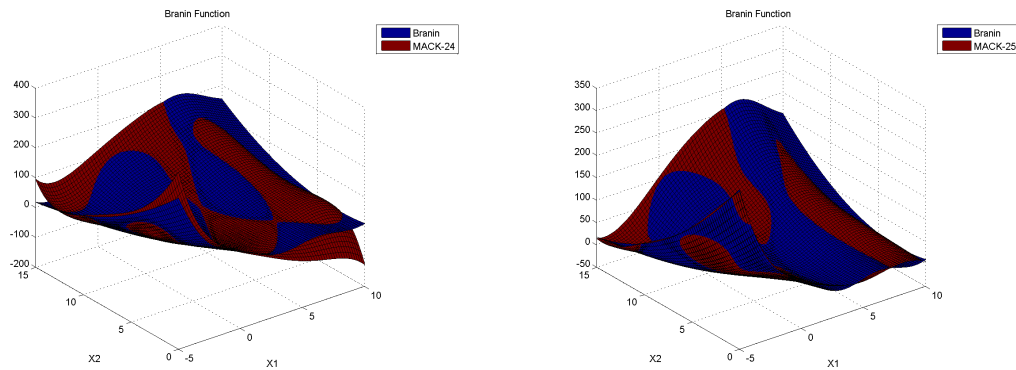


Figure A-19: Increasing the number of points via the MACK Sampler with 24 (left) and 25 (right) samples.

- *Experiment 1:* Sample sizes guided by the literature are not sufficient to model the complexity in the Branin function. This also suggests that the scaling of sample sizes by the number of inputs alone may not be sufficient.
- *Experiment 2:* The sample size required for error estimation is potentially larger than that required to build a metamodel. This may make the estimation of global metamodel error impractical. One potential method is to use small additional samples focused on local areas of interest (optimums or expected design regions) to understand local error.

- *Experiment 3:* A uniform distribution of sample points is more robust and efficient than a non-uniform sample. This experiment also confirmed the conclusion from experiment 1. A sample size of 20 is insufficient for the Branin function, instead 33 samples are required. This value is 16.5 times the number of inputs.
- *Experiment 4:* A smaller initial sample followed by a sequential sampling methods can be more efficient than a larger initial sample. This is because these methods place samples in regions of high error or complexity allowing them to be resolved. Of the three methods available the MACK and EbL methods perform better but are harder to implement than the Lipschitz sampler.
- *Experiment 5:* The 'leave one out' error estimation should be interpreted as a dependency metric rather than an error measure. Used in isolation it can be mis-leading and has the potential to under or over estimate the error depending model. As this estimator is cheap to obtain it should be used, however, only in conjunction with error estimation based on additional samples.

Appendix B

Supporting Documentation for Airbox Project

B.1 Airbox Geometry

This section shows how the airbox input parameters are included in a parametrised CAD model. The simplified geometry is shown in Figure B-1, the primary parameters are listed in Table B.1, these will be varied using the in the optimisation. Table B.2 lists the secondary parameters which will be used, these were used to adjust the final shape of the airbox but are not used in the optimisation. The clean and dirty duct lengths are calculated as a percentage of the total length.

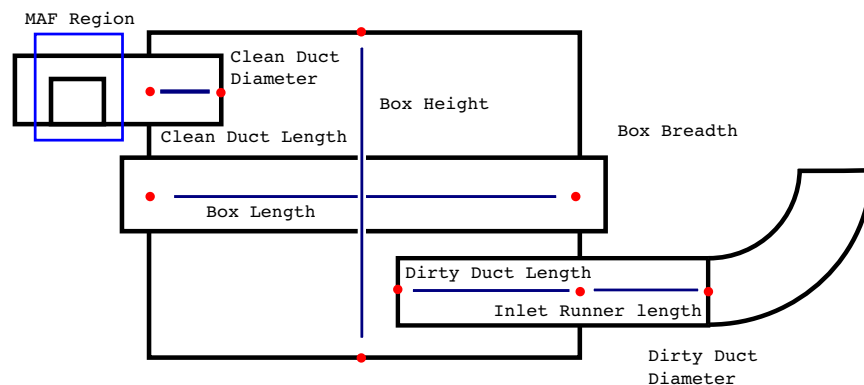


Figure B-1: Simplified Airbox Geometry

Table B.1: Primary Parameters

Parameter	Abbreviation
Total Height	H
Length	L
Breadth	B
Clean Duct Diameter	CDD
Dirty Duct Diameter	DDD
Clean Diffuser Length	CDL
Dirty Diffuser Length	DDL
Inlet Runner Length	IRL

Table B.2: Secondary Airbox Parameters

Parameter	Abbreviation	Value
Bell mouth Radius	BMR	10 mm
Diffuser Thickness	DT	2 mm
Lip Length	LP	10 mm
Filter Thickness	FT	48 mm
Filter Clearance	FC	2 mm
Inlet Runner Radius	IRR	75 mm
Filter Fillet Radii	FFR	2 mm
Box Fillet Radii	BFR	10 mm

The geometry heights was assumed to be symmetrical about the y axis, with the diffuser centre lines an equal distance either side of the filter. The heights are shown in Figure B-2, and the relationships can be defined as;

1. $BH = (H - FT - 2FC) / 2$ (Box Height)
2. $DH = (TH - FT - 2FC) / 4$ (Duct Height)
3. $DCL = DH + FT / 2 + FC$ (Duct Center Line)

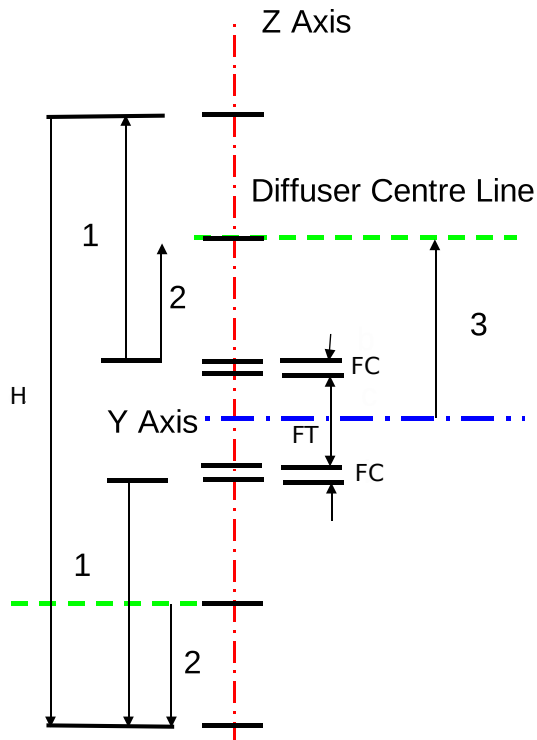


Figure B-2: Airbox Height Definitions

The box length and breaths are defined in a similar manner with an additional 10 mm around the filter section. The length and breath planes are shown in Figure B-3 with the relationships defined as;

1. $HLP=L/2$ (Half Length Plane)
2. $HTLP=L/2+LP$ (Half Total Length Plane)
3. $BLP=B/2$ (Half Breadth Plane)
4. $BTLP=B/2+LP$ (Half Total Breadth Plane)

The implementation clean and dirty side ducts are shown in Figure B-4. Given that the duct length are defined by percentage ingress parameters (Clean Duct Ingress = CDI and Dirty Duct Ingress = DDI), the relationships governing the ducts are;

1. $BBM=C/D \text{ DL-DT}$ (Back of Bell Mouth)
2. $SBM=C/D \text{ DL-BMR}$ (Start of Bell Mouth)
3. $DOR=DD/2+DT$ (Duct Outer Radius)
4. $DMR=DD/2+BMR$ (Duct Mouth Radius)
5. $BOR=BMR-DT$ (Bell Outer Radius)

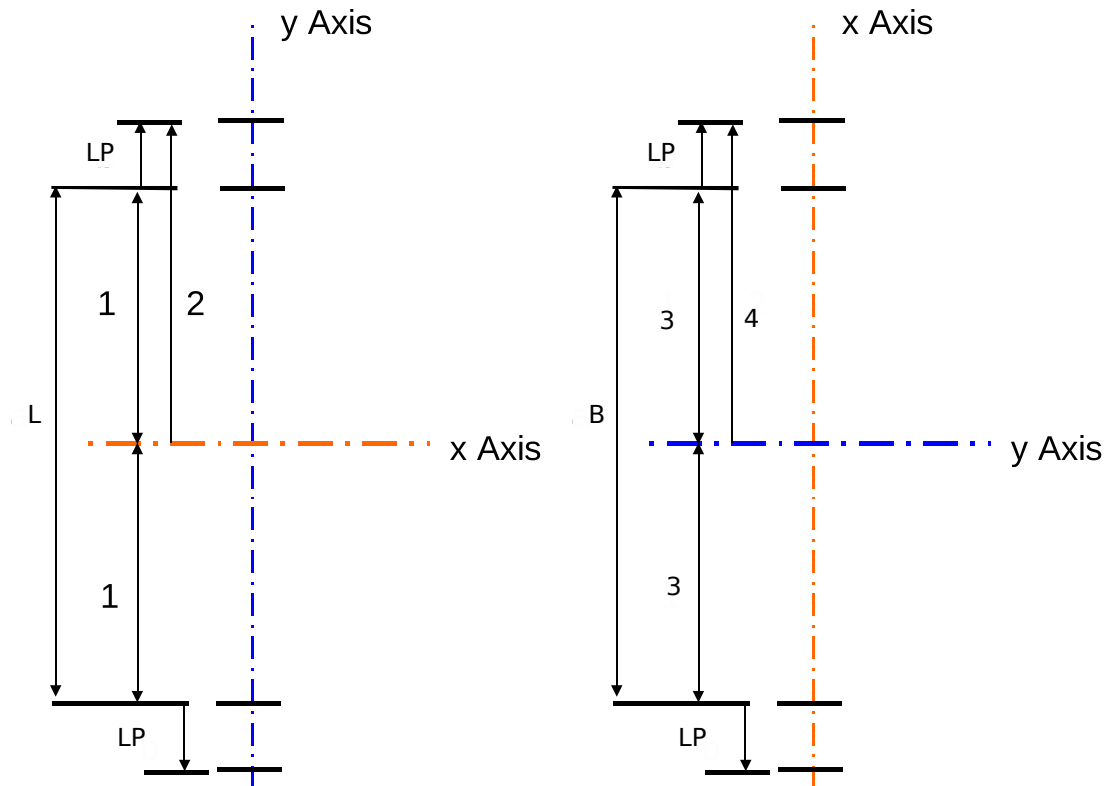


Figure B-3: Airbox Height (l) & Breadth (r) Definitions

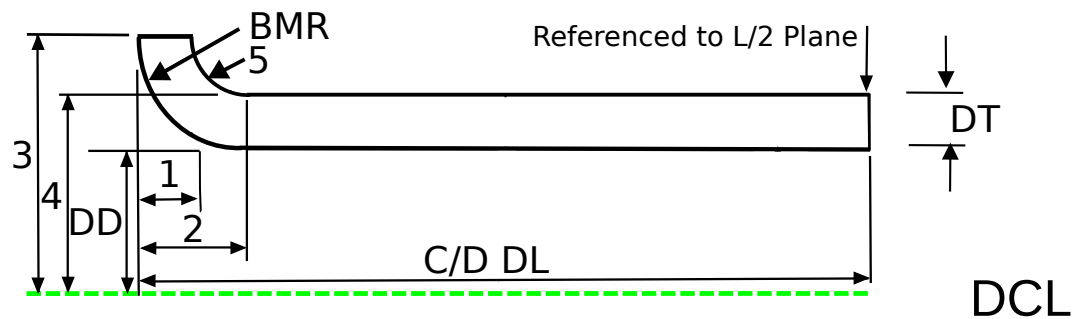


Figure B-4: Airbox Height Definitions

The inlet runner is assumed to be attached to the outside of the box and begins with a 90° bend. The outline of the geometry is given in Figure B-5 and the relationships as;

1. IBH=DCL+IRR (Inlet Bend Height)
2. IRS=L/2-IRL-IRR (Inlet Runner Start)

The MAF sensor geometry was derived from measurements taken of current Jaguar Land Rover devices. This is aimed to be a representative size and shape. The height is proportional to the diameter of the clean air duct. It is also assumed that the MAF is connected directly to the side of

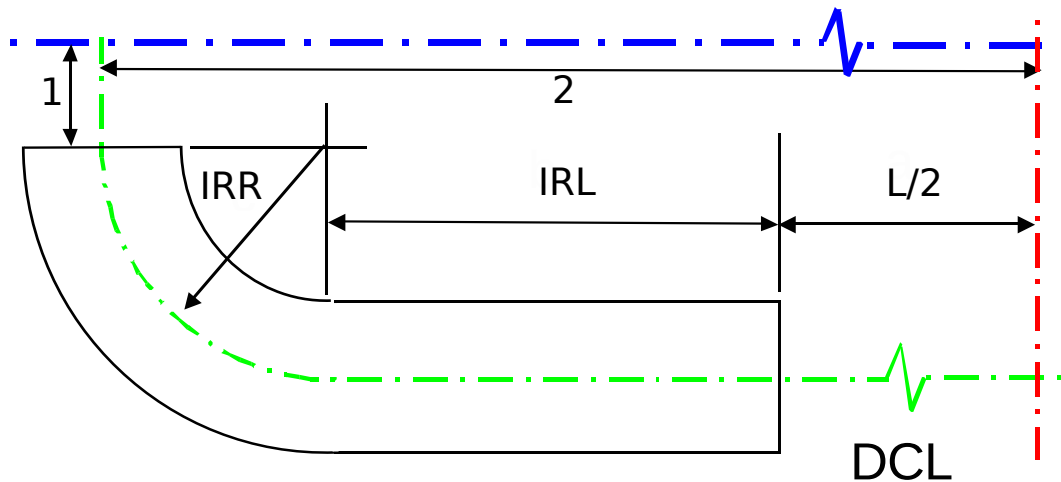


Figure B-5: Airbox Height Definitions

Table B.3: MAF Parameters		
Letter	Description	Value (mm)
a	MAF Width	14.5
b	MAF Box Length	29.8
c	MAF Rounded Length	14.9
d	Difference from Front L/2 Plane	20.0
e	Top rounded distance	10.0

the airbox. The fixed geometry sizes and relationships are shown in Figure B-6 with details in Table B.3.

1. $0.74 \cdot CDD$

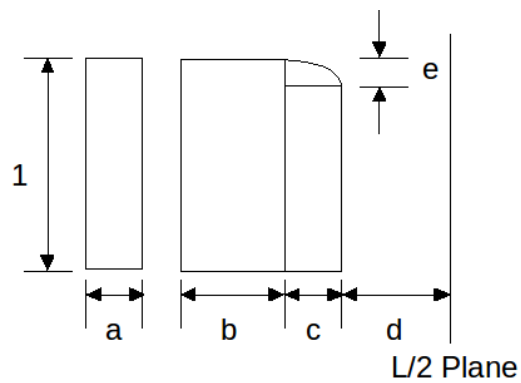


Figure B-6: Airbox Height Definitions

B.2 NVH Metric Method

This NVH metric Matlab script was written to reduce the NVH spectra results to a single value. This was developed by examining preferences expressed by a lead NVH engineer and trying to get the metric to replicate these preferences. The airbox result spectra is compared to the NVH target line and the areas above and below the lines assessed, The two areas are then added together with weightings. these bias the metric to highlight areas of poor performance by giving a larger weight to the area under target.

After the data has been clipped and the target model built, the next step is to find the intersections between the airbox attenuation spectra and the target model. This is done by subtracting the target model from the airbox data. From this the zeros can be found and the intersections added to the data.

```
NTLDATA(:,box)=TLDATA(:,box)-TLTARGET;
flag1=0;
if NTLDATA(1,box)>0
    flag1=0;
else
    flag1=1;
end
FQOUT=[];
len=length(NTLDATA);
n=1;
while n<60
    while flag1==0;
        if NTLDATA(n+1,box)<0
            freq=FQDATA(n,1)-(NTLDATA(n,box)*(FQDATA(n+1,1)...
            -FQDATA(n,1))/(NTLDATA(n+1,box)-NTLDATA(n,box)));
            FQOUT=[FQOUT;box n n+1 freq];
            n=n+1;
            if n==60
                break
            break
            break
        end
        flag1=1;
    else
        n=n+1;
        if n==60
            break
            break
            break
        end
    end
end
```

```

        end
    end
end

while flag1==1;
    if NTLDATA(n+1,box)>0
        freq=FQDATA(n,1)-(NTLDATA(n,box)*(FQDATA(n+1,1)...
        -FQDATA(n,1)))/(NTLDATA(n+1,box)-NTLDATA(n,box));
        FQOUT=[FQOUT;box n n+1 freq];
        n=n+1;
        if n==60
            break
            break
            break
        end
        flag1=0;
    else
        n=n+1;
        if n==60
            break
            break
            break
        end
    end
end
end

end

[x,y]=size(FQOUT);

boxdata=[FQDATA NTLDATA(:,box)];

for i=1:1:x
    L1=FQOUT(i,2)+i-1;
    L2=FQOUT(i,3)+i-1;

    boxdata=[boxdata(1:L1,:); FQOUT(i,4) 0; boxdata(L2:end,:)];
end
NTLBox{box}=boxdata;
clear x

```

```
end
```

Once the intersections have been found, the positive and negative areas can be found. The metric is then calculated by adding together 90% of the negative area and 10% of the positive area.

```
Pos_Factor=0.1;
Neg_Factor=0.9;

AREA_POS=[];
AREA_NEG=[];
ATTRIBUTE=[];

for B=1:L
    L=length(NTLBox{B});
    PA=0;
    PN=0;
    for j=1:L-1
        area=0.5*((NTLBox{B}(j+1,2)+NTLBox{B}(j,2))*(NTLBox{B}(j+1,1)...
-NTLBox{B}(j,1)));
        if area>0
            PA=PA+area;
        else
            PN=PN+area;
        end
    end
    AREA_POS=[AREA_POS; PA];
    AREA_NEG=[AREA_NEG; PN];
    ATTRIBUTE=[ATTRIBUTE; Pos_Factor*PA+Neg_Factor*PN];
end

format long
Output(finum,:)= [finum ATTRIBUTE AREA_POS AREA_NEG];
end
%%%%%%%%%%%%%%%%%%%%%%%%%%%%%%%%%%%%%%%%%%%%%%%%%%%%%%%%%%%%%%%%%%%%%%%%%
```

B.3 WaveBuild 3D Automation

When using the WaveBuild 3D automation script, the latin hypercube data is first imported into Matlab. Running this script will then take each box in turn to generate the appropriate WaveBuild

3D model. The first step is to calculate the required coordinates and lengths then place these values in the correct location of the base files. The script below shows the coding for placing the geometry values in the file. The variable 'line_v' contains the line number and the new geometry value. The geometry value is entered by replacing it using the appropriate regexp command in Matlab. The amended file is then saved in the appropriate directory. The final step is to open the file and mesh the model, then connect the airbox ducts to the test rig in the WaveBuild software.

```
% open inFile
fin = fopen(inFile);
% open outFile for writing
fout = fopen(outFile,'w');

% start on line 1
lineCount = 1;
% get the current line
currentLine = fgetl(fin);
% continue while characters are returned (fgetl returns -1 at EOF)
while ischar(currentLine)
%check if current line is target line
if lineCount==line_v(v,1)
    newValue=line_v(v,2);
    currentLine=regexp(currentLine,'value="(.*?)"', ['value="',num2str(newValue),' "']
    v=v+1;
    if v>13
        v=13;
    end
end
end

%print out the current line to the outfile
fprintf(fout,'%s\n',currentLine);
% get the next line
currentLine = fgetl(fin);
% increment the line count
lineCount = lineCount + 1;
```

B.4 CCM+ Attribute Processing

This script processes the gamma and pressure loss attributes. These are exported from the CCM+ model as a comma separated variable file, these are imported into Matlab as GAMMADATA and

DELTAPDATA matrices. The average and variation of the attribute is then taken over the last 200 increments of the model.

```
NUMITER=200;

%gamma
SIZE=size(GAMMADATA);
ULIMIT=SIZE(1,1);
LLIMIT=SIZE(1,1)-NUMITER;

gamma=GAMMADATA(LLIMIT:ULIMIT,2);
size_gamma=size(gamma);
ave_gamma=sum(gamma)/size_gamma(1,1);
max_gamma=max(gamma);
min_gamma=min(gamma);
delta_gamma=max_gamma-min_gamma;
pc_delta_gamma=100*delta_gamma/ave_gamma;

%Pressure Drop
SIZE=size(DELTAPDATA);
ULIMIT=SIZE(1,1);
LLIMIT=SIZE(1,1)-NUMITER;

deltap=DELTAPDATA(LLIMIT:ULIMIT,2);
size_deltap=size(deltap);
ave_deltap=sum(deltap)/size_deltap(1,1);
max_deltap=max(deltap);
min_deltap=min(deltap);
delta_deltap=max_deltap-min_deltap;
pc_delta_deltap=100*delta_deltap/ave_deltap;

%Tabulating data
gamma_table(i,:)=[i,ave_gamma,max_gamma,min_gamma...
,delta_gamma,pc_delta_gamma];
deltap_table(i,:)=[i,ave_deltap,max_deltap,min_deltap...
,delta_deltap,pc_delta_deltap];
end
```


B.5 ModeFrontier Implementation

Figure B-7 shows the implementation of ModeFrontier for a Multi Objective Optimisation. Here the constraints limit the volume to 9l and the diffuser length to 40 mm. These are entered into the dialogue boxes and entered as equations using the variable names. The DoEs and optimisation approach are entered in at the scheduler and the calculator is set to 100% RSM calculation.

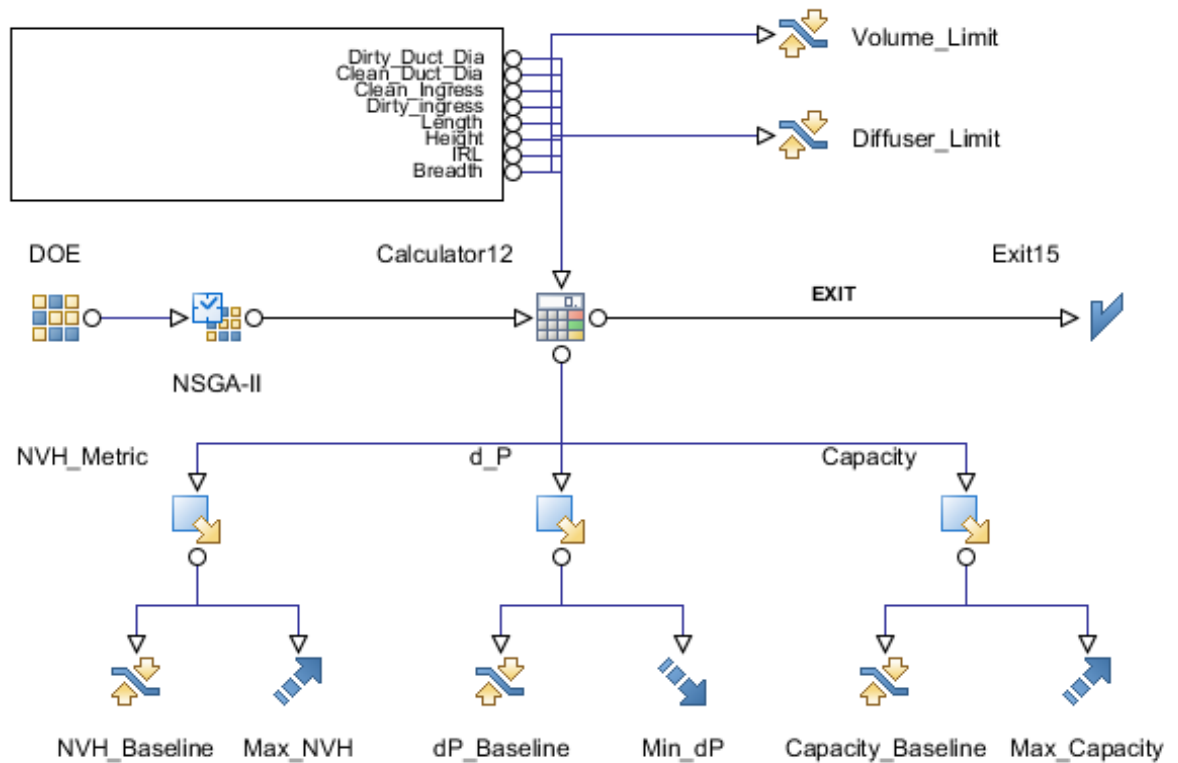


Figure B-7: ModeFrontier implementation for internal assessment of meta models

Figure B-8 shows the implementation of ModeFrontier with the utility function. The Matlab interface automatically calls Matlab and runs the named script. The variable names in Matlab need to be matched to the input and output variable names in ModeFrontier. The input, running and output of this node takes around 1 second per sample and represents a major restriction the process. The script for the utility function is given in Section B.6.


```

%Utility Function of Pressure Drop
if dP<1160
    P_U=1;
elseif dP<2545
    x=[1160;2545];
    y=[1;0.3];
    P_U=interp1(x,y,dP);
elseif dP<3260
    a=-2.197364e-3;
    k=6.886464;
    P_U=a-a*exp(-k*((dP-3260)/1000));
elseif dP>=3260
    P_U=0;
end
%Utility Function of NVH Metric
if NVH<-3000
    NVH_U=0;
elseif NVH<-1850
    x=[-3000; -1850];
    y=[0.3;1];
    NVH_U=interp1(x,y,NVH);
elseif NVH>=-1850
    NVH_U=1;
end
%Calculate Utility
ut_nvh=[0 0.125 0.25 0.375 0.5 0.625 0.75 0.875 1];
ut_p=[0 0.125 0.25 0.375 0.5 0.625 0.75 0.875 1];
pref=[0,1.25,2.5,3.75,5,6.25,7.5,8.75,10;
2.5,4.84375,7.1875,9.53125,11.875,14.21875,16.5625,18.90625,21.25;
5,8.4375,11.875,15.3125,18.75,22.1875,25.625,29.0625,32.5;
7.5,12.03125,16.5625,21.09375,25.625,30.15625,34.6875,39.21875,43.75;
10,15.625,21.25,26.875,32.5,38.125,43.75,49.375,55;
12.5,19.21875,25.9375,32.65625,39.375,46.09375,52.8125,59.53125,66.25;
15,22.8125,30.625,38.4375,46.25,54.0625,61.875,69.6875,77.5;
17.5,26.40625,35.3125,44.21875,53.125,62.03125,70.9375,79.84375,88.75;
20,30,40,50,60,70,80,90,100;];
pval=interp2(ut_nvh,ut_p,pref,NVH_U,P_U);
Utility=Cap_U*pval

```

Appendix C

Fuel Tank Design Study

C.1 Fuel Tank Design Stages

C.1.1 Concept Design

In the Concept Design stage the overall shape of the tank is defined by packaging engineers. The preliminary locations for accessory components are added based on experience. For this, carry over parts from previous vehicle programs or generic models are used as an initial guide for design. The initial wall thickness is estimated from experience and added to the tank shell. These are only preliminary at this stage due to the iterative nature of the supplier analyses. Finally, the tank shell is given rudimentary radii and fillets based upon previous tank models and knowledge of tank forming processes.

The CAE at this stage is completed within the fuel system design team using internal methods. The indicative tank capacity is calculated along with a tank weight calculation. These are then used to generate an initial system cost, which allows the assessment of alternative designs and comparisons to competitor vehicles.

C.1.2 Concept Finalisation

After the concepts have been judged in the Concept Design stage, the design iteration continues with overall shape modifications to allow for the inclusion of clearances and tolerances. The overall tank shape can be modified due to tight packaging space or the need to maximise the total volume within the tank. The methods of locating and placing internal modules within the tank are now included and confirmed with the requirement of a carrier mechanism assessed and detailed. Contact points to the body are located and foam added where required. The external shell is modified to include the tank carrier grooves for straps and fixings. The tank shell thickness is modified as required. However, this is still only estimated until later CAE is completed. Possible materials will be examined to see if any new moulding material grades from suppliers offer better performance. This would allow reduced wall thickness and a weight saving. All sharp edges are

removed by adding in all major external corner and edge radii.

Again the CAE is completed within the fuel system design team. The tank studies include a tip/vent analysis, based on the CAD model, which is used to identify indicative positions for vapour and roll over valves. A low fuel pick-up study is used to identify indicative positions for FDM, jet pumps and senders. The tank capacity calculation is repeated using the latest refined tank CAD models and input from vent valve positions, along with another weight calculation to ensure that the tank is still on target to meet the system requirements.

C.1.3 1st Design Iteration

At the 1st Design Iteration stage, the CAD geometry is becoming more mature as the detail of the model increases. The blanking of CAD models for different variants of camlock ring is given. Detailed internal accessory component geometry including the FDM is completed. The overall tank shell and external geometry is modified to suit the location of fixings to the body. The method of locating fixings are added to the CAD model. This iteration also includes remodelling of the base and sides to suit straps and cradles. The geometry for manufacture, including weld line location and pinch points, is also detailed.

The 1st Design Iteration stage heralds the first usage of the heavyweight CAE applications, with the requests for 'in-house' and supplier analyses. The initial pressure/vacuum cycling, stress/strain and fuel tank blow moulding analyses are completed by the supplier. These processes are iterative and use wall thickness estimates in order to determine the required optimum wall thickness.

The initial 'in-house' crash CAE is requested using initial model data. This analysis uses a generic constant wall thickness and can only approximate the behaviour of multilayer tanks. It must be noted that crash simulations are completed by the crash CAE Team and are not in the remit of powertrain CAE.

Also, the initial 'in-house' NVH slosh evaluation is requested. However, this may not be possible with this level of CAD maturity, as NVH analysis would require accurate tank thicknesses and these will not be detailed until the supplier has reported out. Other slosh evaluations could, however, be completed at this time. These could include the assessment of the need for baffles within the tank or the durability of the internal components. This offers an opportunity for projects to look at fluid structure interaction, for example within the durability analysis of the tank carrier mechanism.

The internal fuel system design team analyses are repeated. The CAE low fuel pick-up study is re-examined and the positions of the FDM, jet pumps and senders are adjusted. The tank capacity is measured on CAD, using the latest refined tank CAD models (including wall thickness), revised vent valve positions and gross volumes of surrogate child-part models (FDM/sender) for comparison to target.

C.1.4 2nd Design Iteration

In this stage the changes to the CAD will be based on the output of the 1st Design Iteration cycle. The exterior tank surface is re-modelled to suit child parts such as weld pads, fuel pipe gullies,

carrier mechanism, pads and kiss-off points. The external fixing locations and the internal and external accessory models are also refined.

The heavyweight CAE is repeated to verify the changes from 1st Design Iteration. The supplier pressure/vacuum cycling analysis is repeated for tank expansion and collapse along with supplier stress/strain analysis. These simulations verify the tank wall thickness by identifying the effects of contact points and the tearing of internal components and joining seams. The supplier also repeats the blow moulding simulation. At this point, the moulding simulations chiefly concentrate on the over-moulding of carrier armatures.

The 'in-house' CAE analysis of crash worthiness of the tank is also completed. The tank mounting durability is assessed using surrogate road load data. Also, initial CAE vibration/modal analyses are used to verify mounting point design and fixing point locations. The tank is again evaluated for NVH and slosh using the tank wall thickness from 1st Design Iteration. The evaluation of slosh could require two or more test iterations; at the start and end of the 2nd Design Iteration design phase. Firstly, fluid motion within an empty tank shell is examined to determine if and where baffles are required. Then secondly, as baffles may be mounted to other internal components within the tank, the effect of introducing these components and their durability need to be examined. This is an opportunity for the application of a multi-physics CAE.

Again, the tip study and vent test are carried out using the frozen tank CAD model along with a capacity calculation. This includes final vent valve positions and detailed child-part models.

C.1.5 3rd Design Iteration

This is the final iteration of the virtual series. The exterior of the fuel tank is frozen and the final details of internal fixings/geometry for auxiliary components are completed. The final CAE loop is to verify the final tank design and allow engineering sign-off. The CAE analyses are repeated and examine the effects of newly available data such as new exhaust routes. The blow moulding simulation, NVH, slosh evaluation, pressure/vacuum cycle simulation, modal analysis and tank mountings durability are all repeated using the latest tank features.

C.2 Summary

This examination of the fuel tank has discussed the maturity of CAD at the various design stages. At the UNV0 stage, the CAE request for an NVH analysis could not be completed due to an insufficient level of CAD maturity. This analysis required the model to have the full tank thickness rather than the basic tank thickness, however the correct data would not be available until the supplier CAE had been completed.

Currently the supplier completes most of the CAE relating to the tank shell. The effort to bring more of the analyses in house may cause some issues. The blow-moulding analysis is part of the supplier's manufacturability test and this provides the tank shell thickness data. The supplier can then use this to complete the other CAE analyses. If the pressure cycling and stress-strain analysis

were brought 'in-house' there may issues, as the supplier may not release the thickness data until the end of 1st Design Iteration. This would delay the analysis to 2nd Design Iteration.

C.3 Application of Method throughout fuel system design team

One of the main aspects of this top-down analysis was to look at when CAE for the fuel system design team would be requested. This would have to be leveraged by the maturity of the available CAD. The process completed from the case study of the fuel tank was then applied across all the systems within the fuel system remit. The results are displayed in tables C.1 and analysing the potential for new CAE processes to cover other areas of issues produced Table C.2. Opportunities for possible research projects in this work are highlighted in bold.

Table C.1: Fuel system design team CAE Lists

Concept Design	1 st Design Iteration	2 nd Design Iteration	3 rd Design Iteration	Design Verification
	Initial pressure/vacuum cycling analysis of fuel tank (supplier /in-house)	Pressure/vacuum cycling analysis of fuel tank repeated		
	Initial stress/strain analysis of fuel tank (supplier /in-house)	Stress/strain analysis of fuel tank repeated		
	Initial blowmould simulation of fuel tank (supplier)	Blowmould simulation of fuel tank repeated, including initial assessment of carrier over-moulding (if applicable)(supplier)	Blowmould simulation of fuel tank repeated, to finalise carrier over-mould parameters (supplier)	
	Initial NVH/slosh evaluation of fuel tank	NVH/slosh evaluation of fuel tank repeated (initial tank internal features added, e.g. basic models of baffles, FDM)	NVH/slosh evaluation of fuel tank repeated, using latest internal child part models	
Initial inj.moulding (mould flow) and stress/strain analysis of new/proprietary parts (supplier-owned) a) New FDM flanges, reservoirs, etc b) New carbon canister c) New fuel filter (head assy)	Supplier inj.moulding and stress/strain analyses repeated (FDM, filter, etc)			
Supplier flow simulations e.g. Vapour flow through canister				
		Initial crash worthiness analysis (fuel tank, fuel filler, filters)	Crash worthiness analyse repeated	Crash worthiness analyses repeated
	Initial thermal analysis of Diesel fuel circuit, to identify hotspots in FDM flange, fuel filter, etc	Initial thermal (RadTherm) analysis of whole vehicle to identify heatsield reqts.	Thermal (RadTherm) analyses repeated	
		Vibration/modal analyses to verify mountings design and fixing point locations	Vibration/modal analyses repeated	

Table C.2: Revised fuel system design team CAE Lists

Concept Design	1 st Design Iteration	2 nd Design Iteration	3 rd Design Iteration	Design Verification
Initial inj. moulding (mould flow) and stress/strain analysis of new/proprietary parts (supplier-owned) a) New FDM flanges, reservoirs, etc b) New carbon canister c) New fuel filter (head assy)	Supplier inj. moulding and stress/strain analyses repeated (FDM, filter, etc)			
Supplier flow simulations e.g. Vapour flow through canister				
	Initial blowmould simulation of fuel tank (supplier)	Initial crash worthiness analysis (fuel tank, fuel filler, filters) Blowmould simulation of fuel tank repeated, including initial assessment of carrier over-moulding (if applicable)(supplier)	Crash worthiness analyse repeated Blowmould simulation of fuel tank repeated to finalise carrier over-mould parameters (supplier)	Crash worthiness analyses repeated
		Initial thermal (RadTherm) analysis of whole vehicle to identify heatshield reqts.	Thermal (RadTherm) analyses repeated	
	Vibration & modal analyses of mountings/fixings/brackets	Vibration & modal analyses to verify mountings/bracket design and fixing point locations (PSD)	Vibration/modal analyses repeated	
	Initial slosh evaluation of fuel tank based upon early internal geometry to determine need for baffling	Slosh evaluation to determine possible damage to internal components based upon detailed CAD of internal components Slosh evaluation for durability of mountings	Slosh evaluation for NVH based upon detailed tank thicknesses	
	Initial thermal analysis of Diesel fuel circuit; to identify hotspots in FDM flange, fuel filter, etc	Pump optimisation & Circuit analyses using AMESIM		
	Modal analysis of F & V Lines.	Pressure/Vacuum cycling analysis of Tank*	Pressure/vacuum cycling analysis of fuel tank repeated*	
		Stress/strain analysis of tank*	Stress/strain analysis of fuel tank repeated*	

* Delayed if brought 'in-house' due to supplier analysis cycle to obtain thickness data.

Appendix D

Slosh Rig Experiments

D.1 Introduction

The aim of this chapter is to discuss the approach taken to correlated the CFD approach to fuel slosh with physiscal rig tests. StarCD uses the the finite volume method with the VoF scalar to predict surface pressures and free surfaces within multi-fluid systems. This must be validated for use as a CAE tool within Jaguar Land Rover powertrain for liquid sloshing in fuel tanks. To achieve this an experiment is required that can measure both the pressures on the walls of a fuel tank and the free surface of the liquid. This chapter discusses the experimental setup, procedure and results obtained in the correlation study for the characterisation of the fuel tank boundary condition.

D.2 Experimental Setup

The experiment will be carried out on the 1/2 scale NVH fuel tank testing rig. This rig was built to study the noise from sloshing of fuel in the tank. The fuel tank to be examined is a saddle style tank, that features two distinct volumes connected by a bridge. The tank is filled with either 4 or 6 litres in the initial tests to examine the effects of fill volume. This experiment required that the pressures and free surfaces within a sloshing fuel tank were measured. Pressure transducers mounted to the tank surfaces were able to detect the pressure changes due to fluid slosh. Rapid prototyping methods allowed for half scale fuel tanks to be created where the surfaces were translucent. The fluid was marked with red, green and blue natural food dyes. This allowed the free surface to be visualised using the marked fluid and a high speed camera. To enable the slosh event to be applied to the StarCD model an accelerometer was used to capture the acceleration profiles during the test. Each of these items and the experimental setup will be described in this section.

D.2.1 The NVH Slosh Rig

The NVH slosh rig features a moving trolley to which the half scale tank is mounted. The trolley is accelerated down the track by a belt drive driven by an electric motor. The speed of the trolley is controlled by varying the voltage and current supplied to the motor. In these experiments the motor is supplied with 15 volts and allowed to draw 8 amps. The trolley is accelerated over a 1.22m long section where it is then released. The tank is brought to a sudden stop using a high tension belt. This action simulates the start stop motion of a vehicle in heavy traffic. The rig is shown in Figure D-1.

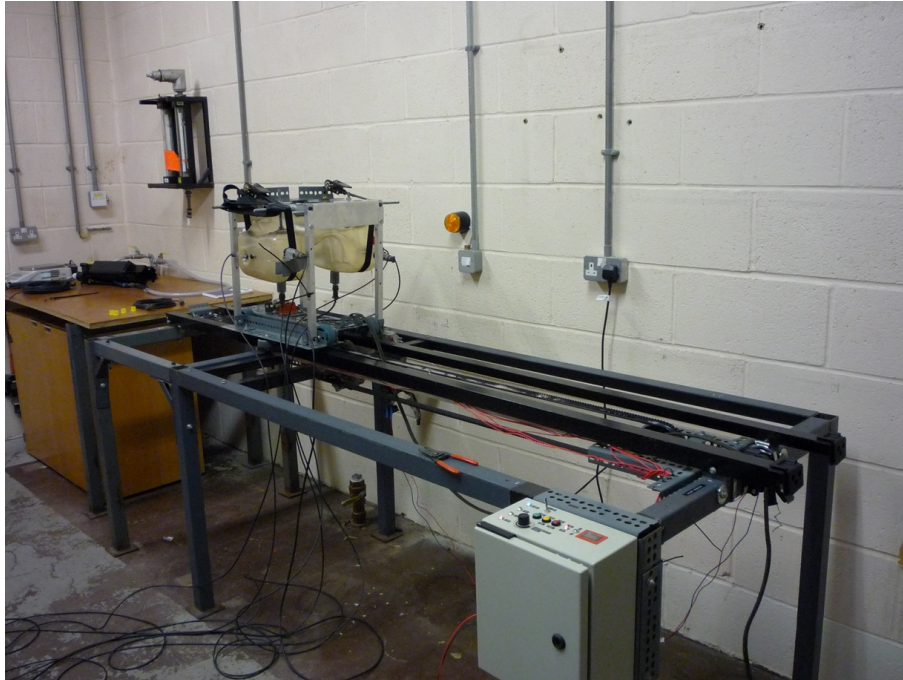


Figure D-1: The slosh rig physical test

D.2.2 High Speed Camera

The high speed camera used was a Kodak HS54540. This camera takes 3072, 256 by 256 pixel, greyscale images. The image sample frequency was set to 250 frames per second which gave 12 seconds of recording time. The field of vision was set to capture the tank as it reached the sudden stop as this was when the most dynamic slosh would occur. The camera was initialised using a 5 Volt input impulse from a switch on the rig. This switch was activated when the trolley was released from the belt drive. Once captured, the video footage was recorded on a laptop at 25 frames per second using the Windows Media Codec pack.

D.2.3 Pressure Transducers

The pressure transducers need to be able to measure both air and water as the sloshing of the fluid will expose the devices to both. The most suitable transducers available within Jaguar Land Rover Instrumentation were the PMP 317 3038 devices manufactured by Druck. These transducers can measure pressures of $\pm 100 \text{ mBar}$, this was the smallest range available within the Company. These transducers feature the 'quick fit connectors' (see Figure D-2), which protect the sensing diaphragm and allow for a standard connection. These were mounted directly on to the tank, where the end of the connector protruded into the fluid. The transducers were connected to data logging equipment via a mil-spec connector and required an input voltage between 7 and 30 Volts. In the initial experiments 8 pressure transducers were used, the calibration is given in Table D.1. The sensitivities and offsets were used in the LMS Testlab setup to give readings in Pascals. The grade represents the accuracy of the device and the channel number gives the location during the experiment, see Figure D-4.

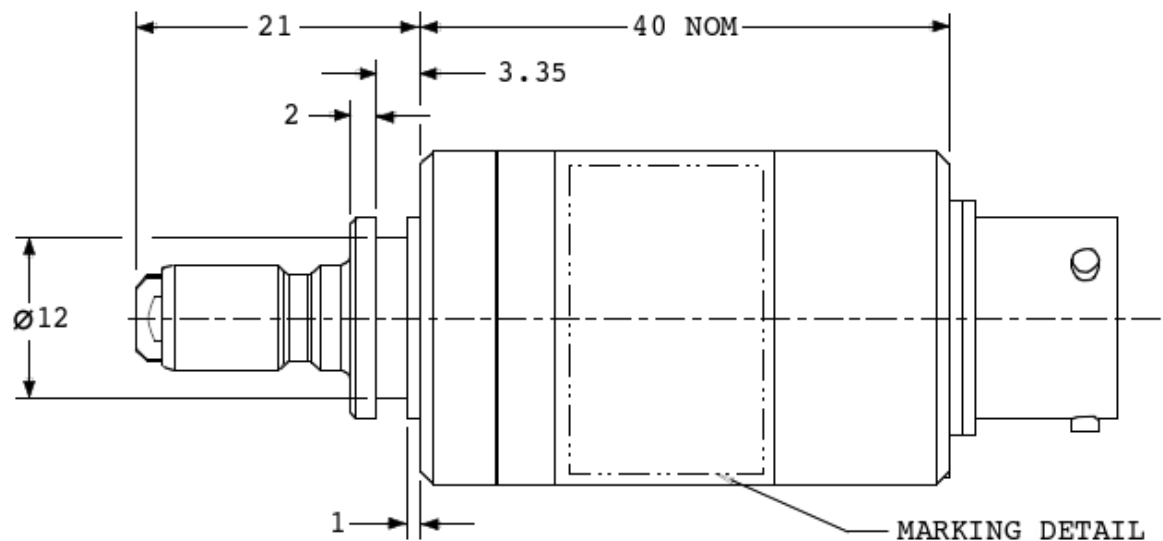


Figure D-2: PMP 317 3038 pressure transducers

Table D.1: Pressure transducer calibration				
Serial Number	Sensitivity (V/mBarG)	Offset (Bar/V)	Grade	Channel
45580	0.02501240	-0.100612	0.03	1
55199	0.02496886	-0.099791	0.04	6
55201	0.02496962	-0.100246	0.01	8
55202	0.02497505	-0.100053	0.04	7
55203	0.02497610	-0.100548	0.03	5
58546	0.02502863	-0.100981	0.07	4
59537	0.02502154	-0.100902	0.04	2
59538	0.02492091	-0.100927	0.09	3

D.2.4 Accelerometer

The accelerometer used on the rig was supplied by the NVH testing department and was a DJB triax charge accelerometer (A31 371) Jaguar Land Rover serial number IS22345. This sensor was aligned with the principal vehicle axes then attached to the tank using Araldite. The calibration of this sensor is given in Table D.2.

Table D.2: Accelerometer calibration			
Axis	Frequency Hz	Sensitivity pC/g	Phase °
X	160	5.61303	-1.71
Y	160	5.58347	-1.55
Z	160	5.57584	-1.76

D.2.5 Communications & Channel Locations

The pressure and accelerometer traces from the experiments were recorded using a Testlab data logger and software. The data connections are shown in Figure D-3. The data logger could only take BNC connections as inputs and could not supply power to the pressure transducers. This problem required the use of 2 break out boxes. These converted the Mil-Spec connectors to BNC whilst supplying 12 volts to the pressure transducers. In order to activate the camera a 5 volt signal pulse was used, this came from the motor cut-off switch on the rig. The signal from this switch was also recorded to enable the accelerometer and pressure traces to be synchronised with the camera images.

The location of the 8 pressure transducers is given in Figure D-4. Channels 1 and 4 are located on the base of the tank, channels 5 & 7 and 6 & 8 are on the front face of the tank either side of the saddle, while 2 and 3 are on the back face. Channel 2 is exposed to air as it is above the stable fill lines in both the 4 and 6 litre cases. An estimation of the hydrostatic pressures is given in Table D.3, these have been estimated from co-ordinate data taken from the StarCD model. The estimated free surface height for the 4 and 6L fill levels are 500.25 and 529.00 mm respectively. The hydrostatic pressures are taken with reference to these values. The pressure in channel 2 is set to zero as this

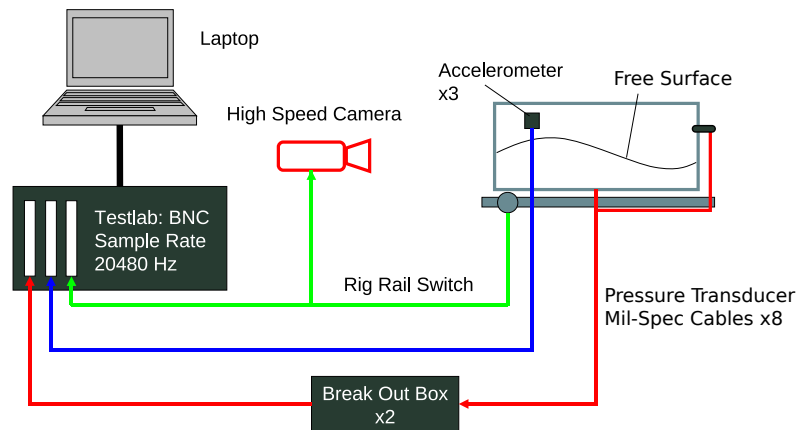


Figure D-3: Communication routes in the experiment

channel is initially exposed to the air and is assumed to be atmospheric.

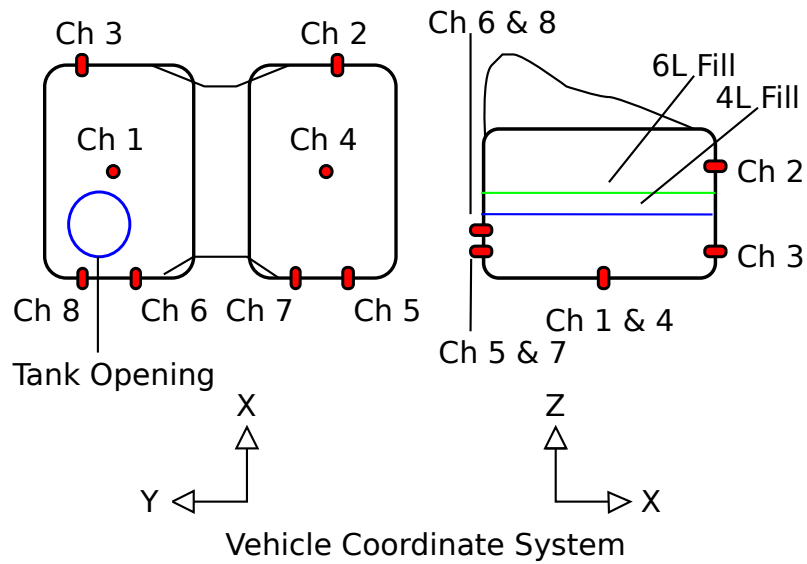


Figure D-4: Pressure transducer channel numbers

Table D.3: Predicted hydrostatic pressures from ρgh approximation

Channel	Height (mm)	4L Pressure (Pa)	6L Pressure (Pa)
1	425.982	727.112	1008.585
2	533.759	0.000	0.000
3	491.451	86.146	367.619
4	425.990	727.034	1008.507
5	483.033	168.561	450.034
6	468.033	315.417	596.890
7	483.033	168.561	450.034
8	468.033	315.417	596.890

D.2.6 Procedure

The procedure for each experimental run is:

1. Move the tank to the start position on the rig, and ensure that it is connected to the belt drive.
2. Allow the fluid to settle and check that the fluid is the same depth on both sides of the saddle.
3. Reset the motor and check the input voltage and current.
4. Set the camera ready to record.
5. Arm the data logger and start acquiring data. Testlab is set up to acquire data at 20480 hz, thus the Nyquist frequency is 10240 hz, this should be much greater than any slosh frequencies contained within the experiment.
6. Press the start button on the rig.
7. Once the trolley has come to a stop and the sloshing has died away stop the data logger.
8. Save the recorded data from the run in Testlab and save the high speed video to a .avi file.
9. To process the data, the Testlab files are exported as a Matlab file, here a 50 hz low pass filter is applied to the data and the relevant plots obtained.

D.3 4 & 6 Litre Pressure Results

The experiment was run three times at the two different fill levels, the pressure traces are shown in Figures D-5 to D-10. Both the 4 & 6L analyses show expected behaviour of channels 2, 5 & 7 and 3, 6 & 8 in terms of nodes and anti-nodes. As sensors are at opposite ends of the tank one would expect that high pressure at one end, caused by liquid impacting on that wall, would correspond to a low pressure seen on the other side. Differences in pressures and timing could be due to the non-rectangular shape of the tank and the sensors being placed at different levels.

In order to compare initial hydrostatic pressures, the average pressure of the first 10 points of each channel is taken, then the average pressure from channel 2 (sensor in air) is subtracted from

all of these values. Table D.4 shows the adjusted values for the 4L cases and Table D.5 the 6L cases. The expected order (based on hydrostatic prediction) would be 1(deepest), 4, 6=8, 5=7, 3 & 2. While some variation between 1 & 4 could be explained by fill level variation, one would expect 6 & 8 and 5 & 7 to be equal, however this is not the case. While channels 5 & 7 are within 20 Pa of each other, channels 6 & 7 show a variation in the region of 100 Pa. One potential reason for this could be aliasing of the sensors during setup or some errors in calibration. However, the pressures are at the correct magnitude and do show some relation to the hydrostatic pressures. When Channels on the Y+ (Channels 1, 3, 6 & 8) side of the saddle change, the opposite change is seen in the Y- side indicating the sensors have some sensitivity to the initial fill levels. However the head changes will not be the same as cross-sectional areas on either side of the saddle are not equal.

Table D.4: 4 litre tests

Channel Number	Raw Data (Pa)			Adjusted Data (Pa)			Hydrostatic (Pa)
	Run 1	Run 2	Run 3	Run 1	Run 2	Run 3	
1	964.52	865.72	1015.64	881.97	879.58	1000.67	727.11
3	155.23	31.08	180.07	72.69	44.94	165.10	86.15
6	399.01	311.50	459.19	316.47	325.36	444.23	315.42
8	277.33	177.59	322.01	194.79	191.45	307.05	315.42
4	832.75	743.16	663.91	750.21	757.02	648.95	727.03
2	82.54	-13.86	14.96	0.00	0.00	0.00	0.00
5	265.05	190.10	113.18	182.50	203.96	98.22	168.56
7	277.69	169.54	89.29	195.15	183.40	74.33	168.56

Table D.5: 6 Litre Tests

Channel Number	Raw Data (Pa)			Adjusted Data (Pa)			Hydrostatic (Pa)
	Run 1	Run 2	Run 3	Run 1	Run 2	Run 3	
1	1107.38	964.19	916.79	1216.11	1135.81	1113.24	1008.59
3	262.24	117.42	72.15	370.97	289.04	268.60	367.62
6	535.37	390.43	344.24	644.11	562.05	540.68	596.89
8	419.79	270.67	229.70	528.53	442.29	426.15	596.89
4	835.02	802.63	796.96	943.75	974.25	993.41	1008.51
2	-108.73	-171.62	-196.45	0.00	0.00	0.00	0.00
5	256.90	184.47	159.13	365.64	356.09	355.57	450.03
7	248.38	178.98	159.03	357.11	350.60	355.47	450.03

All channels also show a degree of drift over the course of the slosh experiment with the pressure being higher at the end of the test than at the start. The drift seems largest after the large slosh event and in the 6l cases. In the 6l cases this pressure rise is approximately 200-400 Pa. Also, the sensors that can be exposed to both air and water seem to be more affected by this than the two channels in the base of the tank. Potential causes of this drift could be:

- The rig test features a shock event which could have caused some vaporisation of the fluid and could potentially change the pressure in the air.
- The experiment was conducted in the presence of a 1000W light for the camera, this continued to run once the rig was stationary until the camera had finished. This could have provided some heating to the tank.
- The design of the pressure transducers with the quick fit connectors could potentially lead to bubbles of air and fluid becoming trapped, this would affect the pressure reading.

These issues require further investigation.

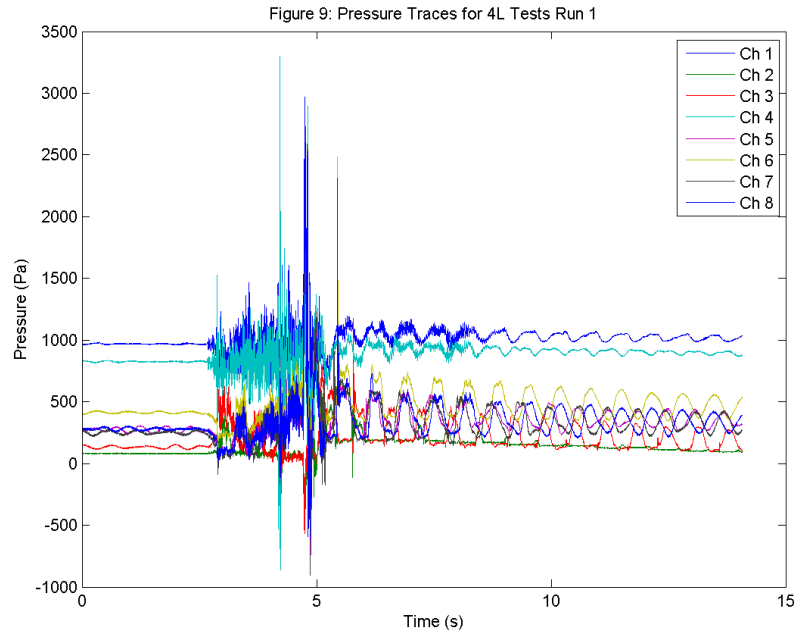


Figure D-5: 4 litre run 1 pressure traces

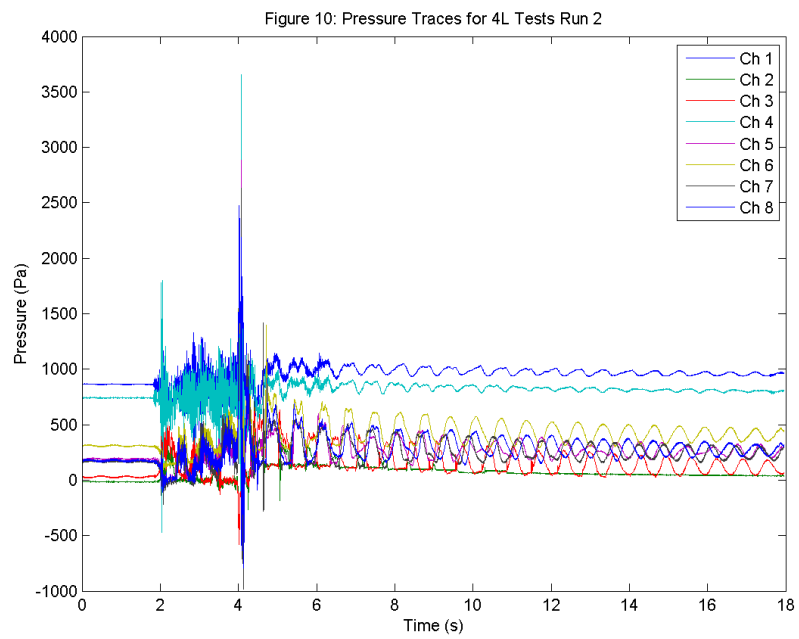


Figure D-6: 4 litre run 2 pressure traces

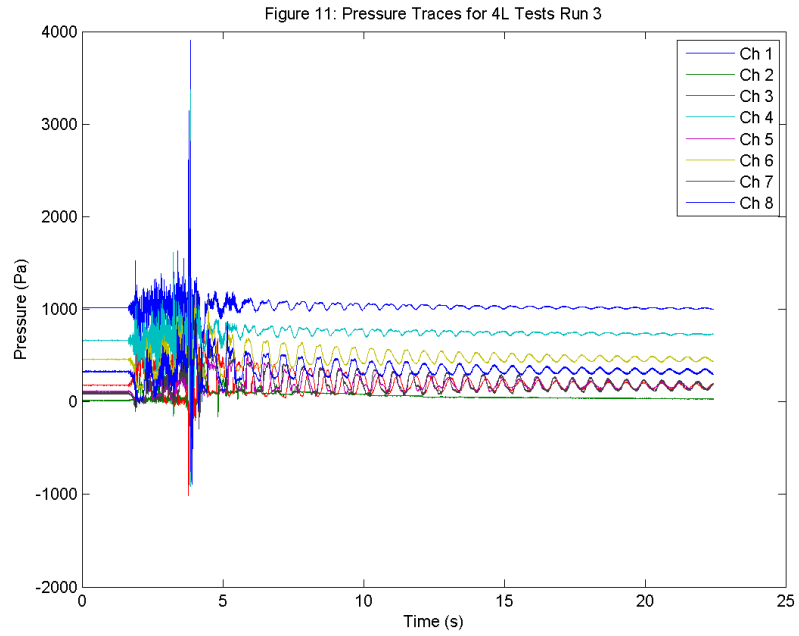


Figure D-7: 4 litre run 3 pressure traces

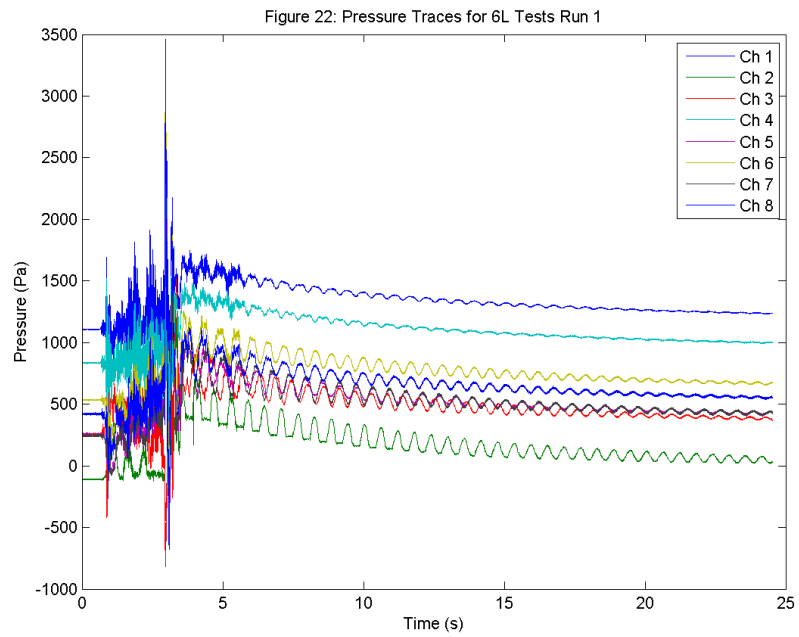


Figure D-8: 6 litre run 1 pressure traces

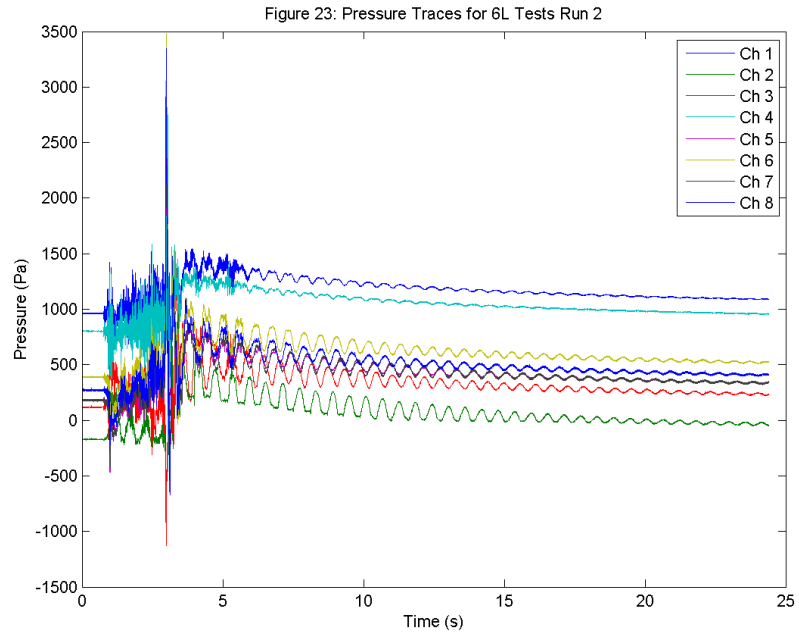


Figure D-9: 6 litre run 2 pressure traces

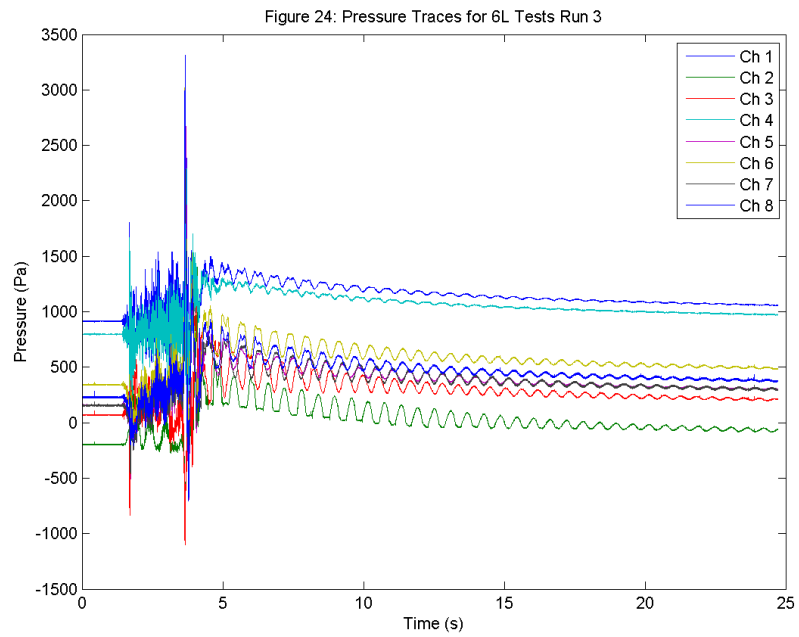


Figure D-10: 6 litre run 3 pressure traces

D.4 Revised Pressure Transducers

The 'quick fit connector' features a small passage of 3.5mm diameter that takes the fluid from the test region to the diaphragm chamber. This passage opens up to a diameter of 22 mm in the sensing chamber with a 1 mm gap to the diaphragm. One theory is this volume is small enough that in tests with multiple fluids, air or fluid may become trapped in the sensing chamber. After the event this fluid is released and the pressure slowly returns to baseline. To test this theory, four pressure transducers were machined to remove the quick fit connectors. The effect of machining is shown in Figure D-11. This is a delicate operation due to the fragility of the diaphragms. To ensure that the transducers were still operational, the calibration exercise was performed before and after the machining process. The calibration data is shown in Table D.6. It was noted during the calibration that the offset of the machined transducer was highly sensitive to the mounting method in the calibration machine. Slight loadings on the sides used to lock the transducer in place would affect the readings. However, the sensitivity of the device was unaffected. This meant that the transducer could no longer be used as an absolute measure of pressure, but could measure relative change during the slosh events.



Figure D-11: The machined pressure transducers

	Channel	Serial Number	Sensitivity (V/mBarG)	Offset (Bar/V)	Grade
Before	CH1	IS48288	0.02504667	-0.100028	0.04
	CH2	IS45587	0.02501069	-0.103994	0.16
	CH3	IS44764	0.0249481	-0.101757	0.18
	CH4	IS59676	0.02500105	-0.100205	0.05
After	CH1	IS48288	0.02502571	-0.108226	0.04
	CH2	IS45587	0.02508476	-0.10124	0.03
	CH3	IS44764	0.02499905	-0.107313	0.03
	CH4	IS59676	0.0249859	-0.0877238	0.04

As only 4 sensors were made available for machining, the setup has been revised as shown in Figure D-12. The pressure transducer calibration data relating to each channel is given in Table D.6. The calibration data was used in the setup of LMS Testlab and the offset was removed in the post-processing phase. The fill level has been set to 5l for these experiments. However, the water

and marker used remained the same. The lighting position was moved to reduce any heating affect from the 1000W lamps.

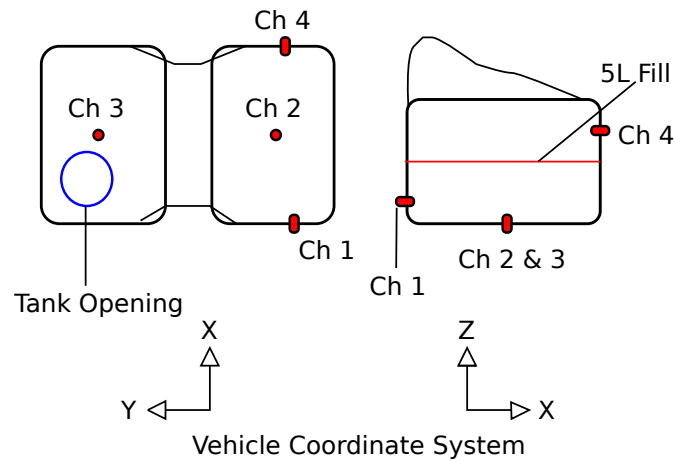


Figure D-12: Revised pressure transducer channel numbers

D.5 Testing With Revised Transducers

D.5.1 Hydrostatic Tests

As there were issues with the calibration of the revised pressure transducers, a hydrostatic test was carried out to ensure that the pressure transducers could measure changes in head. The fluid was put on one side of the tank, then siphoned off before refilling. This was repeated twice on both sides of the tank, the results are displayed in Figure D-13 for channels 1, 2 and 4, and Figure D-14 for channel 3. The head losses were measured with a ruler from the starting fill level to the estimated centre of the pressure transducers. The results, in Table D.7, show that the transducers were working correctly.

Table D.7: Hydrostatic pressure tests

	Channel Number	Head (Pa)	Trans (mm)	Meas (mm)	Head (Pa)	Trans (mm)	Meas (mm)
Test 1	CH1	624.92	63.83	65.00	621.78	63.51	65.00
	CH2	791.38	80.83	80.00	788.74	80.56	80.00
	CH3	127.45	13.02	10.00	123.34	12.60	10.00
	CH4	408.84	41.76	42.00	410.16	41.89	42.00
Test 2	CH1	621.12	63.44	65.00	620.20	63.35	65.00
	CH2	749.64	76.57	77.00	747.08	76.31	77.00
	CH3	122.93	12.56	10.00	118.88	12.14	10.00
	CH4	430.47	43.97	44.00	431.24	44.05	44.00

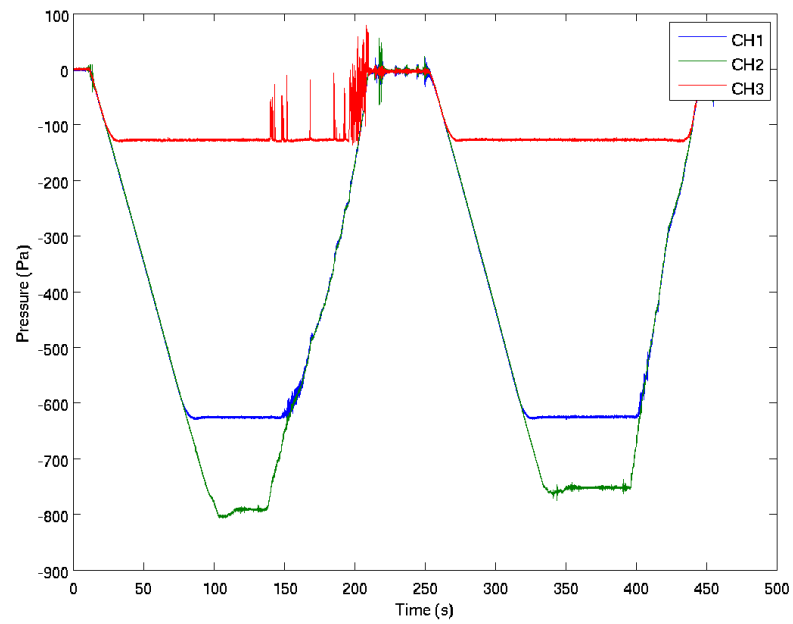


Figure D-13: Hydrostatic test on channels 1, 2 & 4

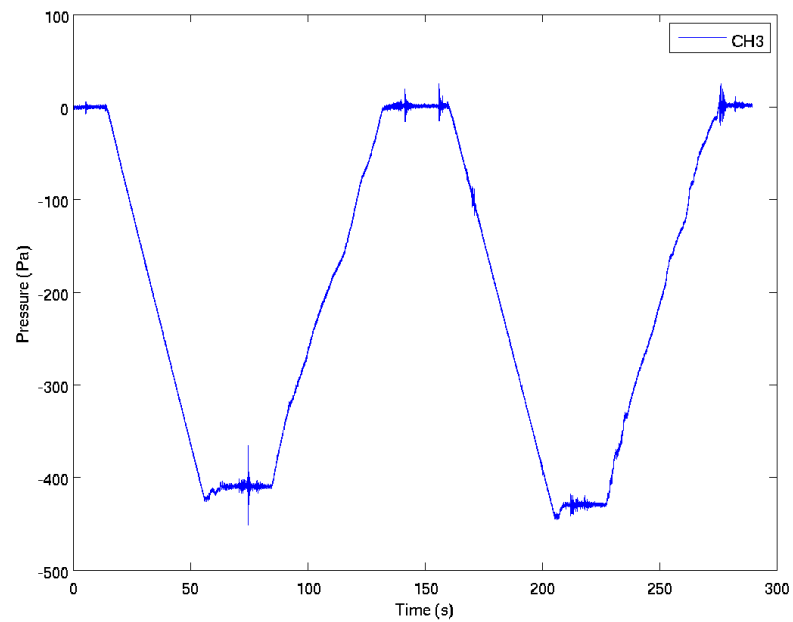


Figure D-14: Hydrostatic test on channel 3

D.5.2 Motored Slosh Tests

As the pressure transducers can give relative pressure changes adequately, the rig was then used for 3 motored runs. The results are displayed in Figures D-15 through D-17. The data from the exposed transducer faces indicates that there are multiple wave forms acting on the tank, particularly present on channel 1. This was confirmed by the high speed camera footage and visual observations of the tank. However, these plots show that the pressure rise behaviour has not been improved by the machining of the pressure transducers. This pressure rise is most notable on the channel exposed to air (channel 4). The test with the revised sensors has eliminated the trapping of fluid in the pressure transducers as a source of error, although the machining of the sensors could have introduced drift or other forms of error. However, as the pressure rise behaviour is present in both tests, the transducers have captured some underlying behaviour in this rig setup that has not been accounted for. As other steps were taken to mitigate the heating of the tank via the lighting, the next step is to consider atomisation or phase changes during the event. Figure D-18 shows the effervescence of the fluid as it was siphoned during the hydrostatic tests, here the dyed fluid gains and holds a froth in the container. This suggests that either the marker fluid or potential contaminants in the test water supply (potentially gasoline or diesel fuels) could be affecting the behaviour in the test. To eliminate this, the tank was emptied and rinsed to remove contaminants and 5 l of unmarked water from a non-contaminated supply were used in the tank.

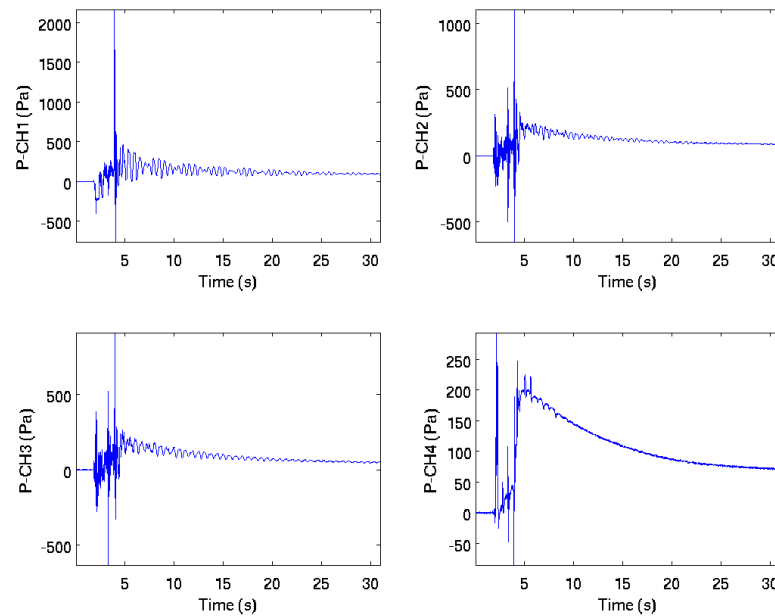


Figure D-15: Full test run 1, channels 1, 2, 3 & 4

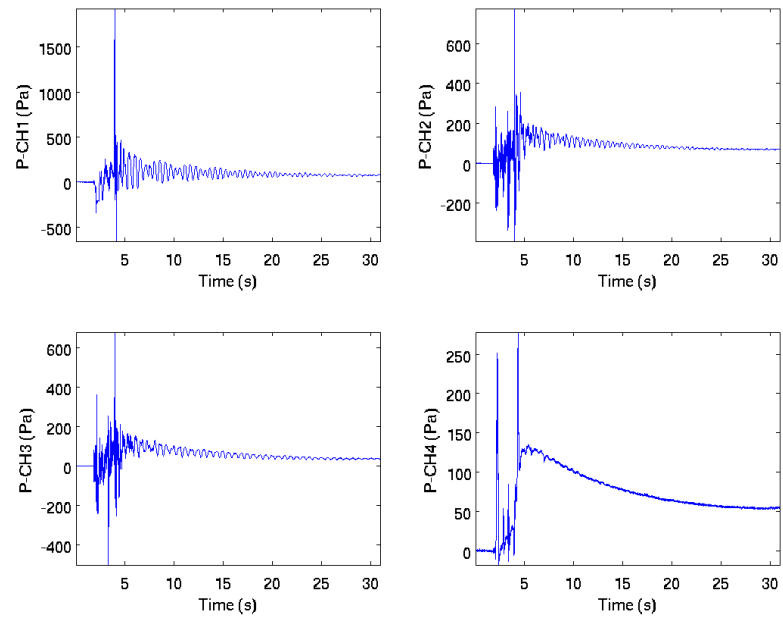


Figure D-16: Full test run 2, channels 1, 2, 3 & 4

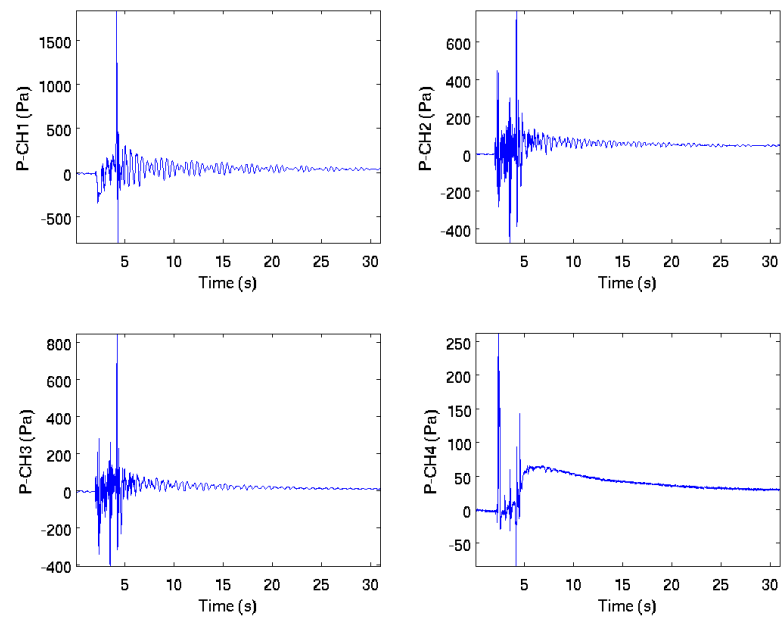


Figure D-17: Full test run 3, channels 1, 2, 3 & 4



Figure D-18: Frothing issue found during hydrostatic tests

D.5.3 Revised Water Supply

The pressure traces from the experiments with the revised water supply are shown in Figures D-19 through D-21. In these tests the pressure rise behaviour has been replaced by a pressure drop of approximately 200 Pa. This could be due to the acceleration in the z direction causing the rig to push down on the top surface of the tank. This has two effects; firstly, the tank is deformed reducing the volume and secondly, the deformation opens up gaps in the seals and cracks in the tank surface allowing air to escape. Once acceleration has reduced, the crack and holes are sealed or become smaller and the volume returns to normal size. However, some small volume of air is lost, creating a pressure loss but the smaller holes and small pressure gradient mean that the pressure rises slowly over time. Assuming a $P_1 \cdot V_1 = P_2 \cdot V_2$ relationship, it can be calculated that a pressure drop of 200 Pa requires a volume loss of 0.012l.

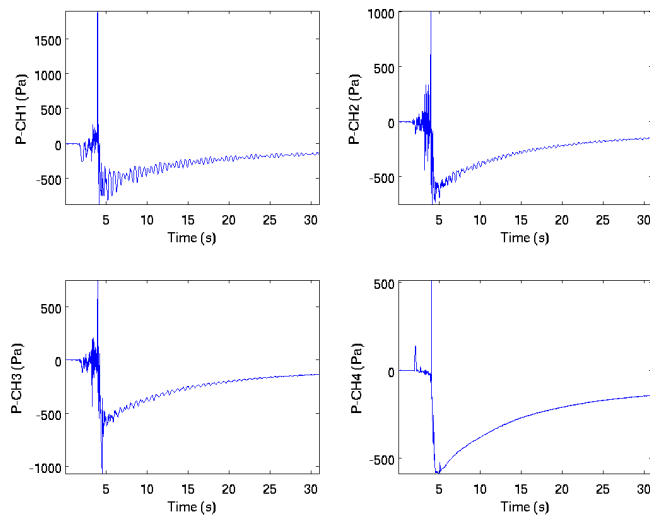


Figure D-19: Clean water full test run 1, channels 1, 2, 3 & 4

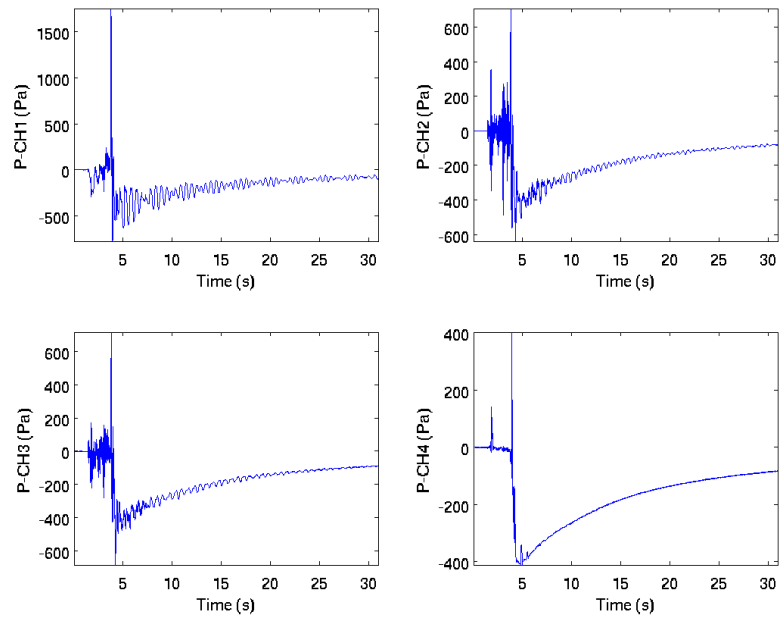


Figure D-20: Clean water full test run 2, channels 1, 2, 3 & 4

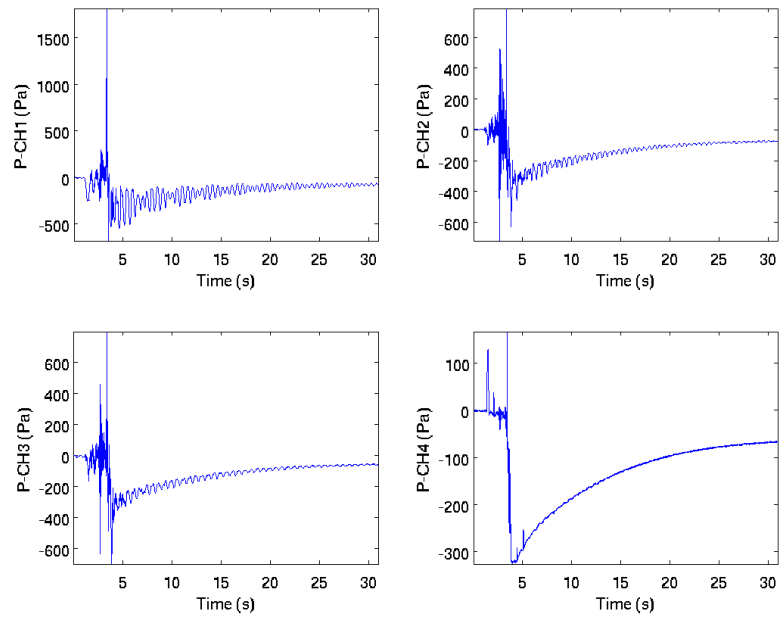


Figure D-21: Clean water full test run 3, channels 1, 2, 3 & 4

D.6 Correlation Study

This section focuses on the steps taken to correlate the StarCD VoF model to the half scale rig.

D.6.1 Rig Test Results

Figure D-22 shows the pressure trace for the front wall transducer, channel 1 (see Figure D-12 on page 256 for transducer locations), for the duration of experiment 33. The initial acceleration of the tank from rest causes the fluid to slosh towards the back of the tank, reducing the head pressure on the front wall. The fluid then sloshes back and forth before the stop event of the rig causes a large pressure rise. This consists of both an increase in hydrostatic head and dynamic pressure as the fluid surges toward the front wall. Within this event the dynamic pressure will be the dominant part. After the stop event, the pressure fluctuates rapidly as the fluid moves about the tank before settling down and forming stationary waves. This run shows an overall pressure drop then slow rise after the stop event. This behaviour is explored in Appendix D.5.3 and will not be discussed here.

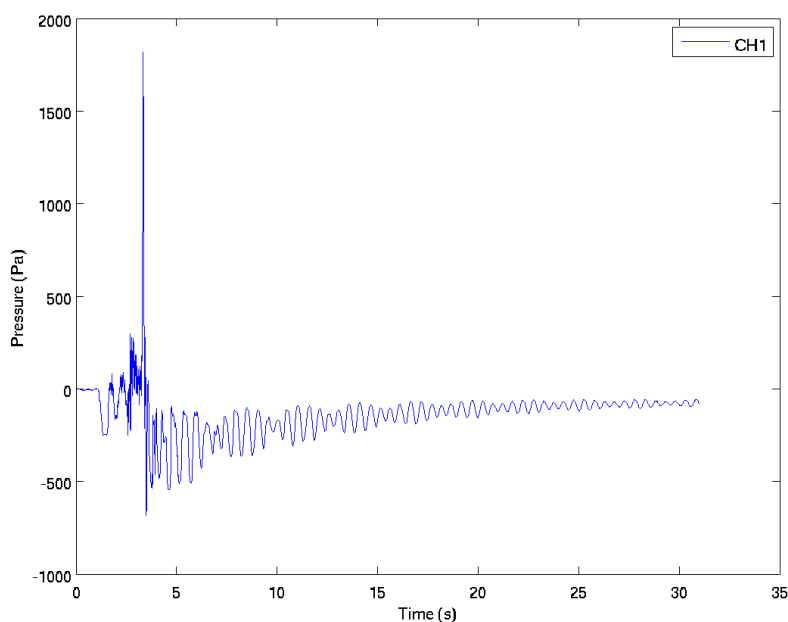


Figure D-22: Run 33 channel 1 pressure trace

D.6.2 CFD Modelling

The StarCD model of the half scale tank uses a 3 mm polyhedral mesh with 3 boundary layer prisms, generated in StarCCM+. This mesh was then imported into StarCD version 4.12.038. The model uses the standard volume of fraction representation of the free surface where the two fluids

are modelled as scalars. The material properties were set to air for the light fluid and $H_2O(l)$ for the heavy fluid. The initial 5 litre fuel fill volume was set by changing cell types based on heights from the tank base and initialising the scalar volume fractions within the cell types accordingly. The input of the acceleration pulse was implemented by using the source momentum user sub-routine *sormom.f* given in Appendix F.1. This read the acceleration profiles from a data file and applied the load as body forces in the three principal directions. The timestep was set to 0.001 seconds for a total runtime of 6 seconds. To compare data, surface pressures at the transducer locations were output along with volume of fraction data at set intervals during the simulation.

D.6.3 Correlation Results

To understand the correlation between the measured rig data and the StarCD model, the pressures traces for Channel 1 will be compared for magnitude and timing. The free surface will also be compared with still images taken from the high speed camera and the VoF fraction from approximately the same time. The red line displayed on the following pressure traces indicated the first frame of the video and was used to synchronise the events with the relevant changes on the pressure traces in Figures D-24, D-31 and D-24.

Accelerometer Input

The first case completed used the filtered x, y and z acceleration pulse from run 33, shown in Figure D-23 with the pressure transducer and model pressure traces shown in Figure D-24. Comparing the StarCD pressures to the rig test shows that the CFD model is severely under-predicting the pressure loading of the fluid. This is seen in both the initial fluid motion and during the sudden stop event. The free surfaces captured in Figure D-25 show the surface approximation in the lead up to the stop event (top). There is less fluid motion predicted after the stop event than actually occurs in reality.

Comparing the free surface images from the StarCD model and high speed camera is difficult to interpret as both are two-dimensional representations of a three dimensional surface and the effect through the tank cannot be visualised. So it is therefore not known if the distribution is across the whole surface or is a near surface effect. However, this visualisation does allow the progression of the slosh event to be examined and help understand the pressure loading events. The reduced amount of sloshing in the initial stages of the StarCD model could mean that the surging behaviour is not correctly predicted as the fluid does not have the correct condition before impact. This caused the reduced peak pressure seen in the StarCD prediction.

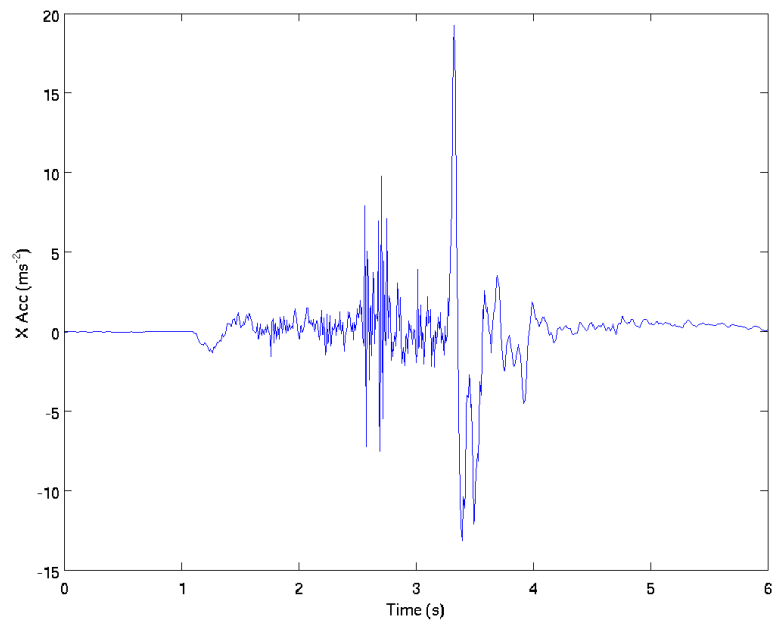


Figure D-23: Run 33 acceleration pulse

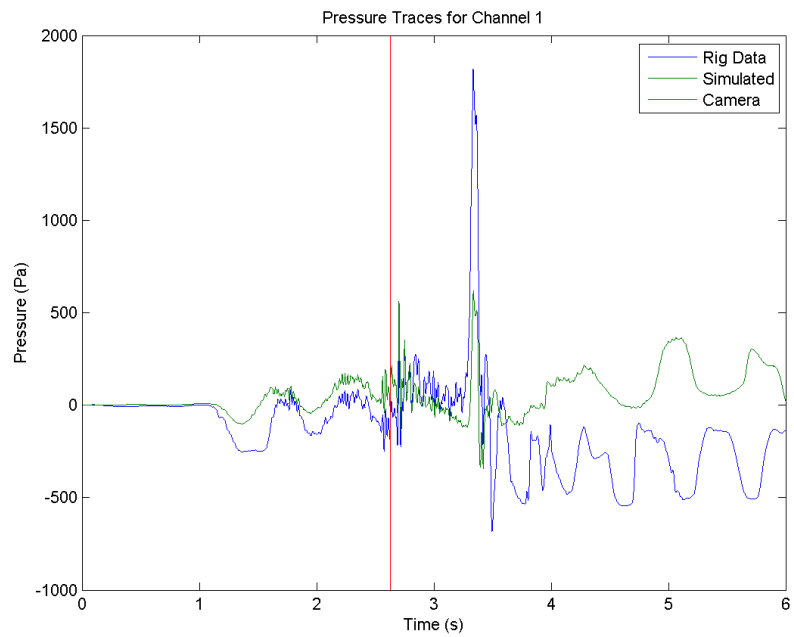


Figure D-24: Channel 1 pressure trace for run 33 acceleration profiles

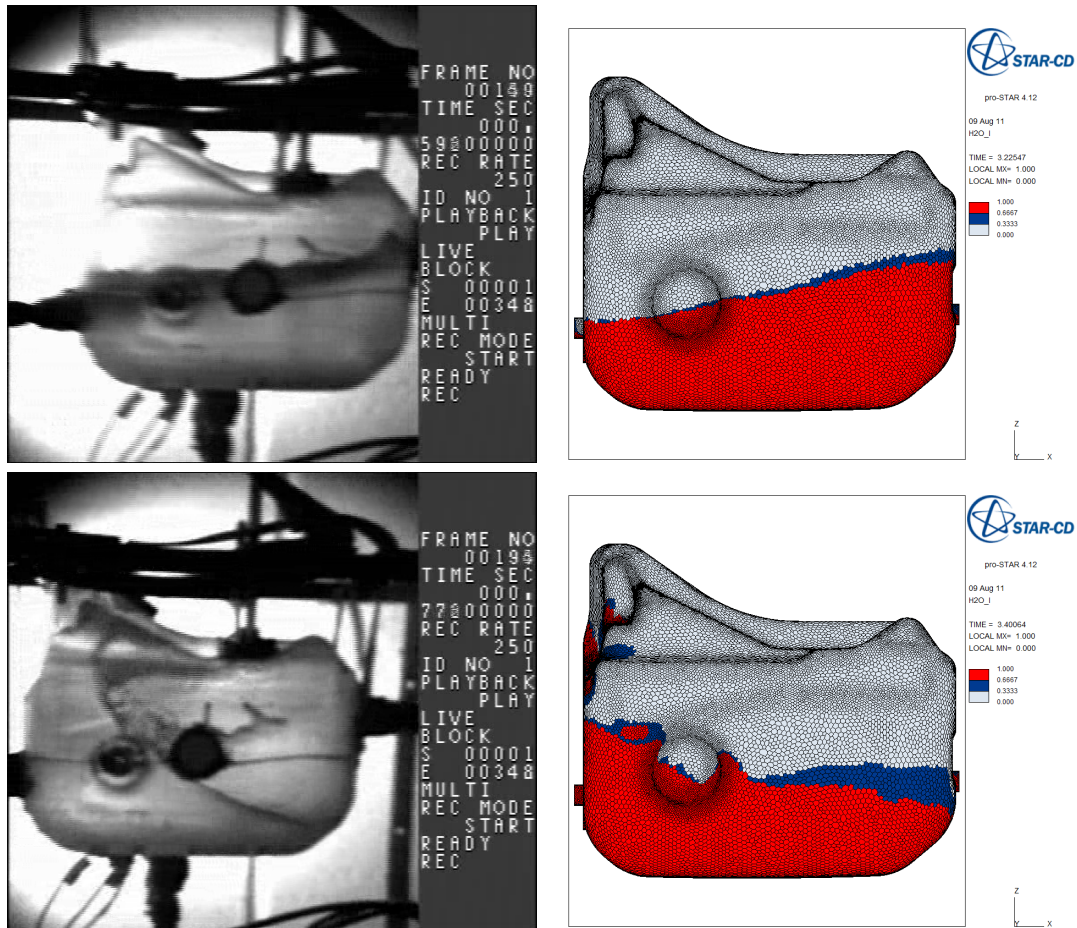


Figure D-25: Free surface comparisons at 3.23 (top images) and 3.40 seconds (bottom images)

There are a number of potential sources for this error in either the rig test or the StarCD model, as follows:

- Rig Test
 - Accelerometers
 - * Type
 - * Set up
 - * Data capture
 - * Filtering & processing
 - Pressure transducers
 - * Effect of modification
 - * Type
 - * Set up
 - * Data capture

- * Filtering & processing
- StarCD model
 - Meshing
 - * Global size
 - * Local refinement
 - * Prism layers
 - Acceleration input methods
 - CFD set up and included models

D.7 Camera Acceleration Input

The selection, set up and use of the accelerometer was reviewed with the equipment owner, where the potential for error was discussed. The result from this was that the accelerometer used may not have been suitable for this application as it behaves like a high pass filter, removing low frequency acceleration signals, the frequency response for the accelerometer is shown in Figure D-26 [145]. While this may not have been an issue during the stopping event, it may have removed some of the initial accelerations. One check for this was to reconstruct the loading pulse from still images from the high speed camera. While the stopping section of test was covered some assumptions were required to reconstruct the initial motion. Here the terminal velocity was estimated from the camera and a velocity profile assumed that met the necessary distance and velocity requirements of the rig.

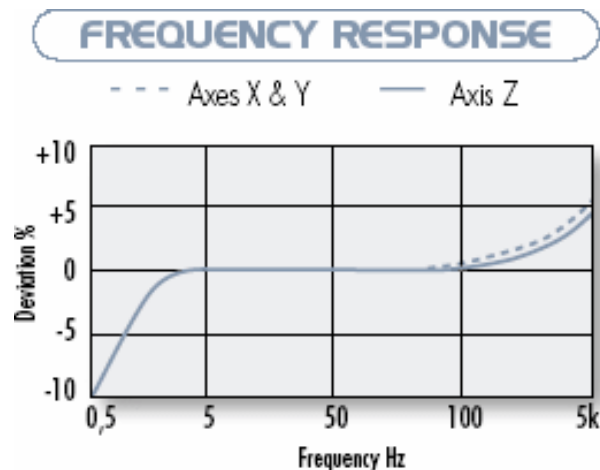


Figure D-26: Accelerometer Frequency Response, taken from [145]

Figure D-26 shows that the low frequency (<5Hz) accelerations have not been captured [145], thus another acceleration profile is required. This can be constructed from measurements on the

high speed video and assumptions about the initial motions of the rig. The third run of the unmarked water experimental test was used and the following steps taken:

1. Establishing scale of the video images.
2. Measurement of distances travelled by known points on the trolley and tank, these can then be scaled to give the actual distances travelled.
3. Post-processing of the distance data to obtain velocity and acceleration profiles.
4. Reconstructing an acceleration pulse for the whole rig test.

Due to the lack of clearly defined edges in video and basic measurement methods, this process can only provide an approximation of the scales and distances travelled. Also, the effect of the change in distance from the camera to the measuring point as the rig moves through the frame is not taken into account.

D.7.1 Establishment of Scale

Establishing scale requires the comparison of known distances to the measured distance in the computerised images. The scaling factors were obtained on later frames where the motion of the tank had subsided. The various points used in the scale and distance measurements are given in Figure D-27, with the scale taken at points labelled B, C, D, E and F. Table D.8 gives the results of the scaling measurements.

Table D.8: Scaling measurements				
Point	Description	Measurement (mm)		Scale
		Actual	Video	
A	Leg Width	19.0	N/A	N/A
B	Front Bolt	8.0	6.0	1.33
C	Mount Bolt	9.5	7.0	1.36
D	Mount Bolt End	15.0	12.0	1.25
E	Bolt Distance	148.0	123.0	1.20
F	Tank Plug Dia	30.0	23.0	1.30
Average				1.29

D.7.2 Measurement of Distances

The distances were measured at three points; the front Leg (1), the front bolt (2) and the mounting bolt (3). The Front leg was only measurable for a short duration of the video as it became aliased with the leg behind. For all measurements a maximum and minimum was taken either side of the fringes in an attempt to reduce error. The measured data was then scaled and the results are shown in Figure D-28.

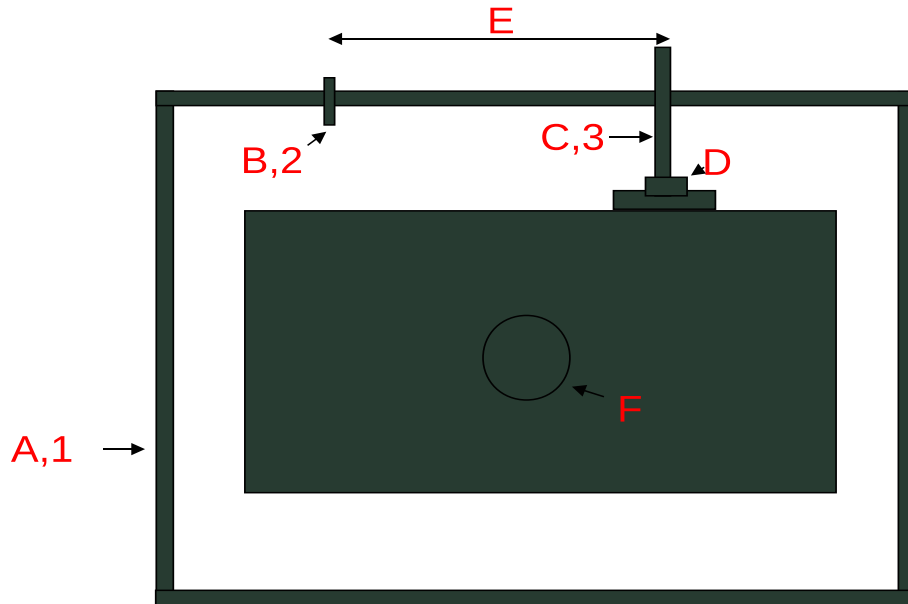


Figure D-27: Measuring points for scale and distance on the fuel tank

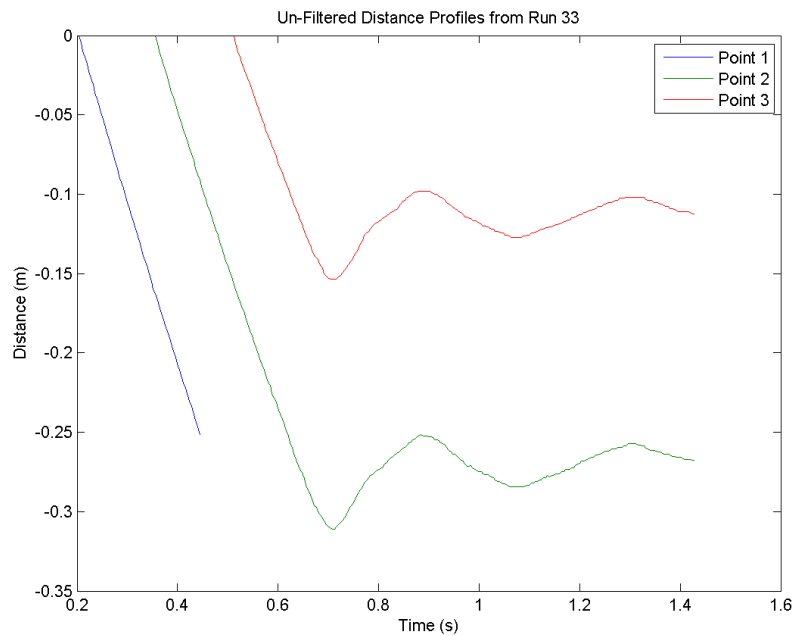


Figure D-28: Measured distances travelled in video images

D.7.3 Processing the Data

The rough nature of the distance measurements led to noise in the velocity and acceleration plots. This was rectified by smoothing the distance data using a 12Hz Filter. The velocity and

accelerations have been calculated using 4th order accurate finite differencing schemes. The acceleration profile is compared to the data obtained from the accelerometer in figure D-29. The acceleration derived from the video gave a reasonable approximation of the loading from the accelerometer. However, as this portion of the rig event is high frequency (>5Hz), it is the initial motions that need to be captured.

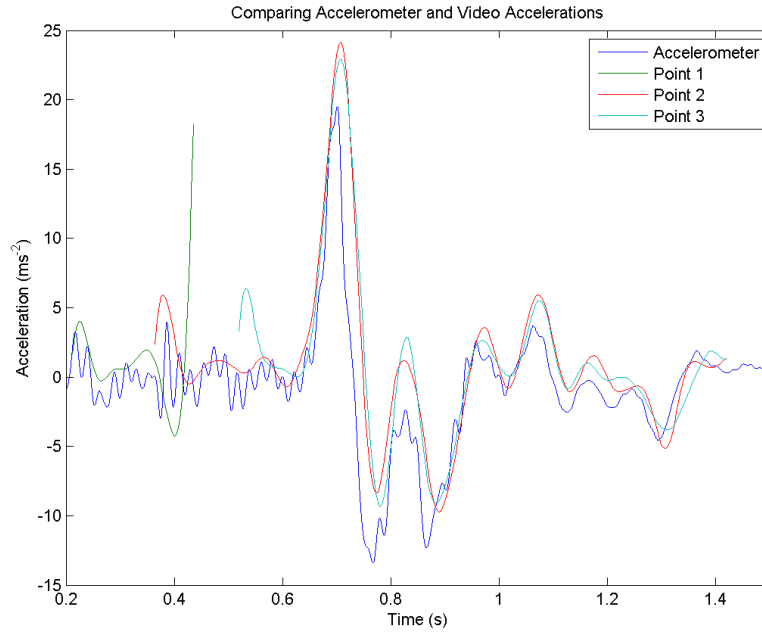


Figure D-29: Comparing acceleration profiles from the accelerometer and video

D.7.4 Reconstructing the Pulse

The first step in reconstructing the initial tank motion was to fit a 2nd degree polynomial to the distance data from point 1 only. The fitted polynomial gave a distance (y) time (x) relationship of:

$$y = 0.3229x^2 - 1.25x + 0.2414 \quad (D.1)$$

$$\frac{dy}{dx} = 0.6458x - 1.25 \quad (D.2)$$

$$\frac{d^2y}{dx^2} = 0.6458 \quad (D.3)$$

This meant that the initial velocity at t=0 (in this instance, when the camera is activated) was -1.25 m/s. From the accelerometer pulse it can be seen that the initial acceleration occurred at 1.04 seconds. Thus, known velocities were 0 m/s at 1.04 seconds and -1.25 m/s at 2.629 seconds when the camera was activated. To obtain the acceleration profile through the simulation an assumption must be made about the velocity of the tank. The assumption was that the velocity followed a

cosine function in the region of $0 < f < \pi$. The time taken to accelerate the tank to terminal velocity was then tuned to cover the correct distance from the start to the camera switch (1.22 m). Once at terminal velocity, the rig was motored up until the switch, when cart was released, after which there was a steady deceleration present as defined in equation D.3. Approximately 0.6 seconds after the switch (3.2 second total simulation time), the acceleration profile of points 2 and 3 was covered the impact event, the acceleration profile was continued until the 4 second mark. The acceleration pulse is shown in figure D-30. While this acceleration profile cannot be used to correlate the StarCD model, it should indicate that accelerometer issues are impacting on the slosh predictions.

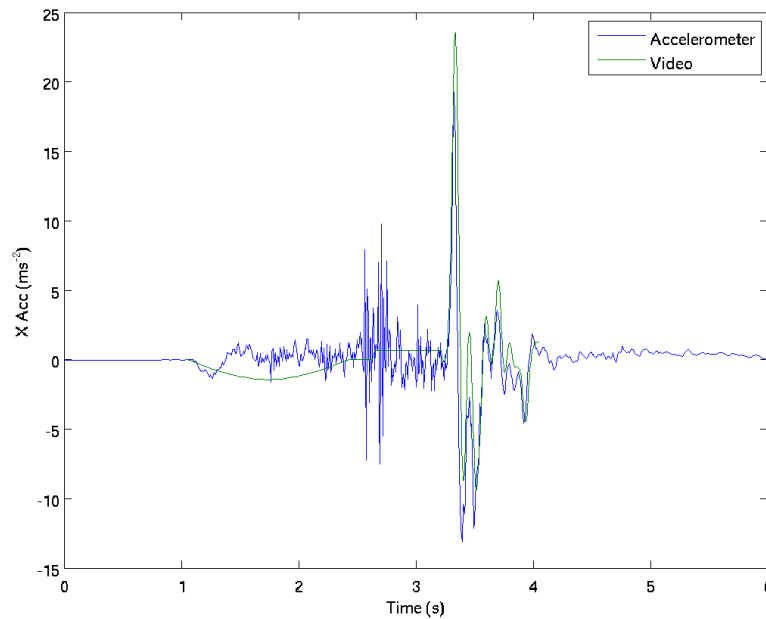


Figure D-30: Assumed acceleration profile compared to accelerometer data

D.7.5 Application of the Video Derived Acceleration Pulse

After using this acceleration pulse, the pressure trace (Figure D-31) shows that the initial fluid motions are not captured. However, the peak pressures in the stop event are captured. When the acceleration pulses are compared, the peak loading obtained from the camera is higher than that obtained by the accelerometer, although the difference is not enough on its own to explain the degree in magnitude by which the predicted pressure changes by. In the first test, with a measured peak acceleration of 20 ms^{-2} , the channel 1 StarCD predicted peak pressure is approximately 500 Pa. The peak acceleration as measure by the camera is approximately 24 ms^{-2} , yet the channel 1 StarCD predicted peak pressure rises to nearly 2000 Pa. This is a close approximation with the peak pressure measured during the rig test. As the camera acceleration pulse improves the prediction of the initial slosh motion then the fluid surge has also been capture. This better

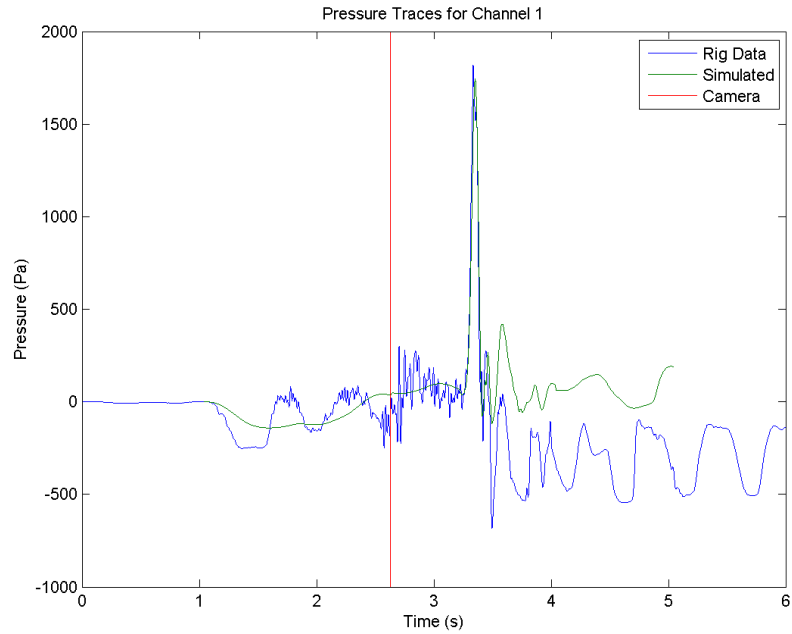


Figure D-31: Channel 1 pressure trace for high speed video derived acceleration profile

represents the velocity conditions within the fluid prior to the stop event must also be acting on the results. However, when the free surface images (figure D-32) are examined the free surface prior to the stop event (3.23 seconds) is much flatter than the camera suggests it should be. Yet, during the stop event (3.40 seconds) the prediction is good. One reason for this could be that the initial rearwards slosh has not been fully captured, but the lower frequency acceleration pulse is giving the fluid some of the surging behaviour that leads to higher peak pressures.

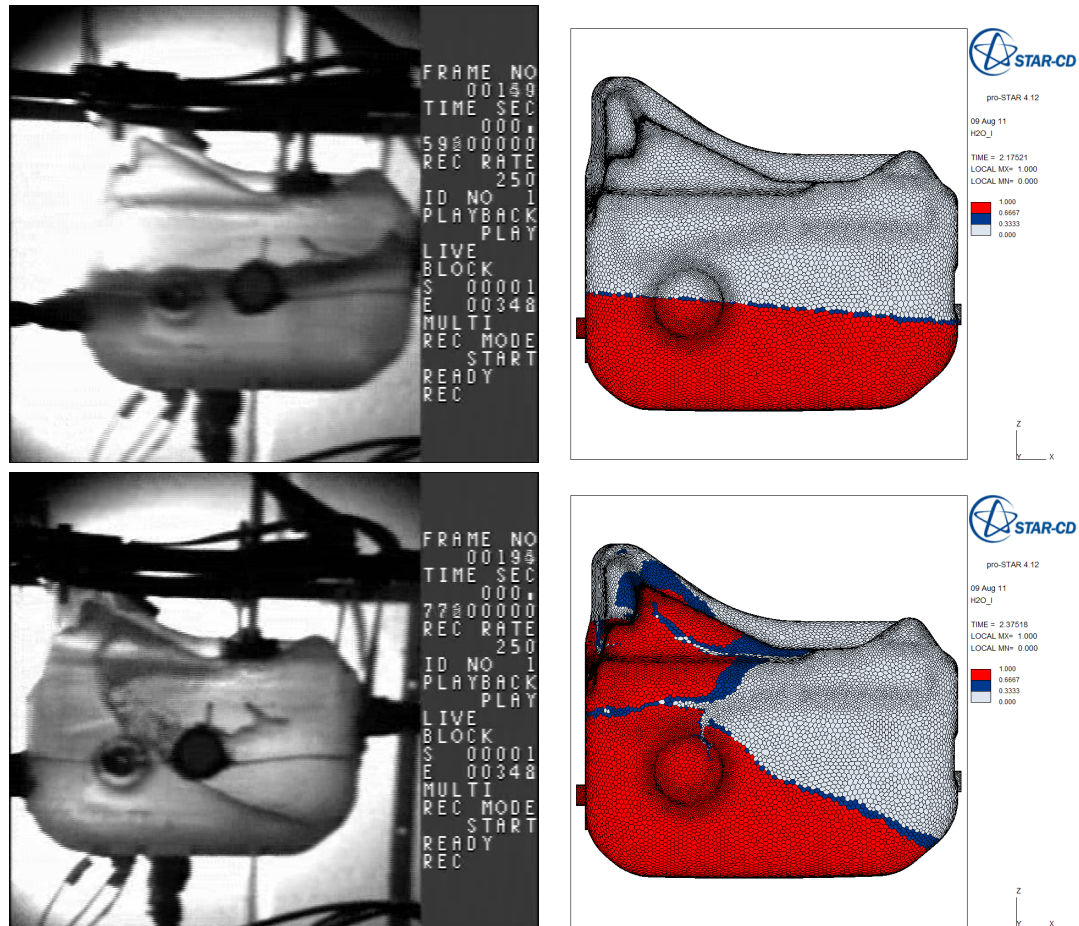


Figure D-32: Free surface comparisons at 3.23 (top images) and 3.40 seconds (bottom images)

Modified Accelerometer Input

In order to improve the initial slosh behaviour prediction the two acceleration pulses can be combined, this would then include the assumed low frequency acceleration which may not have been captured by the accelerometer. The revised acceleration pulse is shown in Figure D-33, the low frequency content is only included up to the camera switch (red line) after which the pulse is solely derived from the accelerometer. The pressure trace shown in Figure D-34 shows that the initial behaviour is improved, however the peak magnitudes of the initial and stop events are still not fully captured. This result is confirmed by the free surface plots shown in Figure D-35.

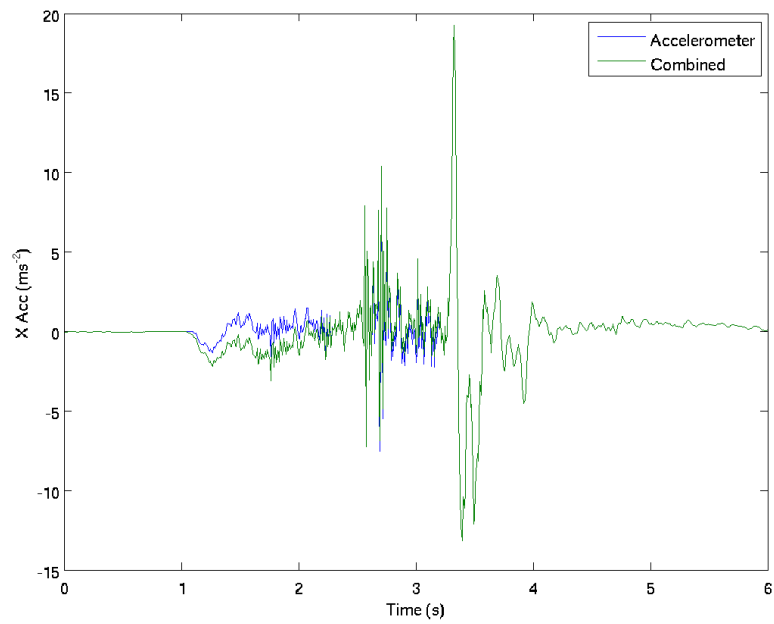


Figure D-33: Run 33 accelerometer and assumed acceleration pulse

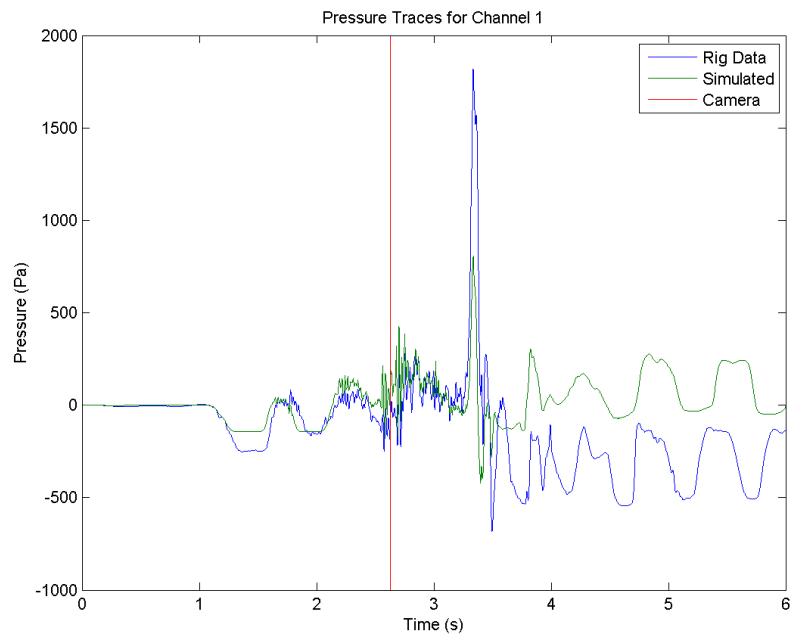


Figure D-34: Channel 1 pressure trace for run 33 acceleration profiles

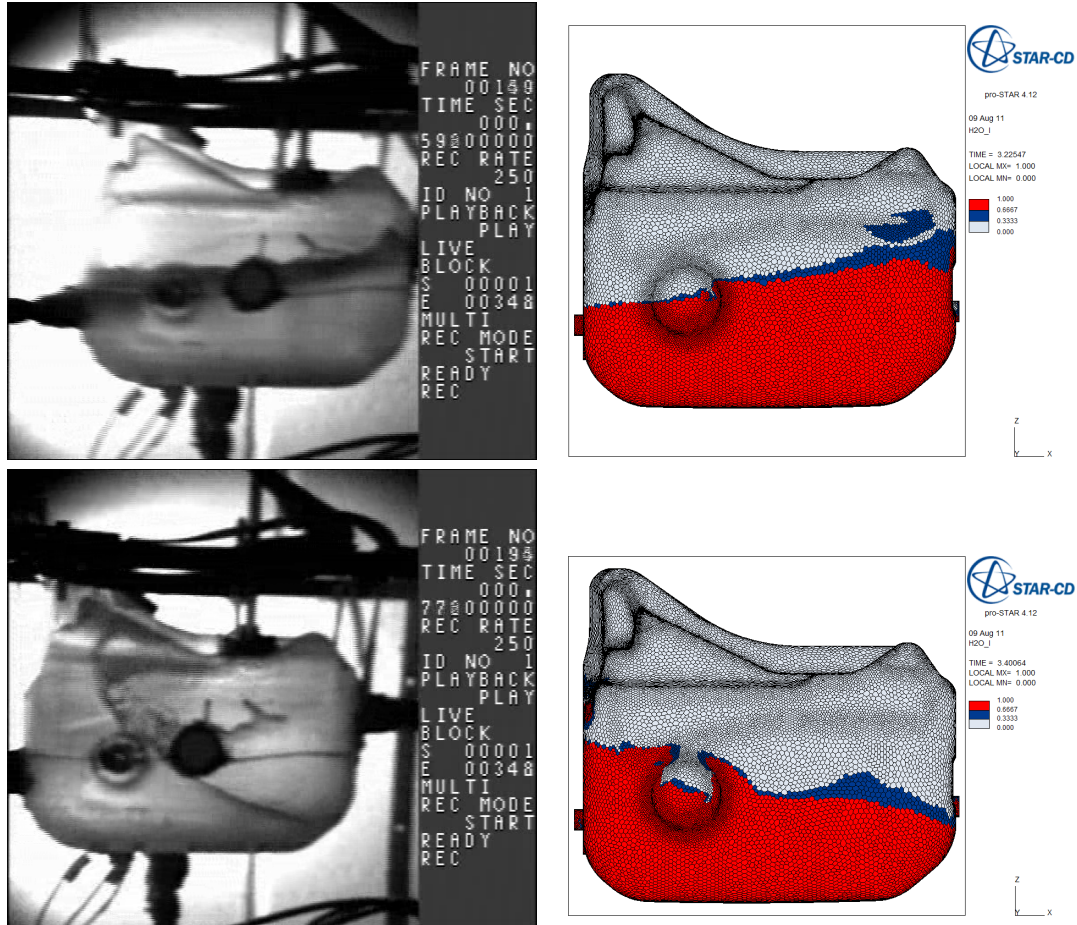


Figure D-35: Free surface comparisons at 3.23 (top) and 3.40 seconds (bottom)

D.7.6 Summary

The current evaluation showed poor correlation between the pressures and free surfaces. One potential cause of this was thought to be the high pass filter behaviour of the accelerometer used in the rig test. The use of the assumed acceleration pulse based on measurements taken from the high speed camera have indicated strongly that the accelerometer used was not applicable for this test. This work has also shown that the loading caused by the fuel slosh is highly sensitive to the fluid condition before the slosh event caused by low frequency accelerations. When acceleration pulses are obtained for future fuel slosh studies the motion before the event must also be included to ensure that the load case is fully modelled. Additional rig tests should be carried out using more suitable instrumentation to capture low frequency acceleration, the velocity or displacement of the rig trolley. This instrumentation should also be included on any acceleration cases obtained from vehicle testing, for example a speed sensor on the drive shaft.

D.8 Conclusion

This chapter has examined the experimental procedure used to obtain pressure loadings and free surfaces during slosh events of a half scale tank. The initial test showed unexpected pressure rise behaviour which was thought to be caused by trapped fluid and air bubbles within the pressure transducers. To eliminate this source of error, four pressure transducers were machined. However, revised tests with these transducers showed similar pressure rise behaviour. Further sources of this behaviour were then discussed, resulting in a change of the water in the tank to remove the marker fluid and any contaminants that may have been introduced. The revised water supply then showed pressure drop behaviour. While this behaviour was also unexpected, this could be explained as a volume loss from the tank. The third test of this set was used in the CFD correlation study.

To resolve issues with the correlation study, the acceleration profile was derived from distance measurements from the high speed camera. The pulse for the whole simulation was then reconstructed using some basic assumptions about the motion of the tank. A review of the CFD shows that the application of this loading pulse to the StarCD model does improve the predictive performance, indicating that the accelerometer used may not have been applicable in this situation.

To correlate the StarCD model to the physical data tests, further tests are required with improved instrumentation to capture low frequency accelerations, velocities or displacement of the tank. Further tests should also be undertaken to understand the underlying causes of the pressure rise or drop, such as a vent in the tank to allow pressure equalisation, or a new un-cracked tank with improved seals.

Although exact correlation has not been achieved, the use of the acceleration pulse from the high speed camera did show that the StarCD VoF method was able to capture pressure rises of the correct order of magnitude. Therefore, it would be acceptable to use the VoF modelling method to compare the various load cases in this exploration of the slosh boundary condition. However, further revised rig tests and correlation studies should be carried out to enable the setup of the mesh and StarCD parameters to be finalised for future analyses.

Appendix E

Exploring the Slosh Boundary Condition

E.1 Introduction

The analysis of the fluid slosh phenomena will require various different load cases to be applied to the model. These load cases must be representative of either testing procedures completed for fuel tanks, or the accelerations the fluid would be subjected to during the use of the vehicle. In the case of real world data, the accelerations would have to be at the extreme of loading to ensure survival of the component during such events. The input cases identified for application to the model were:

- Crash pulses
- Prototype vehicle testing road load data
- Tipping rig testing

Another important factor in the input case is the fill level of the tank. When there is less fuel in the tank, the mass is reduced, leading to lower forces. When the tank is full, the slosh phenomena is reduced as the reduced air space restricts the movement of the free surface. An investigation into the fill level will also form part of this input load case study. In all cases, it is assumed that the fluid is initially in a steady state condition before the acceleration or motion for the event is applied. In this section, the slosh events will be characterised by the loading on the baffle of a simplified test tank.

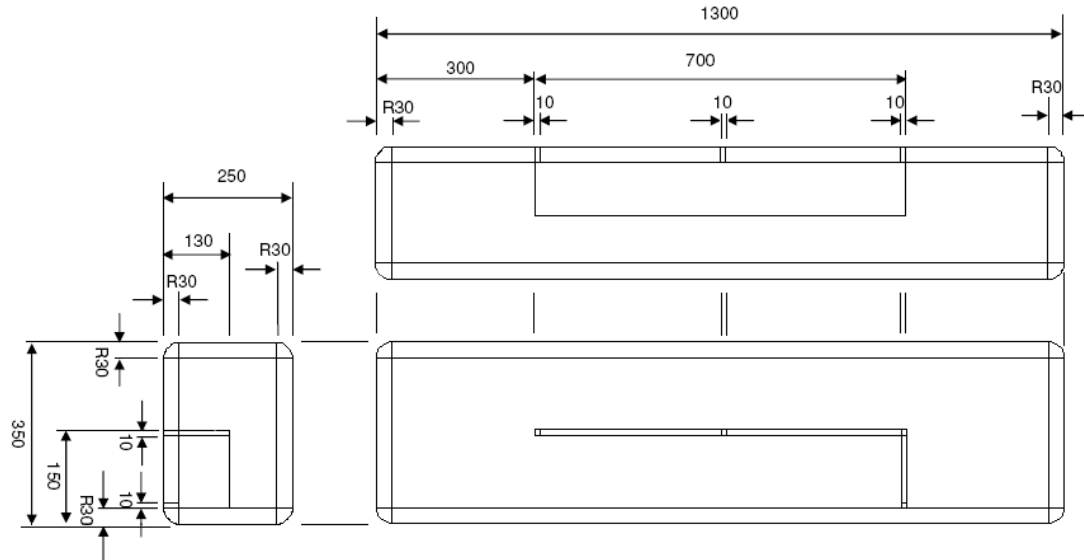
E.2 Details of the Tank Geometry

The geometry of a real automotive fuel tank is highly complex with many internal and external features that are more specific car programs. There are also different varieties of fuel tank depending upon the size of vehicle. The three main classes or shapes of fuel tank are a suitcase, saddle and cigar.

Using a real complex tank would increase the number of elements and nodes required to succinctly mesh the tank. Increasing the computer runtime which, in the context of completing sensitivity studies and method development would prove impractical.

Thus, it was decided that a basic test tank should be set up with a basic baffle to investigate the various problems posed in a fuel tank FSI analysis. The tank would need to be representative in both dimensions and volume and would be cigar like in shape.

The geometry set up is shown below in Figure E-1. The general dimensions are a rectangular volume 1300 x 350 x 250 mm with 30 mm radius fillets on each edge. Within the internal tank volume there is a baffle 10 mm thick running 700 mm down the centre of the tank, the baffle is 130 mm overall height from the base of the tank and is supported on 3 10 x 10 x 30 mm support legs. At one end of the central body, there is a plate located perpendicularly of dimensions 10 x 140 x 100 mm supported on a leg of 10 x 10 x 30 mm at one end. The tank shell is 3 mm thick and surrounds the inner surface. The total volume is calculated in Table E.1, the dead volumes being volumes removed from the rectangle due to fillet radii. The total volume is 111 litres and is comparable to the total volume of current tanks.



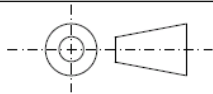
	Paul Sutton (M-Eng AIMEchE)
	Geometry for Fuel Slosh Simulations
	24/06/2008 Jaguar Cars & Uni. Of Bath

Figure E-1: Simplified fuel tank geometry

L	B	H	Fillet r	Total vol	Dead vol	Final Vol
1300	350	250	30	1E+08	1E+06 3E+05 2E+05 1E+05	112179220.8

Baffle Dimensions

Central Body	L	B	H	
	700	10	100	7E+05
Parallel Body	L	B	H	
	10	140	100	1E+05
Feet	L	B	H	n
	10	10	30	4 12000

Scale	cm	Volume - Baffle	<u>-852000</u> 111327220.8
-------	----	-----------------	--------------------------------------

Table E.1: Simplified fuel tank volume calculation

E.3 The StarCD Procedure used for Fluid Modelling

The fuel tank was modelled in CD Adapco StarCD version 4.08 on a polyhedral mesh generated in CCM+. The mesh was developed to aid convergence in the 16 kph crash case, although no

formal mesh dependency study was carried out. This mesh was then applied to all cases. The free surface simulation is modelled as two scalars, one representing the air volume and the other the heavy fluid. The heavy fluid was assumed to be diesel with the initial fill volume set by splitting the mesh into two different cell sets differentiated by height. The volume of fraction is calculated as an additional scalar which allows the interface between the two fluids. The timestep for most cases was set to 0.001 seconds, but to aid convergence in the crash case this was reduced to 0.00001 seconds. The loadings required by the case studies were applied to the tank either by use of the source momentum user sub-routine or by a moving mesh.

Once the mesh files are loaded into Prostar the slosh problem needs to be defined. The definition requires details of the fluids as well as all the solver parameters. The problem can be set up in Prostar either by using the interactive GUI or via the command line. A VOF simulation requires the following steps to be taken;

- The geometry and mesh need to be imported from ICEMCFD.
- The VOF scalar to be activated, this also requires that the transient solver is turned on and cavitation models are turned off.
- Both the heavy fluid (diesel) and the light fluid (air) need to be given material properties such as density and viscosity.
- The fluid properties must then be assigned to the correct cell sets ensuring that the heavy fluid is always at the bottom of the tank.
- Initially turbulence models need to be turned off. An investigation is required to look at the possibility of turning the turbulence on after an initial period of the simulation has been run.
- The buoyancy for air must be turned on; this is to allow bubbles of trapped air to escape to the top of the free surface.
- The parameters for the solver and discretisation scheme need to be set up. For the discretisation scheme, the MARS method is used. However, for all other parameters the StarCD defaults have been accepted.
- Any boundary or measurement probes must be set up. Boundary monitors need to be applied on all baffle surfaces to collect data about the pressures applied to them. This will be outputted using a .erd file which will be discussed in the post processing of data.
- The time step and simulation duration need to be applied to cover accurately the duration of the sloshing event.
- The transient post file needs to be defined. This is the file where the results at given points in time are written to.
- The load case needs to be applied to the model. This includes gravitational forces. StarCD allows for many different types of loads to be applied using a variety of methods which will be discussed in later sections.

- The geometry, problem and model files that the Star solver will use need to be written.

Once the analysis has been run on the clusters it is then post-processed using StarCD, Enight and Matlab. Both the free surface and the engineering data file are interrogated to ensure the simulation has been successfully completed.

E.4 Crash Impulse Loads

The acceleration data for various different crash loadings has been obtained from crash simulations. For the side and rear impacts, the tank was subjected to large deformations of the tank which is beyond the scope of this analysis. The data for the frontal impacts was given in the x-direction only. The impulses were sampled at the base of the B pillar. It was deemed that the internal components would not be expected to survive a 56 kph crash. However, after a 16 kph crash, the tank would still need to operate. The 16 impulse is shown in Figures E-2. To apply the crash accelerations within the CFD, the data was written into a *.dat* file which was then read by the user coding (*sormom.f* Appendix F.1) and the impulse applied according to the elapsed time.

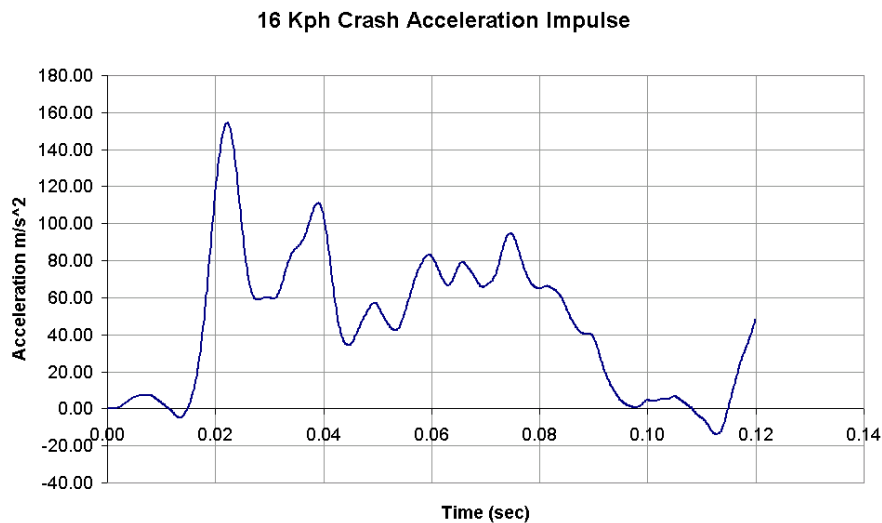


Figure E-2: 16 kph crash impulse

E.5 Prototype Road Testing Event

The prototype road testing event features a number of different obstacles and driving manoeuvres designed to test new vehicles. Accelerometers were placed on various points in the vehicle to record the acceleration experienced, this includes the sensors on the fuel tank mountings. These accelerometers are able to capture the low frequency accelerations of the vehicle during the various test events. The captured data was filtered to remove noise and is currently used in the durability assessment of the fuel tank mounting strategy [131]. The maximum and minimum of the data in the principal directions for all prototype events is given in appendix Table E.2. From this large number of events, five cases were selected based on the intensity and duration of the events which allowed a wide range of boundary conditions to be examined. The events are listed below and the acceleration pulses given in Figures E-3 to E-7. The acceleration is given in the vehicle global coordinate system. The x direction is from the front to the back of the vehicle, the y direction is from right to left and the z direction is from bottom to top.

Case	Name	X Accel (g)		Y Accel (g)		Z Accel (g)	
		Max	Min	Max	Min	Max	Min
ab10	Lock to Lock	0.073	-0.033	0.15	-0.09	0.247	-0.146
ab11	Fig 8	0.161	-0.092	0.642	-0.655	0.033	-0.14
ab12	Lombadas	0.464	-0.182	0.094	-0.227	1.16	-0.852
ab13	Chatterbumps	0.399	-0.348	0.314	-0.269	0.808	-0.752
ab14	Resonance Road 1 & 2	0.725	-0.752	0.781	-0.542	1.32	-1.14
ab15	Body Twist	0.224	-0.039	0.187	-0.095	0.197	-0.24
ab16a	Accel on 5 Bumps A	0.932	-1.14	0.729	-0.567	0.87	-1.11
ab16b	Accel on 5 Bumps B	0.68	-0.02	0.016	-0.042	0.117	-0.088
ab17	Body Twist Platforms	0.065	-0.152	0.252	-0.257	0.195	-0.155
ab18	RR-Crossing	0.749	-0.688	1.07	-0.4	1.17	-1.6
ab19	Kerb Island Strike	1.22	-0.423	0.865	-1.26	1.78	-1.5
ab20	Road 6 D-to-E	0.268	-0.23	0.023	-0.019	0.049	-0.057
af05	Circuit 7	0.837	-0.544	1.31	-1.24	1.18	-0.919
ag07	Comfort Road Split	0.457	-0.284	0.845	-0.867	1.13	-0.737
ag08	Postal Road Brake	1.72	-1	0.687	-0.937	1.04	-1.07
ag10	Slalom Cobblestones	0.165	-0.181	0.543	-0.521	0.331	-0.257
ag11	Chuckholes 18	0.359	-0.279	0.373	-0.235	0.517	-0.285
ag14	Chuckholes 26/30	0.407	-0.434	0.703	-0.471	0.924	-0.513
ar05	Jonce & Reboundholes	0.76	-0.663	0.712	-0.635	0.831	-0.675

Table E.2: Accelerations in the PASCAR events

The acceleration data in these cases was in a similar format to that of the crash case, allowing the source momentum user coding to be applied. However, one difference is that the data is given in all three principal directions. The user coding was modified to apply these additional momentum sources. An example of user coding is given in Appendix-F.1. The events to be examined were:

- Kerb island strike. This is a violent event in which a vehicle is driven at 50 mph into a 6 inch

kerb at an angle of 45° .

- Postal road brake. This represents an extreme braking manoeuvre.
- Acceleration of five bumps. This is representative of driving over speed bumps.
- Chatterbumps. This is a suspension test with out of phase bumps on each side of the car.
- Slalom Cobblestones. This is a steering course on a rough surface where the vehicle is swerving in between obstacles.

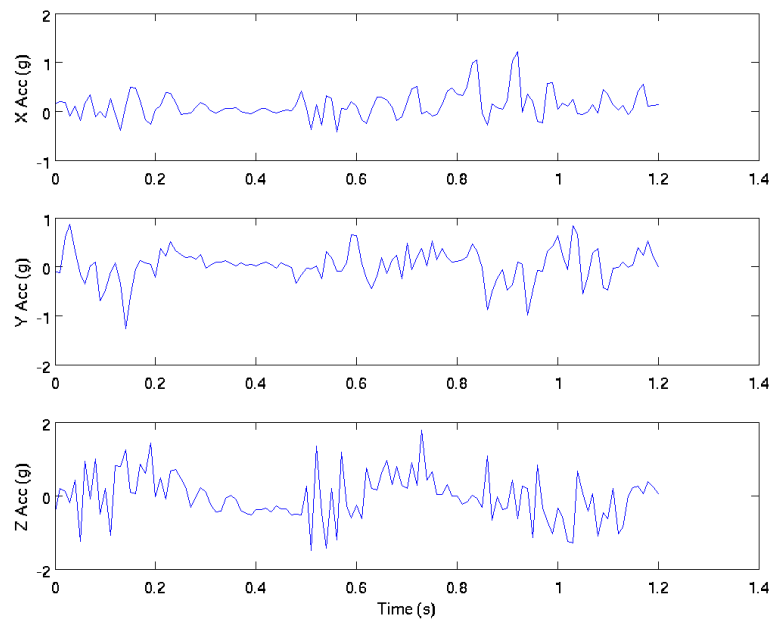


Figure E-3: Kerb island strike x (top), y (middle) & z (bottom) acceleration

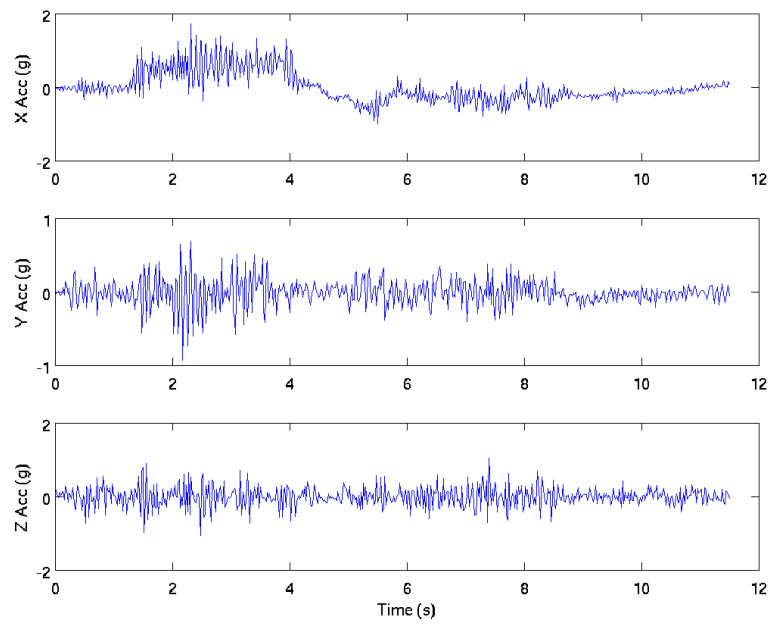


Figure E-4: Postel road brake x (top), y (middle) & z (bottom) acceleration

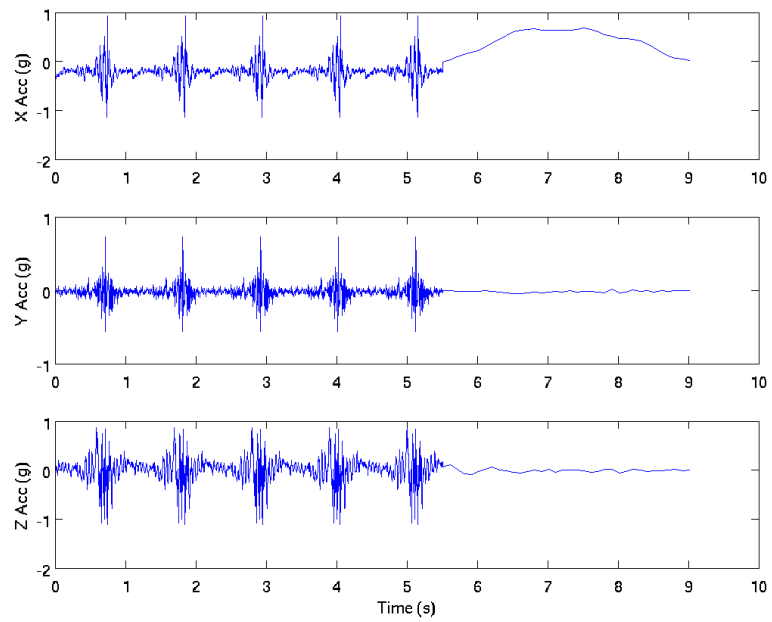


Figure E-5: Accel on 5 bumps x (top), y (middle) & z (bottom) acceleration

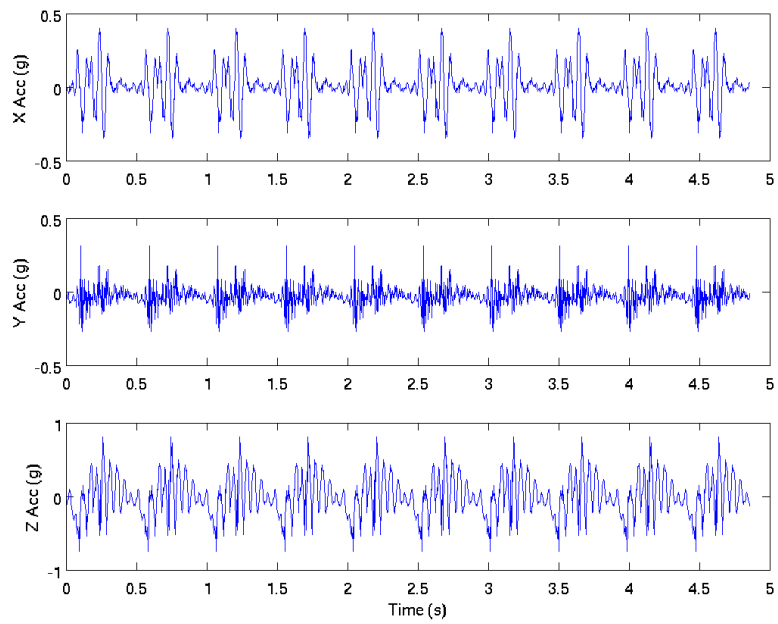


Figure E-6: Chatterbumps x (top), y (middle) & z (bottom) acceleration

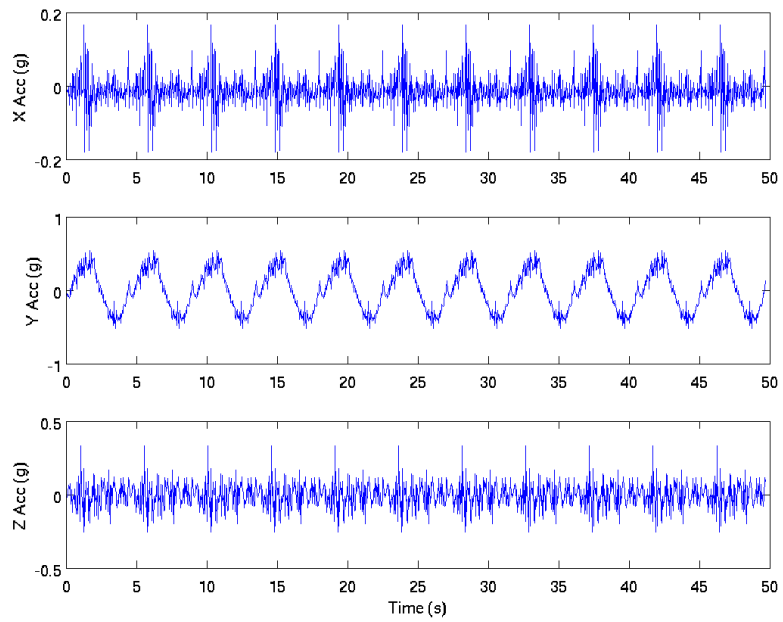


Figure E-7: Slalom cobblestones x (top), y (middle) & z (bottom) acceleration

E.6 Rig Tip Testing

All fuel tanks are subjected to the internal component slosh test. This evaluates the structural integrity of internal components. The test mechanically induces slosh to simulate the dynamic affects of fluid motion due to the acceleration of the vehicle. The test is carried out to Ford procedure [146]. This calls for the tank to be strapped to a tilt table that will rotate the tank through angles of $\pm 15^\circ$ over a 15-second cycle (0.067 Hz) for 100,000 cycles. The procedure also calls for the volume of fuel within the tank to be constantly varied between 25 and 87.5% using the fuel pump working at 10 litres per hour.

The modelling of the tank rotation in StarCD would required the use of a moving mesh rotated around the pivot point (see Figure E-8) at the base of the tank. To do this, an event file with user coding was used. This involved displacing the nodes by an angle determined by the time step. (Details given in Appendix F.2). As this work is only looking at simplified geometry, the variation of the fuel fill was not modelled, as this would have added complexity and increased the execution time of the model. The CFD simulation was only completed for five cycles, this was able to obtain representative cycle to cycle repeatability of loading during the event.

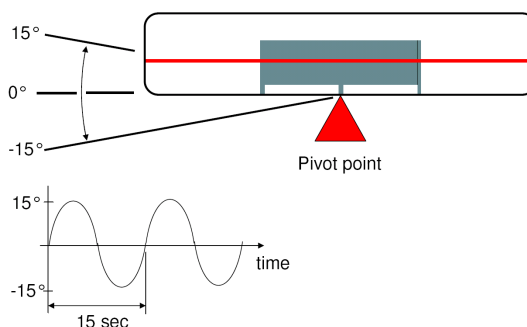


Figure E-8: Rig test modelling setup.

E.7 Case Loading Forces

The first test was to examine the various load cases for loading on the internal baffle. The pressures on each of the baffle faces were exported into the engineering data file (.erd), these were then processed to give the maximum loading in the three principal directions during the event. The loading from the 16 kph crash case can be seen in Figure E-9. Other checks included examining the fluid loading on the baffle and free surface within the tank graphically at given timesteps. Examples of this can be seen in Figures E-10 and E-11.

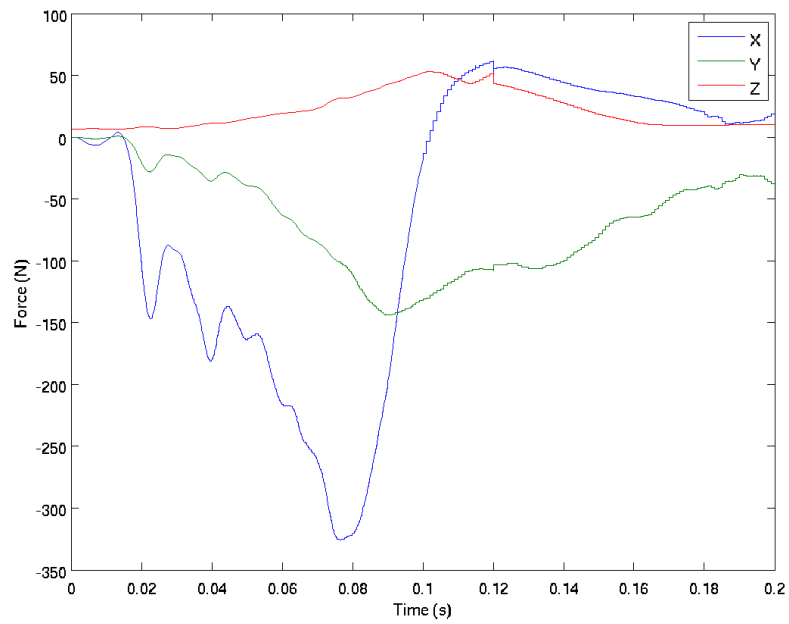


Figure E-9: Forces on the Baffle

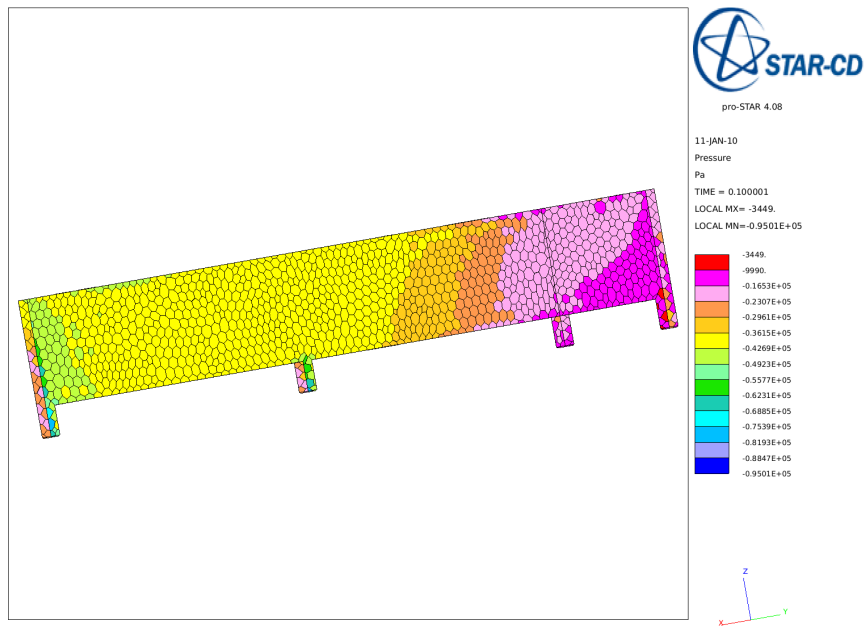


Figure E-10: Pressures on the Baffle

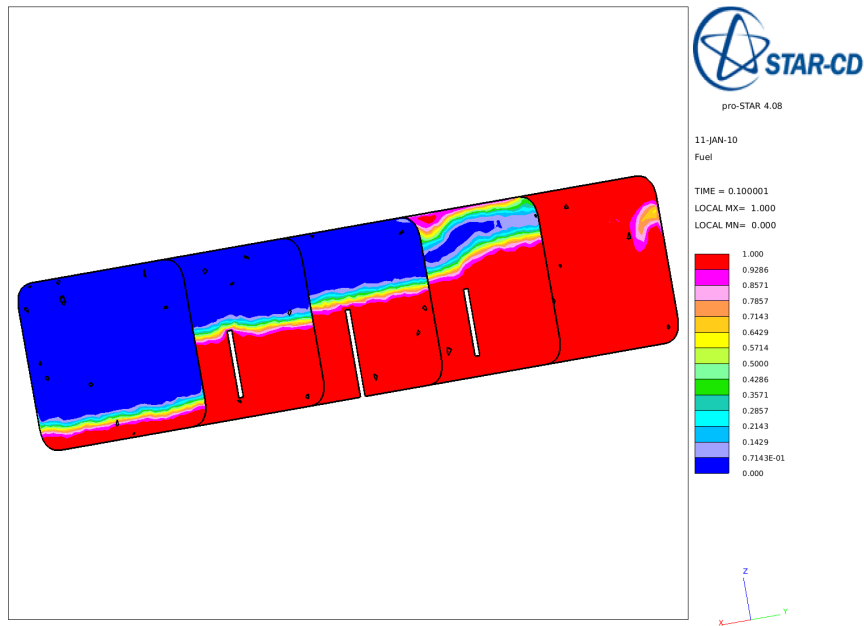


Figure E-11: Free surface within the tank

The load cases were compared by measuring the maximum and minimum force loadings on the baffles in the principal directions. These were obtained from processing the engineering data files and have been summarised in Table E.3. The durability can be categorised by two regimes; high force one off shock loadings and lower force repeated events for fatigue cases. For this reason the number of expected cycles has been included to distinguish between high and low cycle events. The runtimes are also included to understand which cases can be considered the fastest.

The 16 kph crash case exhibits the highest force loading, this is a shock event where the vehicle would only be expected to undergo a single cycle. Due to the decreased timestep this event is one of the longest to run, however due to the strength of the loading this case should be considered within the coupling study. The forces in all prototype testing events give force loadings that are of a similar order of magnitude. Out of this set the kerb island strike shows the highest loading and the fastest turnaround time (this is due to the short duration of the event). However, this is also a low cycle event but as the forces are of a similar magnitude to other prototype cases it will be used in the multi-physics assessment (Chapter 7).

The rig case shows considerably lower forces than all other events. Further assessment is required to examine whether this case is representative of in-vehicle events and is suitable as the fuel tank evaluation method.

Table E.3: Maximum and Minimum Forces of the Baffle								
	Max Force (N)			Min Force (N)			Cycles	Run-Times (s)
	X	Y	Z	X	Y	Z		
16 kph crash	62.96	0.82	55.34	338.32	139.73	6.70	1	101563
Chatterbumps	3.41	9.92	11.57	2.96	8.93	1.32	5120	22425
Slalom Cobblestones	4.05	24.24	8.32	3.54	18.58	4.49	768	134955
Accel on 5 bumps	15.85	18.17	12.76	7.00	11.24	0.53	1024	54965
Kerb Island Strike	14.26	29.51	15.66	11.05	43.32	4.49	80	14995
Postal Road Brake	18.95	21.42	12.86	12.44	14.18	0.03	64	47492
Rig-mvmesh	1.85	0.52	6.91	1.80	0.89	4.49	1.00E+005	38259

E.8 Fuel Fill Sensitivity Analysis

The sensitivity of the loading on the baffle to the fuel fill level was explored to enable any following analyses to be run at the 'worst-case' loading for fluid slosh. The fill levels were varied between 40 and 80%. This was measured as a percentage of the tank depth. As this did not take the volume of the baffle there is some error when examining the exact volumetric fill percentages. The estimated and actual percentage fill are summarised in Table E.4. The table shows that there is an optimum fill level that causes the largest forces on the baffle, this is approximately 60 to 65% fill. Above this fill level, the loadings begin to fall off. This sensitivity to fuel fill is caused by the amount of momentum of the heavy fluid. At lower fill levels, the mass is decreased but the fluid is free to move. As the tank is filled, the mass is increased causing the load to rise until the fluid motion is restricted by decreasing amount of air volume. This reduces velocity, causing the load to lessen.

Table E.4: Maximum and minimum directional forces for each of the load cases

	Fill Level (%)		Max X (N)	Max Y (N)	Min X (N)	Min Y (N)
	Est	Actual				
16kph Crash	50	48.66	32.22	0.56	-274.29	-145.58
	55	54.25	51.73	2.30	-292.96	-148.13
	60	56.66	61.60	0.84	-325.58	-143.93
	65	61.77	69.52	0.87	-313.57	-128.79
	70	66.96	83.28	2.93	-244.22	-102.10
KIS	40	39.64	9.78	16.42	-12.47	-24.97
	45	44.65	11.23	20.74	-13.85	-32.86
	50	48.50	12.03	26.36	-14.33	-36.01
	55	52.08	12.65	29.42	-13.03	-43.17
	60	56.12	13.14	31.28	-12.32	-45.32
	65	59.98	14.09	29.83	-11.93	-43.87
	80	75.45	11.05	24.46	-11.34	-36.04
	80	75.45	10.66	20.86	-11.80	-30.59
Rig	40	39.64	1.91	0.37	-1.58	-1.87
	45	44.65	1.92	0.60	-1.35	-1.46
	50	48.50	1.98	0.86	-1.52	-1.10
	55	52.08	2.03	0.91	-1.72	-0.80
	60	56.12	1.85	0.59	-1.84	-0.93
	65	59.98	2.13	0.50	-2.07	-0.72
	80	75.45	2.22	0.21	-2.94	-0.20

E.9 Conclusions

This chapter examined the steps taken to correlate surface pressures and free surface approximations of a StarCD VOF model with a rig test. While issues with the input to this model prevented a definite correlation being made, the method was deemed to be acceptable for the examination of load cases. The requirements for further correlation work were outlined and discussed the need for additional instrumentation to accurately capture the rig acceleration, velocity or displacement. Similar measurement methods would also need to be in place for load cases obtained from vehicle measurements.

A basic tank was used to examine a number of road load and rig testing cases to find the worst case scenario for internal component durability. This included an assessment of the sensitivity to fuel fill. Of the cases examined, the applicability of the 16 kph crash case and kerb island strike at an approximate fill level of 60% should be the cases considered in any multi-physics method.

Appendix F

Slosh and MPCAE Scripts

F.1 The User Coding for Source Momentum

The 16 kph crash, kerb island strike and postal road brake load cases were all applied to the CFD model using the source momentum facility within StarCD. The non-linearity of the data meant that the data could not be inputted using standard equations, thus, the data was stored in a data file (.dat) which was read using the source momentum user coding (sormom.f). The code allowed for acceleration to be applied to the data in the three principal directions, x, y and z. The code given in the following section is an example of sormom.f.

```
INTEGER k, n, N1, N2, IOUT
COMMON /ACCEL/ TS(576), ACCX(576), ACCY(576), ACCZ(576)
IF (TIME.LT.11.5) THEN
  100   IF (INTFLG(10).EQ.0) THEN
        OPEN (200,FILE='ag08.dat',STATUS='UNKNOWN')
        k=1
        999   READ (200,200) TS(k), ACCX(k), ACCY(k), ACCZ(k)
        200   FORMAT (F10.5,x,F10.5,x,F10.5,x,F10.5)
        IF (TS(k).LT.11.5) THEN
          k=k+1
          GOTO 999
        ENDIF
        1000   CLOSE(200)
        INTFLG(10)=1
      ENDIF
      IOUT=0
      N1=0
      N2=0
      n=0
```



```

DO WHILE (IOUT.EQ.0)
  n=n+1
  IF (TS (n) .EQ.TIME) THEN
    IOUT=1
    N2=n
  ELSEIF (TS (n) .GT.TIME) THEN
    IOUT=2
    N1=n-1
    N2=n
  END IF
END DO
IF (IOUT.EQ.1) THEN
  VALUEX1 = ACCX (N2)
VALUEX2 = 0
VALUEY1 = ACCY (N2)
VALUEY2 = 0
VALUEZ1 = ACCZ (N2)
VALUEZ2 = 0
  ELSEIF (IOUT.EQ.2) THEN
    X1 = (TIME - TS (N1))
X2 = (TS (N2) - TS (N1))
FACTOR= X1 / X2
    VALUEX1 = ACCX (N1) * (1.0 - FACTOR)
VALUEX2 = ACCX (N2) * FACTOR
    VALUEY1 = ACCY (N1) * (1.0 - FACTOR)
VALUEY2 = ACCY (N2) * FACTOR
    VALUEZ1 = ACCZ (N1) * (1.0 - FACTOR)
VALUEZ2 = ACCZ (N2) * FACTOR
  END IF
  S1U=9.81*DEN*(VALUEX1+VALUEX2)
S1V=9.81*DEN*(VALUEY1+VALUEY2)
S1W=9.81*DEN*(VALUEZ1+VALUEZ2)
ELSE
S1U=0
S1V=0
S1W=0
END IF
RETURN
END

```

F.2 The Method Taken to Model the JLR Rig Test

The modelling of the rig test utilised the mvnest commands within StarCD. This called for the creation of an event file which moved the tank by a angle proportional to the timestep around an axis on the base of the tank. The movement was controlled by a change grid file (cgrid.cgrd), the coding is given below.

```
!!Moving grid commands for tipping of a fluid filled tank with baffles
!!
!!Written by P Sutton
!!18th June 2008
!!Ext 7214
!!psutto26@jaguarlandrover.com
!!
!!Based upon
!!
!!Moving grid commands for crankcase breather model
!!
!!Written by S Pierson
!!18th October 2004
!!Ext 7087
!!spierso2@jaguarlandrover.com
!!
*IF,TIME,GT,0.
!!Ensures no mesh motion at Time 0.0
!!
*SET,RDS,4. * 0.1047,0
!!rds is radians per second
!!
CSYS,4
!!
!!Moves mesh in each crank bay
!!
*SET,TANG,TIME * RDS,0
*CALC,ADEF,15.,SIN,TANG,0.,1.
*GET,TPOS,Y,33874
*SET,TPOS,TPOS - 90
*SET,TOFF,ADEF - TPOS
cset news fluid
vset news cset
vgen 2 0 vset,,,0,TOFF,0,1.
*ENDIF
```

F.3 Morphing Mesh Method

The morphing mesh is implemented via the events module in Prostar, this calls up the events file which directs Prostar to use StarMorph.MAC. This file was provided by CD-Adapco in the proof of technology concept for the direct couple.

```
!-----!
!--starting assumptions:
!      The coordinates of the vertex on the
!      fsi interface (region 5) are from the end of the
!      current step and the rest of the vertex are at the
!      beginning of the step.
!-----!
! main control point length scale of influence (m)
*set scl1 0.05
! scale of boundary point length scale of influence (m)
*set scl3 0.05
!-----!
!--set increment frequency for updating reference mesh---!
!-- incrm = 0  => reference grid is always initial grid -!
!-- incrm = 1  => reference grid is always previous step !
!-- incrm = n  => reference grid is updated every nth step
!-----!
*set incrm 10
!*get x10  x 11882
!*get x20  y 11882
!copy the vertices coordinates into the register
vreg copy,, 0,1

*if time eq 0.
! write out the reference grid
vwrit PROSTAR_VERT1.vrt,,,,bloc
*else
! read in the reference grid
vread PROSTAR_VERT1.vrt,,,,bloc
*endif
!reset the morpher
morp clear
!grab the vertices on the fsi interface (region 5)
bset news rlist 5
vset news bset
!morphing in 2d
```

```

morp dime xy
! Line added by NF to invoke inverse multi-quadratics
morp kval -1
!limit number of control points to 20 (there is 346 on the fsi surface)
morp tout 20
!set the control points on the fsi surface
morp vreg 1,vset,,, scl1
!fix the vertices on the bottom plane (region 4)
morp gpla regi 4,, scl3
!allow the vertices on the top, left and right to slide along a plane
morp gsym regi 1,, scl3
morp gsym regi 2,, scl3
morp gsym regi 3,, scl3
!excute the morph
morp exe2
!update the reference grid at requested increments
bset news rlist 5
vset news bset
vreg copy vset 1 0
!*get x11 x 11882
!*get x21 y 11882

*if incrm gt 0
*calc modu,,mod,ITER,,incrm
*if modu eq 0
  writ PROSTAR_VERT1.vrt,,,,bloc
*endif
*endif

```

F.4 Abaqus Direct Cosimulation Cards

```

*CO-SIMULATION, NAME=COSIMULATION_1, PROGRAM=DIRECT,
  CONTROLS=COSIMULATION_CONTROLS_1
*CO-SIMULATION REGION, TYPE=SURFACE, EXPORT
ASSEMBLY_INTERFACE, U
*CO-SIMULATION REGION, TYPE=SURFACE, IMPORT
ASSEMBLY_INTERFACE, CF
*CO-SIMULATION CONTROLS, NAME=COSIMULATION_CONTROLS_1,
  TIME INCREMENTATION=SUBCYCLE, TIME MARKS=YES, STEP SIZE=4.0E-5

```

F.5 Example Abaqus CEL Deck

```
*Heading
** Job name: dam Model name: Model-1
** Generated by: Abaqus/CAE 6.9-1
*Preprint, echo=NO, model=NO, history=NO, contact=NO
**
** PARTS
**
*Part, name=Part-1 %(Solid Baffle)
*Node
(Node Definitions)
*Element, type=C3D8R
(Element Definitions)
%Node, element and surface sets
*Nset, nset=_PickedSet9, internal, generate
*Elset, elset=_PickedSet9, internal, generate
*Nset, nset=s-base
*Elset, elset=s-element, generate
*Nset, nset=s-pos-z, generate
*Nset, nset=s-node, generate
*Nset, nset=s-neg-z, generate
*Elset, elset=_s-force_S3, internal
*Elset, elset=_s-force_S5, internal
*Surface, type=ELEMENT, name=s-force
** Section: Section-1
*Solid Section, elset=_PickedSet9, material=HDPE
,
*End Part
**
*Part, name=Part-2 %(Eularian Volume)
*Node
(Node Definitions)
*Element, type=EC3D8R
(Element Definitions)
%Node, element and surface sets
*Nset, nset=_PickedSet20, internal, generate
*Elset, elset=_PickedSet20, internal, generate
*Nset, nset=f-node, generate
*Elset, elset=f-element, generate
*Nset, nset=f-pos-x, generate
```

```

*Nset, nset=f-pos-z
*Nset, nset=f-pos-y, generate
*Nset, nset=f-neg-x, generate
*Nset, nset=f-neg-y, generate
*Nset, nset=f-neg-z
** Section: Section-2
*Eulerian Section, elset=_PickedSet20, controls=EC-1
Water, Part-1-1
*Surface, type=EULERIAN MATERIAL, name=Part-1-1
Part-1-1
*End Part
**
*Part, name=Part-3
*End Part
**
**
** ASSEMBLY
**
*Assembly, name=Assembly
**
*Instance, name=Part-1-1, part=Part-1
*End Instance
**
*Instance, name=Part-2-1, part=Part-2
*End Instance
**
*Instance, name=Part-3-1, part=Part-3
*End Instance
**
*Nset, nset=_PickedSet9, internal, instance=Part-2-1, generate
*Elset, elset=_PickedSet9, internal, instance=Part-2-1, generate
*Nset, nset=f-node-ini, instance=Part-2-1
*Elset, elset=MySet, instance=Part-2-1
**
**
** INTEGRATED OUTPUT SECTIONS
**
*Integrated Output Section, name=I-Section-1,
    surface=Part-1-1.s-force, project orientation=NO
*End Assembly
**

```

```

** ELEMENT CONTROLS
**
*Section Controls, name=EC-1, hourglass=VISCOUS
0.2, 1., 1.
**
** MATERIALS
**
*Material, name=HDPE
*Density
  8.76e-10,
*Elastic
  903.114, 0.39
*Material, name=Water
*Density
  9.98e-10,
*Eos, type=USUP
  1.5e+05, 0., 0.
*EosShear, type=VISCOUS
  1.003e-09,
**
** INTERACTION PROPERTIES
**
*Surface Interaction, name=IntProp-1
*Friction, rough
**Contact Damping, definition=CRITICAL
**0,
**4,
**
** BOUNDARY CONDITIONS
**
** Name: f-neg-x Type: Velocity/Angular velocity
*Boundary, type=VELOCITY
Part-2-1.f-neg-x, 1, 1
*Boundary, type=VELOCITY
Part-2-1.f-neg-y, 2, 2
*Boundary, type=VELOCITY
Part-2-1.f-neg-z, 3, 3
*Boundary, type=VELOCITY
Part-2-1.f-pos-x, 1, 1
*Boundary, type=VELOCITY
Part-2-1.f-pos-y, 2, 2

```

```

*Boundary, type=VELOCITY
Part-2-1.f-pos-z, 3, 3
**
** PREDEFINED FIELDS
**
** Name: Predefined Field-1   Type: Material assignment
*Initial Conditions, type=VOLUME FRACTION
(Element Volume Fraction Definitions)
**
***Initial Conditions, type=STRESS, GEOSTATIC
***MySet, 0.0, 120, -1.174e-03, 0.0, 1.0, 1.0
**
** INTERACTIONS
**
** Interaction: Int-1
*Contact, op=NEW
*Contact Inclusions, ALL EXTERIOR
*Contact property assignment
, , IntProp-1
*Contact Controls Assignment, Type=SCALE PENALTY
,,0.1
** -----
**
** STEP: Step-1
**
*Step, name=Step-1
*Dynamic, Explicit
, 1
*Bulk Viscosity
0.06, 1.2
**
** BOUNDARY CONDITIONS
**
** Name: BC-1 Type: Symmetry/Antisymmetry/Encastre
*Boundary
Part-1-1.s-base, ENCASTRE
** Name: solid-side-2 Type: Symmetry/Antisymmetry/Encastre
*Boundary
Part-1-1.s-pos-z, ZSYMM
** Name: solid-sides Type: Symmetry/Antisymmetry/Encastre
*Boundary

```



```

Part-1-1.s-neg-z, ZSYMM
**
** LOADS
**
** Name: Load-1    Type: Gravity
*Amplitude, name=Amp-1, definition=SMOOTH STEP
          0.,          0.,          1.,          1.
**
*Dload
, GRAV, 9806.6, 0., 0., -1.
**
** OUTPUT REQUESTS
**
*Restart, write, number interval=1, time marks=NO
**
** FIELD OUTPUT: F-Output-1
**
*Output, field, variable=PRESELECT
**
** FIELD OUTPUT: F-Output-2
**
*Output, field
*Element Output, directions=YES
PRESSVAVG
*Contact Output
CFORCE
**
** HISTORY OUTPUT: H-Output-2
**
*Output, history
*Integrated Output, section=I-Section-1
SOF,
**
** HISTORY OUTPUT: H-Output-1
**
*Output, history, variable=PRESELECT
*End Step

```